Fall 2021

MECHANISTIC MODELLING FRAMEWORK AND LIFE CYCLE ASSESSMENT APPROACH FOR PAVEMENT REHABILITATION USING ASPHALT CONCRETE OVERLAYS

Katie Eileen Haslett
University of New Hampshire, Durham

MECHANISTIC MODELLING FRAMEWORK AND LIFE CYCLE ASSESSMENT APPROACH FOR PAVEMENT REHABILITATION USING ASPHALT CONCRETE OVERLAYS

BY

KATIE E. HASLETT

Bachelor of Science, Civil Engineering, University of New Hampshire, 2018

DISSERTATION

Submitted to the University of New Hampshire

in Partial Fulfillment of

the Requirements for the Degree of

Doctor of Philosophy

In

Civil and Environmental Engineering

September 2021

This dissertation has been examined and approved in partial fulfillment of the requirements for the degree of Doctor of Philosophy in Civil and Environmental Engineering by:

Dissertation Director, Dr. Eshan V. Dave
Associate Professor of Civil and Environmental Engineering

Dr. Jo E. Sias
Professor of Civil and Environmental Engineering

Dr. Weiwei Mo
Assistant Professor of Civil and Environmental Engineering

Dr. Shongtao Dai
Research Operations Engineer at Minnesota Department of Transportation

Dr. Heather Dylla
Sustainable Pavement Engineer for the Federal Highway Administration

Dr. Mirkat Oshone
Pavement Engineer at AECOM

On 15 July 2021

Approval signatures are on file with the University of New Hampshire Graduate School.

"If you believe, you can achieve."

ACKNOWLEDGEMENTS

This dissertation research was made possible by the support and funding of the University of New Hampshire (UNH), and the National Road Research Alliance (NRRA). I want to thank the Department of Civil and Environmental Engineering (CEE) for awarding me a Teaching Assistantship in the Fall of 2018, Fall 2019 and Spring 2021. Thank you to the UNH Graduate School for the Summer Teaching Assistant Fellowship in 2020 and for the numerous travel grants throughout my Ph.D. studies to attend and participate in national and international conferences. I would also like to extend my sincere appreciation to the staff and researchers at Minnesota's Department of Transportation (MnDOT) and full-scale pavement test facility (MnROAD), for their help in collecting and providing data used in this dissertation as well as constructive feedback and input: Ben Worel, Michael Vrtis, Kyle Hoegh, Jerry Geib, Tom Burnham, Joe Voels and Len Palek.

To my advisors, Dr. Eshan Dave and Dr. Jo Sias, thank you. Thank you for supporting me. Thank you for challenging me. Thank you for bringing the best out of me. Thank you for teaching me the importance of being a life learner and most of all, thank you for always believing in me.

I would also like to thank my dissertation committee members, Dr. Weiwei Mo, Dr. Shongao Dai, Dr. Heather Dylla and Dr. Mirkat Oshone for your invaluable feedback and guidance throughout this process. I would like to thank the faculty and staff of the CEE department at UNH, specifically Dr. Erin Bell, Dr. Robert Henry, Dr. Raymond Cook, Dr. Ghayoomi, Dr. Kwiatkowki, Michelle Mancini, Kristen Parenteau and Kelly Shaw for always having an open door to talk or being willing to lend a hand to help. Many thanks to the UNH technology service center, Kevan Carpenter, John Ahern and Noah Macadam for all the help in keeping our equipment running and our research moving forward.

To the asphalt material research group at UNH, past, present and future members, you truly become family throughout this experience. I will cherish every moment I spent getting to know you, learning with and from you during this journey. Thanks to Dr. Mirkat Oshone Dr. Reyhaneh Rahbar-Rastegar, Dr. Mohammad Elshaer, Dr. Rasool Nemati, Dr. Yaning Qiao, Dr. Runhua Zhang, Dr. Francesco Preti, Chris DeCarlo, Chibuike Ogbo, Eric Caron, Danial Mirzaiyanrajeh, Farah Zaremotekhases, Miranda Chiappini, Anh Tran, Wei Fang and Zheng Wang. To my other colleagues, classmates and friends I've made along the way, thank you for your support, many laughs and good memories: Brittany Marshall, Annavitte Rand, Duncan McGeehan, Melissa Gloekler, Matthew McGinnis, Jesse Ross, Masoud Mousavi, and Ian Gates.

Thank you to all my friends, teammates and coaches for the words of encouragement, reminding me to breathe, and not to forget to enjoy the process. A special thank you to Chris DeCarlo for your patience and unconditional support during this chapter of life and cheers to the many chapters to come.

Finally, I wish to thank my family. To my mom, dad, and brother, I could not have done this without your continuous love and encouragement. Thank you for allowing me to spread my wings at just 14 years old to go to school in another country in order to pursue my academic and athletic dreams. I am forever grateful for your love, support and sacrifices over the years.

TABLE OF CONTENTS

LIST OF TABLES

LIST OF FIGURES

LIST OF ACRONYMS

AAPT	Association of Asphalt Paving Technologists
AASHTO	American Association of State Highway and Transportation Officials
AC	Asphalt Concrete
ACOL	Asphalt Concrete Overlay
AMPT	Asphalt Mixture Performance Tester
ANOVA	Analysis of Variance
ASTM	American Society for Testing and Materials
AV	Air Void
AvgRC	Average Reflective Cracking Rate Performance Index
CED	Cumulative Energy Demand
CI	Confidence Interval
CMOD	Crack Mouth Opening Displacement
COV	Coefficient of Variability
CRI	Cracking Resistance Index
CT	Compact Tension
CZM	Cohesive Zone Model
DCC	Damage Characteristic Curve
DCT	Disk-Shaped Compact Tension
Des. Air Void	Design Air Void Level
Des. Gyrations	Design Gyrations
Des. Total AC	Design Total Asphalt Content
DPS	Density Profile System
DTCF	Direct Tension Cyclic Fatigue
EAC	Equivalent Annual Cost

ESAL	Equivalent Single Axle Loads
EPA	Environmental Protection Agency
EPD	Environmental Product Declaration
FE	Finite Element
FEA	Finite Element Analysis
FHWA	Federal Highway Administration
FI	Flexibility Index
FST	Fracture Strain Tolerance
FWD	Falling Weight Deflectometer
G_f	Fracture Energy
G_{mb}	Bulk Specific Gravity
GWP	Global Warming Potential
HMA	Hot Mix Asphalt
HWT	Hamburg Wheel Tracker
IDOT	Illinois Department of Transportation
IRI	International Roughness Index
ISO	International Organization for Standardization
LCA	Life Cycle Assessment
LCC	Life Cycle Cost
LCCA	Life Cycle Cost Analysis
LEFM	Linear Elastic Fracture Mechanics
LTE	Load Transfer Efficiency
M&R	Maintenance and Rehabilitation
Mix ID	Mixture Identification
MnDOT	Minnesota Department of Transportation

NCAT	National Center for Asphalt Technology
NCHRP	National Cooperative Highway Research Program
NMAS	Nominal Maximum Aggregate Size
NPV	Net Present Value
NRRA	National Road Research Alliance
OT	Overlay Tester
PASSRC	Permeable Asphalt Stabilized Stress Relief Coarse
PCC	Portland Cement Concrete
PCI	Pavement Condition Index
PCR	Product Category Rule
PMS	Pavement Management Systems
RAP	Reclaimed Asphalt Pavement
%RC	Percent Reflective Cracking
RCTotal	Total Reflective Cracking Performance Index
RDCI	Rate-Dependent Cracking Index
RTD	Realistic Traffic Data
SCB	Semi-Circular Bend
SPP	Sustainable Pavements Program
S-VECD	Simplified Viscoelastic Continuum Damage
TCF	Truck Conversion Factor
TRR	Transportation Research Record
UTBWC	Ultra-Thin Bonded Wearing Course
Vbe	Volume of Effective Binder
VMA	Voids in Mineral Aggregate

ABSTRACT

MECHANISTIC MODELLING FRAMEWORK AND LIFE CYCLE ASSESSMENT APPROACH FOR PAVEMENT REHABILITATION USING ASPHALT CONCRETE OVERLAYS

Efficient and effective rehabilitation of existing roadways continues to be a top priority for local, state, and federal agencies to provide safe travel of people and goods. Asphalt concrete (AC) overlays on deteriorated Portland Cement Concrete (PCC) are a popular rehabilitation option to extend the service life of a roadway. However, the combination of load and environmentally induced movements at underlying joint locations can cause high amounts of stresses and strains, leading to the formation of cracks in the AC overlay. Ensuring that a suitable asphalt mixture (cracking resistance) and sufficient overlay structure (thickness) are selected is critical to avoid pre-mature failure of overlays and excess funding requirements on pavement maintenance and rehabilitation (M&R).

This dissertation research aimed to improve the decision process of rehabilitation PCC pavements with AC overlays through the development of a Microsoft Excel®-based decision tree tool for screening of asphalt mixtures and overlay designs. A combination of laboratory testing, field performance data from full-scale pavement test sections and predicted modeling results were utilized to assess varying overlay options. The two main outputs from the decision tree tool are (1) a life cycle cost estimate and (2) predicted reflective cracking performance curves with both time and truck traffic.

Furthermore, this dissertation work sought to improve pavement life cycle assessment (LCA) and life cycle cost analysis (LCCA) practices by considering both realistic traffic conditions and future climate projections in the analysis framework. Traditional pavement LCAs are

performed using historical climate data to evaluate pavement performance and provide recommendations for budgeting and planning of M&R strategies in the future. However, due to climate change, this assumption may not be appropriate as pavements' performance is influenced by climate stressors. Research conducted as part of this dissertation showed that incorporating future project climate data and realistic traffic data can lead to a substantial increase in agency LCA impacts (up to 20% for the presented case-study), where the increase is a function of pavement structure and M&R scenario over the analysis period.

1. CHAPTER 1

INTRODUCTION

1.1 Motivation and Background

As pavement infrastructure continuously ages and deteriorates, the preservation, maintenance and rehabilitation of pavements is of critical importance. Asphalt overlays are a relatively simple and cost-effective maintenance solution for the extension of pavement service life. However, the extension of the service life is dependent on the performance of the asphalt overlay. Reflective cracking is one of the most common distresses observed in asphalt concrete (AC) overlays and is the result of both traffic and environmental loading mechanisms. The formation of cracks and high rate of crack propagation is mainly due to the formation of stress concentration in overlays at locations of underlying joints or cracks in the existing pavement. Mechanical properties of the asphalt mixture, layer thickness, composition and the condition of the existing pavement all contribute to reflective cracking performance.

Current state of practice of asphalt overlay material and thickness selection is policy-based and lacking an engineered design approach. The main focus of this dissertation study is to improve the decision process of maintenance and rehabilitation (M&R) of deteriorated Portland cement concrete (PCC) pavements with asphalt concrete (AC) overlays. This is achieved through the development of a simple decision tree-based tool for selecting suitable asphalt mixtures and overlay designs to extend overlay lives by lowering reflective cracking. To develop the decision tree, a combination of laboratory testing, field performance data and predicted modeling results are utilized to assess varying overlay alternatives using a life cycle cost analysis (LCCA) approach. It is anticipated that implementation of the proposed decision tree tool and asphalt materials

recommended from the results of this dissertation study will translate to savings in construction costs and time, improved serviceability of the roadways for users, and reduced life cycle costs.

Simultaneous to the development of simple decision tree solution for practitioners, it is important to develop a life cycle assessment (LCA) and LCCA framework that can consider both realistic traffic conditions and climate change impacts. Typically, pavement LCAs are performed assuming static traffic conditions and historical climate data to plan pavement life expectancy and inform maintenance and rehabilitation decisions. These assumptions may lead to an underestimation of user and agency impacts throughout the use phase of a pavement LCA. With the growing interest in LCAs and LCCAs in pavement management practices, it is important that frameworks provide the ability to include non-static traffic and future climate projections into the analysis process. Therefore, as part of this dissertation work a framework was developed to include realistic traffic conditions and future climate projections in a pavement LCA.

1.2 Dissertation Organization

Dissertation research efforts consisted of analysis of laboratory and field performance data from full scale pavement study sections, development of finite element based reflective cracking mechanistic models, and development of LCCA as well as LCA frameworks. The principal objectives of this research are as follows:

1. Evaluate the suitability of reflective cracking performance measures for asphalt concrete overlays using laboratory, field and predicted model results.
2. Improve pavement LCCA and LCA frameworks by considering realistic traffic conditions and future climate projections in the analysis.
3. Develop a simple decision tree-based tool for selecting suitable asphalt mixtures and overlay designs.

1.3 Overall Research Approach

In order to fulfill the dissertation objectives presented herein, a number of research efforts were undertaken to evaluate the reflective cracking performance of asphalt mixtures overlays on PCC pavement and to develop a LCCA and LCA framework. The research approach adopted in this dissertation work generally included the following activities:

a) Laboratory testing of a range of asphalt overlay mixtures.

b) Evaluation of field performance of 12 full-scale overlay test sections at MnROAD facility.

c) Exploring predictive models of asphalt concrete overlays reflective cracking performances.

d) Statistical analysis of laboratory and field performance results.

e) Developing a realistic traffic and climate change informed LCA-based pavement maintenance and rehabilitation decision framework.

f) Developing an asphalt concrete overlay thickness and material selection decision tree tool.

Figure 1-1 presents a simplified process diagram of the overall research approach. Detailed discussion of each component within the research approach and contributing papers are discussed thereafter.

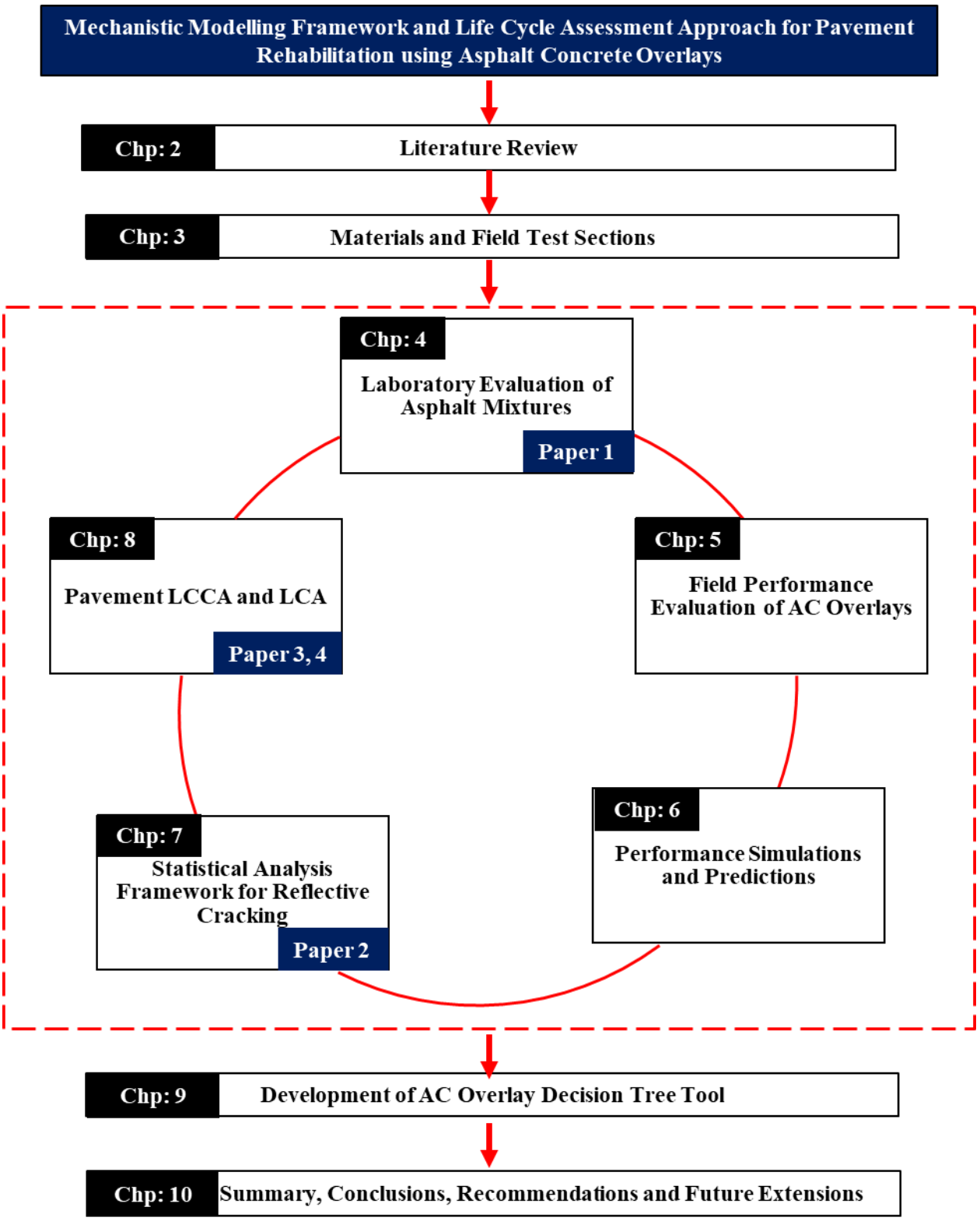

Figure 1-1 Overall research approach.

Chapter 1 is dedicated to the introduction and motivation for this research, as well as the study objectives.

Chapter 2 provides a brief literature review on reflective cracking in asphalt concrete overlays, impact of in-situ density on pavement performance, life cycle cost analysis (LCCA), and life cycle assessment (LCA).

Chapter 3 presents the range of materials that are examined in this dissertation study along with their corresponding full-scale pavement test sections located at the MnROAD test facility. Existing PCC condition in terms of pre-overlay load transfer efficiency (LTE) is discussed along with pre-overlay treatments (e.g. slab stabilization) undertaken to improve reflective cracking performance.

Chapter 4 provides a description of the different laboratory test methods used to evaluate reflective cracking performance of the various asphalt mixtures. There are six different performance test evaluation methods included in this dissertation work. Following a brief description of each test method are the lab performance test results for all asphalt mixtures used in the construction of MnROAD test sections (Cell 984-995).

Chapter 5 includes the field performance data collection methods, analysis, and results of AC overlay test sections. All test sections are studied by driving and passing lane separately, resulting in 24 different sections to compare and contrast. A description of field performance indices used to rank test section performance is also included in this chapter.

Chapters 6 provides an overview of advanced pavement reflective cracking performance evaluation programs that were employed to characterize the asphalt mixtures performance while considering structure, climate and traffic conditions. Two different predictive modeling techniques were adopted in this dissertation work including finite element modeling using Abaqus®

commercial software by Dassault Systèmes®, and AASHTOWare® Pavement ME Design™ software.

Chapter 7 presents a statistical analysis framework that may be adopted to analyze AC mixture's characteristics, laboratory and field performance data. Logistic regression models to predict the probability of reflective cracking occurring were developed and results presented for a scenario where decision makers do not have access to laboratory testing data on AC overlay materials as well as a scenario where common fracture test results are available (e.g. Disk-shaped compact tension, semi-circular bend or overlay tester).

Chapter 8 is devoted to summarizing research efforts on improving pavement LCCA and LCA approaches. A focus is placed on the operational phase of a pavement LCA, specifically looking at the inclusion of realistic traffic conditions and future climate projections.

Chapter 9 summarizes the development of a simple decision tree tool for selecting or screening AC overlay designs. A general overview of the decision tree tool is presented followed by more detailed discussion on the required inputs and expected outputs from the tool.

Chapter 10 summarizes the findings of the research and contribution of this dissertation. Discussion is provided on future extension of this work while identifying current knowledge gaps and areas for improvement.

2. CHAPTER 2

LITERATURE REVIEW

2.1 Reflective Cracking in Asphalt Concrete Overlays

Reflective cracking is one of the most prominent distresses in composite pavement structures [1]. When AC overlays are placed over jointed or severely cracked PCC pavements, stress concentrations form due to thermal, and traffic driven movements near the joint locations and result in cracks initiating and propagating upward through the AC layer. Figure 2-1 shows an example of a reflective crack in a pavement section located on I-94 Westbound in Minnesota.

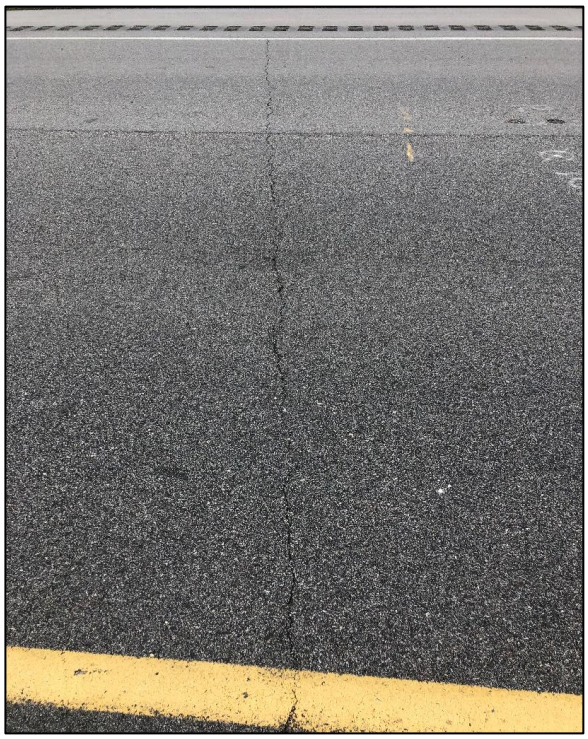

Figure 2-1 Reflective cracking in asphalt concrete overlay.

The formation and propagation of reflection cracking is controlled by the mechanical properties of the asphalt and the condition of the overlaid pavement. One of the major concerns with reflective cracking is not necessarily the crack itself, but rather that it allows for water to

infiltrate into the underlying pavement structure leading to further deterioration and shorten service life of the overlay.

In development of a simple decision tree tool for selection of appropriate AC overlay materials and thicknesses to rehabilitate deteriorated PCC pavements, there are many factors that can influence overlays reflective cracking performance. For example, a sensitivity analysis performed by Hu et al. identified that there are five significant input factors that must be considered when designing an AC overlay. These five parameters are (1) traffic, (2) climate, (3) asphalt overlay thickness, (4) asphalt overlay mix type, and (5) load transfer efficiency (LTE) [2]. As part of this dissertation work, all five of these factors are included and implemented in the development of the decision tree tool. For example, the impact of existing pavement condition is evaluated in terms of LTE, presence of voids and use of slab stabilization prior to overlay construction. Furthermore, there are eight different asphalt overlay mix types included in this study with a combination of traditional designs and some innovative approaches targeting achieving better in-situ density.

2.2 Impact of In-situ Density on Performance

Throughout the development of pavement design, starting in the early 1800's with the basic notion to select an aggregate gradation and a suitable amount of bitumen, achieving a certain level of density has been a priority. Work done in the 1900's by individuals such as Clifford Richardson, Charles Hubbard and Frederick Field, Bruce Marshall, James Rice and Norman McLeod lead to the development of the Marshall mix design method. The Strategic Highway Research program (SHRP), developed in the late 1980's the empirically-based Superpave asphalt design method as an extension of the Marshall design method.

The Marshall method uses an air void design range of 3-5% while compaction specifications during construction result in approximately 8% in-place air voids. In comparison, Superpave requires a 4% design air void and typical in-place air voids are around 7%. The logic behind having higher in-place air voids after construction is that traffic would compact the asphalt mixture to the designed air void level over time. Superpave design focuses on the compactive effort to achieve density at the end of the pavement service life. Another method developed by the Laboratoire Central des Ponts et Chaussées (LCPC) focuses on achieving the desired density of asphalt at the beginning of the pavement in-service life.

In recent years, there has been a heightened interest by many states to adjust asphalt mixtures to achieve higher in place field density to achieve better overall mixture performance. A demonstration project was sponsored by Federal Highway Administration (FHWA) and carried out by the National Center for Asphalt Technology (NCAT), to show that enhanced durability of asphalt pavements through increase in-place pavement density is achievable in the field and not only in the laboratory [3]. A study by Tran et al. in 2016 performed a life cycle cost analysis (LCCA) on two pavement alternatives in which the same asphalt overlay would be constructed to 7% and 8% air voids. Results from the study showed that, “A 1% decrease in air voids was estimated to improve the fatigue performance of asphalt pavements between 8.2% and 43.8% and the rutting resistance by 7.3% to 66.3%. In addition, a 1% reduction in in-place air voids can extend the service life by 10% or more [4].

An article released by the FHWA in July 2021, emphasized that while improved overlays are now available for both asphalt and concrete pavements, providing agencies with the ability to achieve long-life performance under a wide range of traffic, environmental and existing pavement conditions, they are not always targeted to high priority or high maintenance locations (e.g.

interstates, intersections, bus lanes etc.). Therefore, FHWA created the Targeted Overlay Pavement Solutions (TOPS) initiative to help agencies expand the types of overlays they commonly use and apply them in cost-effective situations by developing resources to help select the right overlay product for the right location. Tim Aschenbrener, FHWA's TOPS team co-lead stated that, "The use of overlays is often based on an agency's experience or budget" [5]. This aligns with one of the main motivations of this study to advance current state of practice for overlay designs from policy-based to an engineered design approach. Furthermore, the development of a simple decision tree tool as part of this dissertation can act as a valuable resource for agencies to screen overlay designs (material type and thickness combinations) with the goal of lower the amount of reflective cracking and improving in-situ density. Aschenbrener summarized it well by saying, "While there's no single answer for everyone, by using good project selection practices, we believe every agency can find a targeted solution that is both cost-effective and durable" [5].

As part of this dissertation study, several test sections located at MnROAD test facility have been dedicated to investigating how enhanced density may improve the performance of AC overlays. Permanent deformation is often focused on when considering improvements to the density of the asphalt layer, however there is a lack of research on the impact of in-situ density on reflective cracking or cracking performance in general. There are many approaches to achieving higher in-situ density such as, air void regression, film thickness, minimum asphalt contents, compaction additives, reducing the number of gyrations or modifying design air void targets. Two approaches are being investigated in this study, modifying the design air voids (Superpave5), and the regressed air void method. Further detail on the two approaches is given below.

2.2.1 Superpave5

Superpave5 design (based off the LCPC approach) involves designing at 5% air voids and compacting to 5% in-place air voids. This mixture design approach has gained popularity in recent years after successful laboratory testing and field trials [6]. In comparison to the traditional Superpave (designed at 4% air voids), to achieve a 1% increase in design air voids while maintaining the same volume of effective binder (V_{be}), the voids in the mineral aggregate (VMA) must be increased by 1% as well. In order to increase the design air void by 1% while holding V_{be} constant the aggregate proportions are adjusted to meet the new design criteria.

Hekmatfar et al. (2013) showed that using a 50 design gyration to evaluate Superpave5 that it was possible to compact to 5% air voids in the field without additional compaction effort and laboratory results indicate that the mixtures should have acceptable performance [7]. Huber et al. (2016) concluded based on a laboratory study and two trial sections that an asphalt design at 30 gyrations with 5% air voids and compacted to 5% air voids will perform as well or better than asphalt designed using 100 gyrations and compacted to 7% air voids [8].

2.2.2 Regressed Air Void

The regressed air voids approach, which follows a conventional design (4% air voids) and then increases the amount of additional virgin asphalt binder to obtain 3% air voids. Unlike the Superpave5 method which aims to hold the V_{be} constant while achieving higher in-situ density, the air void regression method typically increases the design asphalt content by up to 0.4%. The premise behind air void regression and increasing in-situ density of the mixture is that it will also decrease permeability, decrease porosity, increase durability and increase film thickness. Recent research led by the National Center for Asphalt Technology (NCAT) focused on the use of regressed air voids for balanced mix design. Results from the study indicated that the regressed air

voids concept can improve mixtures cracking resistance without compromising the rutting resistance of the asphalt mixture [9].

2.3 Life Cycle Cost Analysis (LCCA)

In order to analyze the cost effectiveness of each overlay section, life cycle cost analysis (LCCA) will be used in this dissertation study. LCCA is a technique that identifies and evaluates the costs associated with a piece of infrastructure (a pavement section in this case) during all of the various stages of its useful life. This includes, but is not limited to, costs such as initial construction, maintenance, rehabilitation, operation, and disposal/end of life. The main advantage of LCCA over traditional cost analysis is that LCCA incorporates all the costs endured by an agency throughout the life of the pavement section rather than the traditional way of focusing solely on the initial construction costs. Another significant advantage of LCCA is the ability to incorporate the performance of various sections and its impacts on user costs, which allows for a fair comparison to be made between the sections in terms of cost effectiveness.

There are two different computational approaches to perform an LCCA; deterministic and probabilistic. The more commonly performed deterministic approach involves assigning each LCCA input variable a fixed, discrete value based on historical data or engineering judgment. While sensitivity analysis may be performed to verify the robustness of the input values, the deterministic approach is unable to address simultaneous variations of multiple inputs at a time or convey the level of uncertainty associated with each life-cycle cost (LCC) estimate. In comparison, a probabilistic approach assigns a probability function to each LCC estimate, therefore it is able to express both the range of likely inputs and the likelihood of their occurrence. In recent years, due to the improvement in computer processing capabilities, a probabilistic approach has become more practical to simulate and account for simultaneous changes in LCC inputs. Overall, the

incorporation of an LCCA approach (deterministic or probabilistic) to compare cost effectiveness of various AC overlay alternatives is a critical step in the development of the simple decision tree based tool for the rehabilitation of PCC pavements.

Several research studies have been performed to date using an LCCA approach to compare different rehabilitation and maintenance solutions. A study performed by Tran et al. (2016) illustrated the effect of in-place density on the LCCA of two alternative asphalt overlays (7% and 8% air voids) [4]. LCCA results showed that, "The state highway agency would see a net present value (NPV) cost savings of $88,000 on a $1,000,000 paving project (8.8%) by increasing the minimum required density by 1% of G_{mm}" [4]. However, this savings does not consider other costs such as operation, maintenance, and road user costs. Huang et al. (2009) found that additional fuel consumption and pollutant emissions caused by traffic delays during roadwork periods (maintenance and rehabilitation) are significant and should not be ignored [10]. The inclusion of user costs due to maintenance and operations is a complex task with room for improvement. The LCCA framework presented as part of this dissertation work builds off the LCCA study by Tran et al. (2016) and others such as, Lu et al. (2018), Yu et al. (2012), Zhang et al. (2010) and (2008) and Chan et al. (2008), to incorporate all relevant costs for each alternative to perform a holistic evaluation [4], [11]-[14].

2.4 Life Cycle Assessment (LCA)

International Organization for Standardization (ISO) defines a life cycle assessment (LCA) as an "Environmental assessment tool of a product," where a product is defined as any good or service. There are four key phases in a LCA framework including: (1) goal and scope definition, (2) life cycle inventory analysis, (3) life cycle impact assessment, (4) life cycle interpretation. There are three additional standards that supplement the central ISO 14040 standard by providing

further detail on individual phases one through three (ISO 14041, ISO 14042 and ISO 14042) respectively. Essentially, a LCA is a technique used to assess environmental impacts associated with all stages of a product's life cycle (e.g. pavement system). Figure 2-2 provides an example of the different stages involved in a LCA.

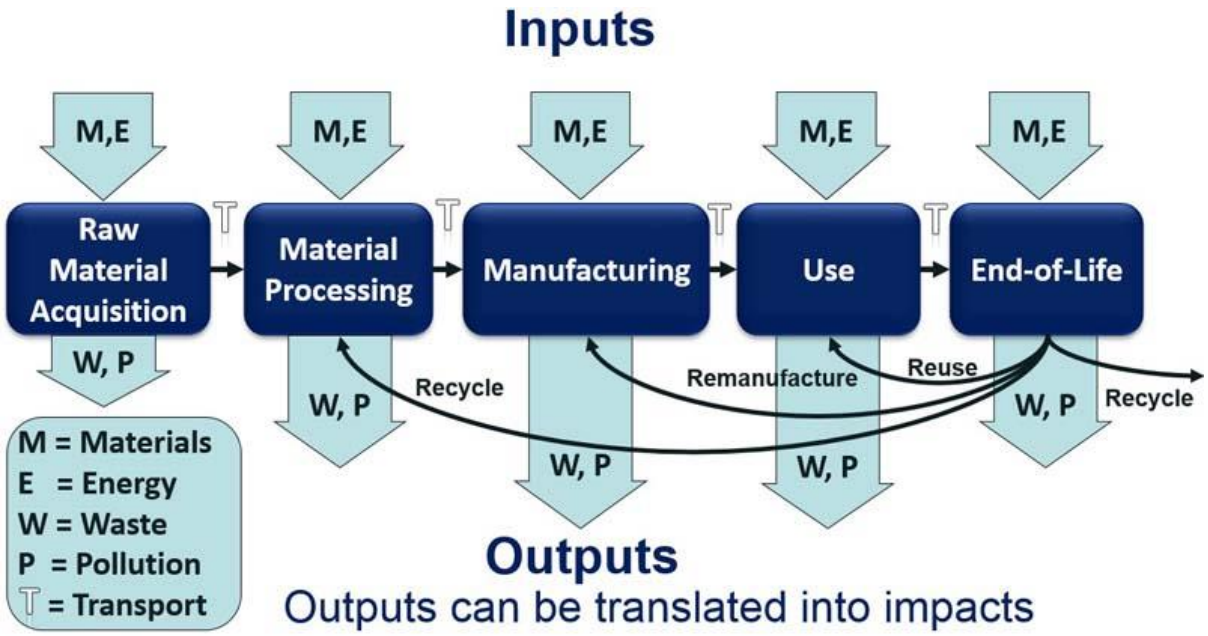

Figure 2-2 Stages of life cycle assessment [15].

A LCA is often employed to determine the tradeoffs associated with different alternatives (e.g. pavement maintenance and rehabilitation options). It is imperative that all life cycle stages be included, and that the life cycle inventory contains quality data sources to make appropriate comparisons among alternatives. While ISO provides a standard method to perform LCA's, specifics vary greatly from one application to another, leading to inconsistencies in pavement LCA applications and comparisons [16].

For example, one of the current weaknesses in a pavement LCA is the lack of a formalized or standard functional unit. Without a uniform functional unit, it is nearly impossible to make a comparison of results from different LCA studies. It was recommended by Azarijafari et al., that

pavement LCA's functional unit consider, "The definition of physical properties of the pavement system, including design structural components, and material properties. Functional unit must also reflect effective exterior factors on the pavement, such as traffic load" [17]. Several researchers have investigated ways to address this weakness by using different functional units in a sensitivity analysis [18]-[20]. However, caution should always be taken when comparing LCA results from one study to another by checking the compatibility of functional units and system boundaries from each study. This leads to a second major weakness of current LCA frameworks, which is the widespread uncertainty regarding selecting system boundaries.

In an ideal world, a LCA would examine all the phases of the products life cycle (i.e. all the pavement life cycle stages from material extraction to end-of-life) in great detail. However due to time, data and knowledge constraints this is rarely achieved. As a result, most pavement LCA frameworks are reduced to assess environmental impacts associated with only a single phase of the LCA (e.g. use phase) based on the goal and scope of the study. By focusing on a single phase of a LCA to meet a specific study objective, it creates a research gap or weakness where the ultimate goal of a true LCA framework following ISO standards is not fully achieved. To address this shortcoming, it is critical that researchers follow ISO guidelines, theory, and intent behind all phases of the LCA framework (goal and scope definition, life cycle inventory analysis, life cycle impact assessment and life cycle interpretation) when performing a simplified LCA study. All phases should still be completed, however the amount of detail and extent of resources spent on each phase may be limited.

While the application of LCA to pavement design is still in the early stages, it presents the opportunity for researchers to address concerns and limitations. One of the objectives of this dissertation work is to improve and advance the state of practice in pavement LCA applications.

A focus was placed on the use stage of the LCA by developing a framework to include realistic traffic conditions and future climate projections. Further detail on this effort is included in Chapter 8 of the dissertation.

3. CHAPTER 3

MATERIALS AND FIELD TEST SECTIONS

3.1 Chapter Introduction

In this dissertation work, a variety of asphalt mixtures with corresponding full scale pavement test sections that utilized different pre-overlay rehabilitation and construction treatments are investigated. In the following sections, detailed information is provided on the eight different asphalt mixtures, 12 field test sections and corresponding pre-overlay PCC conditions. A brief history is also provided on the construction and rehabilitation of test sections (Cell 984-995) located parallel to the MnROAD mainline on I-94 Westbound.

3.2 Materials

Asphalt materials included in this study consisted of a range of mix design approaches. There were three mixtures with a 12.5 mm nominal maximum aggregate size (NMAS) that contained varying air void design from 3 to 5 percent. Two different interlayer mixtures were included in this study, one 9.5 mm NMAS mixture and one ultra-thin bonded wearing course (UTBWC). Further details on the asphalt mixture design properties may be reviewed in Table 3-1.

Table 3-1 Summary of asphalt mixture design properties.

Mix Identification *(Design Approach)*	NMAS (mm)	Binder	Des. Air Voids (%)	Des. Total AC (%)	RAP (%)	Des. Gyrations
SPWEA440E *(Traditional Superpave 9.5 mm)*	9.5	58H-28	4.0	5.8	25	90
SPWEB430E *(Regressed Air Void, 3%)*	12.5	58H-28	3.0	5.7	20	90
SPWEB440E *(Traditional Superpave 12.5 mm)*	12.5	58H-28	4.0	5.4	20	90
SPWEB450E *(Superpave 5%)*	12.5	58H-28	5.0	6.6	15	50
SPWEC440E *(Traditional Superpave, 19mm)*	19.0	58H-28	4.0	5.6	10	90
SPWED430I *(Binder Rich Reflective Cracking Interlayer)*	4.75	58E-34	2.0-3.0	8.2	0	50
PASSRC *(Permeable Asphalt Stabilized Stress Relief Course, Absorbing Reflective Cracking Interlayer)*	9.5	64S-22	-	3.6	0	-
UTBWC *(Ultra-Thin Bonded Wearing Course, Open-Graded)*	9.5	58V-34	-	5.3	0	-

3.3 Field Test Sections

This dissertation work leverages 12 full-scale overlay pavement test sections (Cells 984-995) and one control section (Cell 983) located at the MnROAD's test facility on the original alignment of I-94 westbound (Figure 3-1).

Figure 3-1 Full-scale overlay pavement test sections on I-94 Westbound.

Each pavement test section is 500 feet long with a 100 foot transition zone in-between each section. Overlay designs consist of both single and double lifts. All overlay pavement test sections are AC overlays on 9.5-inch thick PCC pavement over 5-inch MnDOT Class 5 aggregate base material. The original PCC pavement consisted of 27-foot jointed reinforced slabs with skewed joints containing 1.25-inch dowel bars placed in 1973. A brief summary of the asphalt mixtures and their corresponding field test sections is presented in Table 3-2, while Figure 3-2 shows a schematic of the as-designed overlay cross sections included in this study.

Four of the test sections (Cells 988-991) are dedicated to a compaction study evaluating the impact of in-situ density (as well as mix design approaches regarding design air void levels) on reflective cracking performance. These specific test sections have the same overall pavement structure but contain varying surface course materials designed at different air void levels. Two test sections (Cell 992 and Cell 993) make use of a 1-inch interlayer lift prior to applying a

traditional 1.5-inch wearing course. Only one test section (Cell 994) underwent PCC slab stabilization prior to overlay construction. Lastly, Cell 995 was constructed using an ultra-thin bonded wearing course (UTBWC) with a total lift thickness of 0.75 inches.

Table 3-2 Summary of mixtures and corresponding field sections at MnROAD.

Cell	Description	Mixture Type	Comment	Overlay Thickness (in.)
983	Control section	N.A	-	-
984	HMA over concrete (1 lift)	SPWEA440E	Single lift	1.5
985		SPWEB440E	Single lift	1.5
986		SPWEB440E	Single lift + spray paver	1.75
987	HMA over concrete (2 lift)	SPWEC440E	Lift 1	2.5
		SPWEA440E	Lift 2	1.5
988	HMA over concrete (2 lift)	SPWEC440E	Lift 1	2.25
		SPWEB440E	Lift 2	1.75
989		SPWEC440E	Lift 1	2.25
		SPWEB450E	Lift 2	1.75
990		SPWEC440E	Lift 1	2.25
		SPWEB430E	Lift 2	1.75
991		SPWEC440E	Lift 1	2.25
		SPWEA440E	Lift 2	1.75
992	HMA over concrete with interlayer	SPWED430I	Lift 1 (interlayer)	1
		SPWEA440E	Lift 2 (over interlayer)	1.5
993	HMA over concrete with PASSRC	PASSRC	Lift 1	1
		SPWEA440E	Lift 2	1.5
994	HMA over concrete (1 lift)	SPWEA440E	Lift 1 + slab stabilization	1.5
995		UTBWC	Lift 1 + spray paver	0.75

Figure 3-2 Asphalt concrete overlay design cross sections (Test cells 984-995).

3.4 Construction of Asphalt Concrete Overlays

Minimal maintenance had been done on the test sections during previous rehabilitation treatments, with the exception of areas that required full-depth joint replacement or panel replacement as needed. In the most recent rehabilitation project prior to AC overlay construction in 2013, diamond grinding in the driving lane was performed [21]. In general, the PCC pavement was reported to be in fair condition with the primary distress being faulting with mid-panel cracks and spalling also present.

Only one test section (Cell 994) was preceded by a polyurethane compaction grouting and void filling process prior to overlay construction. The objective behind performing slab stabilization is to reduce the potential for high deflections located at joints and cracks in the underlying PCC pavement, thereby reducing the potential for reflective cracking. A direct comparison can be drawn between the performance of Cells 984 and 994, which have the same overall pavement design structure and asphalt mixtures but differ only by the slab stabilization performed in Cell 994.

The use of spray pavers versus conventional pavers was considered in the construction of test sections. Both Cells 986 and 995 were placed with a spray paver that applies a fairly heavy tack (0.17-0.23 gal./yd.^{2}). All remaining test sections were placed using a conventional paver. It should be noted that at the time of construction, samples of all asphalt mixtures were collected for laboratory performance testing described in Chapter 4. Lastly, four of the 12 test sections were instrumented with both joint opening sensors and thermocouples. In-situ temperature data collected from test sections will provide critical thermal loading information that will be implemented in finite element models as part of Chapter 6.

4. CHAPTER 4

LABORATORY EVALUATION

4.1 Chapter Introduction

In the following chapter a description of the six laboratory performance tests used to characterize and evaluate the various asphalt mixtures including in this dissertation is presented. Relevant indices for each test were calculated and results from each test summarized. A paper has been published in the Journal of Testing and Evaluation focused on cracking performance indices derived from disk-shaped compact tension (DCT) testing compared to field reflective cracking performance and is included in Appendix A.1.

4.2 Complex Modulus Test

Complex modulus testing was performed in accordance with the AASHTO T 342 standard using an asphalt mixture performance tester (AMPT) machine [22]. This test was used to characterize the linear viscoelastic properties (dynamic modulus and phase angle) of a given asphalt mixture, which are critical inputs in Chapter 6 of this dissertation work focused on predictive modeling of AC overlay sections. It is important to note that all samples are tested at 7% target air void per AASHTO T 342 standard, regardless of their design air void level. Specimens were fabricated to 150 mm tall by 100 mm diameter cylindrical samples, with three replicates tested per mixture type. Testing was conducted at three different temperatures (4.4, 21.1 and 37.8˚C) and six different loading frequencies (25, 10, 5, 1, 0.5 and 0.1 Hz) using a sinusoidal compression load wave form. Figure 4-1 provides an example of the dynamic modulus specimen test set up in the AMPT and test results.

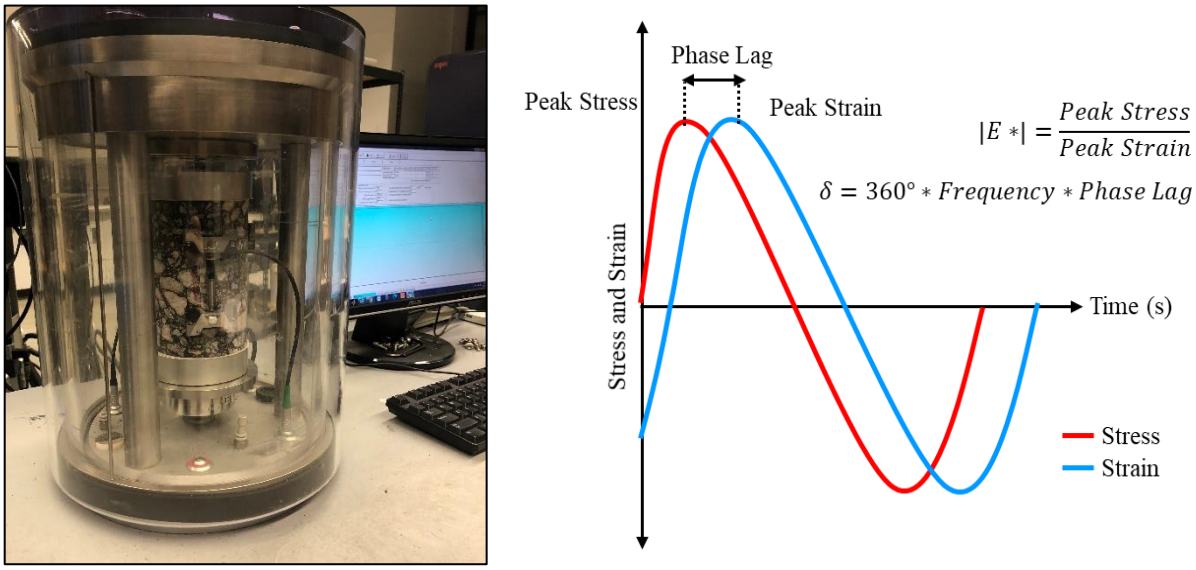

Figure 4-1 Dynamic modulus specimen test set up in AMPT (left), and example test result (right).

4.2.1 Dynamic Modulus |E|*

Dynamic modulus |E*|, which is a fundamental material property, is simply the ratio of stress to strain under oscillatory loading conditions (Equation 1).

$$|E^*| \frac{Peak\ Stress}{Peak\ Strain} \qquad \text{Eqn. 1}$$

Constructing a dynamic modulus master-curve using appropriate time-temperature superposition principle shift factors, provides useful information regarding the relative stiffness and rutting susceptibility of one mixture compared to another. Dynamic modulus results are presented in Figure 4-2. Generally, mixtures with higher stiffness and relatively flatter master-curves may be more prone to cracking.

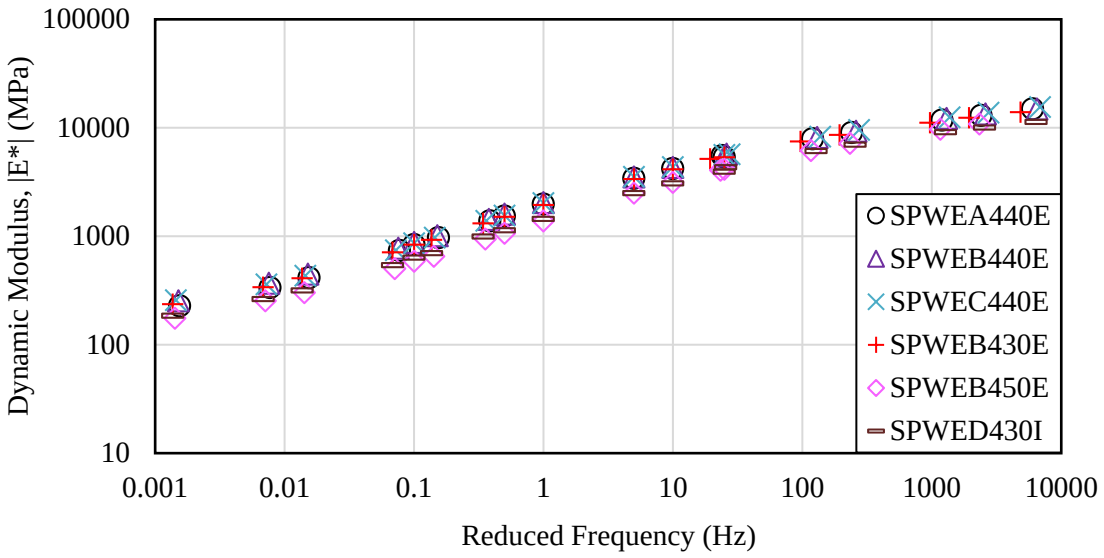

Figure 4-2 Dynamic modulus master curve at a reference temperature of 21.1°C.

It can be observed that as the design air void level increases from 3% to 5%, stiffness decreases (SPWEB430E > SPWEB440E > SPWEB450E). The SPWEB450E mixture exhibits the lowest overall stiffness behavior, denoted by the pink diamond markers. It can also be noted that as NMAS size increases (4.75 mm < 9.5 mm <12.5 mm < 19 mm), stiffness of the asphalt material increases.

4.2.2 Phase Angle (δ)

Phase angle (δ) can be calculated from dynamic modulus testing data using Equation 2.

$$\delta = 360° * t * \omega \qquad \text{Eqn. 2}$$

Where:

δ = phase angle

t = time lag between stress and strain peaks

ω = loading frequency in Hz

The phase angle master curve provides insight on the relative proportion of viscous and elastic behavior of asphalt mixtures at a given temperature and frequency. In general, a higher phase angle means more viscous behavior corresponding to better cracking performance, while lower phase angle (more elastic behavior) may indicate cracking susceptibility. The phase angle for all mixtures is shown in Figure 4-3. Comparing the 12.5 mm mixtures with varying air void designs, SPWEB450E mixture had the highest phase angle while SPWEB430E had the lowest phase angle.

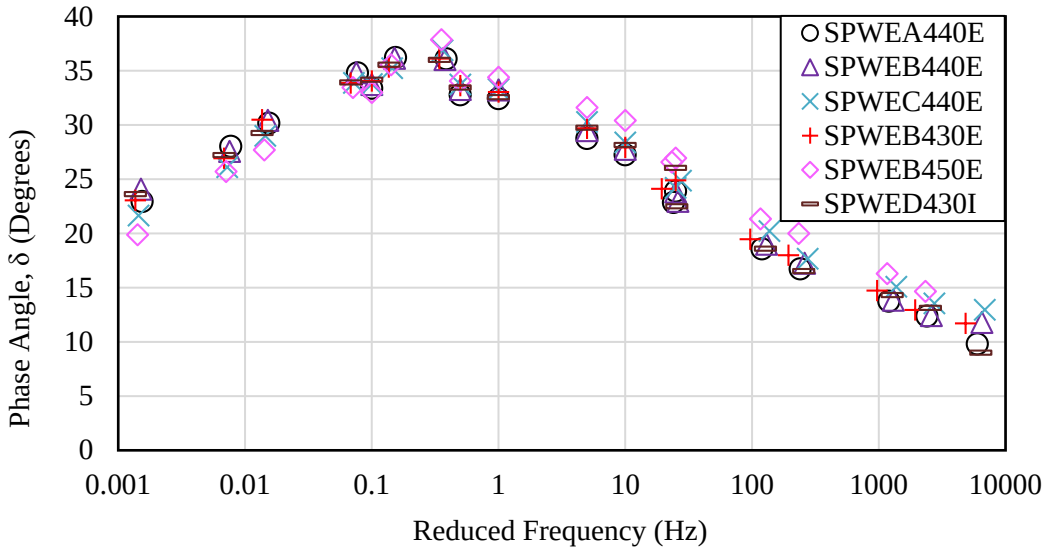

Figure 4-3 Phase angle master curve.

4.2.3 Black Space

Black space, which cross plots dynamic modulus with phase angle, provides another means of visualizing the rheological behavior of a given mixture while eliminating frequency. Mixture cracking resistance is affected by both stiffness and relaxation capabilities as indicated by dynamic modulus and phase angle respectively. Therefore, mixtures which exhibit higher relaxation capability (higher phase angle) with lower stiffness may result in better cracking resistance behavior. Trends in mixture performance in black space (Figure 4-4) are consistent with dynamic

modulus and phase angle master curves. For example, interlayer mixture SPWED430I, exhibits higher phase angle while maintaining relatively lower stiffness compared to other mixtures.

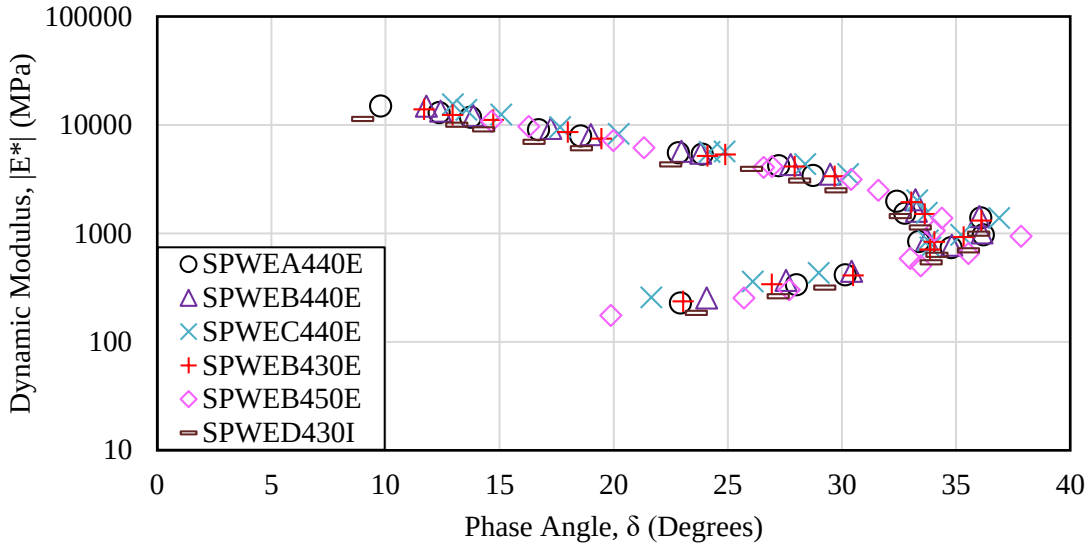

Figure 4-4 Black space diagram.

4.3 Direct Tension Cyclic Fatigue Test

In this study, uniaxial fatigue testing was performed in accordance with AASHTO TP 107 using an asphalt mixture performance tester (AMPT) machine [23]. Specimens were prepared to a height of 130 mm and diameter of 100 mm. Three replicates were tested at a mixture specific test temperature determined by Equation 3 for the corresponding asphalt binder performance grade (PG).

$$Test\ Temperature = \frac{(PGHT+PGLT)}{2} - 3 \qquad \text{Eqn.3}$$

Where:

PGHT = binder performance grade high temperature

PGLT = binder performance grade low temperature

A sinusoidal tensile load is applied at a frequency of 10 Hz in a crosshead-controlled mode until failure using the AMPT. Replicates are tested at varying strain levels to get a range of number

of cycles to failure (N_f). Failure is defined as the cycle where a sudden decrease can be observed in phase angle during continued loading. This typically corresponds to when a macro-crack develops. Figure 4-5 shows an example of the direct tension cyclic fatigue (DTCF) test set-up and results.

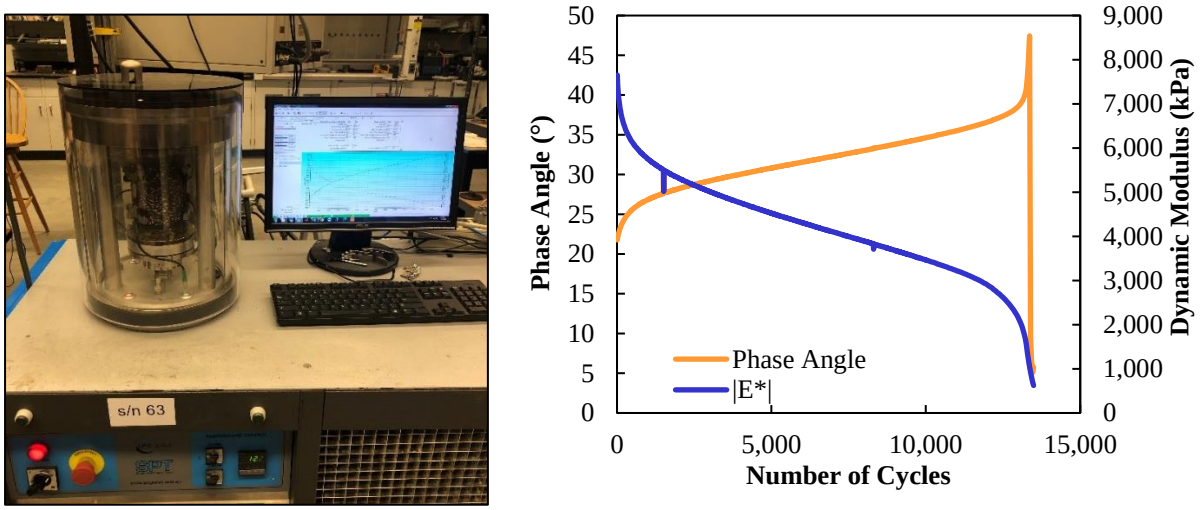

Figure 4-5 Direct tension cyclic fatigue test set up in AMPT (left, and example of test result (right).

The Simplified Viscoelastic Continuum Damage (S-VECD) approach developed by Underwood et al. (2012) was used to analyze the damage characteristics from results obtained during DTCF and dynamic modulus tests [24]. Damage characteristic curves are developed by calculating the secant pseudo-stiffness (C) and the damage parameter (S) at each cycle of loading. These values are cross-plotted to form the damage characteristic curve (DCC) and fitted using Equation 4. An example of a DCC for SPWEA440E mixture is shown in Figure 4-6.

$$C = 1 - C_{11} * S^{C_{12}} \quad \text{Eqn. 4}$$

Where:

C = secant pseudo-stiffness

S = damage parameter

C_{11} and C_{12} = fitting coefficients for the power law form

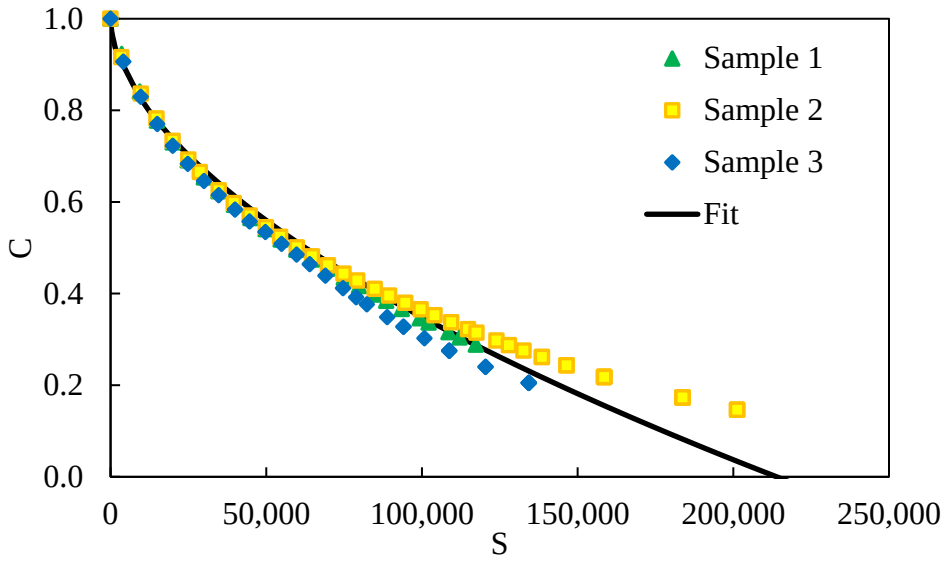

Figure 4-6 Damage characteristic curve for SPWA440E mixture.

A direct comparison between asphalt mixtures using the DCC may not be appropriate because the number of cycles to failure is missing between curves. As a result, three different cracking indices (D^R,$G^R$and S_{app}) were employed to investigate the fatigue properties of asphalt mixtures in this study. In the following subsections, a brief description of each fatigue criterion is provided followed by the results for asphalt mixtures included in this study.

4.3.1 D^R Fatigue Criteria

D^R is defined as the amount of average drop in material integrity $(1 - C)$, per load cycle until failure. D^R fatigue criteria values can be determined using Equation 5 and typically ranges from 0.3 to 0.8. Mixtures with a higher D^R value would be expected to have better fatigue resistance [25].

$$D^R = \frac{\int_0^{N_f}(1-C)dN}{N_f} \qquad \text{Eqn. 5}$$

Where:

$\int_0^{N_f}(1-C)dN$ = accumulated decrease in pseudo stiffness

N_f = number of loading cycles to failure

C = secant pseudo stiffness

Figure 4-7 summarizes the D^R fatigue failure criterion results for six different asphalt mixtures. The best performing mixture was the regressed air void (SPWEB430E) mixture, while the worst performing mixture was the 4.75 mm NMAS interlayer mixture (SPWED430I).

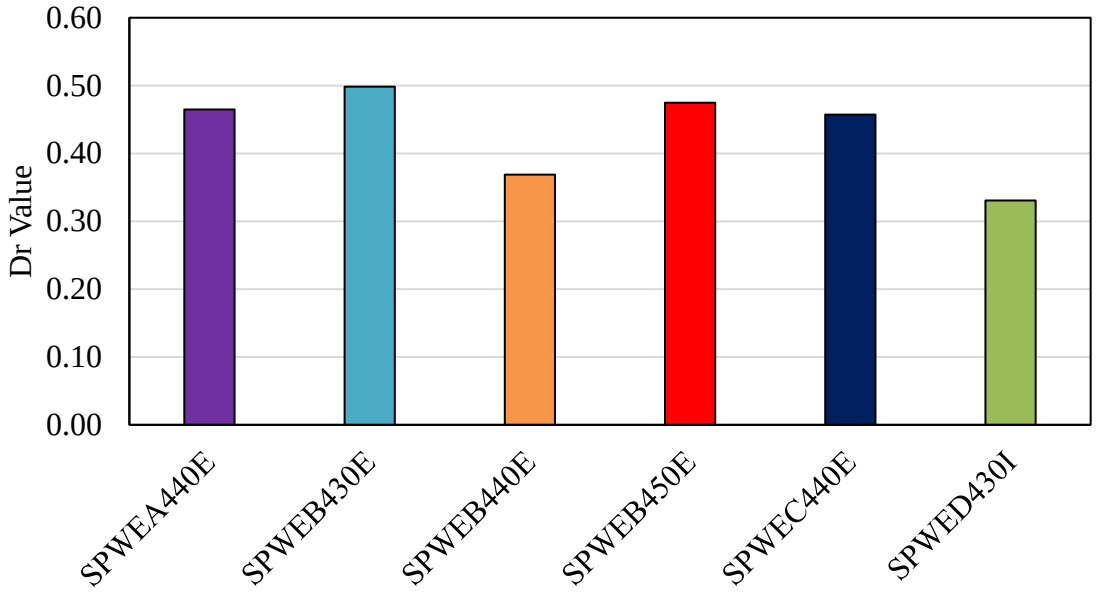

Figure 4-7 D^R fatigue failure criterion results.

4.3.2 G^R Fatigue Criteria

G^R is the rate of change of the averaged released pseudo strain energy throughout the entire loading history until failure. This fatigue criteria indicates the decrease in a mixture's energy storage capacity due to each loading cycle [26]. G^R can be calculated using Equation 6.

$$G^R = \frac{\int_0^{N_f} w_C^R}{N_f^2} \qquad \text{Eqn. 6}$$

Where:

w_c^R = total released pseudo strain energy

N_f = number of loading cycles to failure

Typically, the number of cycles to failure at G^R equal to 100 ($N_f @\ G^R = 100$) is used to rank mixtures as shown in Figure 4-8, with higher values indicating better fatigue performance. The ranking of asphalt mixtures based on $N_f @\ G^R = 100$ fatigue failure criterion is different than that of D^R. For example, SPWEB430E mixture is ranked as the best performing according to D^R, however with respect to $N_f @\ G^R = 100$ criterion the best performing mixture is SPWEA440E.

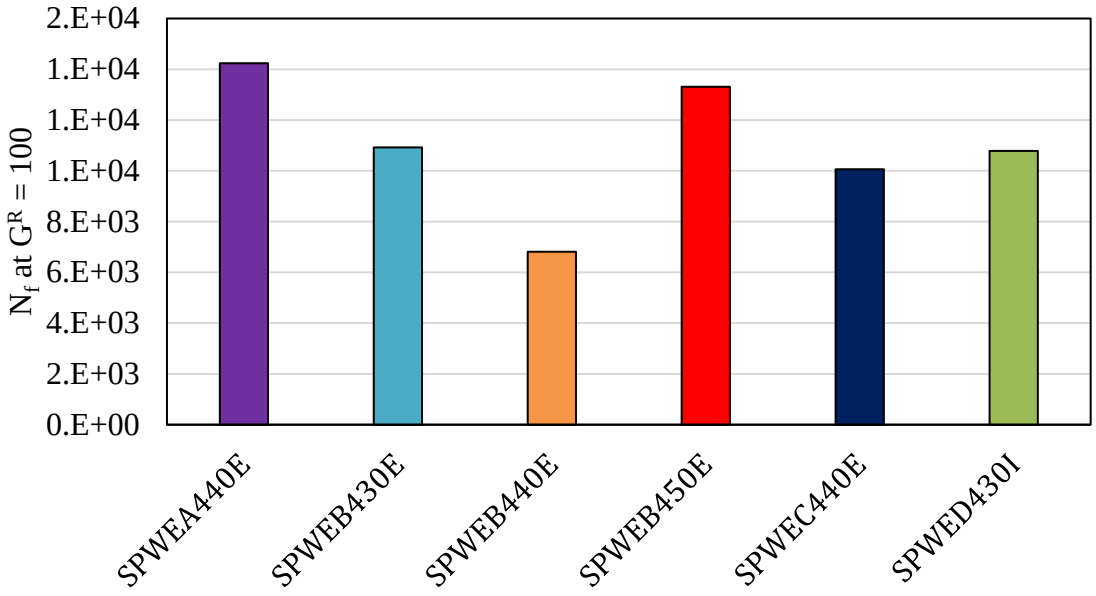

Figure 4-8 N_f at G^R = 100 fatigue failure criterion results.

4.3.3 S_{app} Fatigue Criteria

The last fatigue cracking criteria used to evaluate asphalt mixture fatigue properties was S_{app}, also referred to as the damage capacity at a given temperature. S_{app} can be calculated using Equation 7 and in general, higher S_{app} values are desirable [27].

$$S_{app} = \frac{\left(\frac{\frac{c_{12}}{a_T^{\alpha+1}}}{c_{11}} D^R\right)^{\frac{1}{c_{12}}}}{10{,}000}$$ Eqn. 7

Where:

C_{11} and C_{12} = fitting coefficients for damage characteristic curve

a_T = shift factor

α = fitting coefficient calculated from the relaxation spectrum

D^R = average drop in pseudo stiffness

Figure 4-9 presents S_{app} fatigue failure criterion results for all mixtures. Once again, the ranking of mixture performance varies slightly when compared to D^R or $N_f @\ G^R = 100$ ranking. Both S_{app} and $N_f @\ G^R = 100$ failure criterion rank SPWEA440E mixture as the best performer and SPWEB440E as the worst performer. However, the D^R failure criterion identified SPWEB430E as the best performer and SPWED430I was the worst performer.

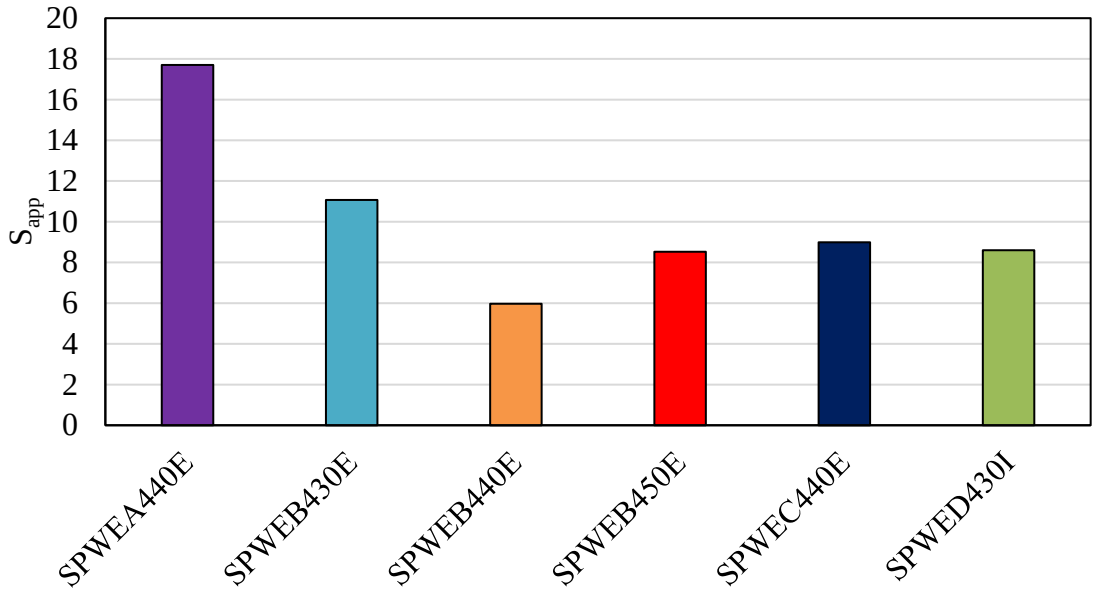

Figure 4-9 S_{app} fatigue failure criterion results.

4.4 Overlay Tester (OT)

The Texas overlay tester (OT) has been proposed as a test method to determine the susceptibility of asphalt mixtures to fatigue or reflective cracking. In this study, OT was performed by Illinois Department of Transportation (IDOT), following the TX-248-F procedure [28]. An example of the overlay test set up and specimen dimensions is shown in Figure 4-10. OT set up consists of two steel plates, one fixed and the other able to move horizontally to simulate the opening and closing of joints or cracks in the underlying pavements beneath an AC overlay. The standard test temperature is 25°C. The test is conducted on specimens 3 inches wide, 6 inches long, and 1.5 inches thick in a controlled displacement mode at a repeated loading rate of one cycle per 10 sec. (5 sec. of loading and 5 sec. of unloading) with a maximum horizontal displacement of 0.025 inches.

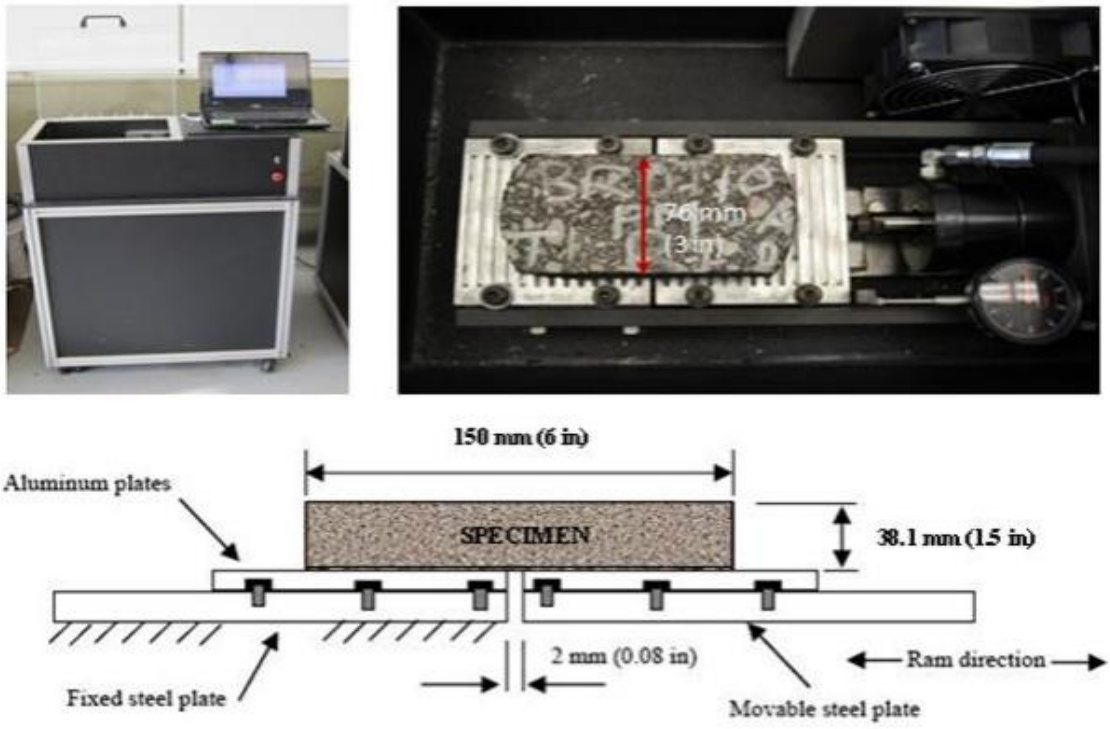

Figure 4-10 Example of overlay tester schematic and specimen dimensions [29].

There are several different ways to analyze OT results, including the most commonly used load reduction as a function of load cycles applied, load reduction at 1000 cycles, and the number of cycles it takes to achieve 93% load reduction (failure). In terms of cracking performance, the higher the number of cycles to achieve failure the better expected cracking resistance. When comparing load reduction at 1000 cycles (single point), lower load reduction is preferred for better cracking resistance performance.

A study conducted for the Texas Department of Transportation explored alternative parameter indices such as, maximum load during first cycle, displacement at maximum load, initial slope, displacement at zero load and energy-based analysis methods to characterize the cracking potential of AC mixtures [30]. The motivation behind exploring these alternative parameters was due to an observation of high variability of the number of cycles to failure, which may linked to the capacity of typical load cells (5000 lbs or 1000 lbs) used in OT devices. As a result, "The precision of the load cell may introduce a considerable level of variability to consistently compute the number of cycles to failure using the current failure criterion" [30].

In this dissertation work however, the percent load reduction at 1000 cycles, and the number of cycles to failure (93% failure criterion) were primarily used to characterize AC mixtures cracking performance from the OT results. In the following subsections, results are presented for the six AC mixtures. An idea for future work may be to expand the data analysis of OT results to consider energy based performance indices and compare results to field performance of test sections.

4.4.1 Load Reduction

Figure 4-11 shows load reduction as a percentage with respect to the number of loading cycles applied for six asphalt mixtures. For each mixture, five replicates were tested and averaged.

It can be observed from this plot that SPWED430I has the lowest load reduction (better performance), while SPWEB440E has the highest load reduction after only approximately 1600 cycles.

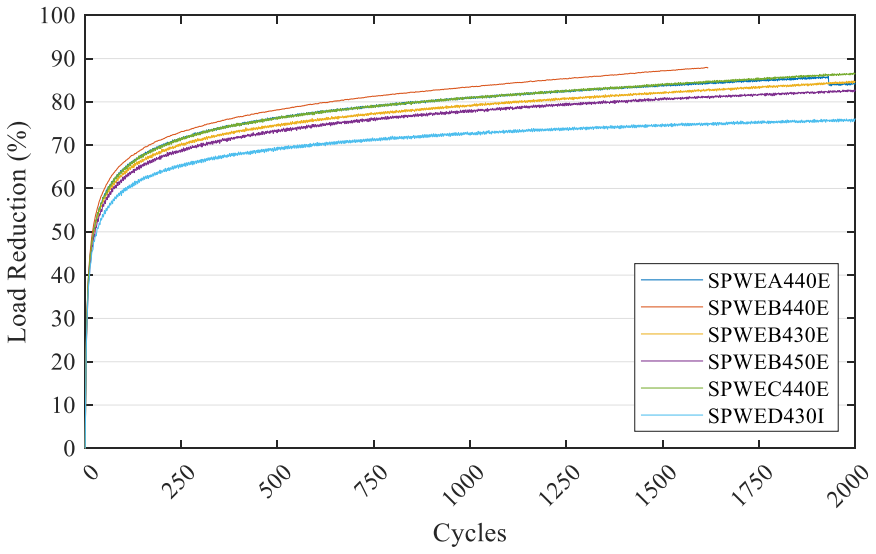

Figure 4-11: Load reduction for all mixtures from overlay tester.

Percent load reduction at 1000 cycles from Figure 4-11 was selected as a comparison point among the six mixtures and is shown in Figure 4-12. Results at the single point comparison point agree with the general trend in ranking of mixtures with SPWED430I ranked as the best performer and SPWEB440E as the worst performer.

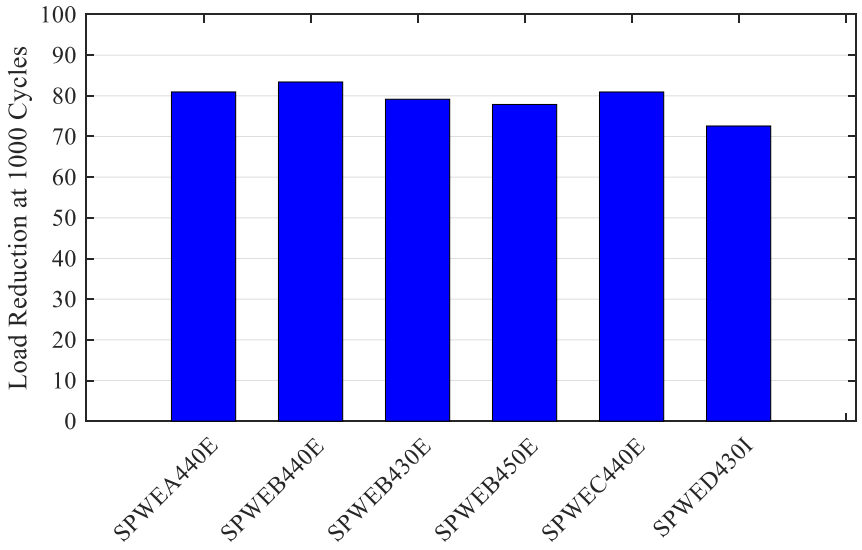

Figure 4-12 Overlay tester results at 1000 cycles.

4.4.2 Cycles to Failure

The number of cycles at 93% load reduction (test failure point), is represented in Figure 4-13. It is more evident in this plot that from OT results, SPWED430I is expected to have better resistance to fatigue or reflective cracking. The five remaining mixtures had relatively comparable failure points, with SPWEB440E having the lowest number of cycles to achieve 93% load reduction.

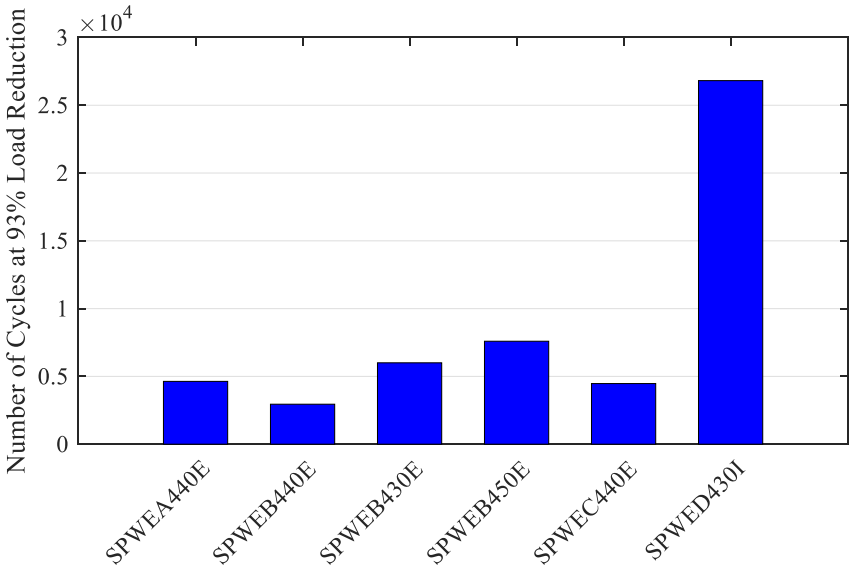

Figure 4-13 Overlay tester results at 93% load reduction.

4.5 Semi-Circular Bend (SCB) Test

Semi-circular bend (SCB) testing was conducted following AASHTO TP 124 by IDOT [31]. From this test, the flexibility index, cracking rate index (CRI) and a rate dependent cracking performance index (RDCI) were calculated. An example of the SCB test set up and commonly plotted load versus displacement data highlighting a few of the key feature on the curve is shown in Figure 4-14.

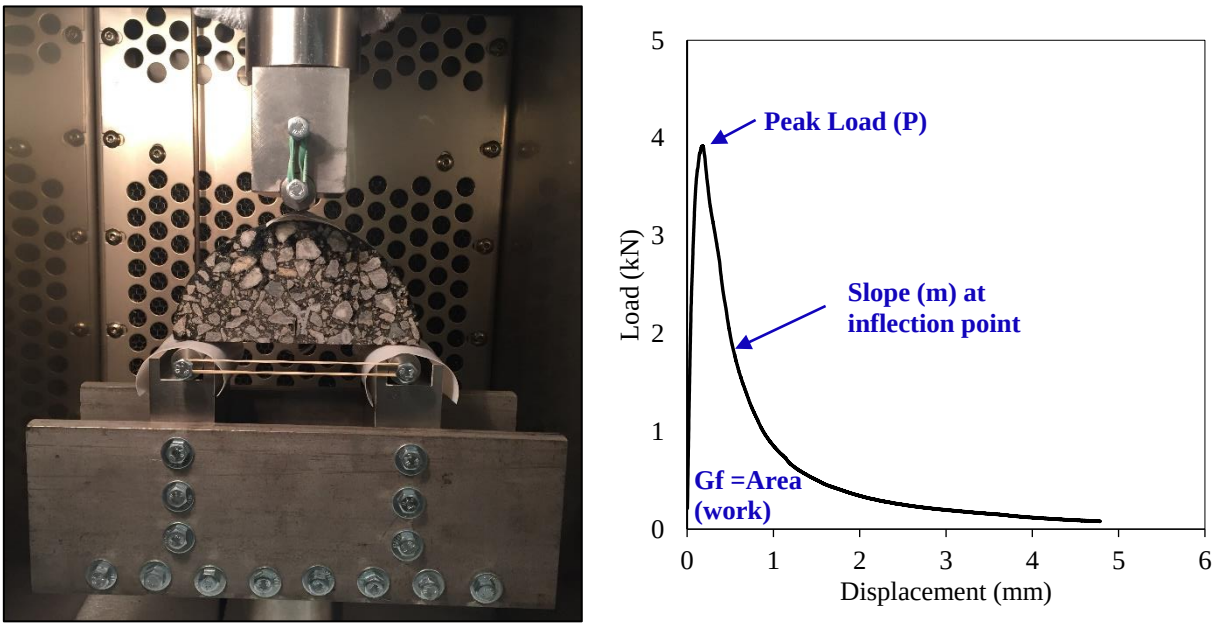

Figure 4-14 Example of semi-circular bend test set up (left) and load versus displacement curve (right)

4.5.1 Flexibility index (FI)

The flexibility index (FI) was developed to correlate the crack growth velocity and the brittleness of a given mixture [32]. Higher FI values are desirable for asphalt mixtures, as it may indicate better crack resistant mixtures. FI may be calculated using Equation 8.

$$FI = A * \frac{G_f}{abs(m)} \quad \text{Eqn. 8}$$

Where:

A = unit correction coefficient (0.01)

G_f = fracture energy (J/m^2)

m = slope at the post-peak inflection point

Figure 4-15 shows that all mixtures had a relatively high FI average value, exceeding the recommend threshold value of eight. Error bars represent one standard deviation. It is not

surprising that SPWED430I had the highest FI value (26.4), since it is a NMAS 4.75 mm mixture with 8.2% asphalt content and designed to be a stress absorbing interlayer mixture.

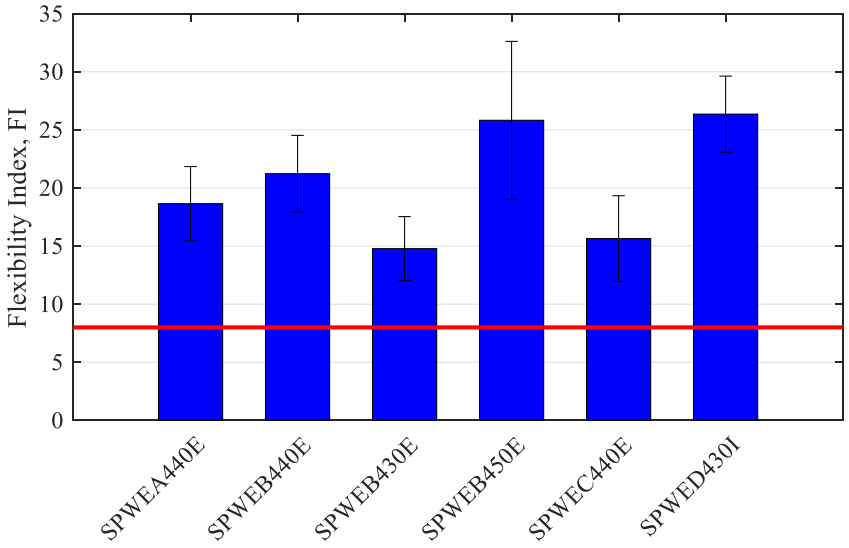

Figure 4-15 Flexibility index from semi-circular bend testing.

4.5.2 Cracking Rate Index (CRI)

Another common performance index used to distinguish cracking resistance is the cracking rate index (CRI) [33]. A higher CRI value is desirable for better crack resistance performance. Rather than using the slope at the post-peak inflection point, the peak load (P_{max}) is used to normalize G_f. CRI can be calculated using Equation 9.

$$CRI = \frac{G_f}{abs(P_{max})} \quad \text{Eqn. 9}$$

Where:

G_f = fracture energy (J/m^2)

P_{max} = maximum load (kN)

Figure 4-16 presents the average CRI results with error bars representing one standard deviation. CRI results agree with the ranking of mixtures using FI.

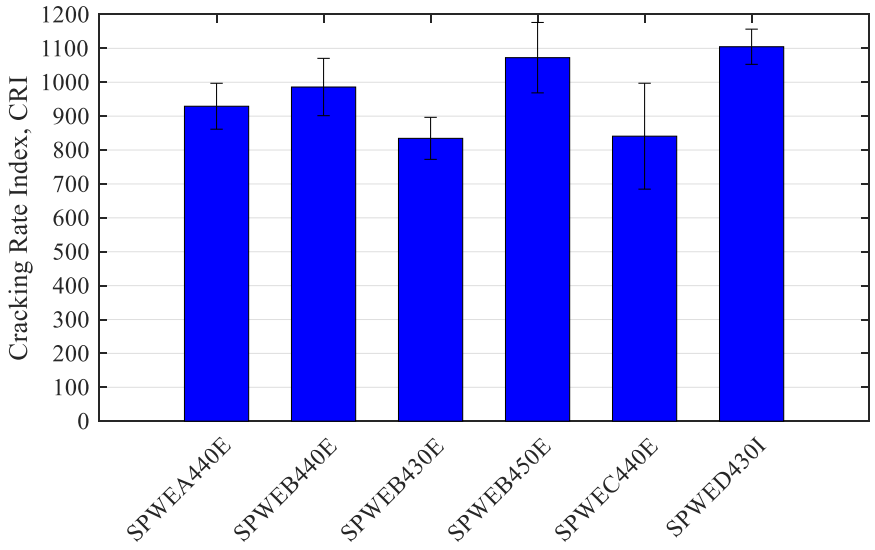

Figure 4-16 Cracking rate index results from semi-circular bend testing.

4.5.3 Rate-Dependent Cracking Index (RDCI)

A rate-dependent cracking index was proposed by Nemati et al. (2019), which utilizes cumulative fracture work potential and instantaneous power calculated from I-FIT results to assess the impulse of the mixture [34]. Analogous to FI which evaluates the fracture energy and crack velocity, RDCI follows a similar process but does so in a rate-dependent manner. By using the cumulative work over time it exhibits the history of the dissipated work during the crack growth phase and can be used to indicate the crack resistance rate at any time during the loading period. The rate of work over time ($\Delta W/\Delta t$) is defined as power (P). Considering a small range of time, such that when Δt approaches 0, it can be reasonably assumed that power is the rate of the work with respect to time (i.e $\Delta W/\Delta t \approx dW/dt$). Typically, this slope is referred to as the instantaneous power (P_t), which can be considered a scalar quantity indicating the instantaneous energy dissipation rate as shown in Equation 10 and simplified to Equation 11.

$$P_t = \frac{dW}{dt} = \boldsymbol{F}\frac{dx}{dt}; \frac{dx}{dt} = \boldsymbol{V} \qquad \text{Eqn. 10}$$

$$P_t = \boldsymbol{F} \cdot \boldsymbol{V}$$ Eqn. 11

Equation 12 can be used to calculate RDCI where $\int_{t_{peak}}^{t_{0.1peak}} W_c \ .dt$ is the post peak area under the cumulative work vs time curve (Figure 4-17), P_{tpeak} is the instantaneous power at peak force, C is a unit correction factor set to 0.01, and the ligament area is the product of specimen thickness and ligament length.

$$RDCI = \frac{\int_{t_{peak}}^{t_{0.1peak}} W_c \ .dt}{P_{tpeak} \times ligament\ area} \times C$$ Eqn. 12

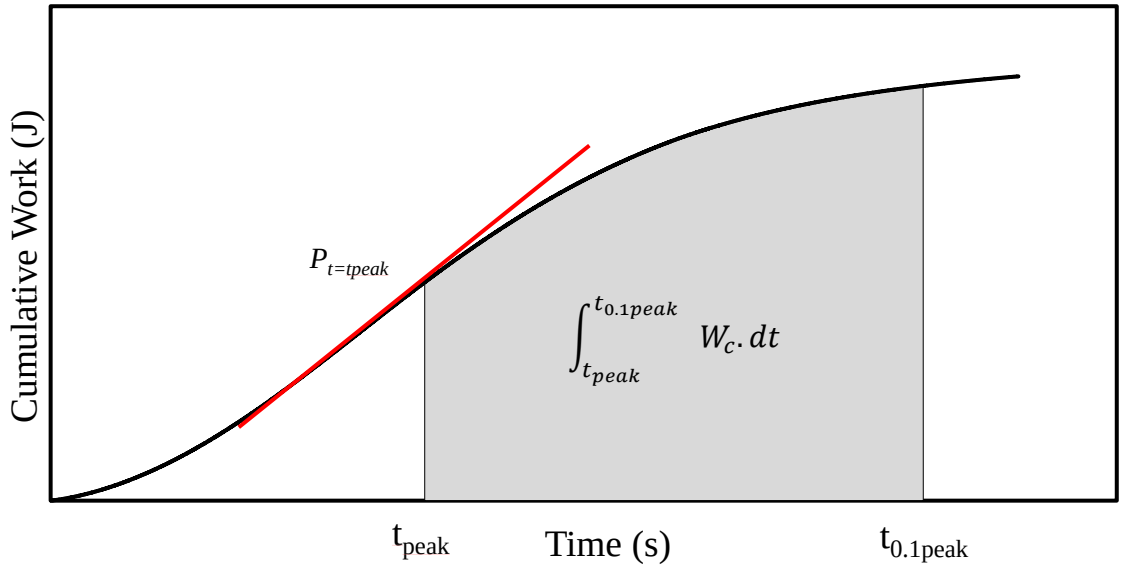

Figure 4-17 Example of the determination of cumulative work between time at peak load and 0.1 of peak load.

Figure 4-18 summarizes the average RDCI results with one standard deviation error bars. Overall the ranking of mixtures for RDCI is consistent with that of FI and CRI.

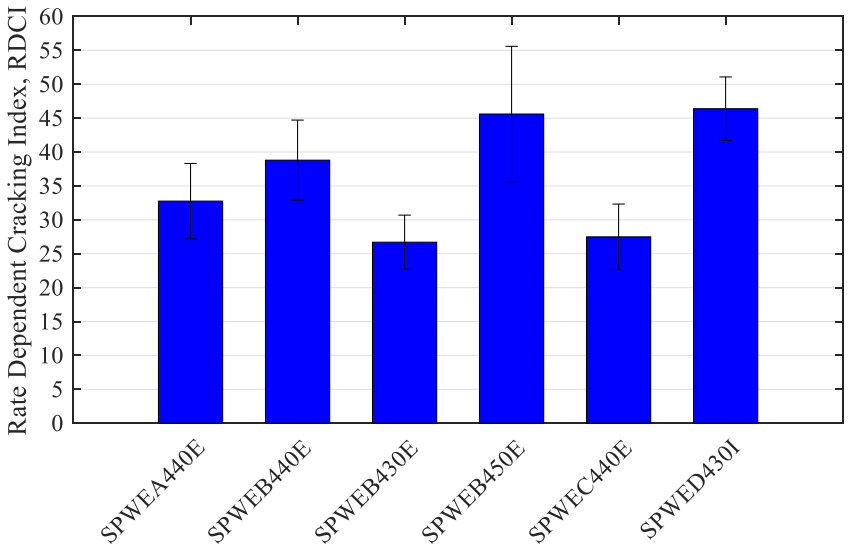

Figure 4-18 Rate-dependent cracking index results from semi-circular bend testing.

4.6 Disk-shaped Compact Tension (DCT) Test

Disk-shaped compact tension (DCT) testing was performed following MnDOT modified procedure for ASTM D7313 [35]. Testing was conducted by the MnDOT Office of Materials and Road Research for six of the study mixtures, with 12 replicates tested per mixture type. The average fracture energy (G_f), fracture strain tolerance (FST) and rate-dependent cracking index (RDCI) performance indices were determined for all asphalt mixtures included in this study except for UTBWC. Evaluation of cracking resistance of UTBWC was determined using the compact tension (CT) test rather than the DCT test due to its unique mixture design and is discussed in the section 4.7. An example of the DCT test set up and typical output in terms of a load versus crack mouth opening curve (CMOD) is shown in Figure 4-19.

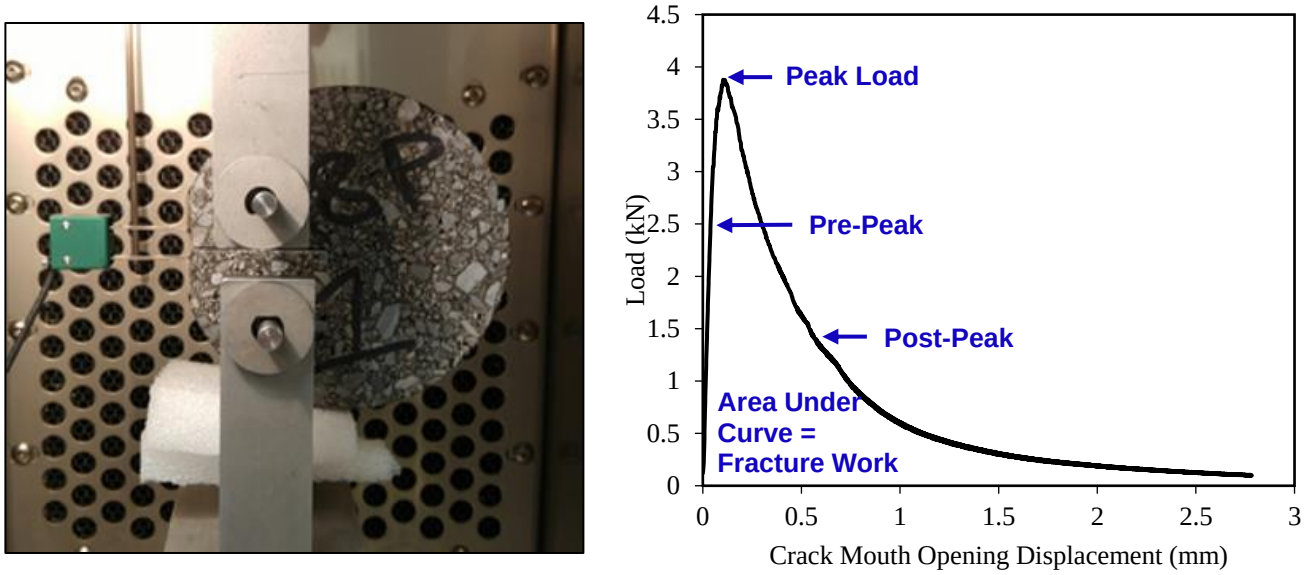

Figure 4-19 Disk-shaped compact tension test set up (left) and typical load versus crack mouth opening displacement curve (right).

4.6.1 Fracture Energy (G_f)

G_f is defined as the amount of fracture work required to generate a unit cracked surface area and can be calculated using Equation 13.

$$G_f = \frac{AREA}{B*(W-a)} \quad \text{Eqn. 13}$$

Where:

G_f = fracture energy (J/m^2)

$AREA$ = area under load vs crack mouth opening displacement curve

B = specimen thickness (m)

$W - a$ = initial ligament length (m)

G_f results are presented in Figure 4-20 with error bars representing one standard deviation. All mixtures are above the typical mix design cracking threshold of 400 J/m^2 as denoted by the

solid red line. SPWED430I mixture had the highest G_f with a value of 572 J/m^2 while SPWEA440E mixture had the lowest value of G_f at 449 J/m^2.

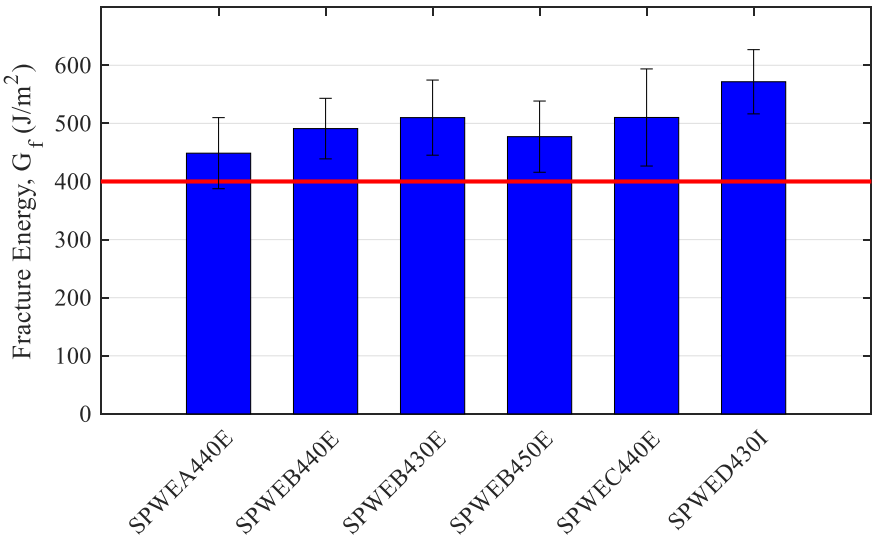

Figure 4-20 Average fracture energy results from disk-shaped compact tension testing.

4.6.2 Fracture Strain Tolerance (FST)

Fracture strain tolerance (FST) is another common index parameter that can be determined from DCT testing [36]. FST normalizes fracture energy (G_f) by fracture strength (S_f) as shown in Equation 14.

$$FST = \frac{G_f}{S_f} \quad \text{Eqn. 14}$$

S_f is defined in Equation 15, where (P_{max}) represents the maximum load, (w) is the specimen width, and (a) is the ligament length.

$$S_f = \frac{2P_{max}(2w+a)}{b(w-a)^2} \quad \text{Eqn. 15}$$

Figure 4-21 summarizes the average FST results for all six mixtures. Again, error bars represent one standard deviation. The asphalt mixtures all yielded comparable ranking where the

mixture with the highest FST value was SPWEB450E at a value of 7.36×10^{-6} m and the lowest mixture was SPWEA440E with a value of 6.15×10^{-6} m.

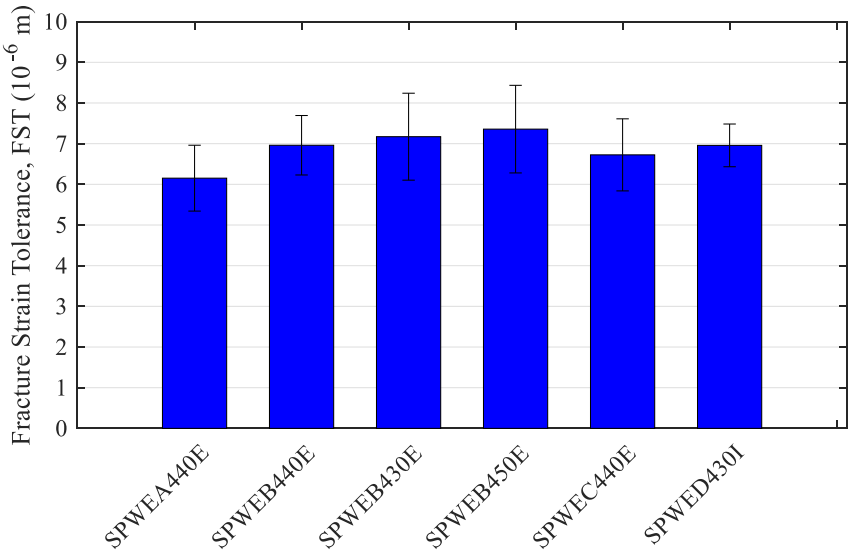

Figure 4-21 Average fracture strain tolerance results from disk-shaped compact tension testing.

4.6.3 Rate-Dependent Cracking Index (RDCI)

While RDCI was originally developed for SCB specimen geometry, in this dissertation study it was also calculated using DCT testing results to compare the ranking of asphalt mixtures using different fracture testing geometries. Both RDCI results from SCB and DCT testing indicate SPWEB450E has a higher cracking resistance. However, the overall ranking of asphalt mixtures varies when RDCI is calculated using SCB versus DCT testing results. For example, SCB results presented in Figure 4-18 indicates that SPWEB430E is the worst performing mixture, followed by SPWEC440E. Based on DCT results in Figure 4-22, SPWEB430E is the next best performing mixture. It should be noted, that the coefficient of variability (COV) increased when calculating RDCI from DCT testing results. The COV from SCB results was approximately 16%, meanwhile for the DCT results on the same asphalt mixtures COV was calculated as 29%.

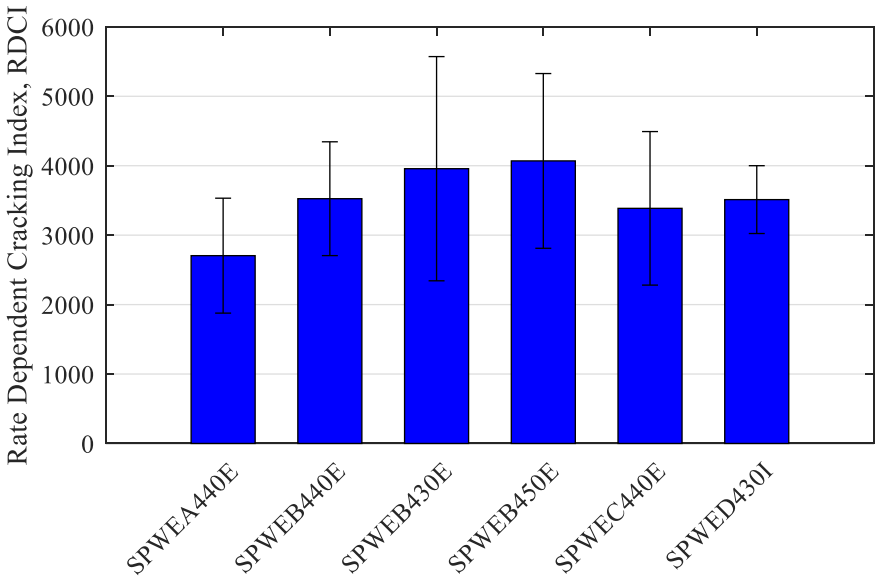

Figure 4-22 Rate-dependent cracking index results from disk-shaped compact tension testing.

4.7 Compact Tension (CT)

Many researchers such as Wagoner et al. (2005a) and (2005b), Li et al. (2006) and Song et al. (2008), have established that a fracture energy based approach for characterization of cracking performance for a quasi-brittle materials at low temperatures is more appropriate than using a linear elastic fracture mechanics approach [37]-[40]. There are many fracture tests developed to evaluate the cracking performance of mixtures such as indirect tension test, four-point bending beam, thermal stress restrained specimen test, disk-shaped compact tension, and semi-circular bend. However, these tests pose a challenge in representing similar sample geometries, thicknesses and use of tack coat in construction of pavement test sections. The direction of crack propagation from these commonly used fracture test varies compared to that observed from reflective cracking. Figure 4-23 illustrates the comparison of required geometry thickness for DCT and compact tension (CT) specimens and their respective direction of crack propagation.

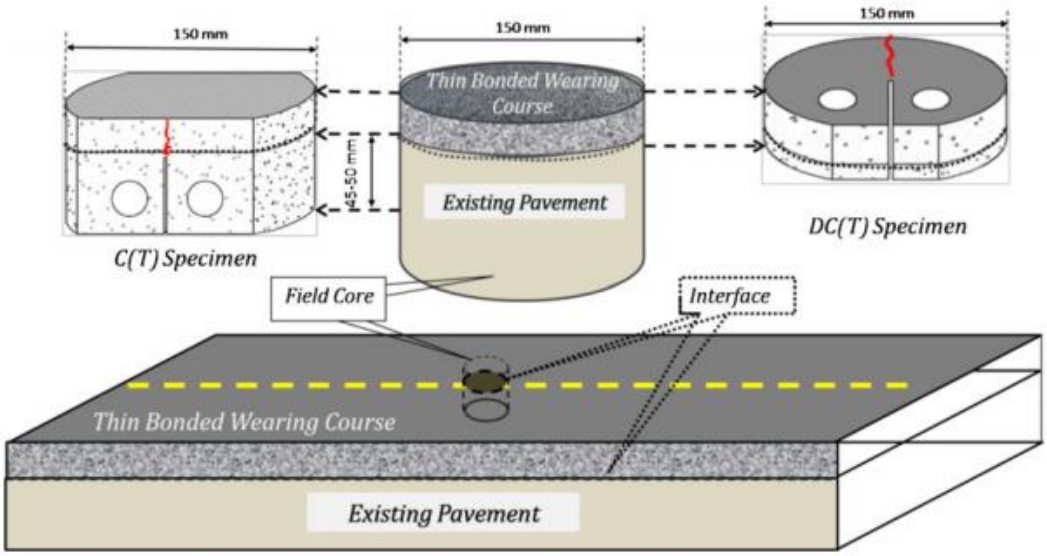

Figure 4-23 Comparison of DCT and CT specimen crack propagation orientation with respect to the pavement structure [41].

The CT specimen geometry is shown in Figure 4-24, and it should be noted that the CT test is run using a constant rate CMOD of 0.017 mm/s, similar to that to the DCT test [38].

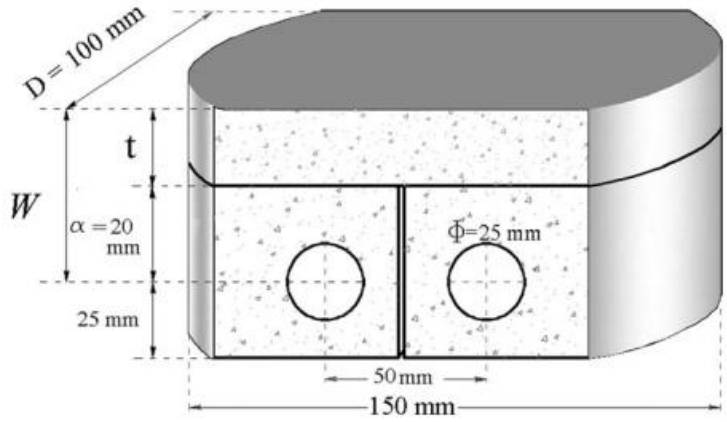

Figure 4-24 Compact tension specimen geometry and dimensions [41].

CT fracture testing was employed in this dissertation work to evaluate the fracture resistance of the UTBWC (0.75-inch thickness) asphalt mixtures included in MnROAD test section Cell 995. Figure 4-25 shows an example of the CT test set up within the MTS loading frame at UNH and a fracture specimen after testing.

Figure 4-25 Compact tension test set up (left) and fractured specimen (right).

Meanwhile, Figure 4-26 summarizes the load vs CMOD curves for the four replicates. It was determined that the average peak load was 1.27 kN and the average G_f was 518 J/m^2 for the UTBWC. The completion of CT testing was significant as it provided necessary material property and damage characteristic inputs for finite element modeling of Cell 995, which discussed further in Chapter 6.

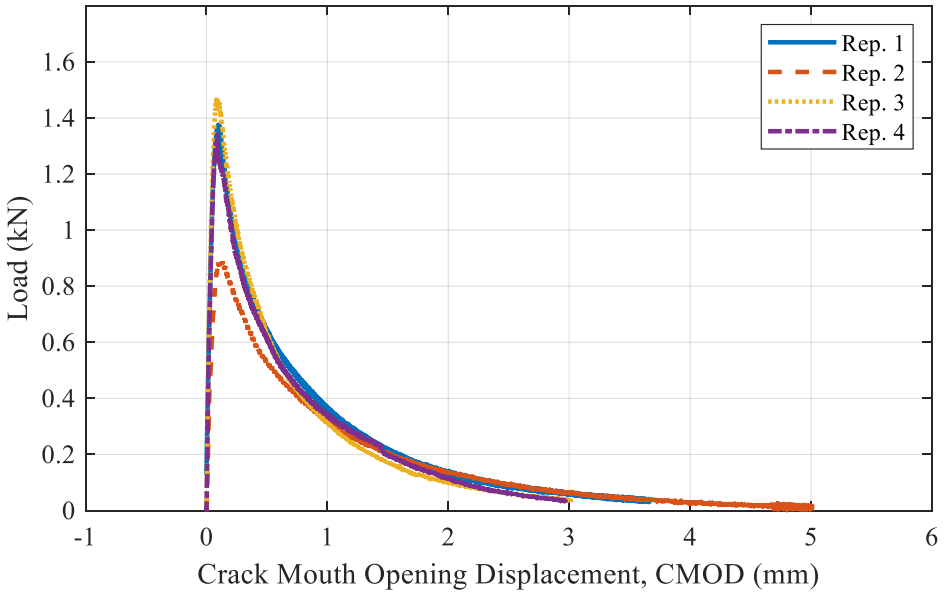

Figure 4-26 Load-CMOD curves from compact tension testing.

4.8 Paper 1 - Assessment of Asphalt Mixture Disk-Shaped Compact Tension Test Indices for Reflective Cracking Performance

This paper directly contributes the first objective of this dissertation work focused on evaluating the suitability of different reflective cracking performance measures for asphalt mixtures using laboratory results. In this paper, cracking performance indices derived from DCT testing are compared to reflective cracking field performance of 10 MnROAD overlay test sections. Furthermore, an equivalent index approach is presented in this paper in order to make comparisons of field test sections that are comprised of multiple lifts (varying thicknesses and asphalt mixture combinations). The abstract of the paper accepted for publication in the journal of testing and evaluation is included below while a full version of the paper may be reviewed in Appendix A.1

4.8.1 Paper 1 Abstract

Disk-shaped compact tension (DCT) testing is a commonly used low temperature fracture test to determine the cracking resistance of asphalt mixtures. The current testing specification only considers the fracture energy (G_f) from load-crack mouth opening displacement (CMOD) test data. However, G_f does not directly take into consideration the behavior of the post peak region of the curve, which may indicate the mixture's ability to resist crack propagation and provide insight into fracture processes (e.g., crack growth velocity). It is possible to have two DCT specimens with similar G_f values but dramatically different load-displacement responses. The main focus of this paper is to make a comparative evaluation of various performance indices developed for DCT fracture testing with respect to field reflective cracking performance of 10 full-scale asphalt concrete (AC) overlay test sections. This study evaluates G_f in addition to three other indices; fracture strain tolerance (FST), rate-dependent cracking index (RDCI) and a proposed DCT_{Index} from Minnesota Department of Transportation (MnDOT), that consider the post-peak load-displacement behavior. An equivalent performance index approach is adopted to make comparisons of test sections with varying overlay structures in terms of thickness and material properties. Results from this study showed there was relatively good agreement between all equivalent laboratory performance indices in identifying the best and worst performing overlay sections according to normalized field performance indices after approximately 3 years of service. In general, the equivalent FST and RDCI laboratory indices rank test sections similarly, while equivalent G_f and DCT_{Index} have comparable ranking.

4.9 Chapter Summary

This chapter presented laboratory performance test results from complex modulus, DTCF, OT, SCB, DCT and CT testing. It was observed from complex modulus testing that as the design

air void level increases from 3% to 5%, stiffness decreases (SPWEB430E > SPWEB440E > SPWEB450E). The SPWEB450E mixture exhibits the lowest overall stiffness behavior. Meanwhile, testing results from OT, SCB and DCT indicate that the binder rich reflective cracking interlayer mixture (SPWED430I) had superior performance compared to other mixtures included in this study. CT testing was conducted on the UTBWC mixture in order to characterize its cracking resistance. Laboratory mixture characterization results presented in this chapter provide necessary material property inputs for the development of predictive models (thermo-viscoelastic material behavior with cohesive zone fracture model) that are discussed further in Chapter 6.

5. CHAPTER 5

FIELD PERFORMANCE DATA ANALYSIS

5.1 Chapter Introduction

This chapter consists of a summary of field performance testing and monitoring performed on MnROAD asphalt concrete overlay test sections included within this dissertation study (Cells 984-995). Two field performance indices are presented that may be used to quantitatively compare reflective cracking performance of field sections while taking into account the rate of cracking, onset of cracking (early versus later) in overlay life, variable pavement cross sections, and service life durations. Density evolution of test sections with traffic and time is explored with an emphasis on in-situ density test sections (Cells 988-991) performance. Moreover, serviceability performance in terms of the International Roughness Index (IRI) is summarized and compared to reflective cracking performance from manual distress surveys. Lastly, the development of life curves for each MnROAD overlay test section in the driving, passing and combination of driving and lanes is presented in this chapter.

5.2 Falling Weight Deflectometer (FWD)

Falling weight deflectometer (FWD) testing was performed prior to overlay construction to assess the structural capacity of the existing PCC on test cell sections 984 to 995. Data was recorded on April 5th, 2017 for the driving and passing lanes respectively and load transfer efficiency (LTE) values are presented in Figure 5-1 with the red dashed box highlighting the four in-situ density test sections. As expected, LTE was higher in the passing lanes for all test sections compared to driving lanes. Among the four in-situ density sections, lower LTE was observed in Cell 990 (3% AV) and Cell 991 (4% AV, 9.5 mm) as compared to Cell 988 (4% AV, 12.5 mm)

and Cell 989 (5% AV). For the thinner overlay test sections, lower LTE was observed in Cell 995 (19 mm thick ultra-thin bonded) as compared to Cell 994 (38 mm conventional overlay with slab stabilization). When comparing Cell 994 to Cell 984 (38 mm conventional overlay without slab stabilization) for both driving and passing lanes LTE is higher in Cell 994. Meanwhile Cell 985, which is also a 38 mm conventional overlay, reported the lowest LTE in the driving lane among all the test sections. The two test sections constructed using interlayers (Cell 992 and 993), showed that the driving lane LTE was lower for both test sections and Cell 992 reported slightly better LTE compared to Cell 993.

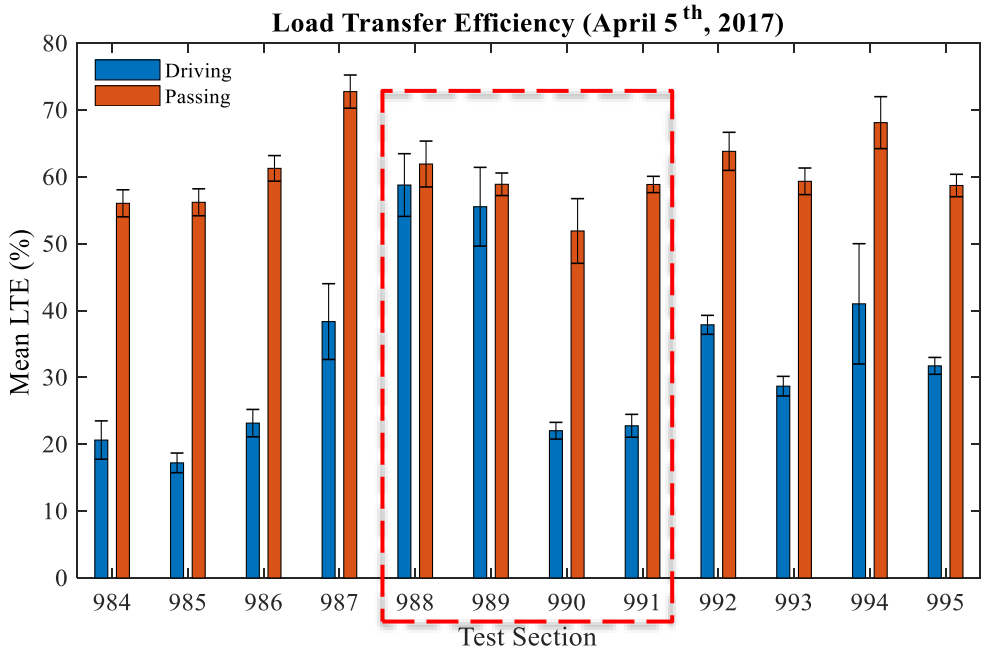

Figure 5-1 Load transfer efficiency data on test sections 984-995.

Two other parameters from the FWD testing conducted prior to AC overlay construction were investigate; (1) central deflection (D1) directly under the load pulse, and (2) the surface curvature index (SCI). Data was analyzed and plotted separately by driving and passing lane for each cell, as well as by the drop location (approach or departure side of joint). Figure 5-2a and 5-2b show the central defection (D1) measured directly under the load pulse before and after joint

locations, respectively. Measured deflection in the driving lane was higher compared to the passing lane for all test sections. This is in good agreement with the LTE data presented in Figure 5-1. Also, a higher deflection is recorded when the drop location is after the joint.

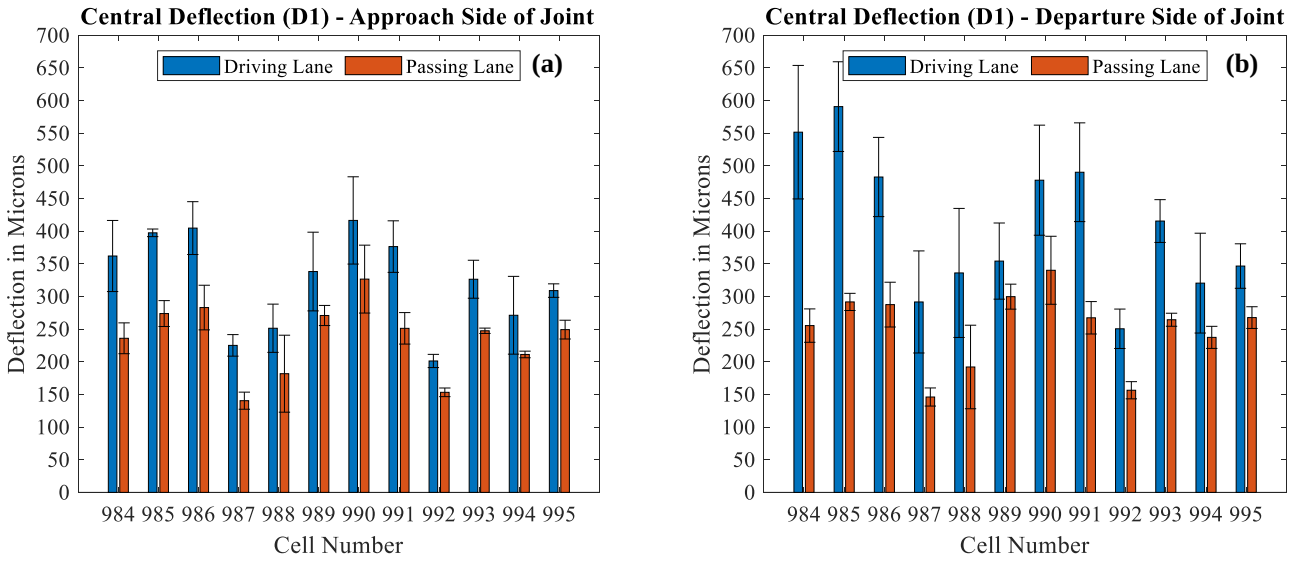

Figure 5-2 Central deflection (D1) measured (a) before and (b) after joint location.

Figure 5-3a and 5-3b present the SCI (also commonly referred to as base layer index, BLI) results; this parameter provides an indication of the structural condition of the base layer [42]. SCI is calculated by taking the central deflection (D1) and subtracting the surface deflection (D3) measured at a distance of 12 inches (300 mm) away from the load. Typically, lower values of SCI indicate better base layer material, providing good load distribution. SCI was determined to be lower in the passing lane compared to the driving lane for all test sections. This agrees with expected trends based on LTE results presented in Figure 5-1, where higher LTE levels correspond to lower SCI values. SCI was investigated further by determining the index using drop locations before (approach) and after (departure) the joint location separately. The difference in calculated SCI between driving or passing lanes differs based on the drop location. For many of the test sections, SCI in the driving lane on the approach side of the joint is double the SCI value calculated

using measurements on the departure side of the joint. For this reason, it can be beneficial to look at the two SCI results calculated separately, rather than taking a single average of all FWD measurements taken within a given test section. Both the central deflection and SCI results agree with the LTE results presented in Figure 5-1 and support the use of LTE as a relatively simple way of evaluating the existing PCC condition prior to overlay construction.

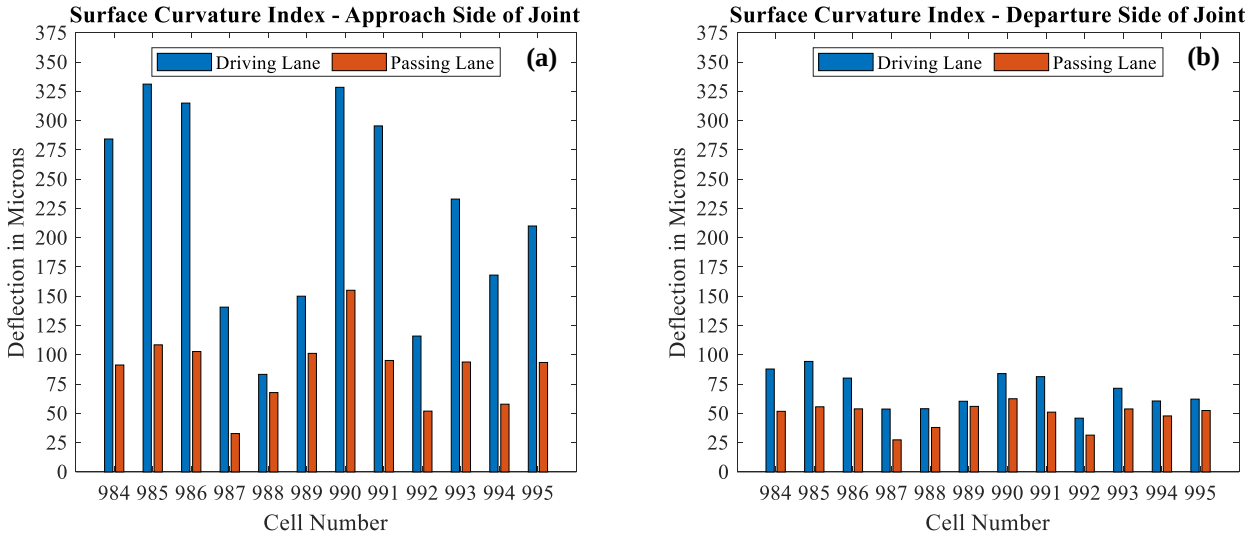

Figure 5-3 Surface curvature index (SCI) determined based on measurements taken (a) before and (b) after joint location.

5.3 Traffic Loading

Field test sections have been subject to approximately 816,000 flexible equivalent single axle loads (ESALs) or 1,165,000 rigid ESALs from the time of construction (September 2017) to May 2020. Table 5-1 provides a monthly trafficking schedule at MnROAD on the respective test cells (typically for a week during each month), while

Table 5-2 breaks down the volume of traffic loading by lane (driving or passing). Car traffic is classified as having MnDOT C1-C3 vehicles, while heavier vehicles (mostly trucks, but also includes buses) are classified as C4-C13. The sum of traffic loading from all vehicle classes on both driving and passing lanes is approximately 7.2 million vehicles. It should be noted that traffic numbers reported in

Table 5-2 are approximate values as they are recorded before traffic enters the lanes on the original alignment of I-94 westbound, and do not account for cases where vehicles change lanes before arriving at a particular test cell.

Table 5-1 Monthly traffic schedule on test sections.

Month	Year			
	2017	2018	2019	2020
Jan				
Feb				✓
Mar		✓	✓	✓
Apr		✓	✓	
May		✓	✓	✓
Jun			✓	✓
Jul		✓	✓	✓
Aug		✓	✓	
Sept	✓		✓	
Oct		✓	✓	
Nov	✓	✓	✓	
Dec		✓		

Table 5-2 Summary of traffic loading on field section lanes from September 2017 to November 2019.

Year	Car Total		Truck Total		Traffic Total	
	Driving	Passing	Driving	Passing	Driving	Passing
2017	202,091	267,134	51,072	16,330	253,163	283,464
2018	940,874	1,352,616	276,569	111,391	1,217,443	1,464,007
2019	1,212,566	1,475,847	369,607	313,991	1,582,173	1,789,838
2020*	240,153	274,703	81,752	30,162	321,905	304,865
TOTAL	**2,595,684**	**3,370,300**	**779,000**	**471,874**	**3,374,684**	**3,842,174**
Sum of traffic loading (Sept 2017- May 2020):						**7,216,858**

*Data collected from January until May 2020.

5.4 Distress Surveys

Manual condition surveys were performed by MnDOT staff at six different instances since overlay construction. Figure 5-4 provides an example of a distress crack map recorded by MnDOT staff for test cell 994. Crack distress maps for each cell were converted into a percentage of joints cracked within each test cell (excluding the transition zones between the cells). This was accomplished by first taking an inventory of all crack maps and quantifying the total crack length at each joint location. The percent of reflective cracking (% RC) within a test cell was calculated by taking the sum of crack lengths (at underlying joints) within a test cell and normalizing by the total length of PCC joints within the test cell (Equation 16).

$$\%\,RC = \frac{Sum\ of\ crack\ lengths\ reported\ at\ joint\ locations}{Total\ linear\ feet\ of\ joint\ underlying\ pavement} * 100 \qquad \text{Eqn. 16}$$

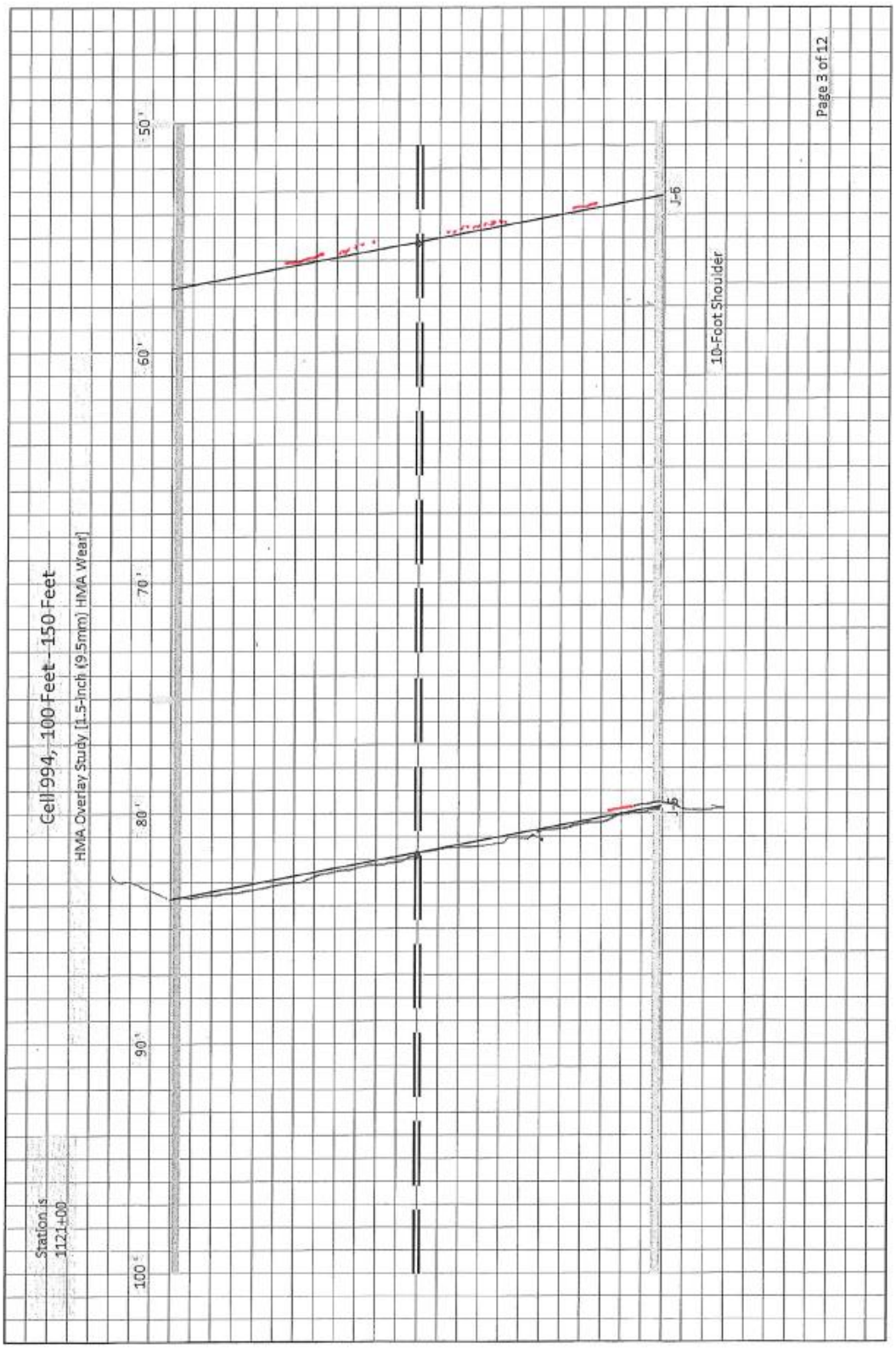

Figure 5-4 Example of distress crack map for Cell 994.

Figure 5-5 and Figure 5-6 summarize the %RC results by driving and passing lane respectively. Figure 5-7 shows the combined results of both lanes for each test section. The red dashed box highlights the four in-situ density test sections. As of the most recent survey date (August 2020), higher %RC was reported in the driving lane in general. In Figure 5-7, the best performing test sections tend to be the thicker overlay sections (4 inches) including Cell 987 and three out of the four in-situ density sections (Cells 988-990). The remaining in-situ density section (Cell 991, traditional Superpave 4% AV, 9.5 mm) showed relatively higher reflective cracking amounts in both lanes compared to other analogous overlay sections in terms of pavement structure.

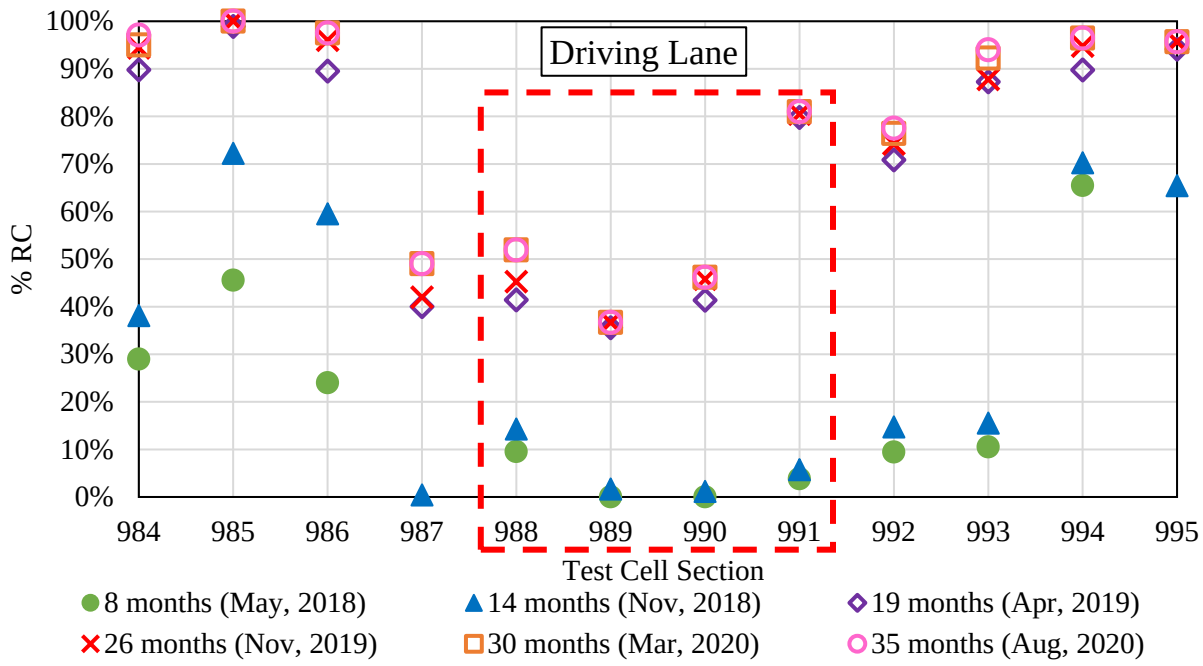

Figure 5-5 Percent reflective cracking (%RC) reported at joints in driving lane (dashed box indicates the four in-situ density study cells).

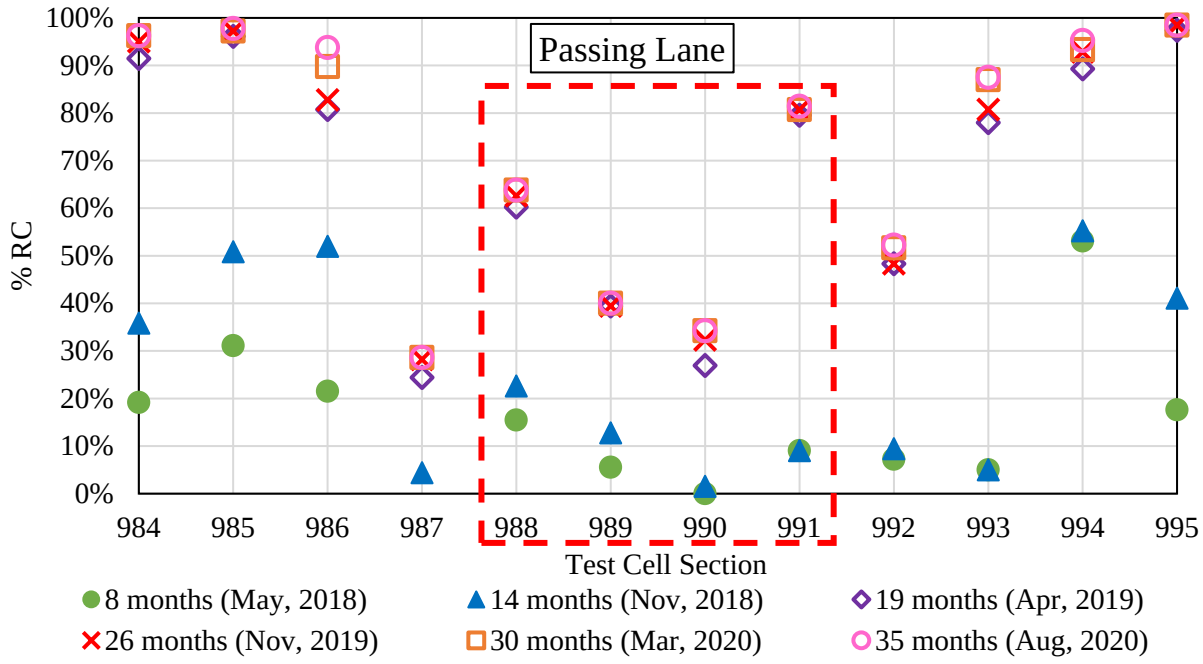

Figure 5-6 Percent reflective cracking (%RC) reported at joints in passing lane (dashed box indicates the four in-situ density study cells).

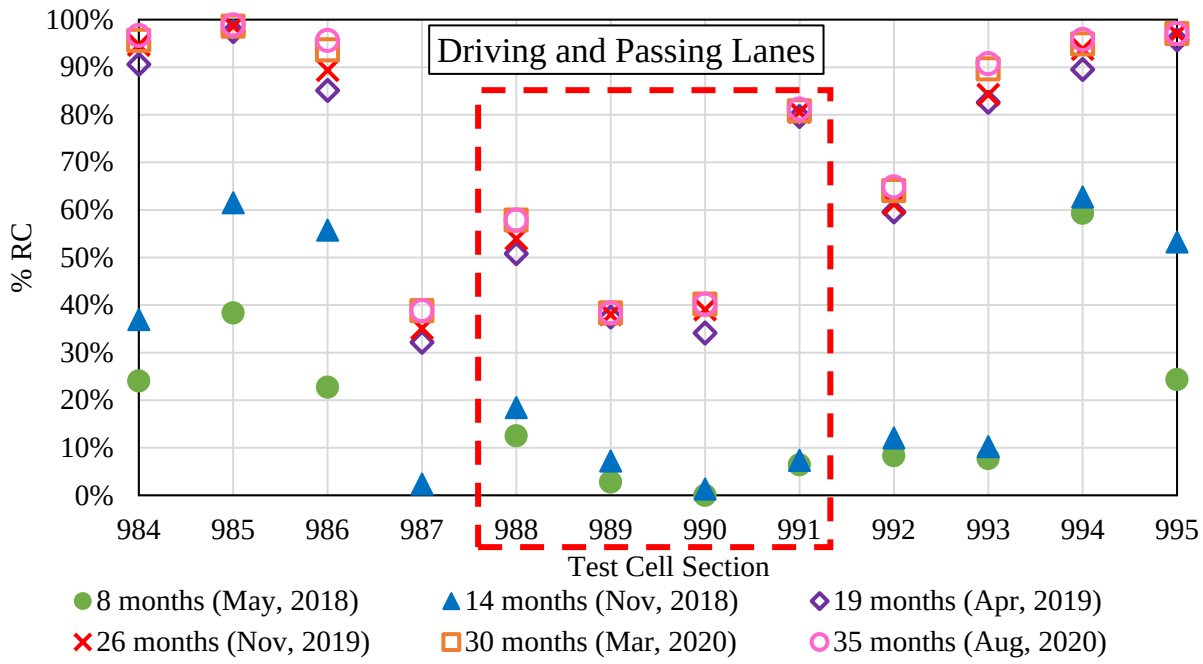

Figure 5-7 Percent reflective cracking (%RC) reported at joints in driving and passing lanes combined (dashed box indicates the four in-situ density study cells).

Another way to visualize the field performance data is to plot %RC with respect to time in service. Figure 5-8 clearly shows the importance of monitoring field performance with time as test sections with good early performance may not necessarily have good long-term performance. Test sections dedicated to studying the impact of in-situ density (Cells 988-991) on reflective cracking are denoted using dashed lines in Figure 5-8. In general, these test sections have experienced less reflective cracking than other sections to date, with the exception of Cell 991 which is the traditional Superpave 4% design with 9.5mm NMAS. Cell 989 (1.75 inch, 12.5 mm (5% AV) and 2.25 inch HMA, 19 mm) is showing the best performance followed closely by Cell 990 (1.75 inch, 12.5 mm (3% AV) and 2.25 inch HMA, 19 mm) and then Cell 988 (1.75 inch, 12.5 mm (4% AV) and 2.25 inch HMA, 19 mm).

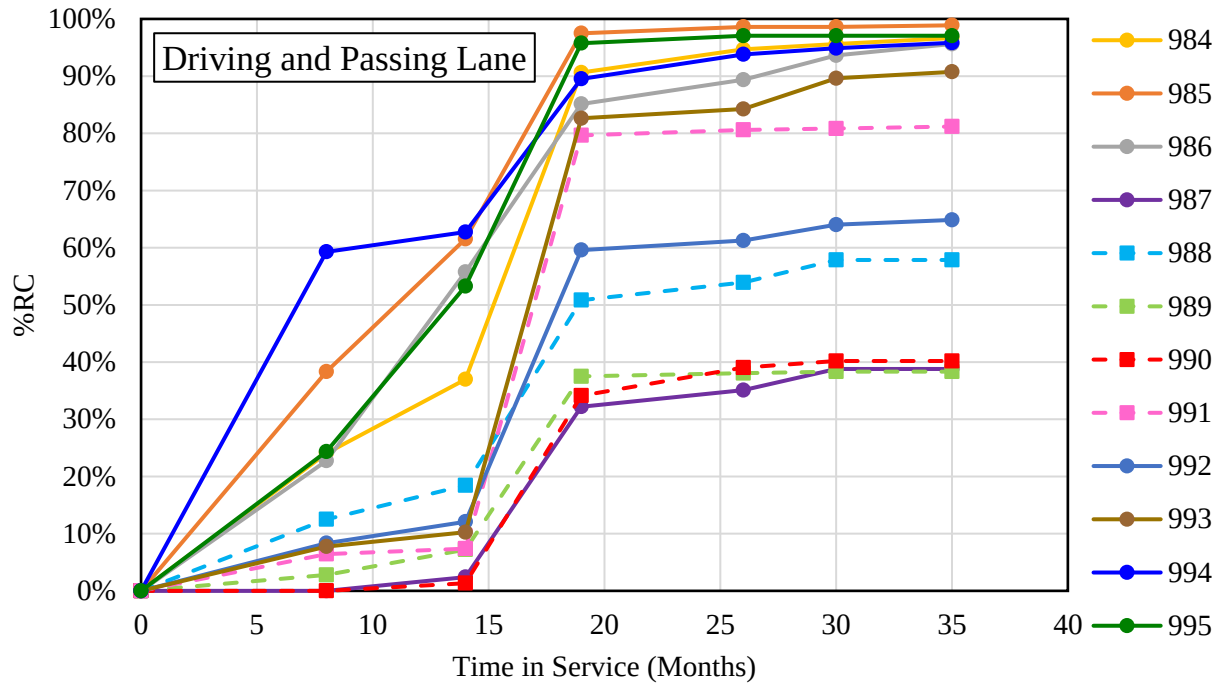

Figure 5-8 Percent reflective cracking with respect to time in service.

5.5 Pavement Condition Index

Distress data from the MnDOT automated pavement distress survey van was collected on all overlays sections in the driving and passing lanes separately. The total reported low, medium, and high severity transverse cracking was used to calculate the pavement condition index (PCI) for each test section. PCI was calculated following the ASTM D6433-20 standard procedure [43]. The PCI calculation was done using two methods, assuming all cracks reported at joint locations on distress surveys are classified as (1) joint reflection cracking (from longitudinal and transverse PCC slabs) and (2) longitudinal and transverse cracking (non-PCC slab joint reflective) distress classification types. Both methods were explored to compare PCI results when cracks are assumed to be from underlying joints versus low temperature material fracture properties of the asphalt mixtures. Table 5-3 summarizes PCI results for both driving and passing lanes separately assuming joint reflection cracking as the primary distress type. All test sections reported good PCI ratings (> 85) except for cell 993 in the driving lane.

Table 5-3 PCI for test sections using joint reflection cracking distress type.

	DRIVING LANE			PASSING LANE		
CELL	**PCI**	**RATING**	**RANK**	**PCI**	**RATING**	**RANK**
984	88	**Good**	10	87	**Good**	11
985	91	**Good**	6	91	**Good**	7
986	89	**Good**	8	90	**Good**	9
987	92	**Good**	4	95	**Good**	2
988	94	**Good**	2	93	**Good**	4
989	96	**Good**	1	96	**Good**	1
990	93	**Good**	3	94	**Good**	3
991	91	**Good**	6	92	**Good**	6
992	92	**Good**	4	93	**Good**	4
993	84	**Satisfactory**	12	91	**Good**	7
994	89	**Good**	8	90	**Good**	9
995	87	**Good**	11	87	**Good**	11

Table 5-4 summaries PCI results assuming longitudinal and transverse distress type. Again, the majority of test sections were classified as having good PCI rating. However, following this calculation method resulted in cells 984 and 995 being classified as satisfactory (PCI between 85-70) for both the driving and passing lanes and cell 993 classified as satisfactory in the driving lane.

Table 5-4 PCI for test sections using longitudinal and transverse distress type.

	DRIVING LANE			PASSING LANE		
CELL	**PCI**	**RATING**	**RANK**	**PCI**	**RATING**	**RANK**
984	85	**Satisfactory**	10	85	**Satisfactory**	11
985	89	**Good**	6	90	**Good**	7
986	86	**Good**	8	89	**Good**	8
987	91	**Good**	4	99	**Good**	1
988	93	**Good**	2	98	**Good**	4
989	94	**Good**	1	99	**Good**	1
990	92	**Good**	3	99	**Good**	1
991	90	**Good**	5	97	**Good**	6
992	90	**Good**	4	98	**Good**	4
993	81	**Satisfactory**	12	89	**Good**	8
994	88	**Good**	7	89	**Good**	10
995	84	**Satisfactory**	11	85	**Satisfactory**	11

In general, the PCI ratings indicate all test sections are in good condition after 3-years of service with very little distinction between them using PCI (majority of reflective cracks to date are low severity). As a result, the development of performance life curves for MnROAD overlay sections will use the percent reflective cracking (%RC) rather than PCI rating in order to differentiate overlay options within the decision tree tool. Furthermore, additional reflective cracking field performance indices using %RC were explored in this dissertation as a means to compare and track test section performance with time as described in the following subsection.

5.6 Reflective Cracking Field Performance Indices

To quantitatively compare reflective cracking performance of field sections, it is important to use cracking performance measures that take into account the rate of cracking, onset of cracking early versus later in overlay life, variable pavement cross sections and service life durations. A study by Oshone et al. (2019) proposed several field cracking performance measures for making recommendations regarding asphalt mix and thickness designs for pavements in cold climates [44]. These indices were developed for transverse cracking in cold climates; therefore they were modified slightly for the implementation in the current study to evaluate reflective cracking performance. As a result, cracking measures considered in this study include average reflective cracking rate (AvgRC, Equation 17) and the total reflective cracking performance index (RCTotal, Equation 18). AvgRC calculates the average reflective cracking rate a pavement experiences per month of service. The RCTotal index uses a concept of cracking work (similar to fracture work), where the total area of the curve between percent cracking and pavement service life is calculated and normalized with respect to the time of the last survey.

$$AvgRC = \frac{Reflective\ cracking\ at\ latest\ survey}{Life\ at\ latest\ survey} \quad \text{Eqn. 17}$$

$$RCTotal = \frac{Reflective\ cracking\ work}{Life\ at\ latest\ survey^2} \quad \text{Eqn. 18}$$

Where:

AvgRC = average reflective cracking rate, % reflective cracking per month

RCTotal = total reflective cracking performance index, % reflective cracking per month

To interpret results of AvgRC, the lower the bar (value) the better the performance. If the height of bars remain constant that means that the rate of cracking is fairly stable, however if an increase in AvgRC is observed between survey dates (sharp spike in bar height), that indicates a higher cracking rate between the two consecutive survey dates. On the contrary, if a decrease in

AvgRC is observed that indicates a lower cracking rate between consecutive survey dates. It should also be emphasized that it is important to make comparisons of test sections with time rather than at a single point. For example, test sections that performed well early by having a lower AvgRC may appear to be performing worse in the current survey date comparison due to more joints being "available to crack" during the given analysis period.

Figure 5-9 and Figure 5-10 present results in terms of AvgRC and RCTotal for all test sections determined at the six different distress survey dates. In general, Cells 984, 985 and 994 had comparable AvgRC performance. One difference between these test sections was the early field performance of Cells 984 and 985 was better than Cell 994 (where approximately 8.5% average reflective cracking rate was reported). Comparing only the in-situ density sections (highlighted in red dashed box), Cell 991 reported the highest AvgRC while Cell 989 reported the lowest amount.

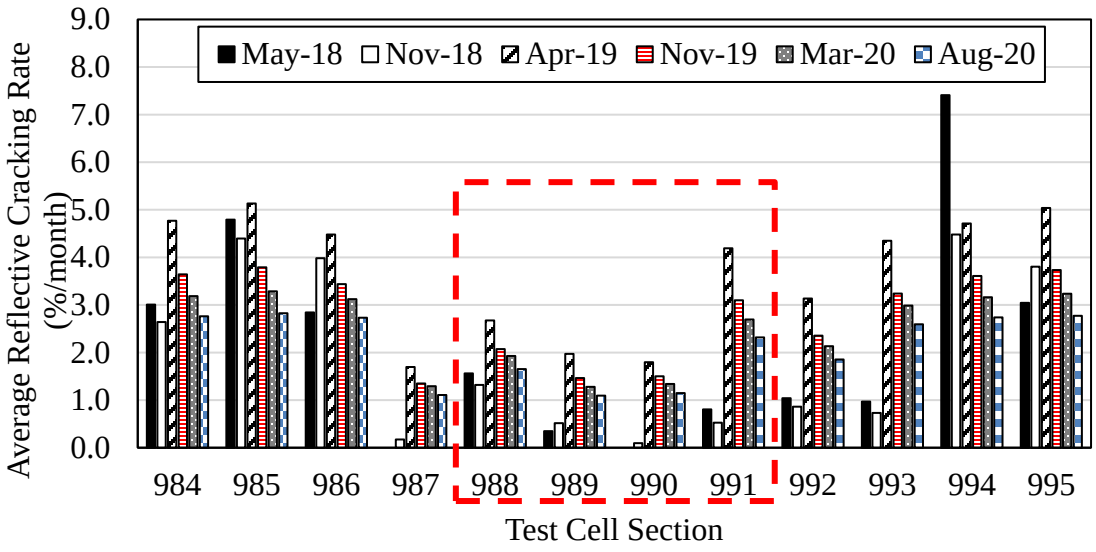

Figure 5-9 Average reflective cracking (AvgRC) rate for all test sections (dashed box indicates the four in-situ density study cells).

RCTotal results shown in Figure 5-10 indicate that the worst performing Cell is 994 while the best performing test cells are Cell 990 and Cell 987. Unlike average reflective cracking rate, since RCTotal encompasses cracking performance over the life of the pavement, the performance measure from latest survey is most reliable for comparisons between various cells. This parameter gives credit to test sections that crack later and have early good performance.

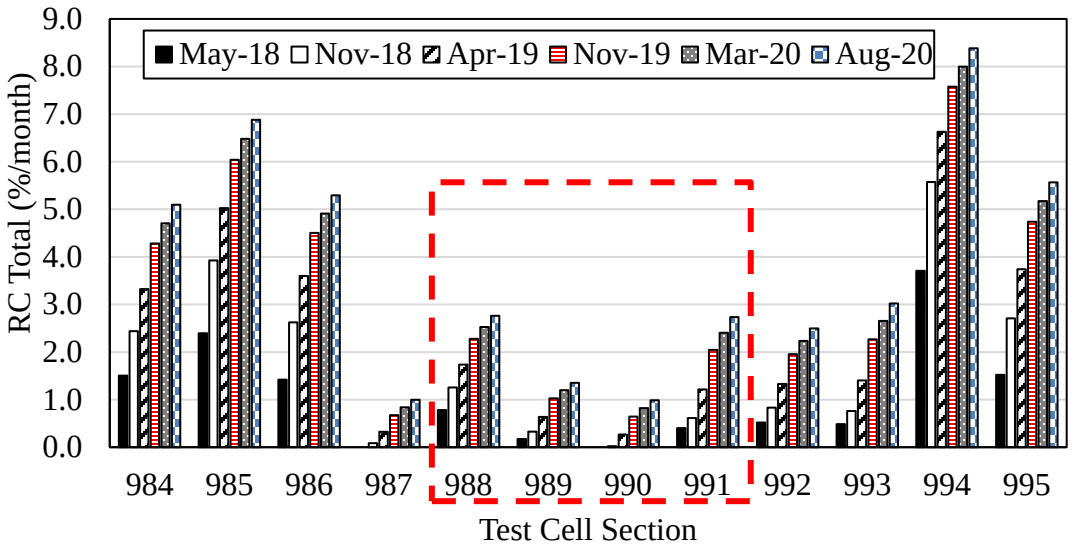

Figure 5-10 Total reflective cracking (RCTotal) rate for all test sections (dashed box indicates the four in-situ density study cells).

Performance indices were also evaluated using a normalized thickness approach to take into account pavement structure. This approach provides a more objective comparison of test sections comprised of varying overlay structures (number of lifts and thickness) and provides the ability to account for the contribution of each individual mixture or layer in the overall structural performance of the pavement. Figure 5-11 and Figure 5-12 show the normalized performance index results for AvgRC and RCTotal respectively. There was no change observed in terms of the best (Cell 995) and worst (Cell 991) performance using the normalized AvgRC index. However, there was a close switch in the best performing test section in terms of normalized RCTotal as of

the August 2020 survey date with Cell 987 reporting the overall lowest normalized RCTotal value followed closely by Cell 990 and Cell 995.

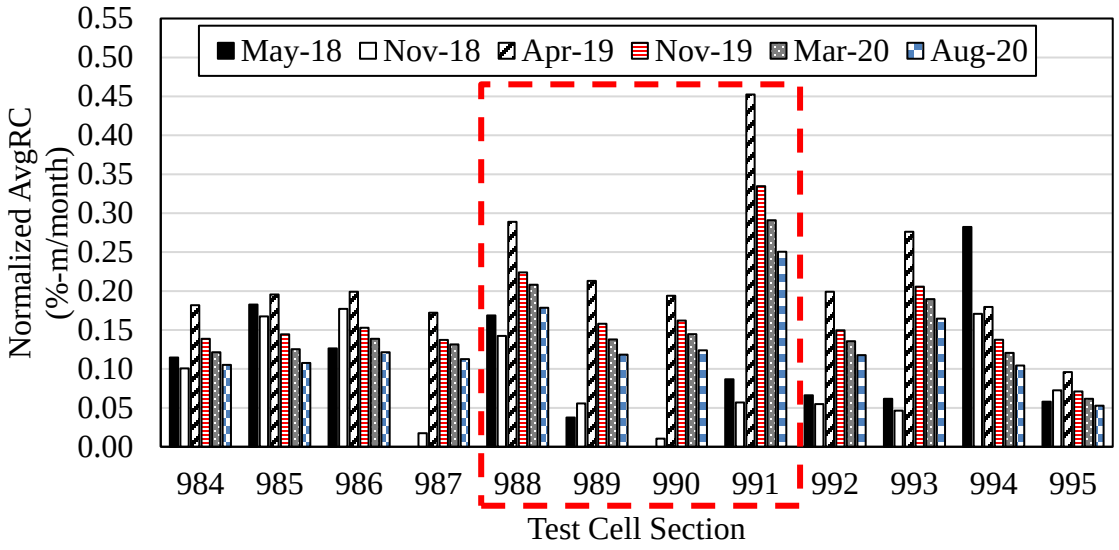

Figure 5-11 Average reflective cracking (AvgRC) rate normalized by overlay thickness for all test sections (dashed box indicates the four in-situ density study cells).

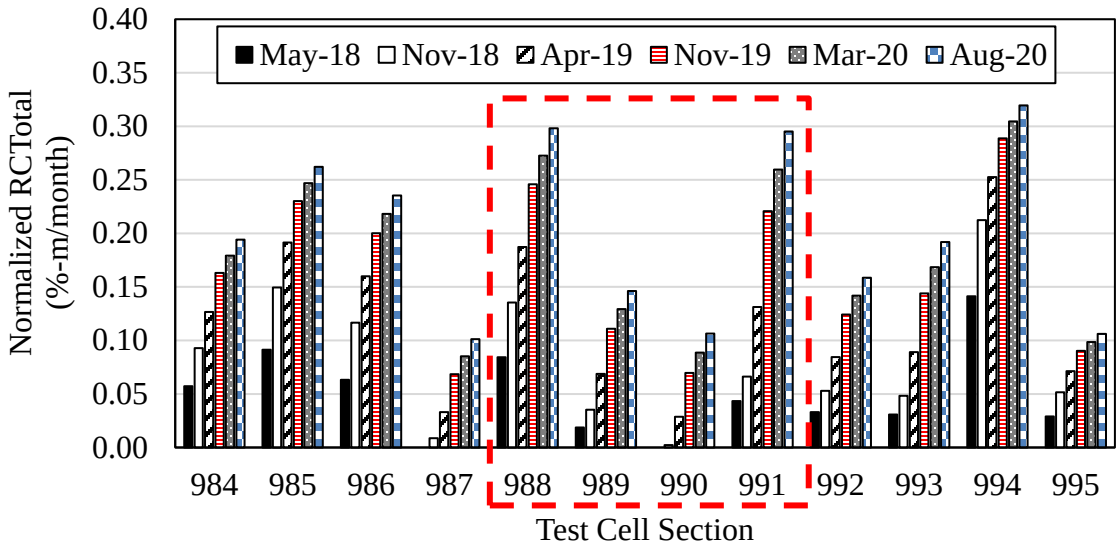

Figure 5-12 Total reflective cracking (RCTotal) rate normalized by overlay thickness for all test sections (dashed box indicates the four in-situ density study cells).

5.7 Density Profile System (DPS)

Dielectric constant data was collected using the MnDOT's density profile system (DPS) for all 12 MnROAD test sections in the driving and passing lanes (Figure 5-13). The dielectric constant refers to a material's ability to transmit electromagnetic waves through its medium. The dielectric constant of an asphalt mixture is derived from the dielectric values of its constituents (air, binder and aggregate). Air and binder both maintain properties of an electrical insulator and have lower dielectrics reflective of a limited ability to translate electromagnetic waves. Bitumen, independent of viscosity, normally has a dielectric ranging between 2.6 to 2.8, while the value for air is even lower. Aggregate, due to its mineralogical nature readily transmit electrons, tends to have a higher dielectric constant ranging from 4.5 to 6.5 [45]. It is expected that a mixture with a higher density would have fewer air voids and a higher dielectric value.

Figure 5-13 Density profile system data collection at MnROAD.

DPS data was collected following overlay construction in 2017 and again in 2019 and 2020. It should be noted that data collected in 2017 represents an average of passing and driving lane dielectric values. Data collected in subsequent surveys (2019 and 2020) includes separate records

for the driving and passing lanes. Density evolution of all test sections is presented in Figure 5-14 using the average dielectric constant collected along the length of each test section (in both driving and passing lanes). As expected, all test sections experience an increase in dielectric constant with time. The relatively lower dielectric constant reported in Cell 995 is not entirely surprising as it is only 0.75 inches thick and the concrete layer may be influencing the measured dielectric constant.

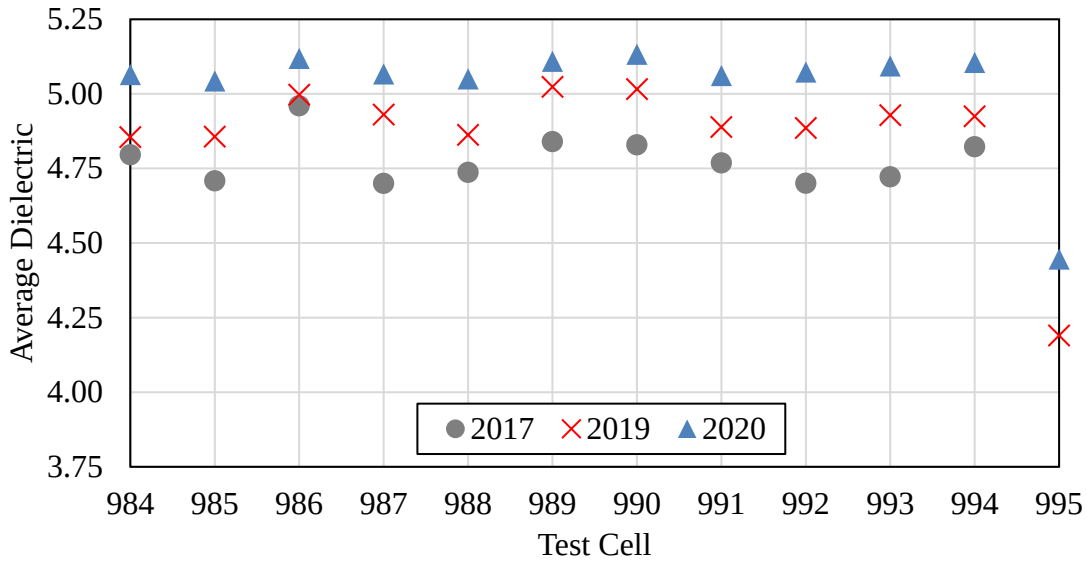

Figure 5-14 Average dielectric constant for all test sections.

To further investigate the density evolution of the various test sections, Figure 5-15 and Figure 5-16 break down the average dielectric results by lane. Standard deviation bars represent positive and negative standard deviation of collected dielectric measurements. It can be observed that the evolution of dielectric values is not consistent between different mixtures, indicating that they may not all densify in the same manner under traffic loading. Typically, the DPS is used on new construction only, as dielectric measurements may become more variable with time and varying environmental conditions (e.g. moisture presence). However, results presented in this study show promise with the application of DPS in monitoring of density with time.

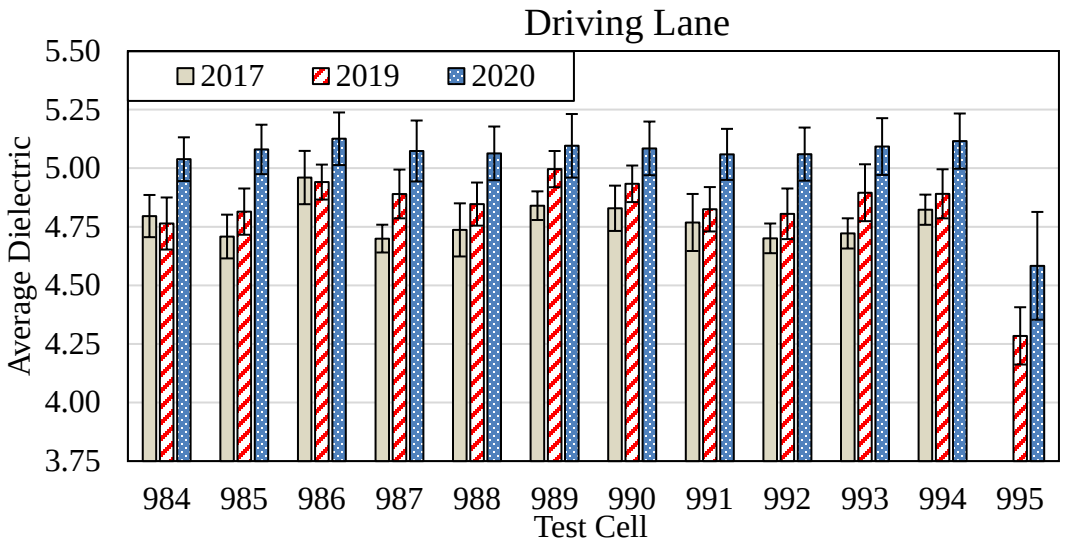

Figure 5-15 Average dielectric in driving lane only.

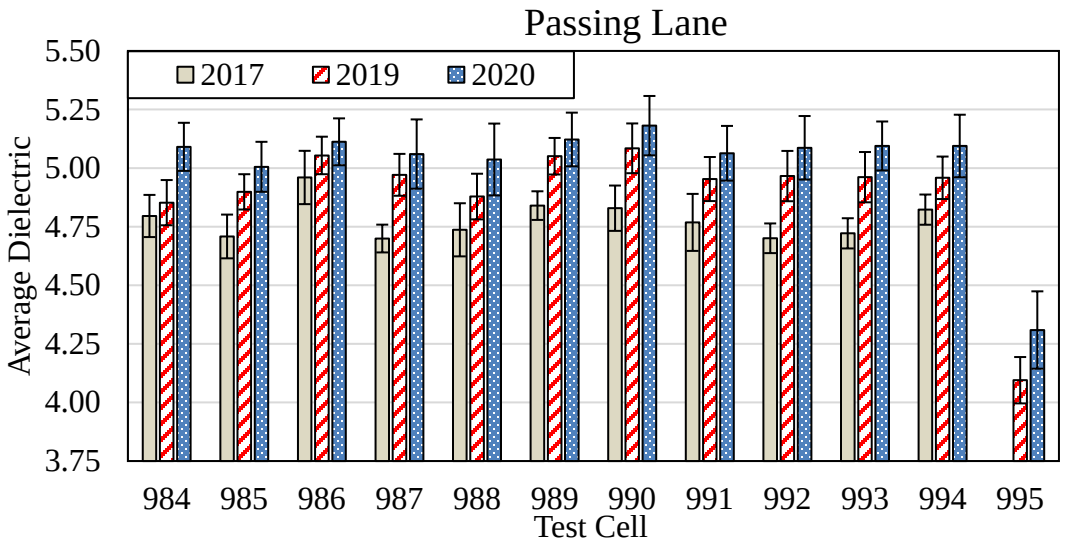

Figure 5-16 Average dielectric constant in passing lane only.

Figure 5-17 and Figure 5-18 highlight the in-situ density test sections (Cell 988-991) results with respect to traffic volume experienced in both driving and passing lanes, respectively. Figure 5-17 shows that all in-situ density test sections are converging in terms of densification of the mixture in the driving lane (approximately at an average dielectric of 5.10). It is also noted that

the rate of densification increased sharply after approximately 3 million vehicle passes in both the diving and passing lanes. However, there does not appear to be any concern of over densification of the in-situ density test sections as compared to the remaining test sections based on dielectric constant and from field distress surveys.

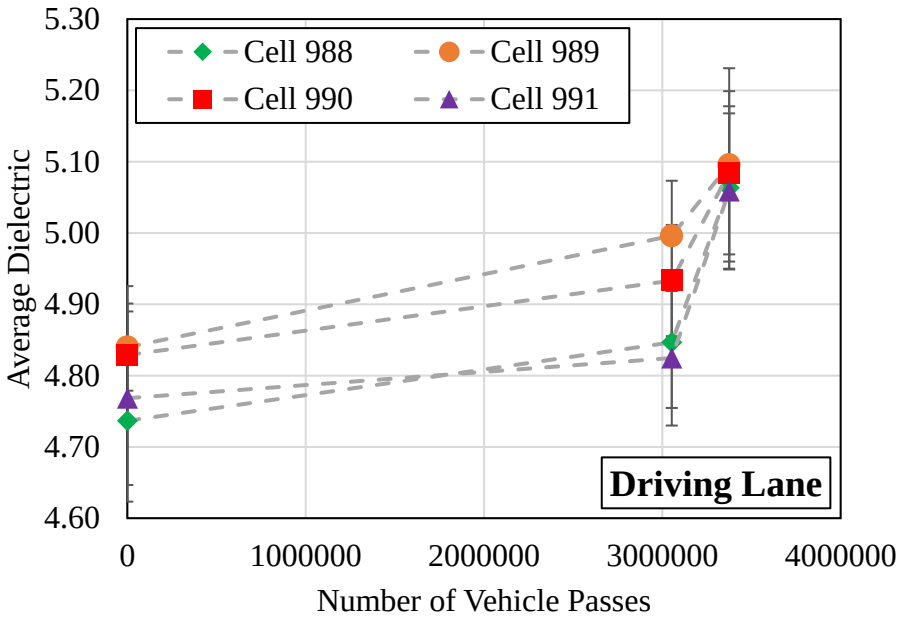

Figure 5-17 Average dielectric of in-situ density test sections with respect to cumulative number of vehicle passes in driving lane.

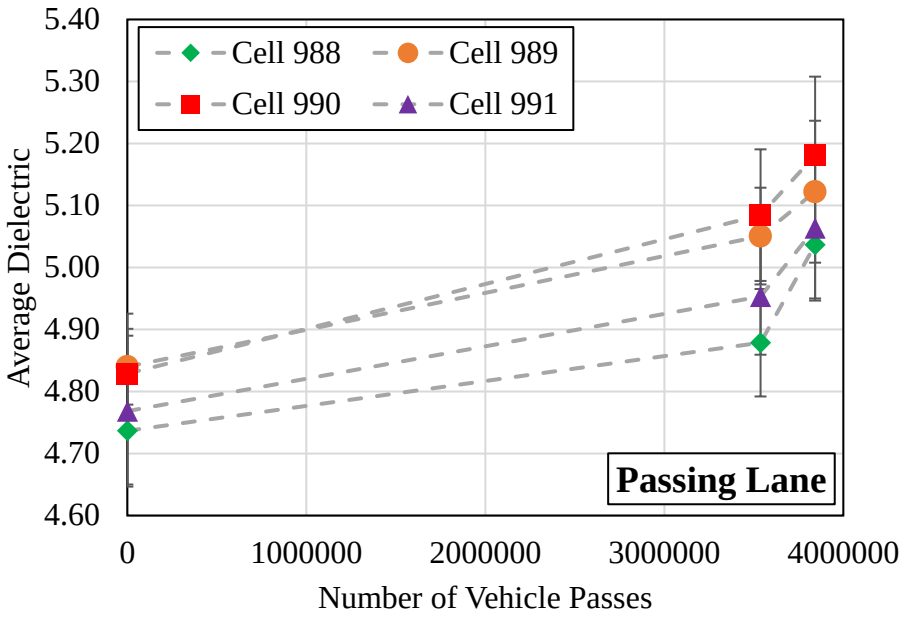

Figure 5-18 Average dielectric of in-situ density test sections with respect to cumulative number of vehicle passes in passing lane.

5.8 Field Cores

Field cores were acquired in the summer of 2019 from transition zones of test sections. A total of 48 cores were sampled, with four cores taken from each test cell: two in the wheel path and two near the joint location. Core locations along the wheel path and joint were selected based on preliminary DPS measurements taken within test sections (by performing a serve test) that indicated these locations were appropriate for sampling representative low and high density areas within each test section. Equations 19 and 20 were used to calculate the low and high target dielectric constant values respectively. DPS equipment was then used to locate areas within the transition zone of each test cell that corresponded to the target low and high dielectric values for coring.

$$Low\ Target = Median\ Dielectric - (2 * Standard\ Deviation) \quad \text{Eqn. 19}$$

$$High\ Target = Median\ Dielectric + (2 * Standard\ Deviation) \quad \text{Eqn. 20}$$

Figure 5-19 provides an example of marking the low (along joint) and high (wheel path) core locations for test Cell 989 prior to extraction. All field cores were measured for in-place thickness prior to trimming for G_{mb} measurements.

Figure 5-19 Example of core location selection.

Lift thickness was verified for each test section by taking the average of the four cores extracted in each transition zone. In general, the in place thickness was higher than the designed thickness. However, it should be noted that these comparisons are made with transition zone cores and not with cores taken in the actual field test section themselves, therefore lift thickness within the actual section may vary.

MnDOT staff then used the Corelok method (AASHTO T 331) to perform bulk specific gravity measurements on field cores that were sampled after approximately two years in service [46]. Most of the air void percentages were within expected ranges compared to design air void levels by mix type. The only exception was the base course (SPWEC440E) used in Cell 987 having a slightly higher average air void content of 11.3% compared to other test sections that contained the same base course mixture with an average air void content of 6.0%.

To investigate the evolution of density with time and traffic within the four in-situ density test sections, quality assurance field cores collected at the time of construction (2017) in transition areas and the field cores collected in 2019 were utilized. Figure 5-20 shows the measured air void percentage for wearing course mixtures used in Cells 988-991 with time. Similar trends and rankings were observed when plotting the measured air void with respect to traffic instead of time.

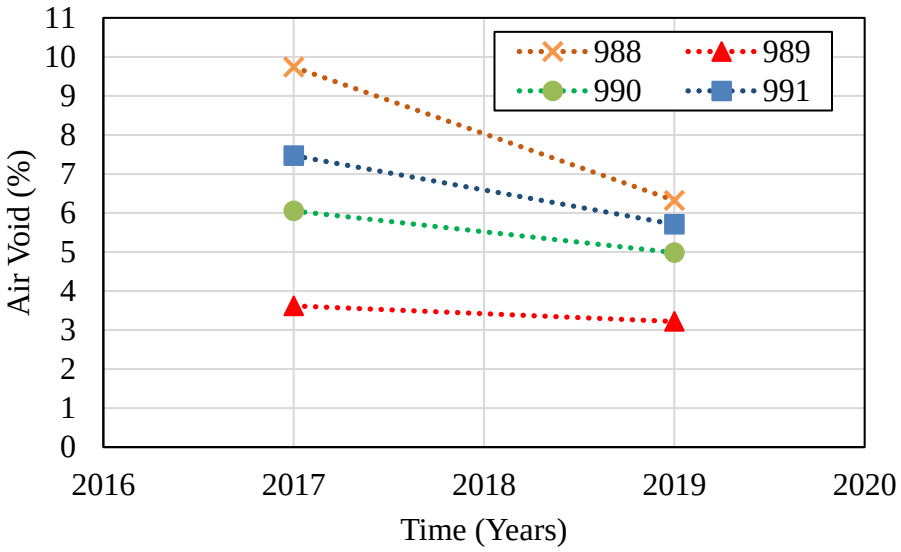

Figure 5-20 Comparison of air void levels with time in wearing course of in-situ density sections.

Figure 5-21 shows the air void content broken down by test section, with the number above the bar representing the rate of change from 2017 to 2019. Cell 989, which contained the Superpave5 mixture, had the lowest rate of change (-0.20 %/yr.). In comparison, Cell 988 had the highest rate of change (-1.71 %/yr.), corresponding to a decrease in air void level of approximately 3.4% after only two years in service. To date, the Superpave5 (Cell 989) and regressed air void (Cell 990) mixtures have experienced less densification than the traditional 4% mixture designs (NMAS of 12.5 mm and 9.5mm) used in Cells 988 and 991 respectively.

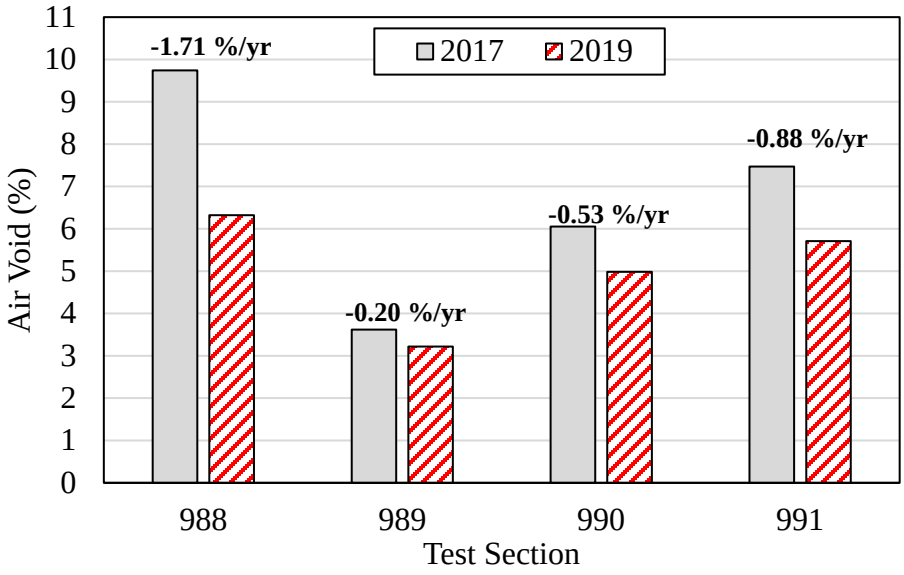

Figure 5-21 Change in air void content from 2017 to 2019 by test section with number above bars showing the rate of change for in-situ air void content per year.

5.9 Serviceability

Serviceability of all 12 overlay field test sections was assessed using the universally accepted standard measure of ride quality, International Roughness Index (IRI). IRI was measured using two different data collection systems at the MnROAD facility: (1) PathRunner van and, (2) Lightweight Inertial Surface Analyzer (LISA). The PathRunner van is a pavement condition data collection vehicle capable of collecting survey data at highway speeds (50 mph), while the LISA equipment is typically used at speeds of less than 15 mph. Both collection methods are included

in this study to explore differences with the measurement methods and impact on ranking of test sections.

Figure 5-22 summarizes the average IRI data collected using the PathRunner van, while Figure 5-23 shows IRI results using the LISA system. Results are shown by driving and passing lane separately and are plotted in terms of time (days since construction, where Day 0 is selected as the date of construction). Negative values represent survey data collected prior to overlay construction.

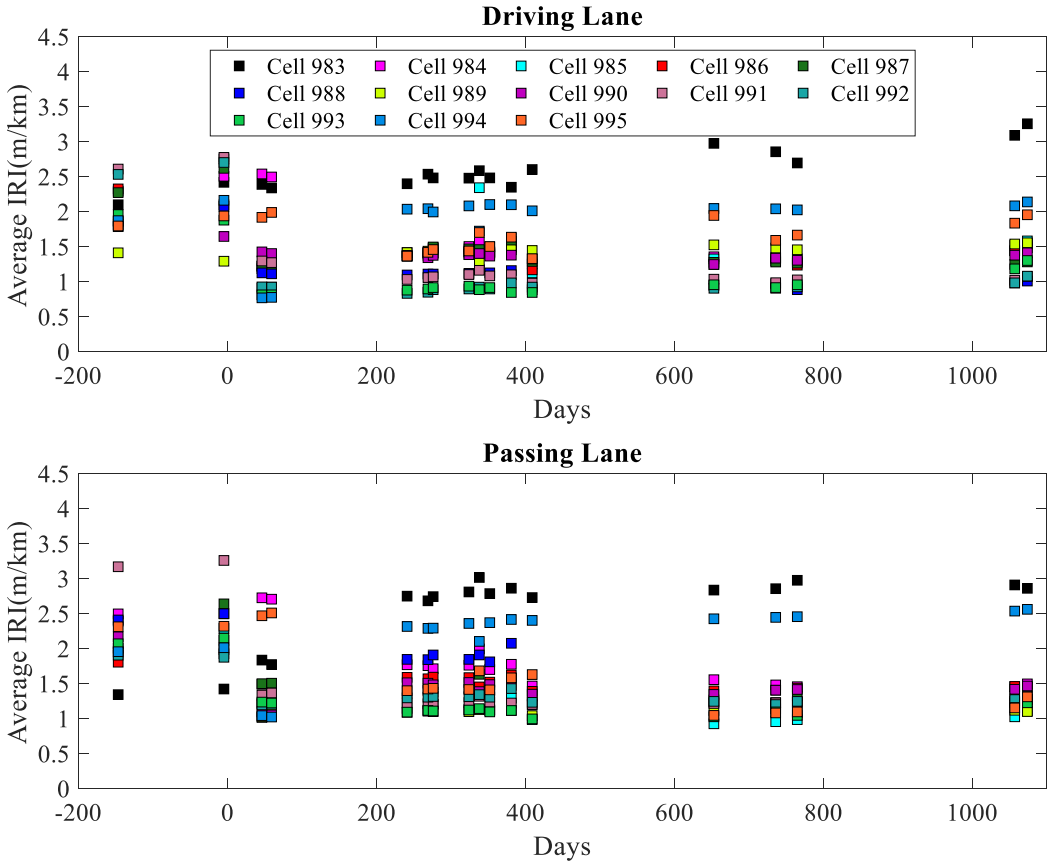

Figure 5-22 International roughness index (IRI) data obtained from PathRunner van.

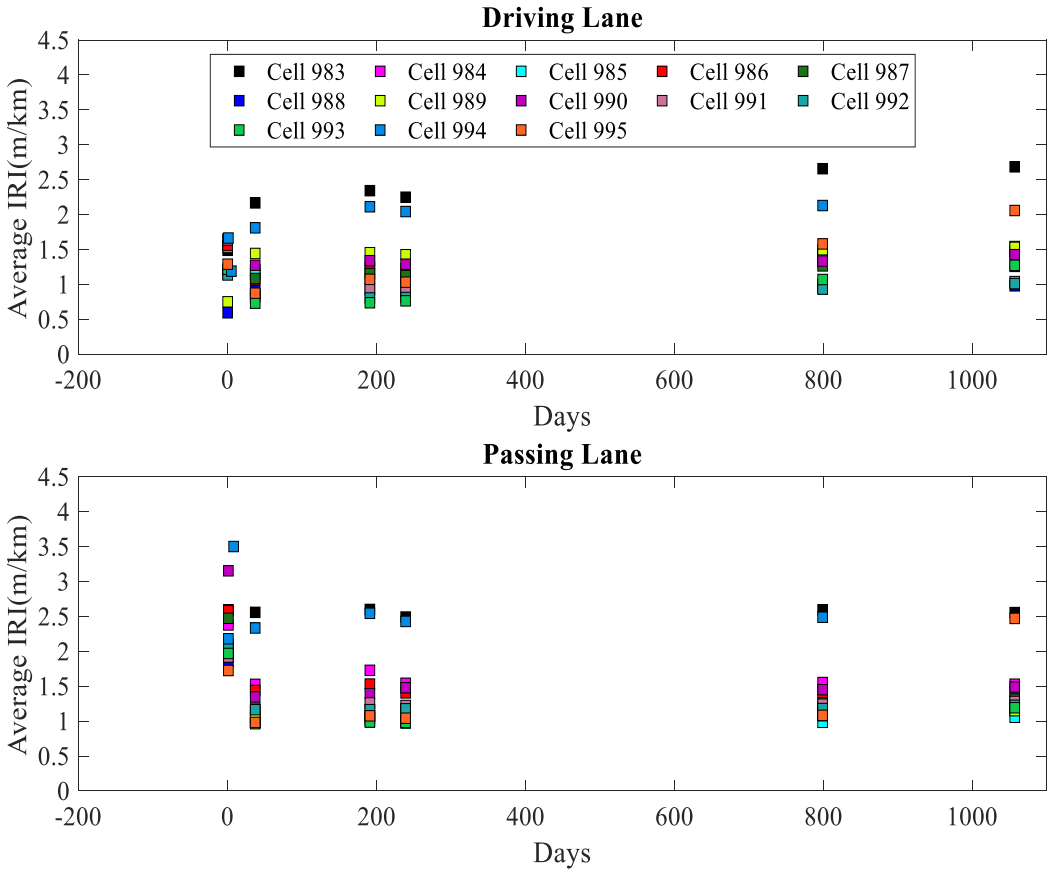

Figure 5-23 International roughness index (IRI) data obtained from lightweight inertial surface analyzer (LISA).

Table 5-5 and Table 5-6 provide the ranking of test sections based on the IRI collection methods as of the most recent survey for driving and passing lanes, respectively. The change in IRI (Δ IRI) from pre-overlay construction to the most current distress survey using data collected from the PathRunner van is shown in the last column of each table. A larger negative value indicates better ride quality since overlay construction, while positive values indicate that the current IRI is higher than the value measured prior to overlay construction. Also included for reference in each table is the %RC for all test section as of August 2020. In general, there was some variation in early IRI performance ranking between the Pathways van and LISA collection methods, however later IRI performance shows comparable ranking of serviceability performance.

Some discrepancy exists when comparing the ranking of test section based on reflective cracking versus serviceability. As an example, Cell 987 had the lowest %RC (Ranked 1st) but had relatively poor IRI performance (Ranked 8th) when comparing results from the passing lane.

Table 5-5 Driving lane serviceability ranking table (number within parenthesis denotes ranking).

Driving Lane					
Cell	**RC (%)**	**LISA IRI (m/km)**	**Pathways IRI (m/km)**	**IRI Pre-Overlay (m/km)**	**Δ IRI From (Pathways)**
984	97.1 (10)	1.4 (8)	1.33 (9)	2.51 (8)	-1.18 (6)
985	100 (12)	1.44 (9)	1.29 (7)	2.10 (6)	-0.81 (8)
986	97.5 (11)	1.32 (6)	1.24 (5)	2.76 (11)	-1.52 (3)
987	49 (3)	1.27 (5)	1.27 (6)	2.62 (9)	-1.35 (4)
988	51.9 (4)	0.95 (2)	**0.89 (1)**	2.08 (5)	-1.19 (5)
989	**36.7 (1)**	1.50 (10)	1.46 (10)	**1.30 (1)**	0.16 (12)
990	46.2 (2)	1.34 (7)	1.31 (8)	1.65 (2)	-0.34 (9)
991	81.0 (6)	1.00 (3)	1.03 (4)	2.78 (12)	-1.75 (2)
992	77.5 (5)	**0.93 (1)**	0.93 (2)	2.71 (10)	**-1.78 (1)**
993	94 (7)	1.07 (4)	0.96 (3)	1.88 (3)	-0.92 (7)
994	96.4 (9)	2.13 (12)	2.03 (12)	2.17 (7)	-0.14 (11)
995	95.7 (8)	1.58 (11)	1.67 (11)	1.94 (4)	-0.27 (10)

Table 5-6 Passing lane serviceability ranking table (number within parenthesis denotes ranking).

Passing Lane					
Cell	**RC (%)**	**LISA IRI (m/km)**	**Pathways IRI (m/km)**	**IRI Pre-Overlay (m/km)**	**Δ IRI (Pathways)**
984	96.3 (10)	1.55 (11)	1.46 (11)	2.50 (9)	-1.04 (7)
985	97.8 (11)	**0.98 (1)**	**0.99 (1)**	2.29 (7)	-1.30 (3)
986	93.8 (8)	1.41 (9)	1.44 (10)	1.99 (3)	-0.55 (11)
987	**28.6 (1)**	1.26 (8)	1.33 (8)	2.64 (11)	-1.31 (2)
988	63.8 (5)	1.12 (5)	1.24 (5)	2.50 (9)	-1.26 (4)
989	40 (3)	1.11 (4)	1.09 (3)	1.93 (2)	-0.84 (8)
990	34.2 (2)	1.45 (10)	1.42 (9)	2.12 (5)	-0.70 (9)
991	81.4 (6)	1.24 (7)	1.24 (5)	3.26 (12)	**-2.02 (1)**
992	52.2 (4)	1.18 (6)	1.25 (7)	**1.88 (1)**	-0.63 (10)
993	87.5 (7)	1.08 (2)	1.05 (2)	2.15 (6)	-1.10 (6)
994	95.2 (9)	2.49 (12)	2.46 (12)	2.02 (4)	0.44 (12)
995	98.5 (12)	1.08 (2)	1.1 (4)	2.32 (8)	-1.22 (5)

To examine the ranking of field test sections further, percent discrepancy was calculated between all performance parameters and test sections separately for the driving and passing lanes. Percent discrepancy was determined by taking the absolute ranking difference divided by the maximum possible difference in the ranking (i.e. 12-1=11). The average percent discrepancy for each performance parameter is summarized in Table 5-7 and

Table 5-8. A lower percent discrepancy for a given performance parameter pairing indicates the parameters rank test sections similarly. As expected, there is fairly good agreement between PathRunner and LISA collected IRI data with the lowest discrepancy reported in both driving and passing lanes. The highest percent discrepancy in the driving lane is observed between PathRunner IRI, Δ IRI and %RC. Δ IRI and %RC produced the highest percent discrepancy in the passing lane. This observation is important, since it is demonstrating that the level of reflective cracking in an overlay may not be directly correlated to the level of serviceability degradation. This is the case

for the 12 MnROAD test cells. Furthermore, the overall comparison of reflective cracking amount and the IRI values also indicates that depending on the measure/threshold used by an agency for a maintenance and rehabilitation (M&R) decision, the resulting recommendation and its timing could be significant different. For example, the structural life will be the dominant one in M&R decision as opposed to the loss of serviceability thresholds and may impact the timing of future required M&R treatments.

Table 5-7 Driving lane average percent discrepancy in ranking.

	%RC	LISA IRI (m/km)	Pathways IRI (m/km)	Δ IRI From Pre-Overlay
%RC	N/A	33.3	36.4	36.4
LISA IRI (m/km)		N/A	7.6	15.2
Pathways IRI (m/km)			N/A	18.2
Δ IRI From Pre-Overlay				N/A

Table 5-8 Passing lane average percent discrepancy in ranking.

	%RC	LISA IRI (m/km)	Pathways IRI (m/km)	Δ IRI From Pre-Overlay
%RC	N/A	35.6	37.1	37.9
LISA IRI (m/km)		N/A	6.1	23.5
Pathways IRI (m/km)			N/A	28.0
Δ IRI From Pre-Overlay				N/A

5.10 Development of Overlay Life Curves

A common technique used in infrastructure asset management to predict the timing of maintenance and rehabilitation is to construct life or performance curves. A life curve typically

plots a given performance measure (e.g. reflective cracking) with time in service (life of the overlay). A performance curve is a graphical representation of the deterioration of an asset where the slope indicates the anticipated rate of deterioration while the length of the curve typically represents the service life of the asset until a functional failure threshold (e.g. serviceability) is reached.

In development of the life and performance overlay curves for the decision tree tool, the possibility of using different measures such as field cracking performance (%RC), serviceability (IRI) or simulated performance from advanced software such as AASHTOWare® Pavement ME Design™ or finite element modeling was initially explored. Based work comparing the ranking of test sections using %RC, IRI and calculated field performance indices it was observed that %RC will control the structural life of an overlay. As a result, %RC was determined to be the most suitable measure to use for purposes of conducting life cycle analysis to support decision process of selecting materials and overlay structure/treatments within the proposed decision tree tool.

All available field performance data collected from the 12 MnROAD test sections over the six different distress surveys were analyzed. Three individual life curves were plotted for each test section based on distress survey data from the driving lane, passing lane and the combination of both lanes. In general, the pavement life curves follow a sigmoidal shape which is common among other infrastructure life curves (e.g. bridges or pipelines). A threshold of 50% reflective cracking reported at joints within a given test section is shown by the solid red line. However, the decision tree tool will allow users to input a desired cracking threshold (e.g. 90% of joints reflected). For the majority of test sections, all three life curves reached the 50% threshold as of the most recent distress survey date performed in August 2020. However, three test sections (Cell 987, 989 and 990) reported lower than 50% reflective cracking as of August 2020; therefore, the data was

linearly extrapolated to the threshold value. This approach involved determining the maximum winter and summer average cracking rate for each section by individual lane or combined performance. AvgRC performance index is highly dependent upon the number of joints remaining undamaged compared to the number of joints fully cracked. In other words, a test section that has experienced severe cracking early on may have relatively low AvgRC values between subsequent distress survey dates and vice versa. As a result, when taking an average of the AvgRC performance index calculated between the six different distress survey dates a biased AvgRC rate was produced. Therefore, the maximum AvgRC performance index calculated between distress survey dates was selected as a conservative approach to extrapolate results. Table 5-9 summarizes the maximum winter and summer average reflective cracking (AvgRC in %/month) rates experienced in each test section since construction. Table 5-10 shows when each cracking rate was applied based on six months of the year being assigned a winter cracking rate and 6 months a summer rate.

Table 5-9 Maximum winter and summer average reflective cracking (AvgRC) rate (%/month).

Test Cell	Combined		Driving		Passing	
	Winter	Summer	Winter	Summer	Winter	Summer
Cell 987	1.69	1.35	2.11	1.62	1.28	1.08
Cell 989	1.97	1.46	1.87	1.41	2.08	1.52
Cell 990	1.80	1.50	2.18	1.76	1.42	1.24

Table 5-10 Monthly allocation of cracking rate.

Month	Applied Cracking Rate
January	Winter
February	Winter
March	Winter
April	Winter
May	Summer
June	Summer
July	Summer
August	Summer
September	Summer
October	Summer
November	Winter
December	Winter

Figure 5-24 to Figure 5-35 show the life curves constructed using distress survey data (percent reflective cracking) for MnROAD test cells 984-995. Each test section has three curves; (1) combined performance of driving and passing lanes, (2) driving lane and (3) passing lane.

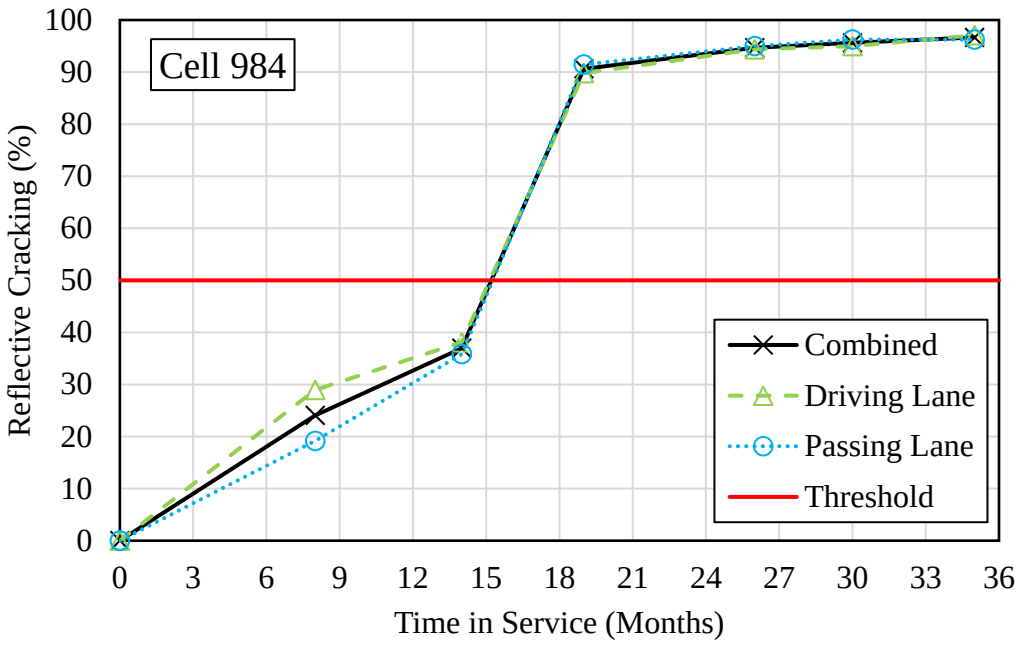

Figure 5-24 Cell 984 life curves.

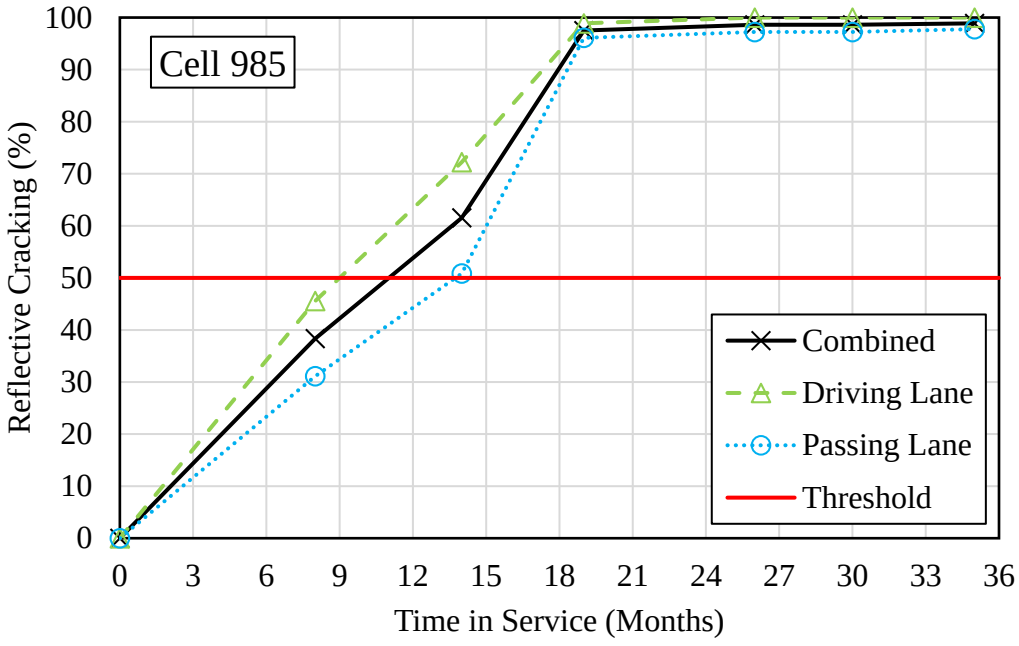

Figure 5-25 Cell 985 life curves.

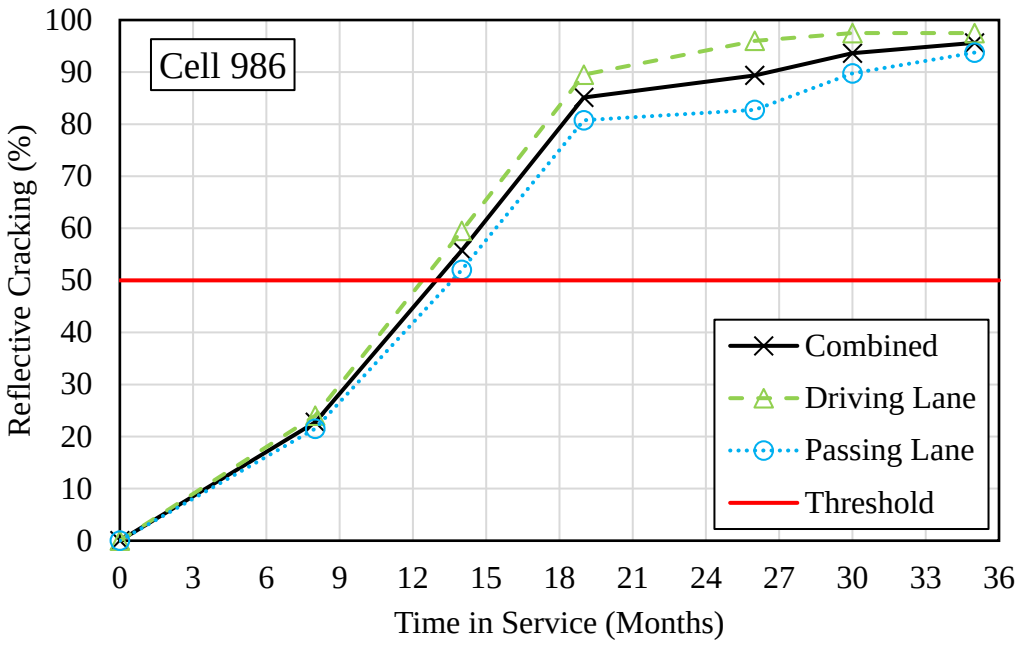

Figure 5-26 Cell 986 life curves.

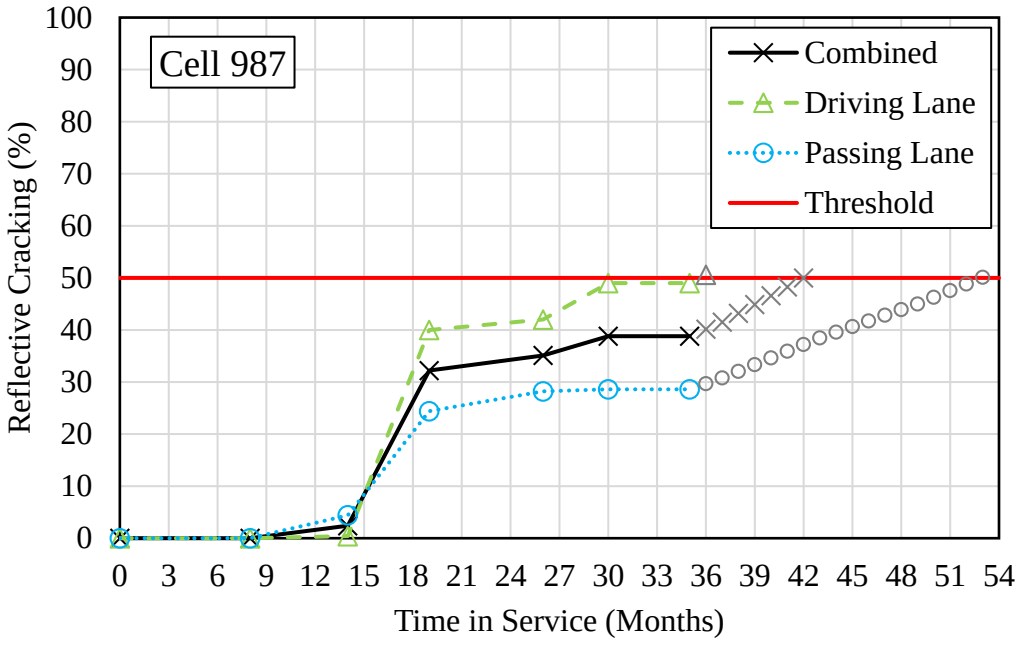

Figure 5-27 Cell 987 life curves.

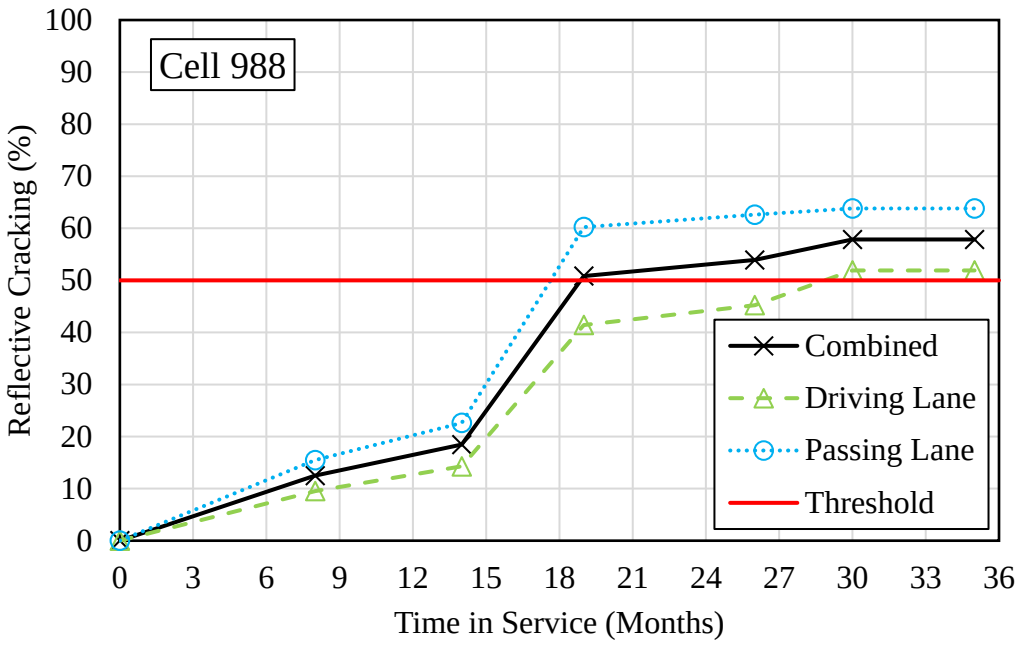

Figure 5-28 Cell 988 life curves.

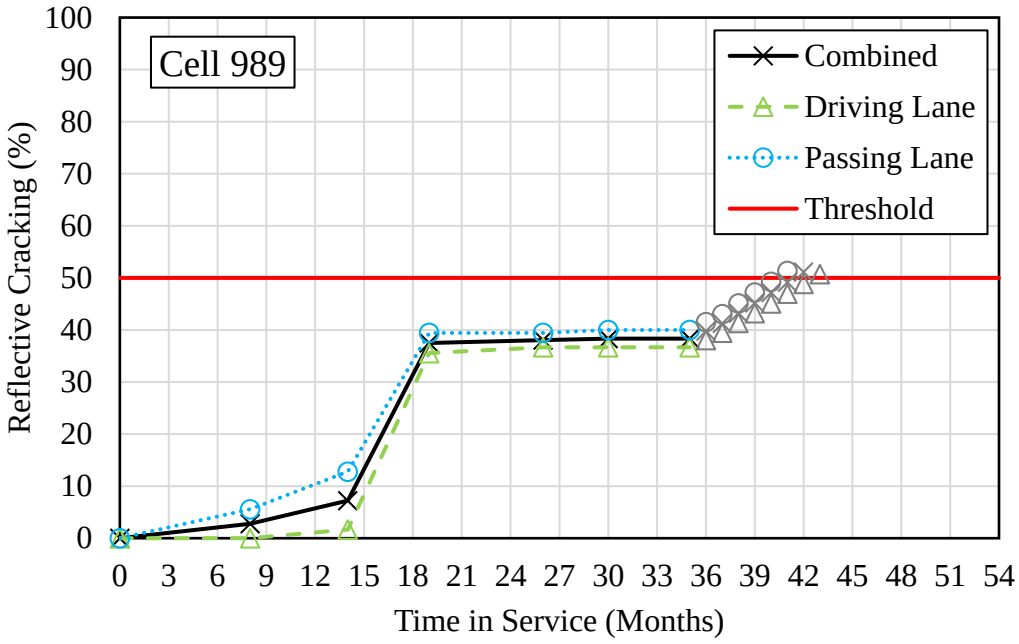

Figure 5-29 Cell 989 life curves.

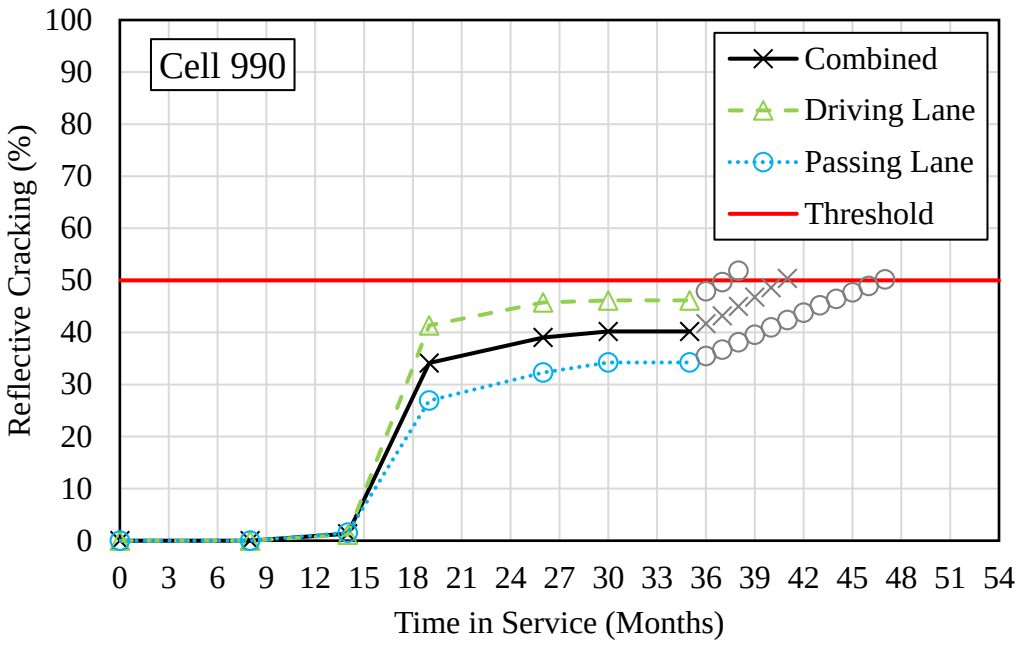

Figure 5-30 Cell 990 life curves.

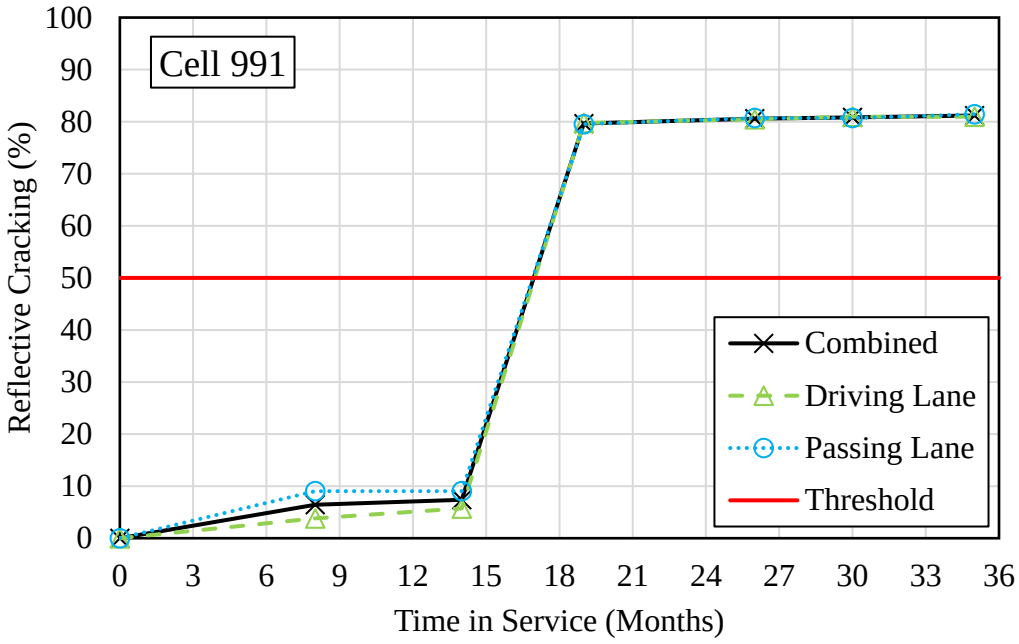

Figure 5-31 Cell 991 life curves.

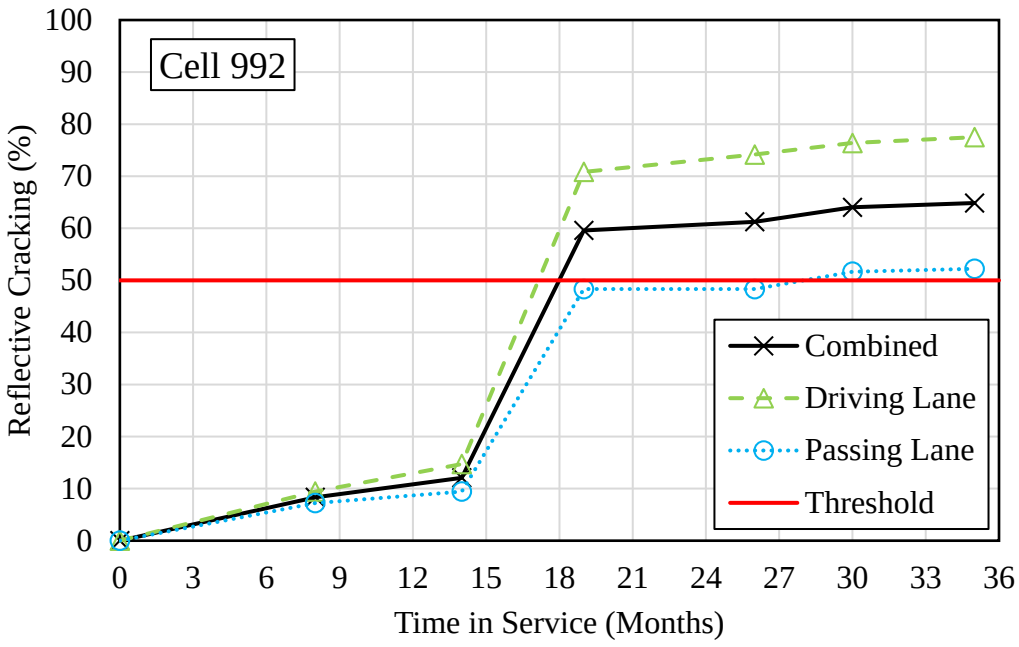

Figure 5-32 Cell 992 life curves.

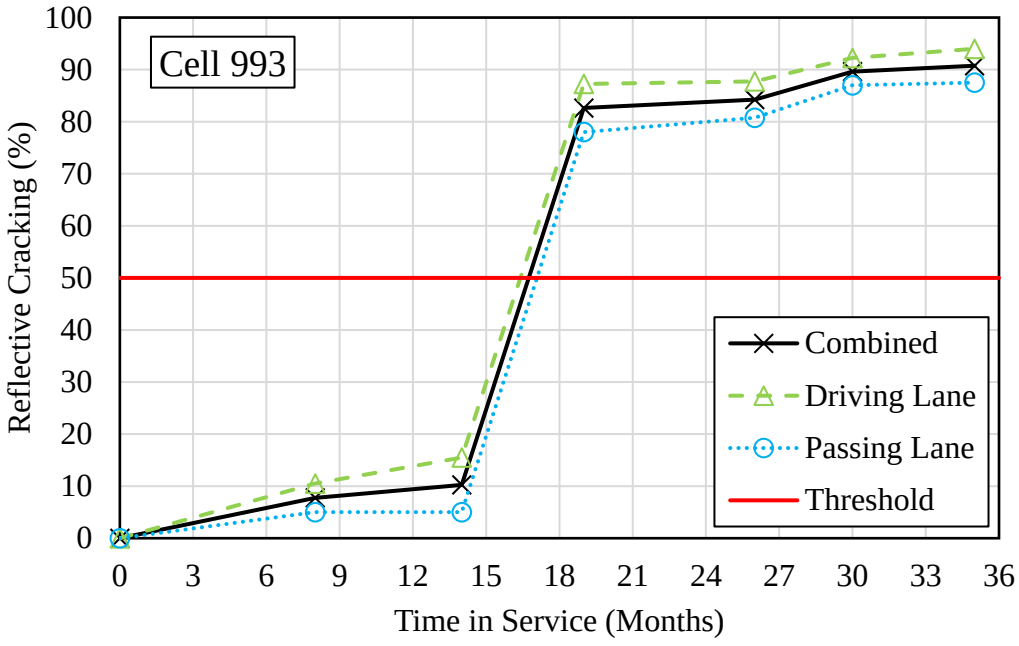

Figure 5-33 Cell 993 life curves.

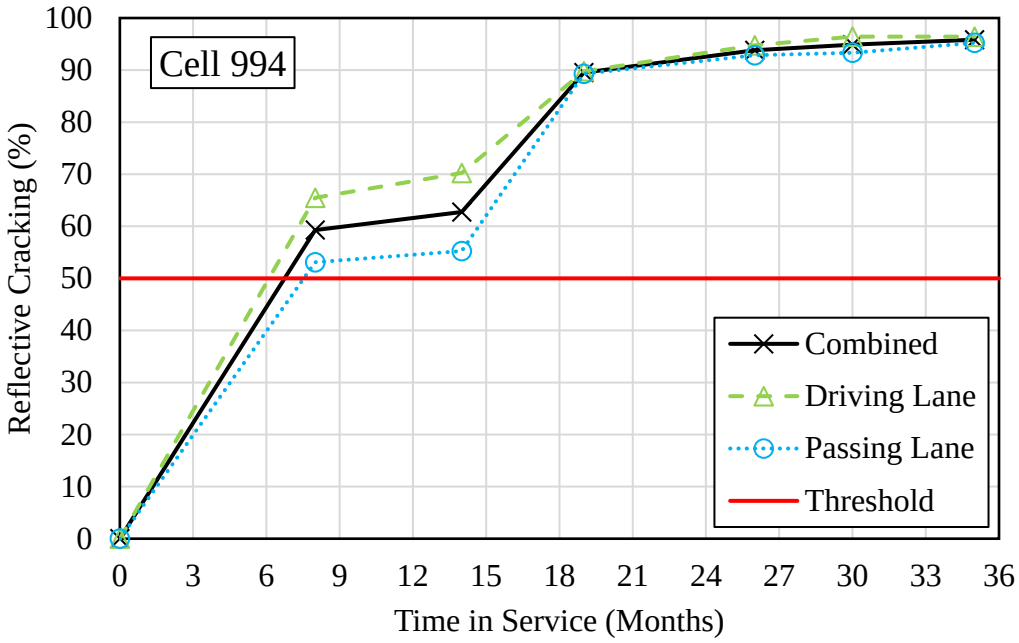

Figure 5-34 Cell 994 life curves.

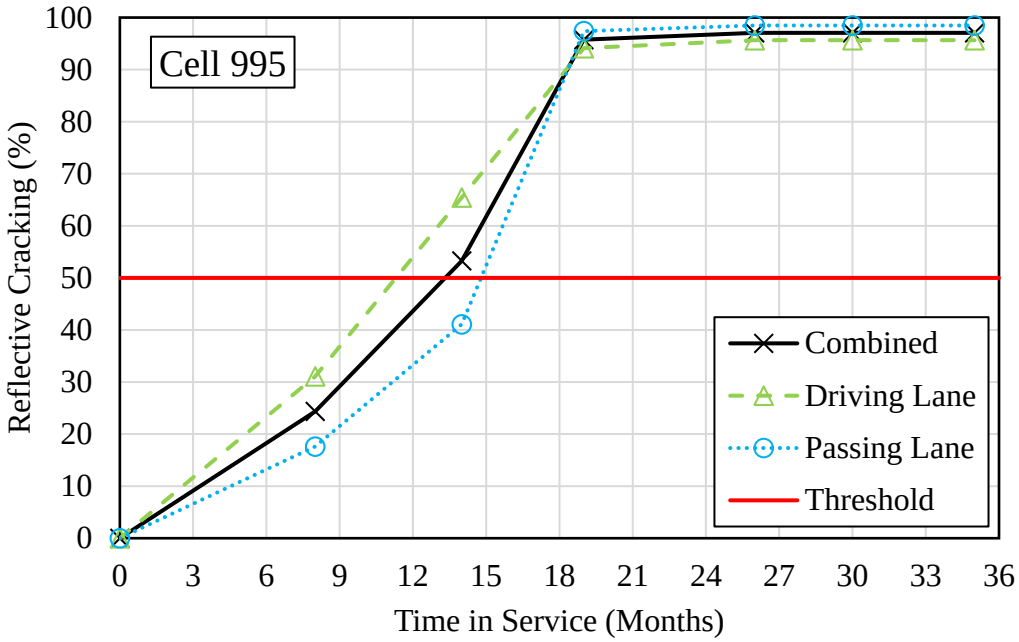

Figure 5-35 Cell 995 life curves.

5.11 Chapter Summary

This chapter summarizes monitoring efforts and field performance results of MnROAD test cells 984-995. Field test sections have been subject to approximately 816,000 flexible equivalent single axle loads (ESALs) or 1,165,000 rigid ESALs from the time of construction (September 2017) to May 2020. Two field performance indices (AvgRC and RCTotal) were presented and recommended to quantitatively compare reflective cracking performance of field sections while taking into account the rate of cracking, onset of cracking, variable pavement structures and service life durations. In general, thicker asphalt concrete overlay sections (4 inches total thickness) such as Cell 987 and in-situ density sections (except Cell 991) are the best performers. An increase in dielectric constant was observed among all test sections and there does not appear to be any concern of over densification of the in-situ density test sections (Cells 988-991) thus far. Discrepancy exists in ranking of test sections based on serviceability (IRI) versus reflective cracking performance. In general, the PCI ratings following ASTM D6433-20 indicate that test sections are in good condition after 3-years of service with very little distinction between them using PCI (majority of reflective cracks to date are low severity). As a result, the development of performance life curves for MnROAD overlay sections will use the percent reflective cracking (%RC) rather than PCI rating in order to differentiate overlay options within the decision tree tool.

6. CHAPTER 6

PERFORMANCE SIMULATION AND PREDICTION METHODS

6.1 Chapter Introduction

As part of this dissertation work, predictions models with as-built properties comparable to the 12 MnROAD AC overlay test sections were developed as well as additional overlay models with different pavement structures (Number of lifts, total thickness and varying combination of asphalt mixtures). Models were constructed using the National Cooperative Highway Research Program (NCHRP) 1-41 model (now built into AASHTOWare® Pavement ME Design™ software) and commercial finite element software Abaqus®. The main motivation behind conducting this modeling effort was to increase the number of overlay options that may be included in the overlay decision tree tool beyond the 12 MnROAD test sections. With limited resources and construction constraints, pavement performance prediction using finite element analysis (FEA) is an effective alternative to assess overlay designs and material selections beyond those constructed in form of actual full scale monitored pavement sections.

Model inputs were based on laboratory measured material properties (Chapter 4) and simulation results were compared with initial reflective cracking performance data available from MnROAD test sections (Chapter 5). Parametric evaluation was performed to expand the datasets that compare overlay material types, structures and PCC pre-treatment against reflective cracking performance. The expanded dataset that includes both the field performance data from MnROAD test cells, as well as results of calibrated model outputs, is used in development of overlay performance curves within the decision tree tool to screen potential overlay designs.

The two different modeling systems and approaches (a mechanistic-empirical pavement design and analysis system, and a cohesive zone fracture model based composite pavement finite element model with critical cracking phase loading) were utilized in this dissertation study to explore MnROAD test sections long term predicted pavement performance as well as investigate different overlay designs (thickness and asphalt material combination). Table 6-1 summarizes potential considerations when selecting which modeling approach is most appropriate to use based on the intended research modeling objective, as well as some key advantages and disadvantages of each software.

Table 6-1 Predictive modelling comparison.

	AASHTOWare Pavement ME Design	Finite Element Analysis (ABAQUS)
Ability to convert mechanistic measures into pavement distresses and serviceability measures (e.g. transverse cracking, rutting, IRI, etc.) through use of calibrated transfer functions.	**X**	
Predicted mechanical response (e.g. stress, strain, displacement, etc.)		**X**
Long-term pavement performance predicted	**X**	
Advanced mechanistic modeling of fracture process zone		**X**
Post processing of predicted results required		**X**
Ability to manual adjust thermal loading history and modelled thermal loading scenarios		**X**
Model development intensive		**X**
Analysis run time intensive		**X**
Ability to easily model different traffic spectrums and loading configurations	**X**	
Ability to model asphalt layers as viscoelastic, other loading conditions, and pavement boundaries (e.g. friction between layers).		**X**
User interface (UI) for conducting pavement specific analysis is more straightforward	**X**	
Relies on Miner's Law of cumulative damage and as a result can simulate progression of distresses along with combination of traffic and environmental loading effects (e.g. subsurface moisture changes)	**X**	

In the following subsections, detailed information on each modeling approach (FEA and Pavement ME) adopted in this study along with predicted results from each software's are presented. Next, a three-way comparison of results from FEA, Pavement ME and field

performance is provided. Finally, discussion on the two different modeling effort undertaken in this dissertation and their respective contribution is given.

6.2 Finite Element Analysis

In modeling of AC overlays, it is paramount to ensure proper translation of field information to relevant simulation parameters to achieve accurate pavement model predictions. In development of a finite element (FE) model, it is necessary that the geometry, in-situ material properties, climatic and traffic conditions are correctly translated to the model. Previous research conducted by Paulino et al. (2006), Dave et al. (2010), Ahmed et al (2013) and Dave et al. (2018) demonstrating an effective modeling framework was used in the present study in modeling of asphalt concrete overlays to predict reflective cracking [47][50]. In terms of modeling crack nucleation, initiation, propagation within the fracture process zone, the Cohesive Zone Model (CZM) was adopted as a simple, yet powerful and computationally efficient phenomenological model. CZM allows for spontaneous crack nucleation, crack branching and fragmentation, as well as mode-I and mixed-mode crack propagation without an external fracture criterion.

Key attributes of the FE model included finite element mesh, constitutive models for material behavior, boundary conditions, loading conditions and post processing of results. In order to achieve computational efficiency, graded mesh schemes were utilized with smaller size elements used in the area of interest with higher gradients of stresses, strains and deformations. Meanwhile, transition elements were used to go from smaller to larger elements sizes moving away from the area of interest. To model bulk material behavior at low and intermediate temperatures the generalized Maxwell model was adopted to represent the relaxation modulus of the viscoelastic AC material. For the remaining layers of the FE model, linear elastic material properties can be reasonably assumed. Another important material property required to model AC undergoing

thermal and mechanical loading (causing thermal straining), is the coefficient of thermal expansion and contraction. Interaction properties between layer surfaces in the model were considered using frictional behavior allowing for sliding and shear traction translation. Lastly, infinite elements were used at the boundary of the finite element domain to represent the semi-infinite nature of the soil and subgrade.

6.2.1 Fracture Model

A cohesive fracture model approach was adopted in this study because of its ability to simulate cracking in asphalt concrete materials as demonstrated by Song et al. in 2006 [51]. Due to the large fracture process zone in asphalt concrete, the Linear Elastic Fracture Mechanics (LEFM) approach may not be a suitable method to predict damage. Challenges such as the highly nonlinear stress and strain fields within the fracture process zone near the crack tip due to asphalt heterogeneity and the need to model cracking of the entire paving structure as a moving boundary problem led researchers to adopt a cohesive fracture model. Figure 6-1 provides an illustration of the fracture process zone highlighting the crack tip region and the cohesive zone (where softening and cracking occurs leading to the formation of a macro crack).

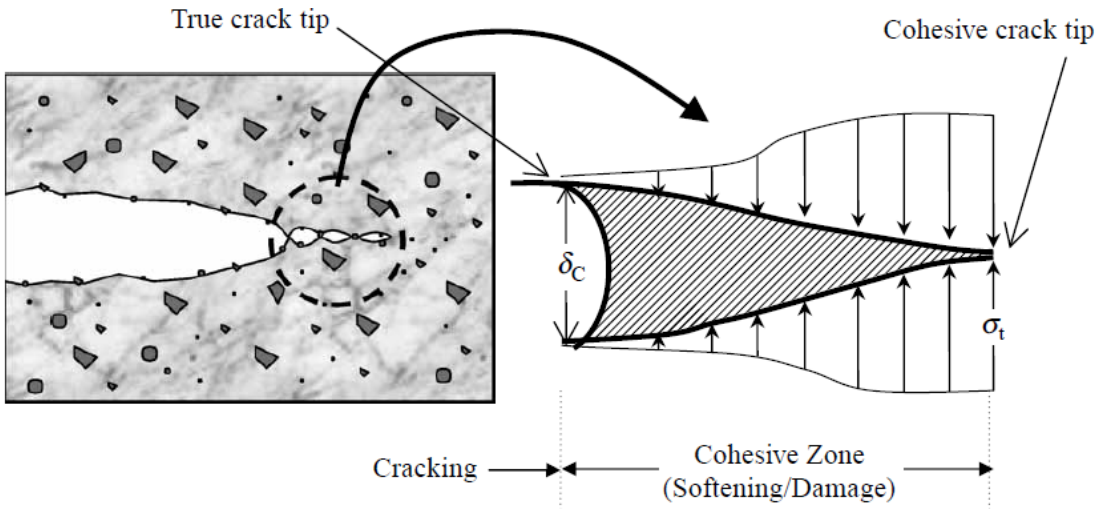

Figure 6-1 Example of crack tip and fracture process zone [48].

The cohesive fracture approach assumes that as a material starts to undergo loading, it remains undamaged until the material along the crack path reaches its tensile strength (σ_t), the displacement jump ($\Delta\delta$) corresponding to the tensile strength is indicated as softening initiation displacement (δ_s). The material then undergoes softening until $\Delta\delta$ reaches the critical displacement jump (δ_c), where complete separation of materials occurs resulting in zero load carrying capacity along the crack path and formation of a macro crack. Figure 6-2 provides a schematic of the bilinear cohesive zone model used in this study and Table 6-2 summarizes the corresponding fracture properties of the various overlay materials. DCT testing data provided the necessary fracture energy values while peak load values from fracture testing were used to estimate tensile strength using the IlliTC software. For the UTBWC mixture, fracture energy and peak load were determined using the CT test. The lack of lab measured fracture properties for the PASSCR mixture (as well as lack of sampled material) required the estimate of fracture energy and tensile strength for Cell 993 based on readily available properties from similar mixtures used by New Hampshire Department of Transportation [52].

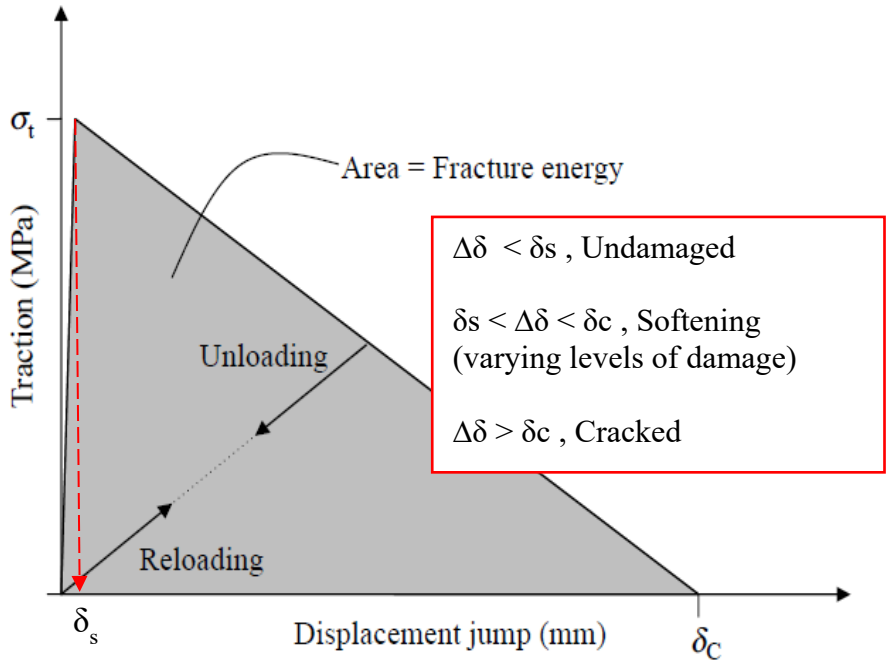

Figure 6-2 Example of bilinear cohesive zone model damage criteria [48].

Table 6-2 Fracture properties of overlay mixtures.

Mix Name	Test Temperature (°C)	Fracture Energy (J/m^2)	Tensile Strength (MPa)
SPWEA440E	-21.4	449	5.87
SPWEB440E	-21.4	491	5.66
SPWEB430E	-21.4	510	5.73
SPWEB450E	-21.4	477	5.19
SPWEC440E	-21.4	510	6.05
SPWED430I	-21.4	572	6.46
SPWED440E	-21.4	466	5.69
UTBWC	-24	518	1.85

6.2.2 Material Properties

It is well established that asphalt concrete is a viscoelastic material, especially at intermediate and low temperatures. To model bulk material behavior at low temperatures, the

generalized Maxwell model was adopted to represent the relaxation modulus of asphalt concrete. The relaxation moduli used in this study were obtained though interconversion from complex modulus data following the AASHTO T 342 specification (Chapter 4). For reference, the functional form of the generalized Maxwell model is provided in Equation 21 and a summary of the viscoelastic material inputs including Prony series parameters and Williams-Landel-Ferry (WLF) time-temperature shift factors by mixture type are provided in Appendix B.1

$$E(\xi) = \sum_{i-1}^{M} E_i[\exp(-\xi/\tau_i)] \quad \text{Eqn. 21}$$

Where;

E_i =Elastic coefficient of the spring in i^{th} Maxwell unit

Relaxation time of i^{th} spring-dashpot pair, $\tau_i = \eta_i / E_i$

η_i = Viscosity of i^{th} dashpot

Reduced time, $\xi = t/a_T$

t = time

a_T = Time-temperature shift factor

Another important material property required to model HMA overlay pavement structures undergoing thermal and mechanical loading (causing thermal straining), are the coefficient of thermal expansion and contraction (CTEC) for each mixture and the PCC layer. Table 6-3 provides a summary of the CTEC values used in this study by mixture type. The values for asphalt mixtures were estimated using the CTEC prediction equation that is part of the Pavement ME software. This equation utilizes asphalt mixture volumetric information to estimate CTEC.

Table 6-3 Coefficient of thermal expansion and contraction.

Mixture Name	CTEC (mm/mm/ºC)
SPWEA440E	2.29E-05
SPWEB440E	2.34E-05
SPWEB430E	2.30E-05
SPWEB450E	2.56E-05
SPWEC440E	2.21E-05
SPWED430I	2.82E-05
SPWED440E	3.00E-05
UTBWC	2.5E-05
PCC Layer	1.00E-05

For all PCC, granular base and subgrade material layers, linear elastic material behavior was assumed and typical values for elastic modulus and Poisson's ratio by material type are provided in Table 6-4. The base and subgrade properties were estimated from the MnPAVE software using late spring seasonal values to simulate a critical condition.

Table 6-4 Elastic material properties.

Layer/Mix Type	Elastic Modulus (MPa)	Poisson Ratio
PCC	20,684	0.22
Granular Base	156.4	0.4
Subgrade	44.2	0.45

6.2.3 Finite Element Mesh and Boundary Conditions

In this dissertation study to reduce simulation time of FE models, a two-dimensional (2D) model assuming plane strain conditions was adopted. The in-plane stresses (x, y, and xy) are calculated, while the out-of-plane (or through thickness) z strain is assumed to be zero. In other words, the plane strain analysis assumption only allows strains in-plane to occur while constant through thickness z stresses are developed. This assumption is often used to simplify FE model structures with substantial thickness in one plane, which is often the case for pavement cross sections. Figure 6-3 shows a schematic of an asphalt concrete overlay on existing pavement structure located at MnROAD test facility consisting of a PCC, aggregate base and subgrade layer.

The superimposed plane (light blue box) in Figure 6-3 denotes the 2D simplification of pavement FE models.

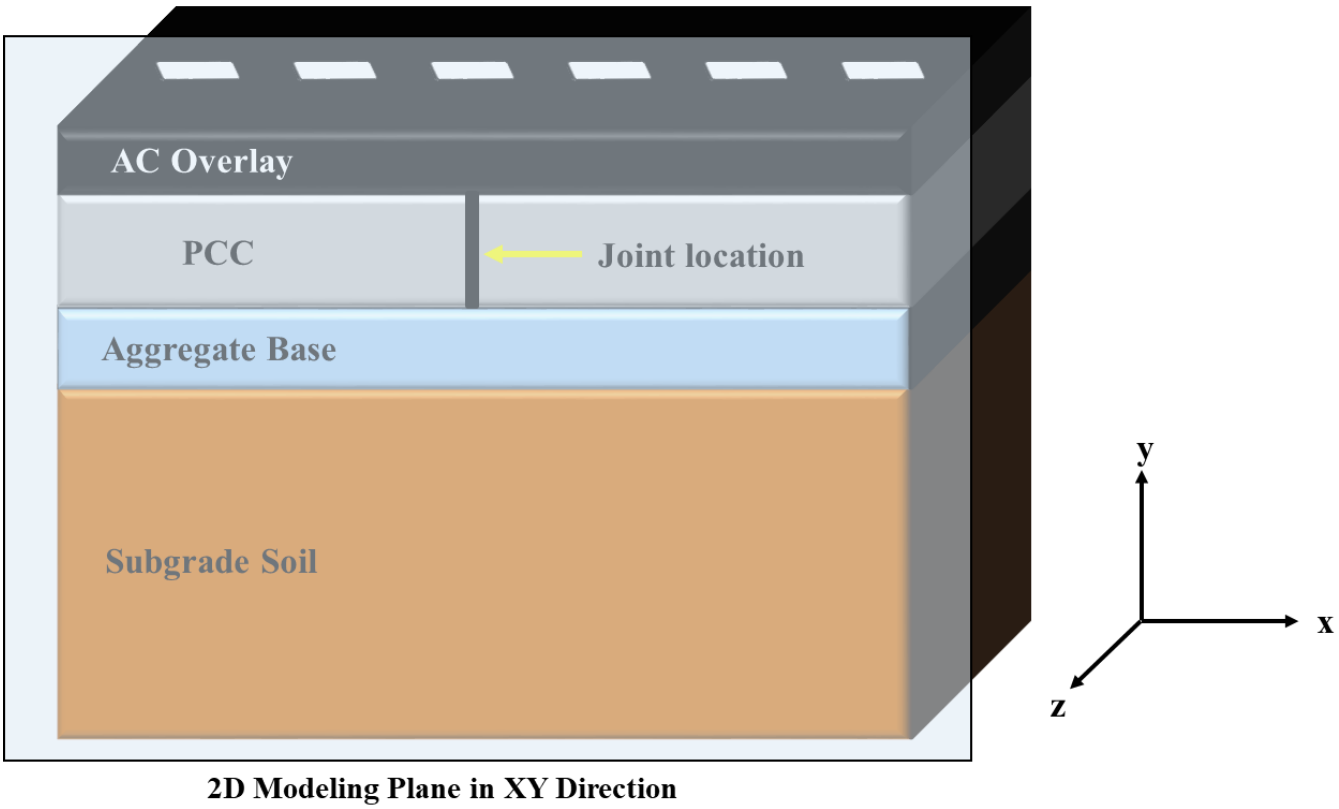

Figure 6-3 Schematic of asphalt concrete overlay on PCC pavement cross section and the simulated 2D modeling plane.

All models were constructed using four node quadrilateral (Q4) elements to represent the pavement structure. Figure 6-4 shows an example of the entire pavement cross section mesh while Figure 6-5 shows a close up of the mesh near the PCC joint location. To achieve computational efficiency a graded mesh scheme was utilized. Smaller size elements were used in areas of interest (e.g. near PCC joint location) with higher gradients of stresses, strains and deformations expected. As a reference, along the cohesive zone elements located directly above the PCC joint, the average element size was 0.7 mm (1/32 inches). Transition elements were then used to go from smaller to larger size elements moving away from areas of interest.

Boundary conditions of the pavement structure were addressed by using infinite elements to model the semi-infinite nature of soil subgrade material at the edge of the finite domain in the subgrade layer as shown in Figure 6-4. Interaction properties between layer surfaces in the model assumed finite frictional sliding. The shear behavior along the layer interfaces are simulated using frictional behavior, with a friction coefficient of 0.7 to allow for sliding and shear traction translation [53].

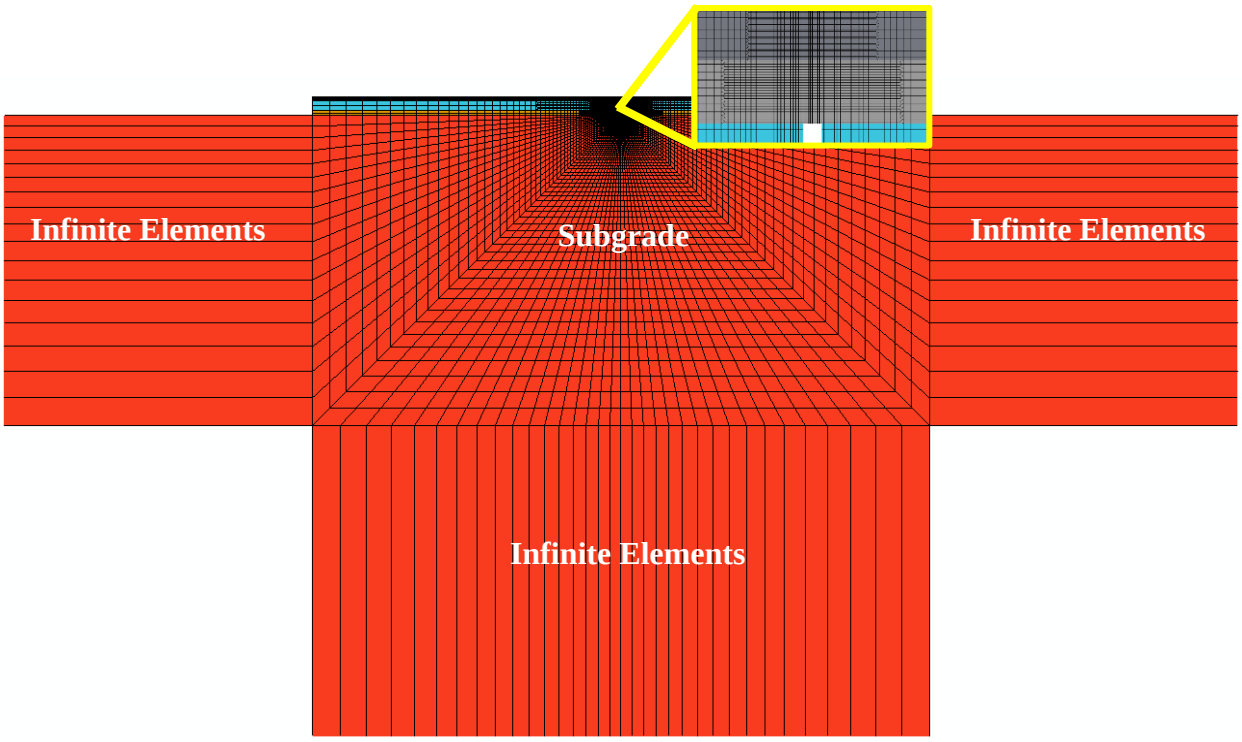

Figure 6-4 Example of mesh generated for finite element models.

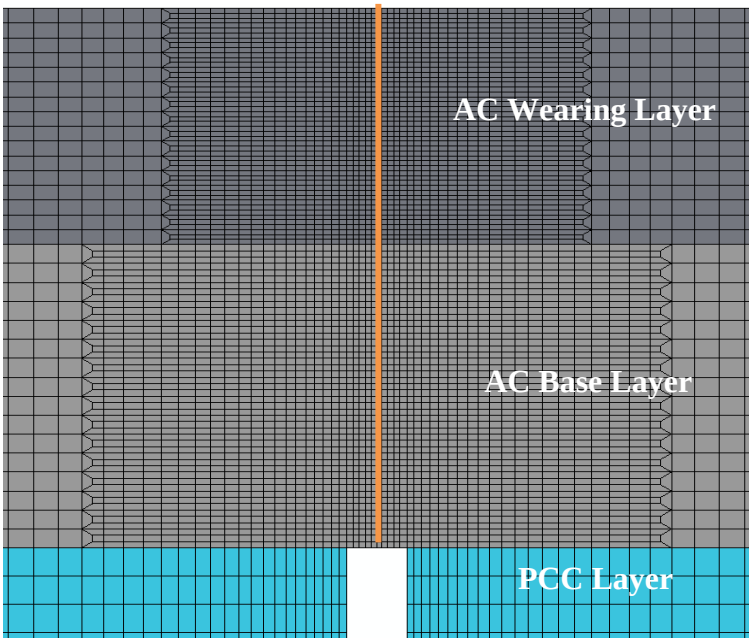

Figure 6-5 Zoomed-in mesh near PCC joint highlighting (orange line) the cohesive zone element locations.

6.2.4 Loading Conditions

Once the finite element mesh was generated and all necessary material properties inputted, a gravity load was imposed. The gravity load utilizes the bulk density of each material type to impose the self-weight conditions. The next step was to apply a thermal load, and then if the overlay was able to withstand thermal loading without a fully formed reflective crack, then a tire load was added directly above the PCC joint location. In the finite element analysis conducted in this project, a critical cracking conditions approach was adopted. This approach has been used by multiple researchers in past to simulate thermal and reflective cracking in asphalt and composite pavements [48],[53]-[55]. The use of a critical cracking conditions approach is necessary when using a full-scale finite element model with highly non-linear and history dependent material responses (such as viscoelasticity and fracture response in asphalt mixtures and frictional interfaces between pavement layers) to ensure realistic simulation times. The approach utilizes simulation of a worst-case loading condition, as manifested by the lowest asphalt mixture in-

service temperatures (when material has high stiffness, low relaxation capability, high brittleness and very high thermal stresses).

Pavement temperature variations (both in time and depth) were computed using the Enhanced Integrated Climate Model (EICM), which is also used in the AASHTOWare® Pavement ME Design™ software. Essentially, EICM uses various factors (e.g., air temperature, sunshine, precipitation) to generate temperature profiles as a function of time and depth, providing a means to generate historical critical thermal loading events. For each of the pavement cross section types (6 total for the MnROAD cells studied herein), separate EICM simulations were performed to obtain asphalt concrete and PCC temperatures profiles for a 10-year duration. Figure 6-6 provides an example of the AC and PCC layer surface temperatures over 10 years for cell 995 generated using the EICM model.

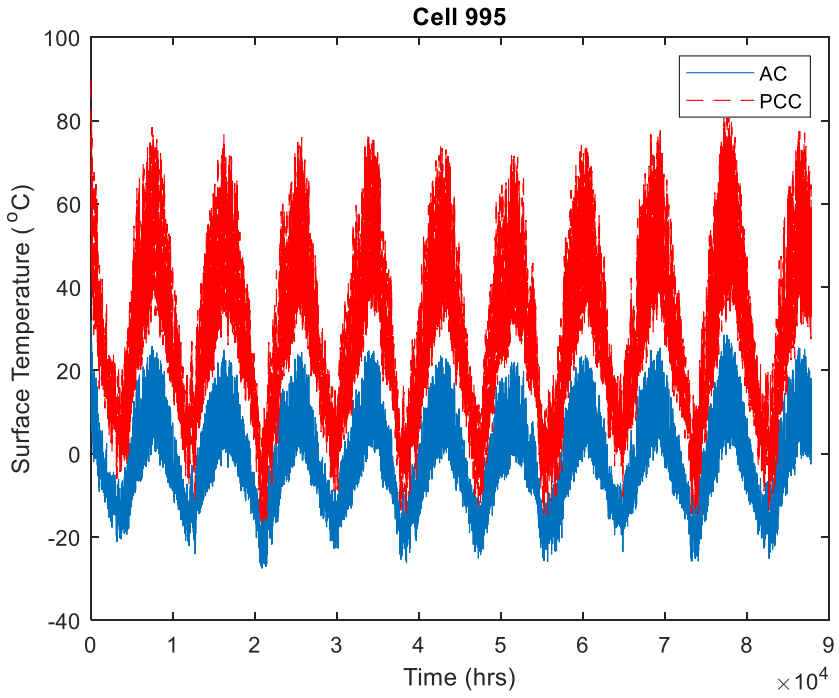

Figure 6-6 Example of surface temperature output for AC and PCC layers in test cell 995 from EICM.

To determine the critical conditions for thermal loading simulation, the lowest surface temperature experienced in the AC layer and the time it occurred during the simulation was identified as shown in Figure 6-7. This approach for identifying the critical cracking conditions builds upon previous work by Dave et al. [48], [50], [55], [56]. These previous approaches have shown very good correlation between the model predictions and field cracking performance for accelerated reflective cracking experiments as well as for MnROAD test cells.

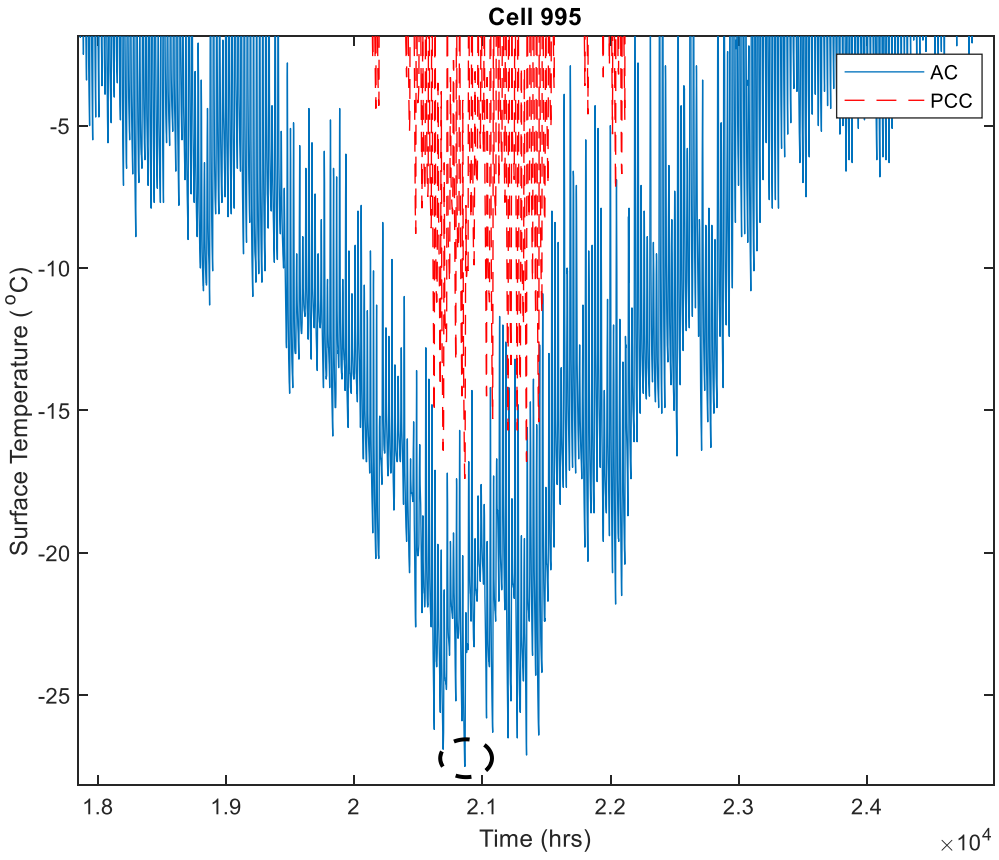

Figure 6-7 Identifying lowest surface temperature in AC layer (shown with dashed circle).

Once this historical critical condition was identified, approximately 16 hours prior (cooling period) and 7 hours after (warming period) this point were simulated for a total of 24 hours (1 day) of thermal loading in each model. During the analysis period, nodal thermal conditions are

imposed in hourly increments (steps). The main reason for simulating the "warm up" time period is to allow for the PCC temperature (red line) to reach its lowest value as there may be a time delay in reaching the peak low temperature in PCC with respect to pavement surface temperature, this can be seen in Figure 6-8 for cell 995.

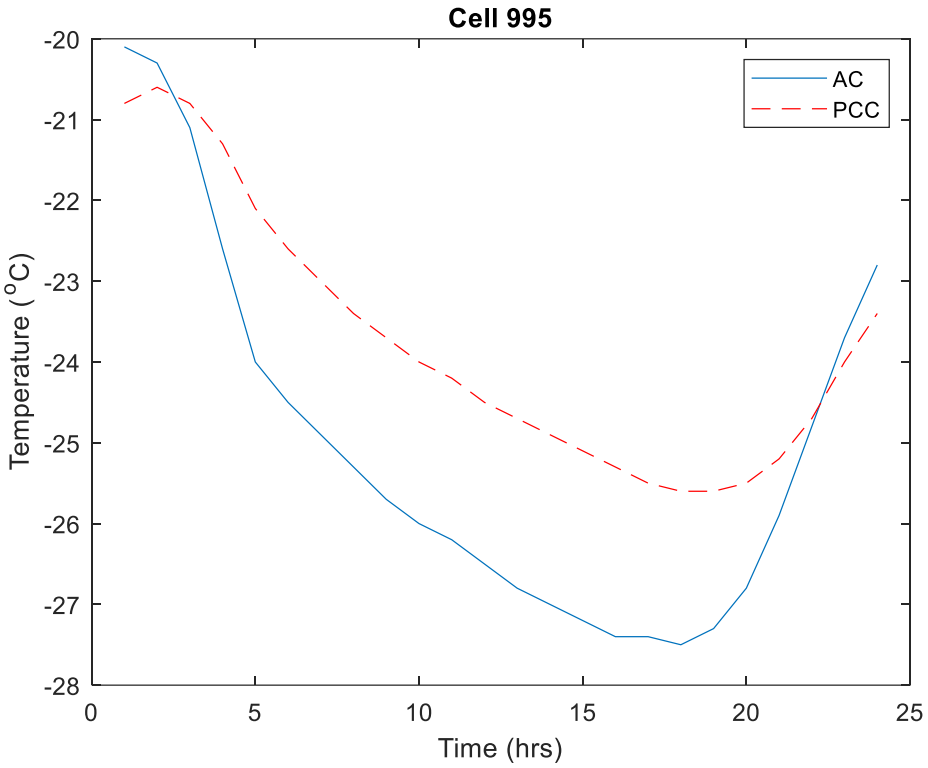

Figure 6-8 Example of thermal loading cycle for cell 995 during 24 hour detailed analysis.

For all models that were able to withstand the historical critical thermal loading event without experiencing a fully formed reflective cracking immediately above the PCC joint, a tire load was applied directly above the PCC joint location. The timing of this tire load was determined by review of the displacement along the cohesive zone elements (along the crack path). The tire load was applied immediately following the condition when maximum cohesive zone element displacements occurred from thermal loading. A 9,500 lbs. tire load with 120 psi tire pressure was

applied for a time increment corresponding to 70 mph speed. Detailed tire loading information can be reviewed in Table 6-5.

Table 6-5 Tire loading input.

Tire Loading		
Load Type	Distributed	
Pressure	0.8274 MPa	120 psi
Load	42258 N	9500 lbs
Tire Radius	127.5 mm	5.02 in.
Load Time Increment	0.008 sec	

In addition to the historical critical thermal loading event, thermal loading data from instrumented field test sections was used to develop supplementary FE models. Three pavement test sections (Cell 984, 989 and 992) with varying pavement structures in terms of number of lifts and total thickness were instrumented at the time of overlay construction. A similar process as outlined above was followed to identify the critical low surface temperature in the AC and PCC layers respectively. Care was taken in selecting the thermal loading simulation duration to account for the time lag in the PCC layer reaching the lowest temperature. As an example, Figure 6-9 shows a time series plot of thermocouple data from the three instrumented test sections from November 2017 to April 2018. It should be noted that, due to instrumentation recording issues in Cell 989, the critical thermal loading event over the winter of 2017-2018 was not available (missing data at bottom of AC (blue line) and top of PCC (red line) layers). As a result, the critical thermal loading event was reconstructed based on available AC surface temperature data and average temperature offset with depth values from the critical thermal loading event over the winter period in 2017, 2019 and 2020.

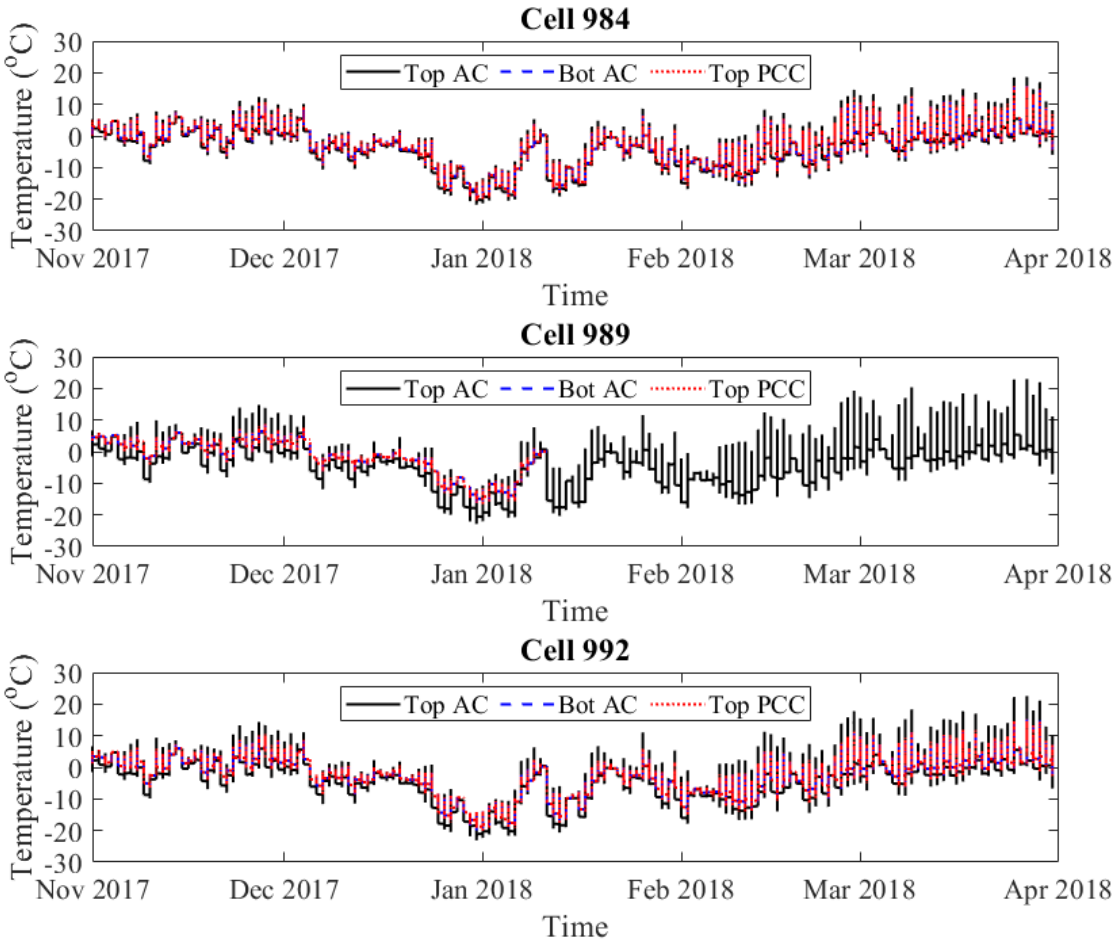

Figure 6-9 Time series plot (daily max. and min.) of thermocouple data from November 2017 to April 2018.

Taking a closer look at the variation of temperature with depth in a given pavement structure, Figure 6-10 shows a week's worth of temperature data for a thin (Cell 984) and thick (Cell 989) overlay cross section. A temperature gradient can be clearly seen as the top of the AC layer temperature varies from the bottom of the AC and subsequently the top of PCC layer. There is close agreement between the bottom of AC (blue dashed line) and the top of PCC layer (red dotted line). As expected, the difference in temperature from the top of the pavement structure to the bottom is greater for the thicker pavement section. However, the difference in temperature gradient within the pavement structure is not constant with time. For example, Cell 989 on January

1st shows roughly a 5 ˚C difference from the top to the bottom of the AC layer and the PCC layer. However, as the temperature remained cold over the course of the week, by January 7th the difference in temperature gradient had decreased to less than 1˚C. This information is particularly important when modeling the response of asphalt layer separately from the PCC layer and the differential movement due to temperature loading. The insulating effects of thicker overlays in PCC is also evident in Figure 6-10, the peak-to-peak 24 hour temperature variation for the week's duration for PCC is approximately 9 ˚C for Cell 984 versus less than 4 ˚C for Cell 989.

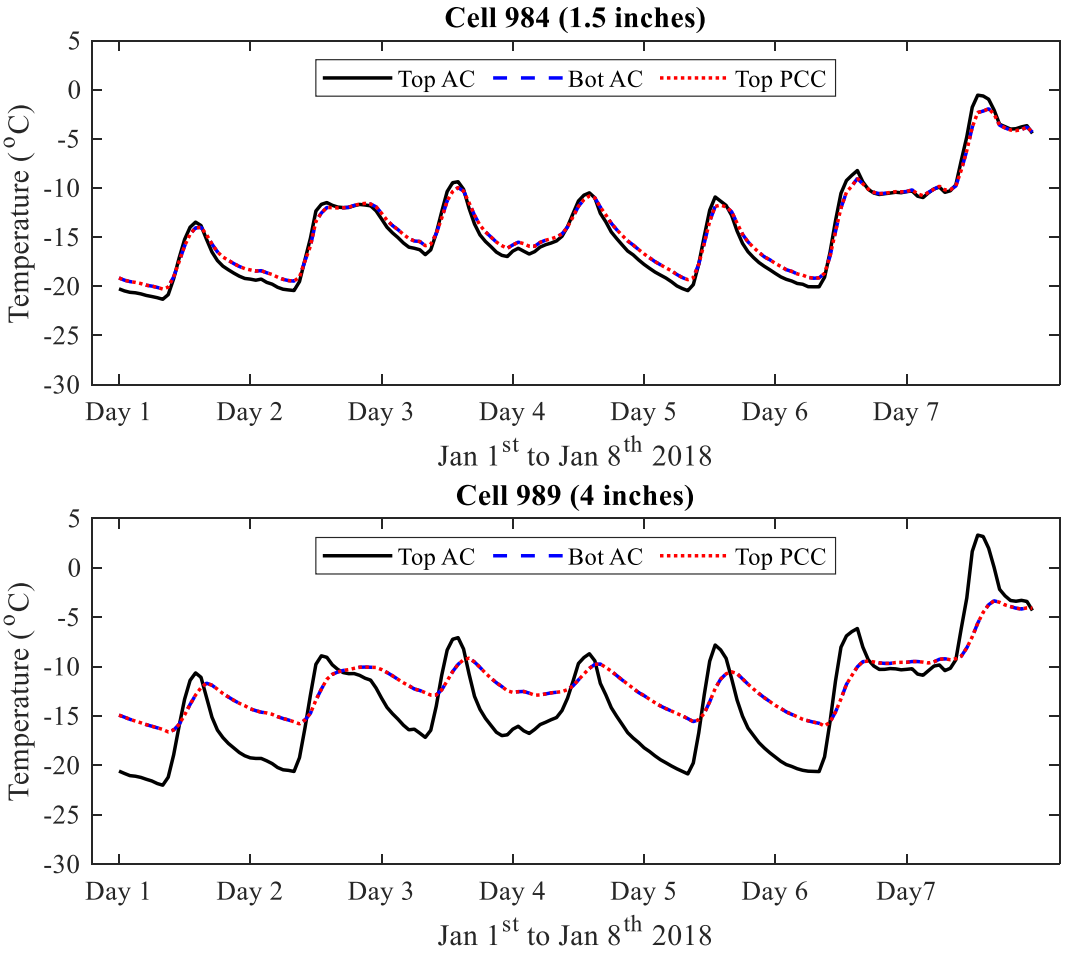

Figure 6-10 Temperature versus depth for week of January 1st - 8th, 2018 for Cell 984 and Cell 989.

Figure 6-11 summarizes the extracted thermocouple temperature data with respect to depth in the pavement structure for three instrumented test sections during the critical thermal event, defined as the lowest recorded pavement temperature. For all three-pavement structures, a total of 20 hours of thermal loading data was extracted based on when the lowest temperature was reached in both the AC and PCC layers and ensuring that sufficient cooling and warming periods are included in the thermal loading cycle. The dark blue line corresponds to the design interface depth of 304.8 mm (12 inches). Due to variability in construction of various layer thicknesses, it is hypothesized that the interface Cell 992 is actually lower as denoted by the light blue dashed line. The deepest thermocouple in Cell 992 was instrumented at the bottom of the PCC layer and was reported to be at a depth of exactly 304.8 mm, implying that the PCC- granular layer interface is slightly lower.

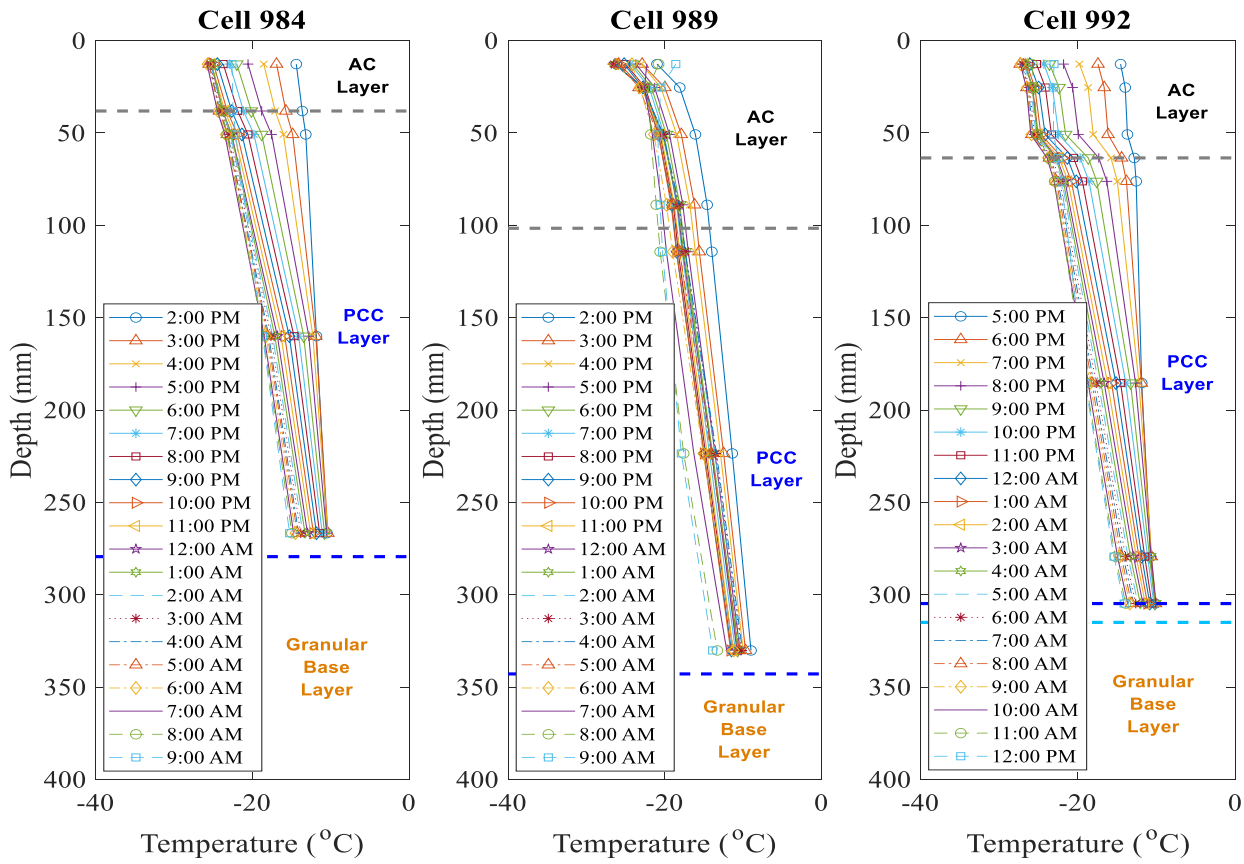

Figure 6-11 Thermocouple temperature data versus depth for instrumented test sections during.

The following subsection (6.2.5) will describe the post processing of FE model results from the EICM generated historical critical thermal loading event models and the select number of models with instrumented thermal loading data from MnROAD field sections.

6.2.5 Post Processing of Finite Element Results

Upon completion of the FE simulations, several post-processing techniques were used to extract key results from the model output and summarize the findings. As an example, Figure 6-12 shows a model undergoing thermal loading where a stress concentration region (red and gray contours) clearly develops in the overlay in the vicinity of the PCC joint. Effectively, horizontal

stresses are shown in the direction perpendicular to the direction of reflective crack formation. This is similar to observations made by Dave and Buttlar (2010) with respect to thermal reflective cracking in asphalt overlays [48]. Figure 6-13 shows a model undergoing thermal and tire loading with the stress concentration moving vertically upwards with the propagation of a crack. The tire load induces compression near the pavement surface (denoted by blue and black contours). Separation of cohesive zone elements is observed in the base course asphalt layer near the top of the PCC joint (denoted by white crack), as well as high stress concentration.

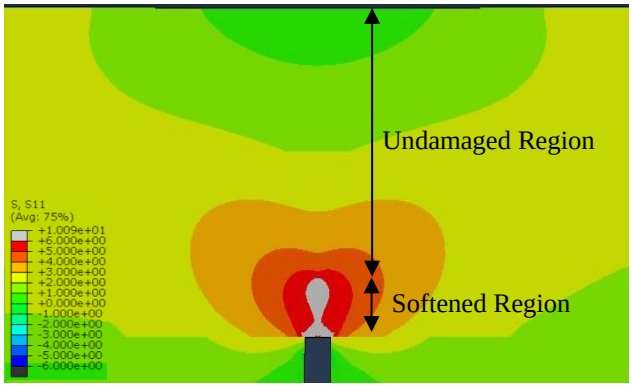

Figure 6-12 Stress concentration at crack tip due to thermal loading showing undamaged region and softened region.

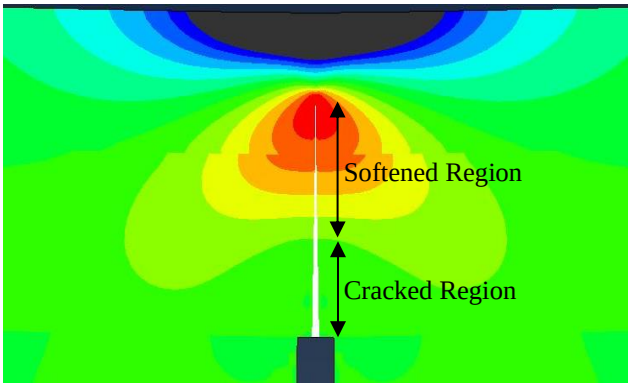

Figure 6-13: Stress concentration at crack tip due to combination of thermal and tire load showing softened region and cracked region.

To quantify the amount of damage along the crack path, two primary thresholds in the cohesive fracture model were utilized: (1) Softening initiation displacement (δ_s); and, (2) Critical displacement (δ_c). Use of these thresholds along with result from FEA along the cohesive zone elements provided three main outcomes for a given overlay:

(1) When the amount of displacement ($\Delta\delta$) at any point along the crack path was less than the δ_s value, the overlay was considered to be undamaged ($\Delta\delta < \delta_s$ shown in green).

(2) When displacement at any portion along the crack path exceed the δ_s value but was less than the critical displacement value associated with the development of a macro-crack (δ_c),

that portion of overlay was considered to be in a damaged or softened condition ($\delta_s < \Delta\delta < \delta_c$ shown in orange)

(3) When displacement values for a portion of the overlay exceeded δ_c, this portion is considered to be fully cracked ($\Delta\delta > \delta_c$, shown in red).

Figure 6-14 provides an example of the undamaged, softened and cracked cohesive elements as a percentage of overlay thickness corresponding to the stress contour results shown in Figure 6-12 and Figure 6-13 respectively.

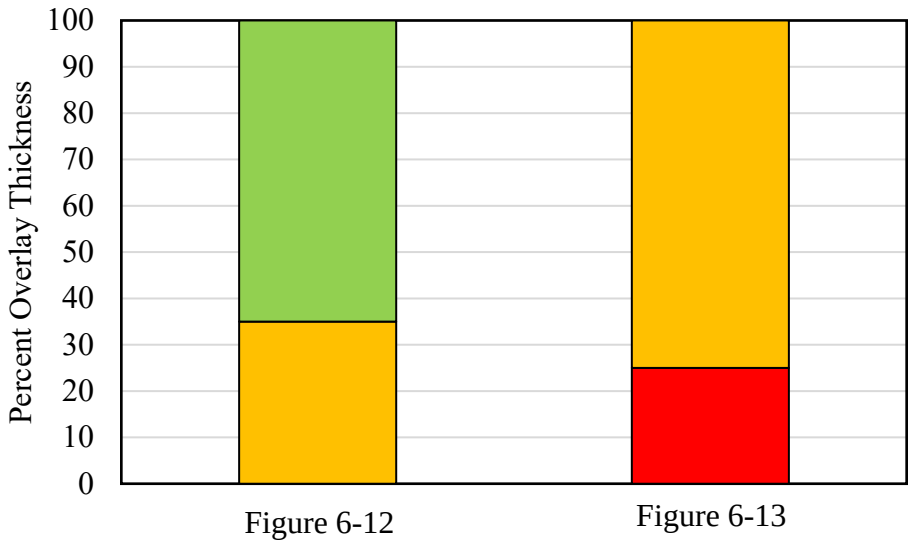

Figure 6-14 Finite element results broken down by cohesive fracture zones where undamaged is green, orange is in softening and red is cracked.

In order to differentiate further between the degree of damage when the portions of overlay are in a damaged state ($\delta_s < \Delta\delta < \delta_c$), FEA results were further post-processed to determine the displacement jumps along the crack path. Figure 6-15 provides sample FEA results showing the displacement jumps along the crack path after thermal and combined thermal and tire loading cases.

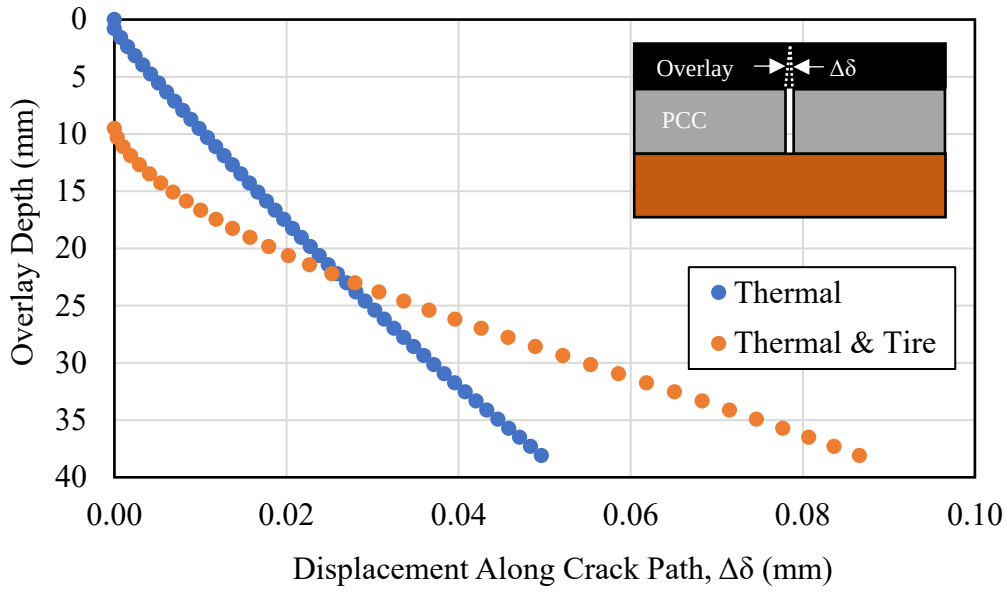

Figure 6-15 Damage along cohesive zone line under thermal and the combination of thermal and tire loading.

A damage ratio was calculated by taking the ratio of reported damage along the crack path (A) to the critical damage level (B), whereby the critical damage level represents a fully formed reflective crack. Figure 6-16 provides a schematic of the damage ratio concept where A and B are calculated using Equations 22 and 23 respectively.

$$Damage\ Area\ (A) = \int_0^t \delta\, dt \qquad \text{Eqn. 22}$$

Where;

t = thickness of overlay

δ = displacement along the cohesive zone elements

$$Critical\ Damage\ Level\ (B) = (\delta_c) * (Overlay\ Thickness) \qquad \text{Eqn. 23}$$

Where;

δ_c = Critical displacement where macro-crack forms for a given overlay mixture

Lastly, the damage ratio percentage (from 0 to 100) was computed using Equation 24.

$$Damage\ Ratio\ \% = \frac{A}{B} \quad \text{Eqn. 24}$$

Where;

A = Damage area calculated using Equation 22

B = Critical damage level area calculated using Equation 23

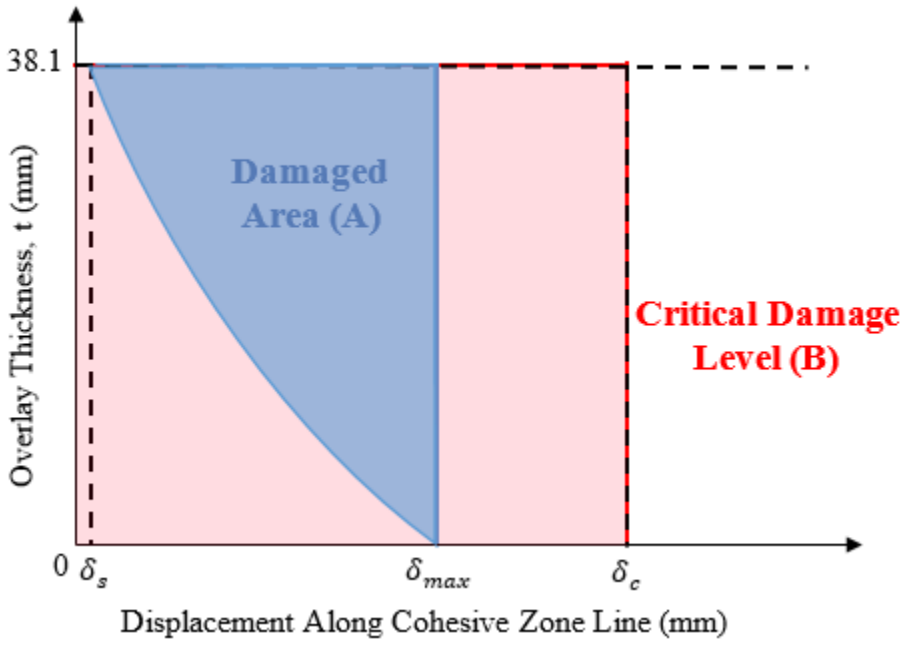

Figure 6-16 Schematic of damage ratio concept.

6.2.6 Finite Element Results for Historical Critical Thermal Event

Figure 6-17 summarizes the revised FE model results simulated using a historical critical thermal event determined from EICM. Solid color bars represent simulated results with thermal loading, while hashed bars show results with the combination of thermal and tire loading. Cell 993 was excluded from the FE model results presented below as viscoelastic material properties for PASSRC were not available.

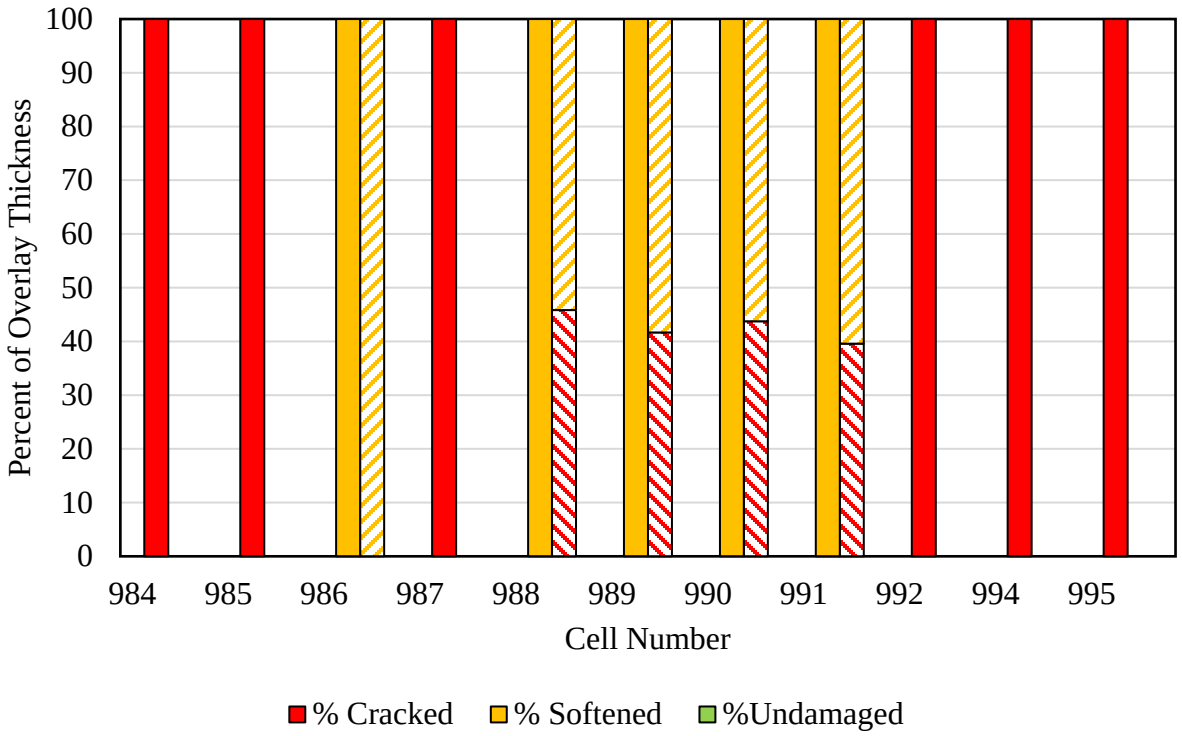

Figure 6-17 Finite element analysis results for models with historical thermal loading (solid color bar) and combination of thermal and tire loading (hashed bar).

All four in-situ density sections (Cell 988-991) and Cell 986 were able to withstand thermal loading and as a result a tire load was applied directly on top of the joint location. In-situ density test sections experienced cracking damage in the lower lift of the overlay with the addition of the tire load application. Cell 986 (44.45 mm overlay thickness, NMAS of 12.5 mm) was the only simulated test section to remain in the softening phase and not develop a fully formed macro crack with both thermal and tire loading. It can also be concluded that in general, thinner overlay sections performed worst with a fully formed macro crack along the entire thickness of the overlay after thermal loading (solid red bars).

Damage ratio results of all simulated models with thermal loading are summarized in Table 6-6, while Table 6-7 presents thermal and tire loading results. Damage ratio values equal to 100% represent overlays in which a fully-formed macro crack has occurred through the entire overlay

thickness. Test cells 984, 985, 987, 992, 994 and 995 were fully cracked after the thermal loading simulation. The remaining test sections were subjected to both thermal and tire loading and Cell 986 was the best performer (lowest damage ratio) overall with a damage ratio of 17.4%. Among the in-situ density test sections, Cell 989 was the best performer followed by Cells 990, 991 and 988.

The improvement to crack resistance due to the combination of material selection and overall pavement structure can be observed when comparing Cell 986 to other comparable test sections. The asphalt mixture in Cell 986 had a relatively higher fracture energy value (491 J/m^2) compared to other overlay mixtures and a greater overlay thickness (44.45 mm overlay thickness). These findings are in good agreement with field reflective cracking performance for Minnesota overlays as observed by Oshone et al. in 2019 [44]. For example, the difference between Cell 985 (fully cracked and uses SPWEB440E overlay mixture) and 986 (fully softened and uses SPWEB440E overlay mixture) is 6.35 mm (0.25 inch) extra of overlay thickness. The extra pavement thickness provides sufficient structure to resist thermal-reflective cracking potential and minimize the damage ratio from 100% (Cell 985) to 6.2% (Cell 986) for a critical loading scenario.

Table 6-6 Summary of thermal (historical critical event) loading damage ratio results.

Thermal Loading				
Cell #	Layer	Thickness		Damage Ratio (%)
		(in)	(mm)	
984	Wearing	1.5	38.1	100
985	Wearing	1.5	38.1	100
986	Wearing	1.75	44.45	6.20
987	Wearing	1.5	38.1	100
	Base	2.5	63.5	
988	Wearing	1.75	44.45	0.5
	Base	2.25	57.15	
989	Wearing	1.75	44.45	0.33
	Base	2.25	57.15	
990	Wearing	1.75	44.45	0.48
	Base	2.25	57.15	
991	Wearing	1.75	44.45	0.37
	Base	2.25	57.15	
992	Wearing	1.5	38.1	100
	Base	1	25.4	
994	Wearing	1.5	38.1	100
995	Wearing	0.75	19.05	100

Table 6-7 Summary of thermal (historical critical event) and tire loading damage ratio results.

Thermal and Tire Loading				
Cell #	Layer	Thickness		Damage Ratio (%)
		(in)	(mm)	
984	Wearing	1.5	38.1	Fully Damaged from Thermal loading
985	Wearing	1.5	38.1	Fully Damaged from Thermal Loading
986	Wearing	1.75	44.45	17.4
987	Wearing	1.5	38.1	Fully Damaged from Thermal Loading
	Base	2.5	63.5	
988	Wearing	1.75	44.45	56.2
	Base	2.25	57.15	
989	Wearing	1.75	44.45	51.2
	Base	2.25	57.15	
990	Wearing	1.75	44.45	51.9
	Base	2.25	57.15	
991	Wearing	1.75	44.45	53.9
	Base	2.25	57.15	
992	Wearing	1.5	38.1	Fully Damaged from Thermal Loading
	Base	1	25.4	
994	Wearing	1.5	38.1	Fully Damaged from Thermal Loading
995	Wearing	0.75	19.05	Fully Damaged from Thermal Loading

To illustrate the impact of thermal stress generation within a pavement structure, the damage ratio contributions from thermal, tire, and the combination of thermal and tire loading were compared. Simplified 3-step models were explored for the four in-situ density test sections (Cell 988-991) and simulated as follows:

1. An initial thermal load was applied to the model, equal to the coldest AC pavement temperature for a given overlay structure (critical thermal event temperature).
2. Apply gravity load to entire model.
3. Apply tire load on AC surface directly above PCC joint.

Model results (damage ratio) from the combination of thermal and tire loading where subtracted from the model results for the 3-step models to determine the contribution of damage from thermal loading at the critical thermal event temperature. Table 6-8 summarizes the calculated damage ratio values for each model under the three different loading scenarios. The contribution of thermal loading was approximately 79% the total damage ratio (thermal and tire). This finding emphasizes that for cold regions, such as Minnesota, damage from thermally induced loading comprises a significant portion of the damage ratio. As a result, it is important to consider thermal loading history in reflective cracking FE analysis of viscoelastic materials such as asphalt concrete.

Table 6-8 Summary of damage contribution at critical thermal event temperature.

Model Cell Number	Thermal and Tire Damage Ratio (%)	Tire (3-Step Model) Damage Ratio (%)	Thermal Δ Damage Ratio (%)
988	56.2	11.4	44.8
989	51.2	10.6	40.5
990	51.9	10.7	41.2
991	53.9	11.3	42.6

6.2.7 Finite Element Results for MnROAD Critical Thermal Event

Using the temperature versus depth profile data shown in Figure 6-11 from January 2018 (coldest thermal event recorded), thermal loading equations were developed and implemented into the respective FE models. Table 6-9 summarizes the damage ratio results for all applicable test sections under thermal loading only. Due to the relatively high cooling rates of the simulated thermal event (3˚C/hr. or higher), all models reported fully formed macro cracks along the entire overlay thickness (100% damage ratio). This is not entirely surprisingly as: (1) field distress surveys from this winter period reported a sharp increase in reflective cracking amounts across all test sections, and (2) FE models are set-up to simulate critical loading events with a degree of built-in factor of safety that utilizes worst-case scenario approach. The AvgRC performance index was generally the highest between distress surveys that overlap with this specific thermal loading event (Figure 5-11, April 2019 survey date). This observation reinforces the importance of thermal loading in formation of reflective cracks in AC overlays on PCC pavement continues to appear as a dominant mechanism that needs to be incorporated in overlay design and material selection criteria.

Table 6-9 Summary of thermal loading damage ratio results from thermocouple data.

Thermal Loading				
Cell #	Layer	Thickness		Damage Ratio (%)
		(in)	(mm)	
984	Wearing	1.5	38.1	100
985	Wearing	1.5	38.1	100
987	Wearing	1.5	38.1	100
	Base	2.5	63.5	
988	Wearing	1.75	44.45	100
	Base	2.25	57.15	
989	Wearing	1.75	44.45	100
	Base	2.25	57.15	
990	Wearing	1.75	44.45	100
	Base	2.25	57.15	
991	Wearing	1.75	44.45	100
	Base	2.25	57.15	
992	Wearing	1.5	38.1	100
	Base	1	25.4	
994	Wearing	1.5	38.1	100

6.2.8 Varying LTE and Voids under PCC Slab

As part of a parametric analysis of model input and assumptions, FE model simulations with varying LTE and voids under the PCC slab were conducted. The purpose behind performing additional FE model simulations was to gain a better understand of the impact of initial LTE and voids under PCC slabs on predicted reflective cracking performance. To evaluate varying LTE level in the existing PCC pavement, falling weight deflectometer (FWD) test simulations were performed in FE Software. This was accomplished by building an FE model that consists of PCC, granular base, subgrade and infinite elements. A tire load was located at the edge of one side of the PCC joint and the ratio of unloaded to loaded deflection calculated. Based on measured LTE from MnROAD test sections prior to overlay construction (Table 6-10), an iterative process followed to determine the appropriate stiffness (K-value) of spring elements (acting as dowel bars) between PCC slabs (Table 6-11). The goal was to determine LTE values similar to those reported

in the driving, passing and average of both lanes. In Table 6-11, highlighted iteration rows correspond to target LTE levels presented in Table 6-10 for the driving, passing and average of both lanes.

Table 6-10 Average load transfer efficiency (LTE) in MnROAD test sections prior to overlay construction.

	LTE (%)
Driving Lane	33
Passing Lane	61
Average of lanes	47

Table 6-11 Finite element simulations with varying load transfer efficiency (LTE).

Individual K-Value (N/mm)	K*Num. of Spring Elements (N/mm)	Ratio (unloaded/loaded)	LTE (%)
-	-	0.190	19.0
0.005	0.24	0.339	33.9
0.01	0.48	0.428	42.8
0.02	0.96	0.449	44.9
0.023	1.10	0.464	46.4
0.025	1.2	0.498	49.8
0.05	2.4	0.539	53.9
0.1	4.8	0.612	61.2
0.2	9.6	0.712	71.2
0.5	24	0.843	84.3
1	48	0.861	86.1
10	480	0.979	97.9
100	4800	0.998	99.8

Next, a series of FE simulations with varying amounts of voids under the PCC joint location to represent scenarios where pumping and joint faulting may have occurred in the field. To simulate voids underneath the PCC slab, the modulus of granular base material directly under and on either side of PCC joint was reduced by 10%. The “damaged” granular material property represents a void with an extent of 1ft (≈ 300 mm) to the left and right of the joint and

approximately 0.23 to 0.31 inches (6-8 mm) deep. Figure 6-18 shows an example of the extent of the simulated void directly under the PCC slab highlighted in orange.

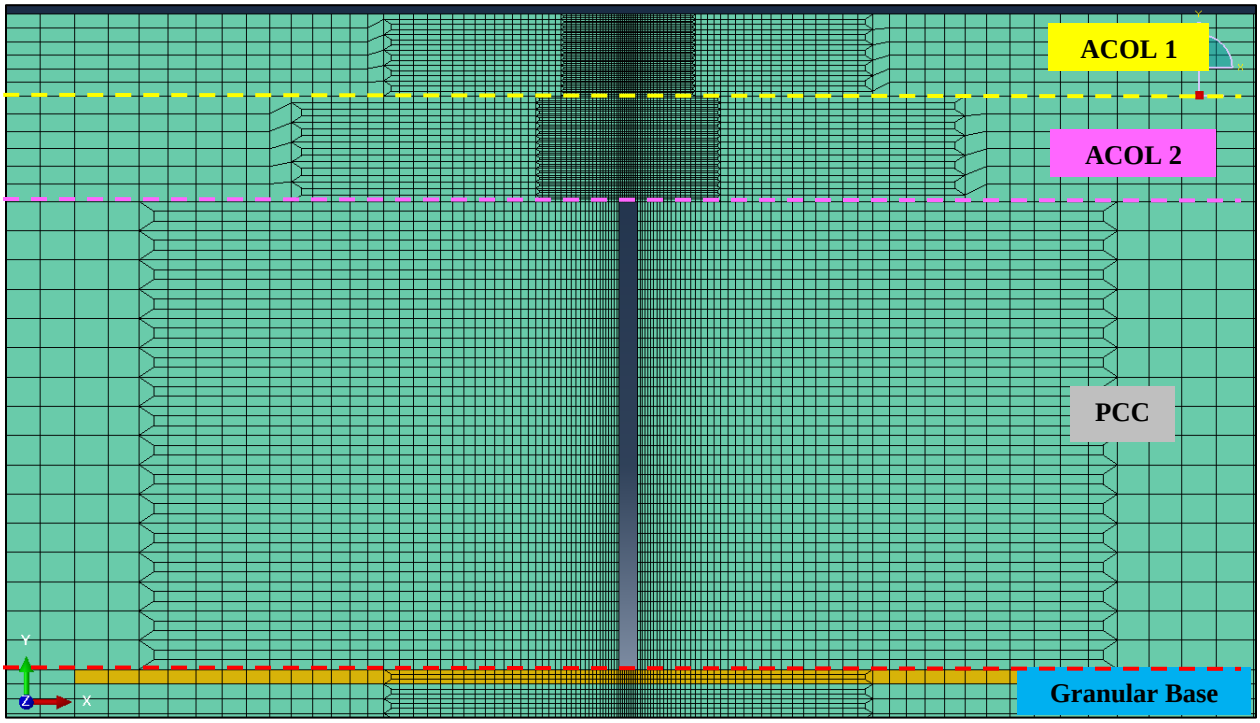

Figure 6-18 Void under PCC slab with damaged granular base material highlighted in orange.

To investigate the impact of the presence of a void in the granular base layer, two different pavement structures (thin and thick) were selected as base line models (Cell 986 and Cell 990). Damage ratio results from thermal and tire loading simulations with and without the presence of the void are compared in Table 6-12. Detailed information on the selection of a historical critical thermal event for each overlay pavement structure and applied tire load was provided in section 6.2.4 of this dissertation. It is observed that approximately a 2% increase in total damage occurred when a void was present in the thicker pavement structure (Cell 990), while minimal increase in total damage resulted in the thinner pavement structure (Cell 986).

Table 6-12 Damage ratio results of models with and without voids.

Model Description	Layer	AC Layer Thickness	Damage Ratio (%)
Cell 986, No void	Wearing	44.45	4.58
Cell 986, Void	Wearing	44.45	4.80
Cell 990, No Void	Wearing	44.45	51.7
	Base	57.15	
Cell 990, Void	Wearing	44.45	53.6
	Base	57.15	

The impact of the presence of a void in the granular base layer with the combination of varying levels of LTE was also explored. FE model results with LTE levels based on FWD testing in MnROAD sections (Table 6-10) and presence of a void are summarized in Table 6-13. It should be noted that the models where no spring elements were used (Cell 990, No void and Cell 990, void) assumed an LTE level of approximately 19% (Table 6-11). It can be concluded from this analysis and given model parameters, when LTE is less than 61%, the controlling factor in the amount of damage from thermal and tire loading is driven by the presence of the void rather than the level of LTE.

Table 6-13 FE model damage ratio results with void and varying levels of LTE.

Model Description	Layer	AC Layer Thickness	Damage Ratio (%)
Cell 990, No Void	Wearing	44.45	51.7
	Base	57.15	
Cell 990, Void	Wearing	44.45	53.6
	Base	57.15	
Cell 990, Void + LTE from driving lane	Wearing	44.45	53.6
	Base	57.15	
Cell 990, Void + LTE from passing lane	Wearing	44.45	53.6
	Base	57.15	
Cell 990, Void + Average LTE	Wearing	44.45	53.6
	Base	57.15	

6.2.10 Material Property Parametric Evaluation

Parametric analysis of AC fracture material properties (fracture energy and tensile strength) was undertaken on select models to investigate optimization of the combination of material properties and overlay structure design (thickness) to reduce reflective cracking potential. This is a major advantage of FE analysis in that it provides the ability to simulate different pavement structures and material property combinations beyond the 12 MnROAD field test sections. Previously developed models with as-built material properties and the combination of thermal and tire loading for MnROAD test sections were used as control models. Two different test sections (Cell 986 and 988) with varying overlay structures were selected to perform the parametric analysis. Cell 986 was ranked as the best performing test section overall among all MnROAD test sections with the lowest reported damage ratio, while Cell 988 was considered the worst performing test section among the four in-situ density test sections.

The tensile strength and fracture energy values for Cell 986 were decreased by 12.5% and 25%; Table 6-14 summarizes the resulting damage ratio values. It can be observed that as tensile strength decreases while holding fracture energy constant the material behaves more brittle, resulting in poor cracking resistance. Similarly, as fracture energy was decreased while holding tensile strength constant, the damage ratio increased. By decreasing tensile strength by -12.5% it resulted in a fully cracked overlay (100% damage ratio), while decreasing fracture energy by -25% produced a fully cracked overlay.

Table 6-14 Cell 986 parametric results with decreasing material properties.

Damage Ratio (%)

Cell 986		Fracture Energy (G_f)		
		Control (491 J/m^2)	-12.5%	-25%
Tensile Strength (σ_t)	Control (5.66 MPa)	17.4	21.4	100
	-12.5%	100	100	-
	-25%	100	-	-

Table 6-15 summarizes parametric analysis results for Cell 988 where fracture material properties were increased by 25% or 50% in an attempt to improve its cracking resistance performance. As expected, when fracture energy was increased at a constant tensile strength, the damage ratio decreased. When tensile strength was increased at a constant fracture energy, an increase in damage ratio was observed as the material behaved more brittle under thermal and tire loading. When both fracture energy and tensile strength were increased a tradeoff was created, where the damage ratio improved but not as much compared to when tensile strength was held constant.

Table 6-15 Cell 988 parametric results with increasing material properties.

Damage Ratio (%)

Cell 988		Fracture Energy (G_f)		
		Control (Wear = 491 J/m^2) (Base = 510 J/m^2)	+25%	+50%
Tensile Strength (σ_t)	Control (Wear = 5.66 MPa) (Base = 6.05 MPa)	56.2	34.9	24.2
	+25%	74.5	46.9	28.9
	+50%	90.7	56.7	34.5

While this is an academic exercise in nature, this type of analysis can help to demonstrate to pavement designers the tradeoff that exists when considering how to improve cracking performance of overlays by altering material properties or changing the pavement structure (number of lifts, individual lift material properties, and total thickness of overlay). A key implication of the findings from this parametric analysis for pavement designers and agencies is that a focus should be placed on increasing ductility (fracture energy) over increasing tensile strength to improve cracking resistance.

6.3 AASHTOWare Pavement ME Simulations

6.3.1 Overview of Pavement Simulations

AASHTOWare® Pavement ME Design™ software was used to predict pavement performance of 11 MnROAD test section (Cell 984-995). Cell 995 was not included in the analysis as dynamic modulus data was not available for the UTBWC mixture and is a critical input in level 1 design. Target distress values assumed for all test sections at the specified reliability are summarized in Table 6-16. All Pavement ME simulations assumed a reliability of 90% for a 20-year design period.

Table 6-16 Specified distress target values for all models.

Distress Abbreviation	Distress	Target
IRI	Terminal IRI (in/mile)	172
RUT	Permanent deformation - AC only (in)	0.25
AC-BF	AC bottom-up fatigue cracking (% lane area)	25
AC-TR	AC total transverse cracking: thermal + reflective (ft/mile)	2500
AC-T	AC thermal cracking (ft/mile)	1000
AC-TF	AC top-down fatigue cracking (ft/mile)	2000
JPCP-T	JPCP transverse cracking (percent slabs)	15

6.3.2 Pavement ME Results

Initial Pavement ME results were simulated for each test cell using available default climate data from the closest weather station (Champaign, Illinois) to MnROAD test sections. Predicted results are presented in Table 6-17. Green formatted values denote that the design criteria was achieved (passed), while values that did not meet the specified design criteria (failed) by exceeding the distress tolerance value are highlighted in red. AC total transverse cracking (Thermal + reflective (ft/mi)) and AC thermal cracking only (ft/mi) were predicted to exceed the target design criteria in all but two cells (Cell 989 and cell 990). Only cell 986 failed the JPCP transverse cracking (percent slabs) criterion.

Table 6-17 Summary of predicted distress levels assuming default weather station data from Champaign, Illinois. Green cells passed the specified design criteria while red cells failed.

Test Cell Number	Distress Result						
	IRI	RUT	AC-BF	AC-TR	AC-T	AC-TF	JPCP-T
984	127	0.18	1.45	5558	2112	1173	12.9
985	124	0.17	1.45	4610	2112	1140	13.2
986	127	0.25	1.45	4374	2112.0	1543	15.4
987	149	0.56	1.45	3640	1912.0	11312	1.9
988	151	0.59	1.45	3989	2112.0	11729	2.2
989	158	0.79	1.45	1843	34.2	12971	2.2
990	143	0.63	1.45	2443	19.8	5273	2.2
991	151	0.60	1.45	3936	2112.0	11790	2.2
992	139	0.43	1.45	5061	2112.0	5826	4.6
993	139	0.43	1.45	5061	2112.0	5826	4.6
994	127	0.18	1.45	5558	2112.0	1173	12.9

Figure 6-19 shows the predicted performance curves for each cell in terms of the international roughness index (IRI) in/mi. Test cell 989 appears to be the worst performing cell while the best (lowest terminal IRI after 20 years) is test cell 985. However, it should be noted that all models passed the design criteria (less than 172 in/mi) at the specified reliability (90%).

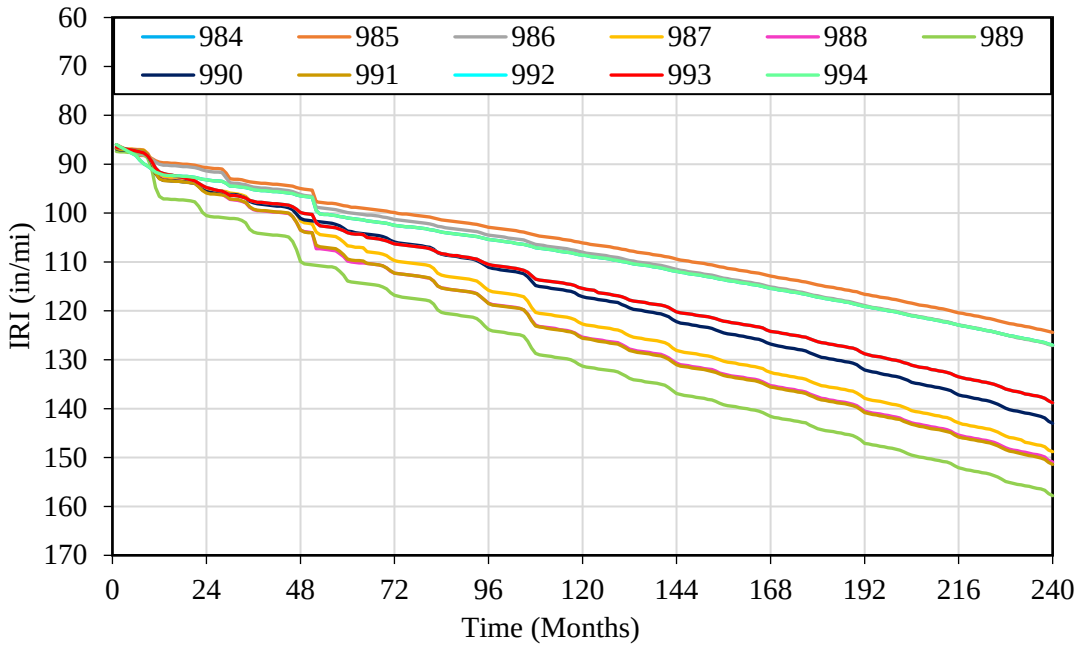

Figure 6-19 Performance curves from Pavement ME for a 20-year design period with default climate data from Champaign, Illinois.

After approximately 3 years of service, MnROAD weather station data was collected and manually added to the climatic input in Pavement ME software. Inputs included air temperature, wind, percent sunshine, precipitation, humidity and water table from 2017 to 2019. A constant water table depth of 10 feet was assumed based on estimates from geological atlas of Wright County, Minnesota. Predicted distress results using the three years of weather station data located at MnROAD is summarized in Table 6-18. Again, green formatted values denote that the design criteria was achieved (passed), while values that did not meet the specified design criteria (failed) by exceeding the distress tolerance value are highlighted in red.

Table 6-18 Summary of predicted distress levels using MnROAD weather station data. Green cells passed the specified design criteria while red cells failed.

Test Cell Number	Distress Result						
	IRI	RUT	AC-BF	AC-TR	AC-T	AC-TF	JPCP-T
984	124	0.16	1.45	3787	2112	1868	49.4
985	124	0.15	1.45	3796	2112	1824	49.7
986	126	0.22	1.45	3437	2112	2295	50.6
987	148	0.48	1.45	3129	2112	13083	2.7
988	149	0.51	1.45	3108	2112	13185	3.1
989	156	0.67	1.45	3535	2112	13494	3.1
990	146	0.54	1.45	3135	2112	9111	3.1
991	150	0.52	1.45	3192	2112	13286	3.1
992	139	0.36	1.45	3149	2112	9714	10.3
993	139	0.36	1.45	3149	2112	9714	10.3
994	124	0.16	1.45	3787	2112	1868	49.4

Meanwhile, Figure 6-20 shows the predicted IRI performance curves over the 20-year design period. In general, the predicted distress results from both climate scenarios (historical data from Champaign, Illinois weather station data versus MnROAD weather station data) agree on which distresses meet target values and which fail to meet the 90% reliability target values. However, the magnitude of certain predicted distresses results vary between the two sets of results. For example, the predicted AC top-down fatigue cracking (ft/mile) or the predicted JPCP transverse cracking as a percentage of the number of slabs (JPCP-T) was higher for models simulated with MnROAD weather station data and holding all other inputs constant. In terms of AC total transverse cracking (AC-TR) and AC thermal cracking only (AC-T), all models were predicted to exceed the target design criteria.

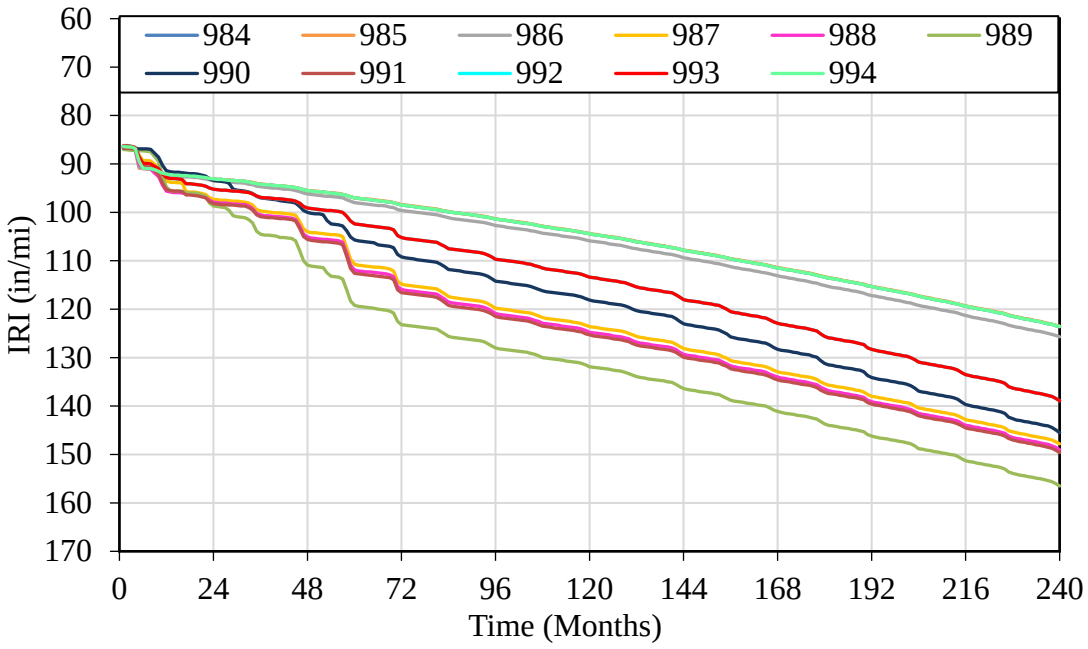

Figure 6-20 Performance curves from Pavement ME for a 20-year design period with climate data MnROAD weather station.

6.4 Comparison of Finite Element, Pavement ME and Field Performance

FE results from thermal and tire loading may be considered comparable to Pavement ME distress output for asphalt concrete total transverse cracking, which includes both thermal and reflective cracking. Field performance results indicate that the best performing test sections (lowest reflective cracking) are in-situ density test sections 989 (5% AV design) and 990 (3% regressed AV design) and Cell 987. Meanwhile the worst performing test section are generally the thinner overlays such as Cell 984, 985, 994 and 995. A three-way comparison of results from Pavement ME, FEA results (FE thermal and FE thermal and tire), and field performance data has been made using historical climate data. The results were broken down into three categories (A, B or C) based on the respective level of cracking/damage predicted or measured. Ranges were selected based on the given spread in data to provide good distinction between results, these are shown in Table 6-19. Table 6-20 summarizes the three-way comparison results from Pavement ME, FEA and field

performance from the August 2020 distress survey. Meanwhile, the limited three-way comparison results using MN climate and relevant models can be reviewed in Appendix B.4.

Table 6-19 Field performance, Pavement ME and FEA result ranges for grouping of test cells.

Field performance: Percentage of joints reported as cracked during August 2020 survey	
Category	**Damage Level**
A	< 40 %
B	40 - 70 %
C	> 70 %
Pavement ME: Predicted asphalt concrete total transverse cracking	
Category	**Damage Level**
A	< 3000 ft/mile
B	3000-5000 ft/mile
C	>5000 ft/mile
FE Thermal: Damage Ratio Percentage	
Category	**Damage Level**
A	< 5 %
B	5 – 50 %
C	> 50 %
FE Thermal + Tire: Damage Ratio Percentage	
Category	**Damage Level**
A	< 15 %
B	15 – 75 %
C	> 75 %

Table 6-20 Summary of grouped performance comparisons between Pavement ME and FEA model results (historical climate) with field performance as of August 2020.

Cell Number	Field Performance (<50; 50-70; >70)	Pavement ME (<3000, 3000-5000, >5000)	FEA Thermal (<1; 1-50; >50)	FEA Thermal + Tire (<30; 30-60; >60)
984	C	C	C	N.A.
985	C	B	C	N.A.
986	C	B	B	A
987	A	B	C	N.A.
988	B	B	A	B
989	A	A	A	B
990	A	A	A	B
991	C	B	A	B
992	B	C	C	N.A.
993	C	C	N.A.	N.A.
994	C	C	C	N.A.
995	C	N.A.	C	N.A.

In general, there is fair agreement with FE model results with field performance data. The impact of pavement structure and material selection (fracture properties) in providing sufficient resistance to withstand the combination of thermal and tire loading with minimal damage was observed. The damage ratio concept proves to be an effective manner to distinguish performance of modeled test section that reported softening damage along the cohesive zone line but had not yet formed a macro-crack.

FE model ranking of in-situ density test sections from lowest damage ratio percentage to highest is cell 989, 991, 990 and 988 (Table 6-6). Interestingly, this ranking does not exactly line up with current field performance ranking of cells where 990 is the best followed by 989, 988 and 991. A possible explanation for the disagreement in ranking can be observed by taking a closer look at the damage (percent cracked) by asphalt layer or lift. FE models are predicting transverse cracking originating in the base course rather than in the wearing course (crack movement from bottom to top). All 4 of these test sections report softening damage in the wearing course and

cracking damage in the base course only. A limitation of the given field performance data is that it was collected by means of visual distress maps and only cracks visible from the surface are reported, therefore the underlying damage or potential for cracks in the base layers cannot be accounted for. This can lead to a disagreement in ranking of FE model results and %RC results from visual distress surveys.

Comparison of asphalt concrete total transverse cracking (thermal + reflective) from Pavement ME software to field performance data as of August 2020 is shown in Table 6-21, where the number in parenthesis denotes the rank of the test cell section. Pavement ME results show good agreement between field ranking and total transverse cracking predicted in Pavement ME model test sections. It should be noted that there is less than a 2% difference in field performance ranking of cell 987, 989 and 990, while the difference in total amount of transverse cracking reported for the two sections is larger with cell 989 being the best performer (1843 ft/mi) and cell 987 the worst (3640 ft/mi).

Table 6-21 Field rank comparison to Pavement ME rank for total transverse cracking.

Cell Number	Field Performance (%)	AC Total Transverse Cracking (ft/mi)
984	96.7 (10)	5558 (10)
985	98.9 (12)	4610 (7)
986	95.6 (8)	4374 (6)
987	38.8 (2)	3640 (3)
988	57.9 (4)	3989 (5)
989	**38.3 (1)**	**1843 (1)**
990	40.2 (3)	2443 (2)
991	81.2 (6)	3936 (4)
992	64.9 (5)	5061 (6)
993	90.8 (7)	5061 (8)
994	95.8 (9)	5558 (10)
995	97.1 (11)	-

6.5 Chapter Summary

This chapter was dedicated to summarizing performance simulations and predictive modelling efforts undertaken as part of this dissertation research. Detailed information on the modeling approaches adopted and preliminary results from Abaqus and Pavement ME software's were presented. The main motivation for conducting this modeling effort was to increase the number of overlay options that may be included in the overlay decision tree tool beyond the 12 MnROAD test cells 984-995. Comparisons show that the Pavement ME models are in good agreement with latest field performance (August 2020) ranking of test cells and ranking of FE models were in fair agreement using a historical critical thermal loading event. All FE models simulated using instrumented thermocouple weather data resulted in fully formed macro cracks along the entire overlay thickness due to the relatively quick cooling rate that was simulated based on selecting a critical thermal event. A key finding from modeling effort undertaken as part fo this dissertation study was that thermal loading is critical to reflective cracking, especially in cold climate regions. Field performance data (AvgRC performance index) agrees with this finding where the highest value was observed between distress surveys that overlap with this specific thermal loading event. This observation reinforces the importance of considering thermal loading stress generation in FEA of viscoelastic materials such as asphalt concrete. The contribution of thermal loading to the formation of reflective cracks should be consider when selecting an overlay design (thickness of overlay and material type).

7. CHAPTER 7

STATISTICAL ANALYSIS FRAMEWORK FOR REFLECTIVE CRACKING

7.1 Chapter Introduction

Ensuring that a sufficient overlay design and material selection is used to meet a target service life if critical. A step towards gaining a better understanding on what variables may significantly affect reflective cracking performance is to perform statistical analysis of mix design properties, initial design considerations such as existing load transfer efficiency (LTE), and reflective cracking performance indices. Included in this chapter are examples of statistical analysis carried out between laboratory testing, mixture volumetric properties and field reflective cracking performance after approximately 3 years of service. An abstract is provided for Paper 2, where a statistical analysis framework to evaluate reflective cracking performance of asphalt concrete overlays is presented. The full version of the paper may be reviewed in Appendix C.1.

7.2 Statistical Analysis of Laboratory and Field Performance Data

7.2.1 Pearson Correlation

A common statistical method that is used to evaluate the strength of correlation between volumetric and laboratory mixture performance data is the Pearson correlation. The Pearson correlation is a measure of how much two variables change together. It is typically reported on a scale from 1 to -1 where, 1 represents a strong positive correlation and -1 represents a strong negative correlation. Table 7-1 summarizes the Pearson correlation for select volumetric properties and performance test results. A color designation was used to identify strong, medium and weak correlation using the following criteria:

- Strong correlation (green): $0.7 \leq |x| \leq 1$
- Medium correlation (orange): $0.3 \leq |x| \leq 0.7$
- Weak correlation (red): $|x| < 0.3$

Table 7-1 Pearson correlation summary.

Variables	PGLT	UTI	NMAS	AC (%)	Adj. AFT	AV (%)	VMA	RAP	Gyr	% Passing #4	% Passing #200	SA	G_f	FI	CRI	RDCI	IDT (500 cycles)	IDT (3500 cycles)	IDT (Dry)	TSR (500)	TSR (3500)	OT % Load Reduction (2000 cycles)
PGLT	1.00	-	-	-	-	-	-	-	-	-	-	-	-	-	-	-	-	-	-	-	-	-
UTI	-0.34	1.00	-	-	-	-	-	-	-	-	-	-	-	-	-	-	-	-	-	-	-	-
NMAS	0.17	-0.31	1.00	-	-	-	-	-	-	-	-	-	-	-	-	-	-	-	-	-	-	-
AC (%)	-0.24	0.34	-0.74	1.00	-	-	-	-	-	-	-	-	-	-	-	-	-	-	-	-	-	-
Adj. AFT	-0.28	-0.07	0.43	0.21	1.00	-	-	-	-	-	-	-	-	-	-	-	-	-	-	-	-	-
AV (%)	-0.36	-0.46	0.38	-0.40	0.36	1.00	-	-	-	-	-	-	-	-	-	-	-	-	-	-	-	-
VMA	-0.27	0.19	-0.83	0.85	-0.08	-0.17	1.00	-	-	-	-	-	-	-	-	-	-	-	-	-	-	-
RAP	0.38	-0.50	0.46	-0.69	-0.12	0.28	-0.76	1.00	-	-	-	-	-	-	-	-	-	-	-	-	-	-
Gyr	0.42	-0.65	0.40	-0.63	-0.39	-0.04	-0.53	0.56	1.00	-	-	-	-	-	-	-	-	-	-	-	-	-
% Passing #4	-0.17	0.30	-0.94	0.83	-0.35	-0.52	0.88	-0.63	-0.32	1.00	-	-	-	-	-	-	-	-	-	-	-	-
% Passing #200	-0.16	0.37	-0.89	0.82	-0.34	-0.55	0.90	-0.74	-0.35	0.98	1.00	-	-	-	-	-	-	-	-	-	-	-
SA	-0.10	0.30	-0.93	0.77	-0.44	-0.57	0.86	-0.62	-0.27	0.99	0.99	1.00	-	-	-	-	-	-	-	-	-	-
G_f	0.15	0.29	-0.14	0.60	0.27	-0.72	0.25	-0.40	-0.20	0.37	0.42	0.38	1.00	-	-	-	-	-	-	-	-	-
FI	-0.50	0.32	-0.40	0.61	0.36	0.06	0.44	-0.22	-0.71	0.34	0.31	0.29	0.35	1.00	-	-	-	-	-	-	-	-
CRI	-0.47	0.28	-0.51	0.71	0.34	0.00	0.54	-0.26	-0.69	0.46	0.41	0.40	0.38	0.99	1.00	-	-	-	-	-	-	-
RDCI	-0.48	0.34	-0.41	0.62	0.37	0.05	0.45	-0.23	-0.74	0.34	0.31	0.29	0.35	1.00	0.99	1.00	-	-	-	-	-	-
IDT (500 cycles)	0.54	-0.01	0.36	-0.10	0.11	-0.63	-0.48	0.25	0.42	-0.20	-0.19	-0.18	0.59	-0.34	-0.32	-0.34	1.00	-	-	-	-	-
IDT (3500 cycles)	0.12	-0.27	-0.23	0.48	0.08	-0.51	0.25	-0.10	0.29	0.44	0.40	0.43	0.72	0.19	0.29	0.17	0.50	1.00	-	-	-	-
IDT (Dry)	0.29	-0.31	0.71	-0.84	-0.07	0.20	-0.93	0.88	0.58	-0.80	-0.83	-0.76	-0.26	-0.28	-0.38	-0.30	0.35	-0.15	1.00	-	-	-
TSR (500)	-0.05	0.33	-0.61	0.87	0.08	-0.60	0.75	-0.80	-0.37	0.80	0.83	0.77	0.63	0.16	0.28	0.18	0.15	0.49	-0.86	1.00	-	-
TSR (3500)	-0.13	0.08	-0.68	0.88	0.03	-0.49	0.81	-0.68	-0.22	0.86	0.86	0.83	0.62	0.31	0.44	0.31	0.05	0.72	-0.79	0.90	1.00	-
OT % Load Reduction (2000 cycles)	0.11	-0.28	0.75	-0.98	-0.17	0.44	-0.81	0.62	0.55	-0.82	-0.79	-0.76	-0.55	-0.48	-0.61	-0.50	0.01	-0.47	0.83	-0.89	-0.86	1.00

To highlight a few of the key results from the Pearson correlation, a strong relationship exists between the overlay tester results and several volumetric properties including asphalt content (AC), nominal maximum aggregate size (NMAS), voids in mineral aggregate (VMA), percent passing #4 and #200 and surface area (SA). OT is also strongly correlated with IDT results from dry testing condition and TSR results after 500 and 3500 conditioning cycles. TSR results after both 500 and 3500 conditioning cycles showed a strong correlation for AC, VMA, percent passing #4 and #200 and SA. It is also not surprising that TSR results after 500 cycles and 3500 cycles are strongly correlated with each other as they are evaluating similar performance characteristics but simply different conditioning durations.

There was no significant correlation observed between PG low temperature (PGLT), or useful temperature interval (UTI), which is the difference between PG high and PG low temperatures. Also, RDCI has a perfect correlation (value of 1) between CRI and FI, which is not surprising since they are related to each other and are calculated using same test results. Among all the performance test included in the statistical analysis, OT shows the most sensitivity with respect to volumetric properties and other performance tests.

7.2.2 Laboratory Performance Compared to Volumetric Properties

To evaluate the relationship between laboratory performance tests to volumetric properties, DCT, SCB and OT test results were selected to be investigated further. For demonstration purposes, asphalt content and NMAS were selected as volumetric properties to be plotted against DCT, SCB and OT results. Figure 7-1 shows the relationship between fracture energy and fracture strain tolerance determined from DCT testing with respect to asphalt content.

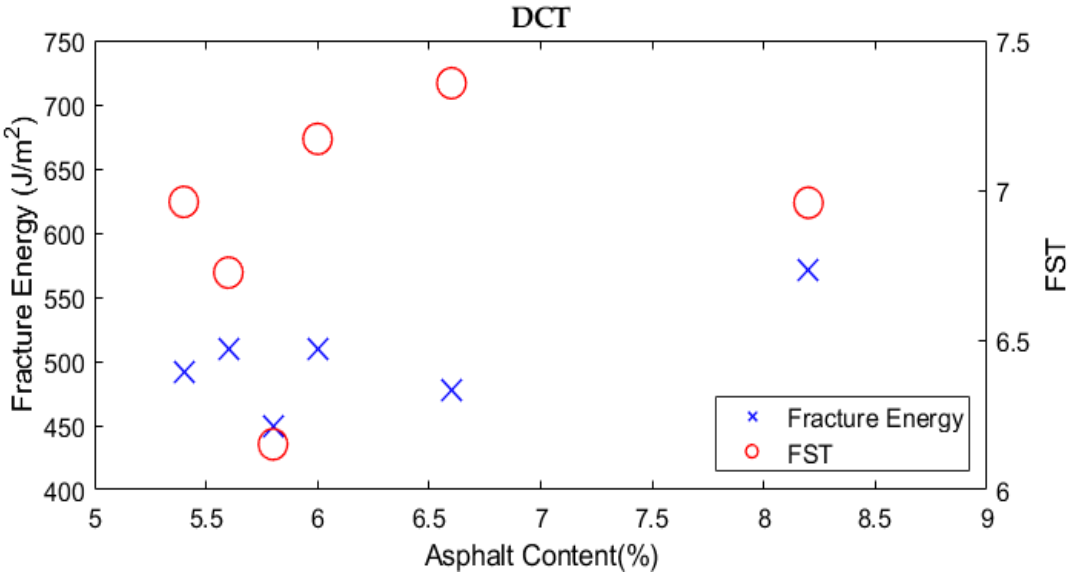

Figure 7-1 DCT performance indices versus asphalt content.

Figure 7-2 shows the relationship between FI, RDCI and CRI with respect to asphalt content. It is expected that as asphalt content increases the performance of mixtures increases for all three indices.

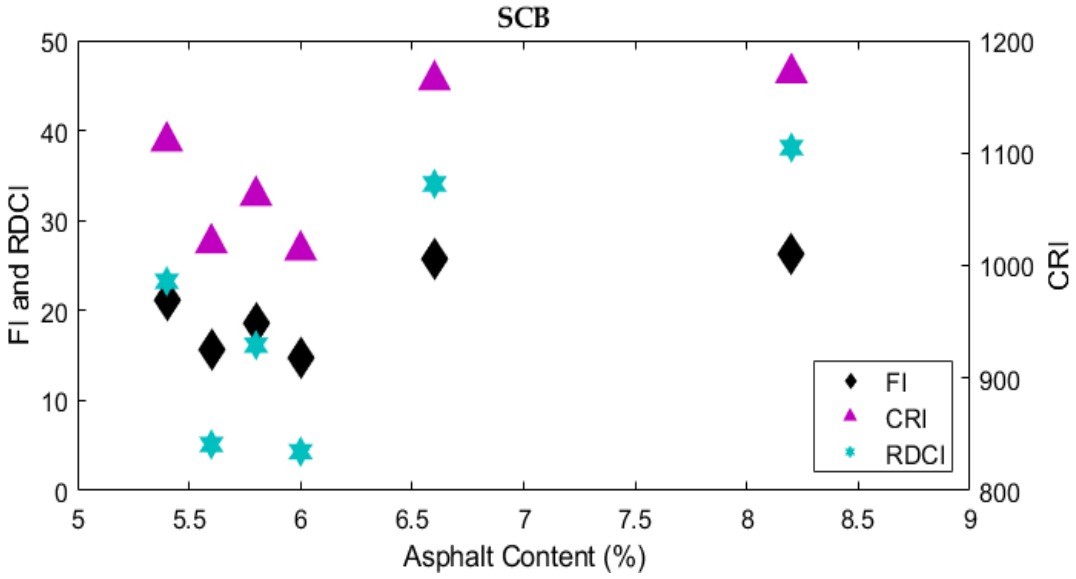

Figure 7-2 SCB performance indices versus asphalt content.

Two different points of interest from the overlay tester were plotted with respect to asphalt content, the number of cycles at 93% load reduction and the load reduction value at 1000 cycles. A higher number of cycles at 93% reduction is desirable and a lower load reduction at 1000 cycles indicates better cracking resistance. A relatively linear increase in the number of cycles at 93% load reduction is observed as asphalt content increases (Figure 7-3). This trend makes sense as the percentage of asphalt content increase typically corresponds to an increase in cracking resistance.

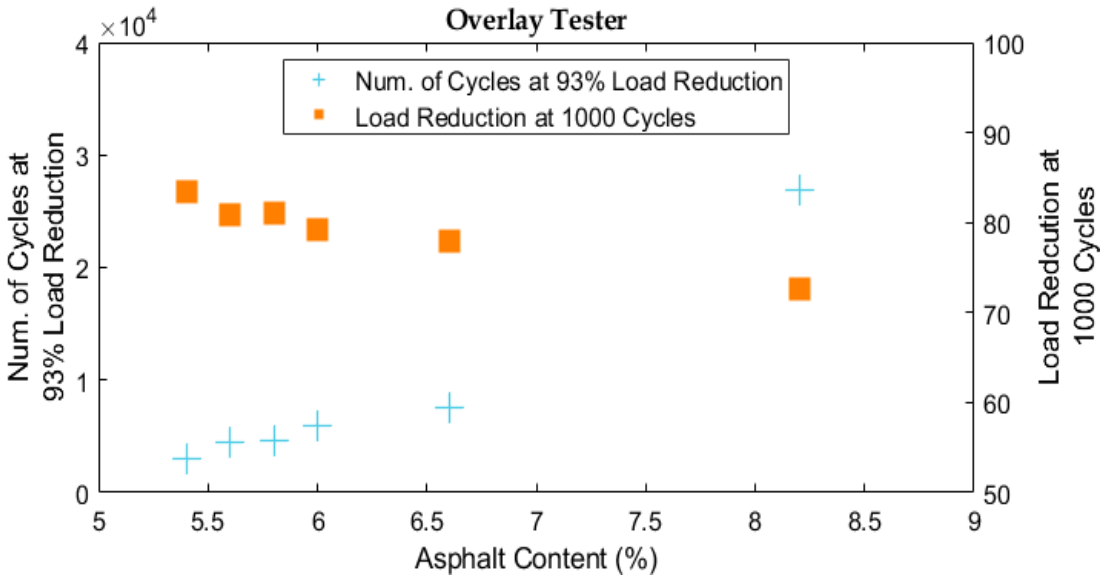

Figure 7-3 Overlay tester performance indices versus asphalt content.

The same performance indices from DCT, SCB and OT testing were plotted with respect to NMAS to identify any relationships among laboratory testing and performance. There was no significant trend in performance from DCT testing results with respect to NMAS as shown in Figure 7-4.

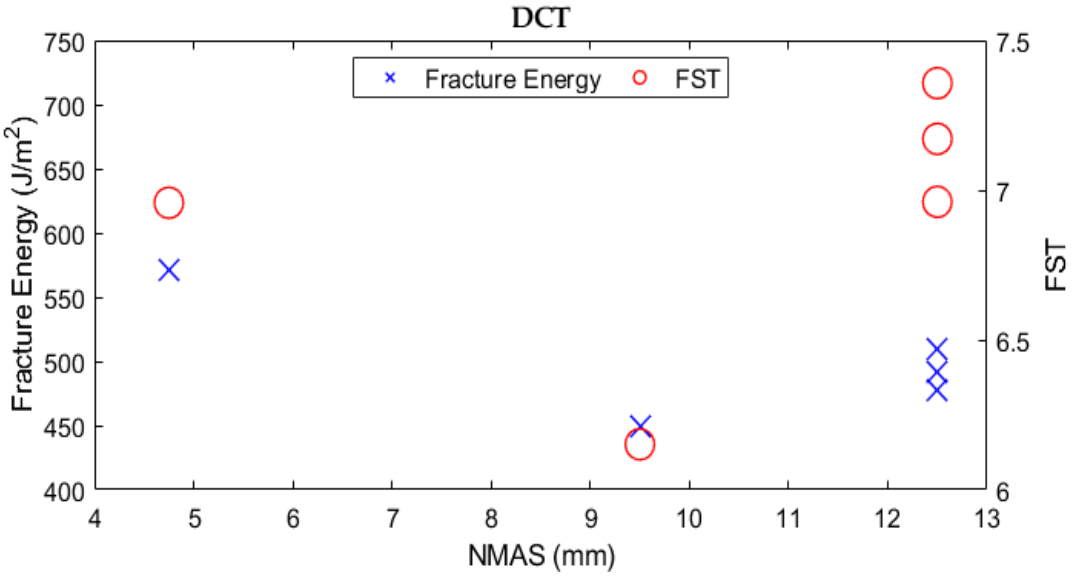

Figure 7-4 DCT performance indices versus NMAS.

A slight decrease in SCB performance results is observed as the NMAS increases (Figure 7-5). This trend also makes sense because mixtures with lower NMAS contain higher amounts of asphalt content (Table 3-1), which helps to improve cracking resistance.

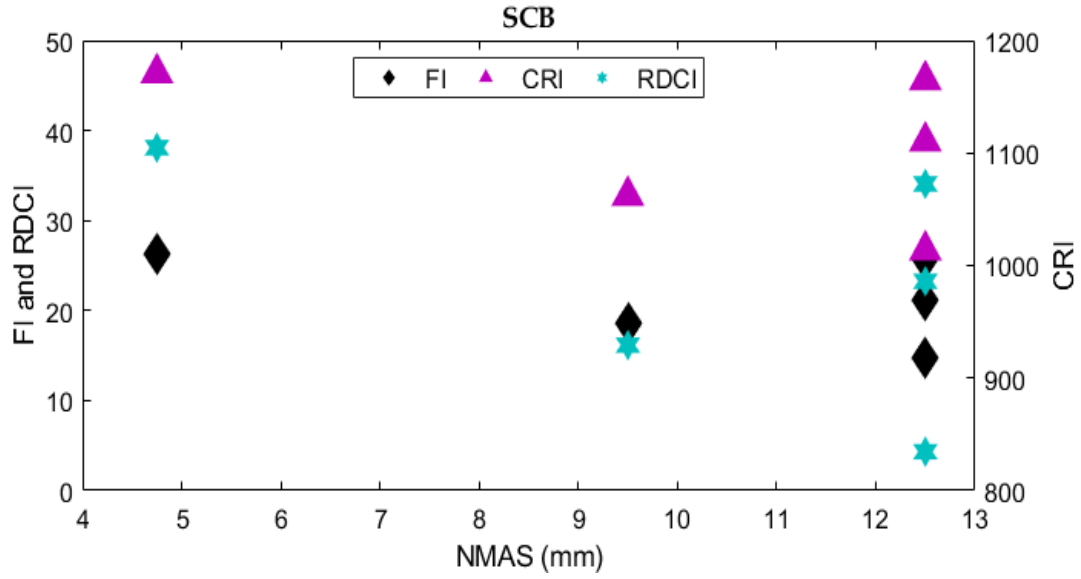

Figure 7-5 SCB performance indices versus NMAS.

Lastly, OT results were plotted with respect to NMAS in Figure 7-6. A positive linear increasing trend in load reduction at 1000 cycles results as NMAS size increases. In comparison, the number of cycles at 93% load reduction decreases linearly with an increase in NMAS size.

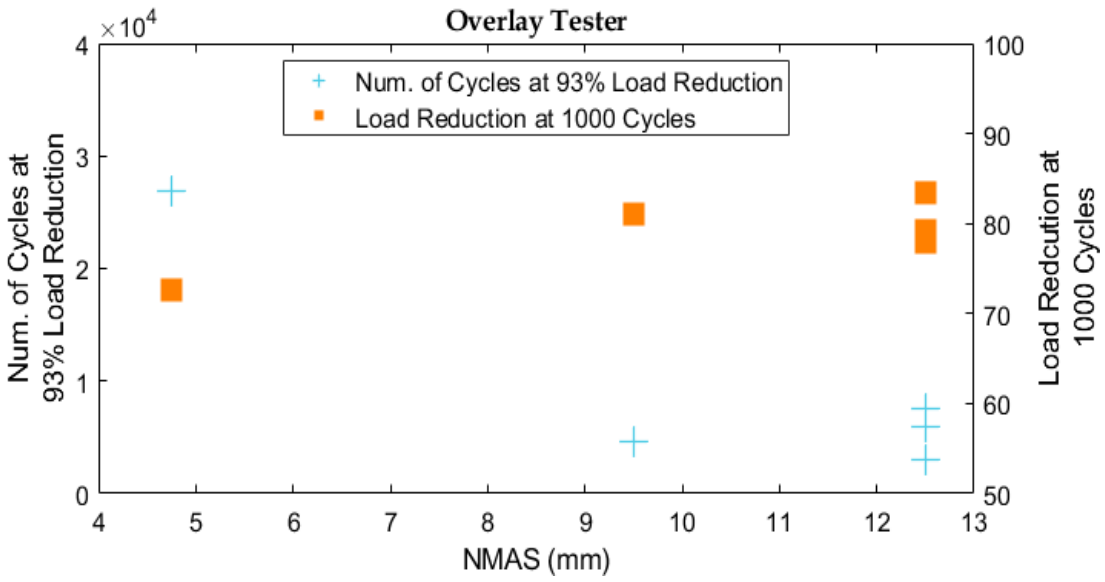

Figure 7-6 Overlay tester performance indices versus NMAS.

7.2.3 Laboratory Performance Compared to Field Performance

Laboratory performance data from DCT, SCB and OT was compared to field performance data in the form of percent cracking located at joints (%RC) for all surface course mixtures. Distress crack maps were used to quantify the percent of joints cracked within each test cell (both driving and passing lanes) and that value was then assigned to the surface course within that test section. While this is a simplification and does not account for the overall structure of each test section, it provides an initial method to estimate the correlation of laboratory performance tests with field performance. Figure 7-7 to Figure 7-9 present comparison results from DCT, SCB and OT performance tests with respect to cracking reported at joints (%RC) as of the August 2020 distress survey. It is observed that there is no strong correlation between any of performance

indices derived from DCT, SCB or the OT performance tests with respect to non-normalized (either for time in service or overlay structure) reflective cracking field performance.

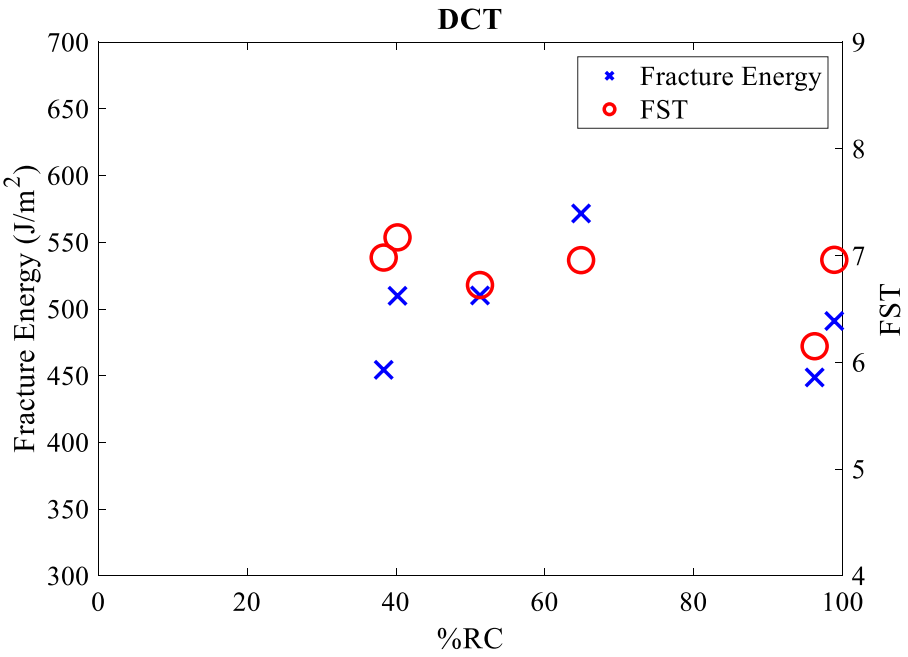

Figure 7-7 DCT performance indices versus percent cracking reported at joint as of August 2020.

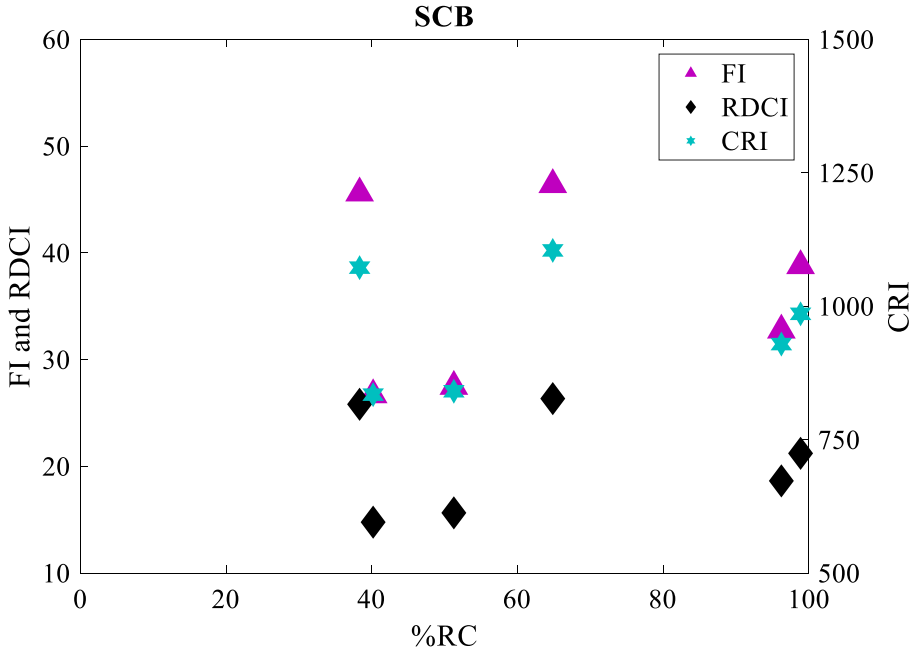

Figure 7-8 SCB performance indices versus percent cracking at joints as of August 2020.

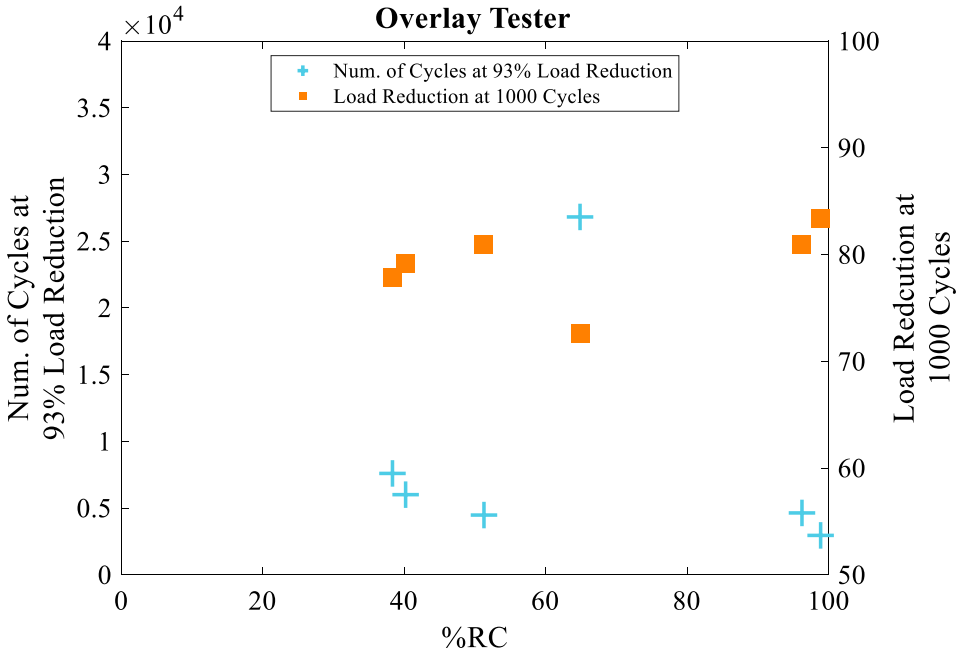

Figure 7-9 OT performance indices versus percent cracking at joint as of August 2020.

As a next step, correlations between the RCTotal field performance index (which takes into account the life of an overlay test section) with a combined parameter called ‘‘Total fracture resistance of overlay,” proposed by Oshone et al. in 2019 were explored [44]. This combined parameter is the product of the average DCT fracture energy of the asphalt mixture and the thickness of the overlay; thus it represents the required energy to form a reflective crack per unit thickness of the overlay (Equation 25).

$$Total\ Fracture\ Resistance = Fracture\ Energy * Overlay\ Thickness \quad \text{Eqn. 25}$$

Figure 7-10 shows the comparison between the two parameters with the in-situ density sections denoted by the hollow markers. In the top left portion of the figure, the cluster of best performing test sections are the in-situ density sections and Cell 987. This is not entirely surprising

as these test sections are thicker in overall pavement structure. To the bottom right portion of the figure are worst performing test sections. When the structure of an overlay (total fracture resistance of overlay) as well as the evolution of cracking over the service life (RCTotal) are taken into account, it more fairly compares the thin lift to thicker lift overlays. For example, comparing Cell 995 (UTBWC) to Cell 994, which has double its lift thickness yet has a lower RCTotal value.

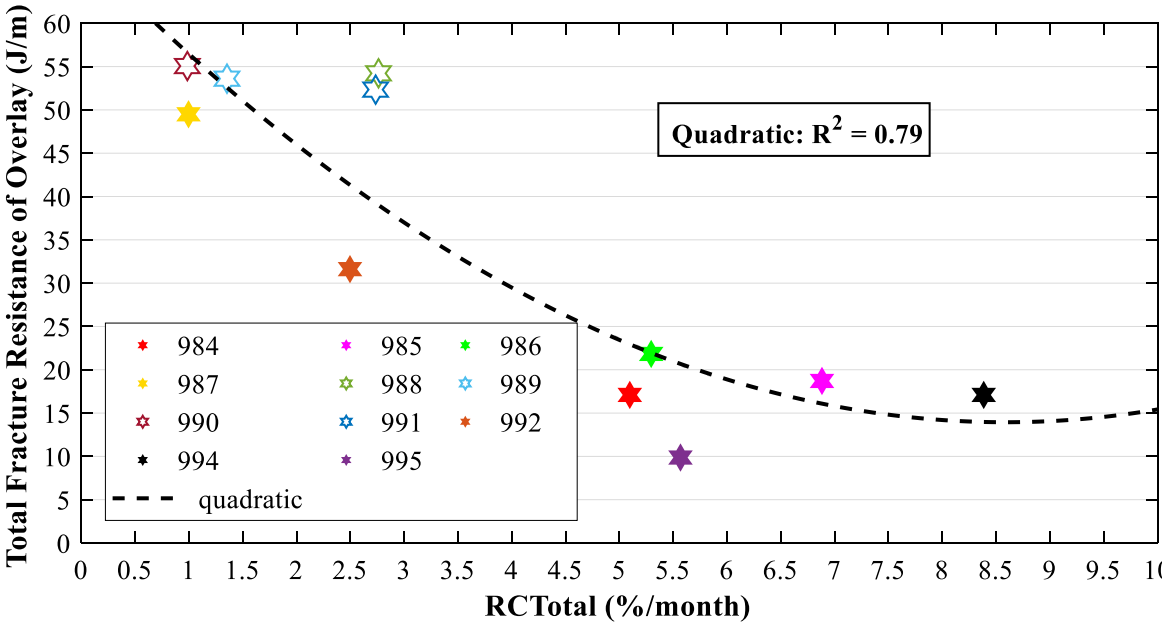

Figure 7-10 Comparison between total fracture resistance of overlay and RCTotal.

An R^2 value of 0.79 was observed when a quadratic fitted function was applied to the data in Figure 7-10, which is typically considered a strong correlation coefficient for pavement field data. This reinforces the importance of considering both material properties and structure in selecting an overlay design and the impact on field pavement performance. Using such an approach allows for designers to make a trade-off between material costs and overlay thickness to achieve a desired service life at an optimized cost.

7.3 Paper 2 A Statistical Analysis Framework to Evaluate Asphalt Concrete Overlay Reflective Cracking Performance

The intention of this paper is to use various statistical analysis methods to evaluate reflective cracking performance while presenting a simple exploratory data analysis framework that may be adopted in other studies. This paper directly contributes to the first objective of this dissertation work focused on evaluating the suitability of different reflective cracking performance measures for asphalt mixtures using laboratory and field performance results. Paper 2 has been submitted to the Association of Asphalt Paving Technologist (AAPT) as a special issue in the Transportation Research Record (TRR). The abstract may be reviewed below while the full paper is included in Appendix C.1.

7.2.1 Abstract

The purpose of this paper is to provide a robust process to statistically analyze reflective cracking field performance data. There is often a lack of consistency and transparency in performing statistical analysis of pavement field performance data, which may not satisfy ANOVA or regression modeling assumptions. A total of 12 full-scale asphalt concrete (AC) overlay pavement test sections located at the MnROAD test facility are used to demonstrate the statistical framework. The percentage of cracking reported at joint locations (%RC) is used to represent reflective cracking performance, and its relationship to pre-overlay load transfer efficiency (LTE), truck traffic, overlay thickness and common performance indices determined from laboratory tests are investigated. The three laboratory tests considered in this study are the disk-shaped compact tension (DCT), semi-circular bend (SCB) and overlay tester (OT). Logistic regression models were used for estimation. Predictive abilities of various models are compared in terms of the percent odds (%odds) of reflective cracking. This is done while assuming varying ability to perform

asphalt mixture laboratory performance testing. An example of such a model, where no laboratory performance testing variables are included, showed that a one-unit increase (1-inch) in AC overlay thickness may result in approximately a one-third decrease in the %odds of reflective cracking. A logistic regression model developed that considers laboratory performance data from DCT, SCB and OT resulted in the most optimal model that balances the best fit and best prediction properties without overfitting.

8. CHAPTER 8

MAINTENANCE AND REHABILITATION DECISIONS USING A LIFE CYCLE COST ANALYSIS AND LIFE CYCLE ASSESSMENT APPROACH

8.1 Chapter Introduction

Throughout this dissertation work, considerable effort was made on advancing the state of knowledge of pavement LCCA and LCA. Specifically, two papers have results from research efforts of this doctorate dissertation thus far, these focus on the implementation of realistic traffic conditions and future climate projections in the operational phase of a pavement LCA. In the following sections, abstracts are provided for each paper separately. Results and discussion within these papers directly contribute to the second objective of this dissertation focused on the improvement of pavement LCCA and LCA applications. Following the two paper abstracts, is a brief discussion on the importance of data quality, compatibility and harmonization of LCA practices in order to routinely use LCA as a tool in pavement management decision making.

8.2 Paper 3 - Realistic Traffic Condition Informed Life Cycle Assessment: Interstate 495 Maintenance and Rehabilitation Case Study

Incorporating an LCA-LCCA approach into the pavement design and maintenance and rehabilitation (M&R) process can help to improve the pavement management of highway infrastructure systems [57]-[59]. It can also help to identify explicit and implicit costs incurred by both agencies and users. The motivation of this study was to use a LCA-LCCA approach to evaluate pavement performance over the design life with the inclusion of realistic traffic conditions, different pavement M&R alternatives, and pavement material characteristics. A framework to include realistic traffic conditions was proposed and a case study utilized to

demonstrate the approach. A sensitivity analysis on fuel price, traffic growth and vehicle efficiencies on cumulative energy demand was performed. A copy of the published manuscript in the Sustainability journal is attached to this dissertation proposal in Appendix D.1.

8.2.1 Abstract

As construction costs continue to rise and adequate amounts of funding continues to be a challenge, the allocation of resources is of critical importance when it comes to the maintenance and rehabilitation (M&R) of highway infrastructure. A Life Cycle Assessment (LCA) methodology is presented here that integrates realistic traffic conditions in the operational phase to compare M&R scenarios over the analysis period of a 26-km stretch of Interstate-495. Pavement International Roughness Index (IRI) were determined using AASHTOWare® Pavement ME Design™ software. Meanwhile, vehicle fuel consumption and emission factors were calculated using a combination of Google Maps®, the U.S. EPA's Motor Vehicle Emission Simulator, the SHRP2 Naturalistic Driving Study, and MassDOT's Transportation Data Management System. The evaluation of pavement performance with realistic traffic conditions, varying M&R strategies and material characteristics was quantified in terms of Life Cycle Cost (LCC), Global Warming Potential (GWP) and Cumulative Energy Demand (CED) for both agencies and users. The inclusion of realistic traffic conditions into the use phase of the LCA resulted in a 6.4% increase in CED and GWP when compared to baseline conditions simulated for a week long operation duration. Results from this study show that optimization of M&R type, material selection and timing may lead to a 2.72% decrease in operations cost and 47.6% decrease in construction/maintenance costs.

8.3 Paper 4 - Impacts of Climate-Change and Realistic Traffic Conditions on Asphalt Pavement and Rehabilitation Decisions using Life Cycle Assessment

The motivation of this paper was to build upon paper 3 to include both realistic traffic conditions and future climate projections into a pavement LCA and LCCA decision process. Traditionally, pavement LCAs are performed using historical climate data to plan pavement life expectancy and inform maintenance and rehabilitation plans. However, pavement systems are constantly exposed to the natural environment and impacts of climate change, therefore it may not be applicable to use historical climate data to inform decisions about future pavement performance. An abstract is provided below, while a full version of paper 6 may be referenced in Appendix D.2

8.3.1 Abstract

Typical pavement Life Cycle Assessment (LCA) are performed using historical climate data to evaluate pavement performance and provide recommendations for budgeting and planning of M&R strategies in the future. However, due to climate change, this assumption may not be appropriate as flexible pavements' performance is influenced by climate stressors. This study explores the impacts of future climate data and realistic traffic data (RTD) in the pavement M&R evaluation process. A 26-km stretch of Interstate-495 was used to evaluate costs and environmental impacts with varying M&R scenarios and pavement structures. Predicted performance using historical and future projected climate data in combination with RTD is used for life cycle cost and global warming potential estimation. Results show that incorporating future project climate data and RTD can lead to a substantial increase in agency LCA impacts (up to 20% for the presented case-study), where the increase is a function of pavement structure and M&R alternative.

8.4 Life Cycle Assessment in Pavement Management Decision Making

There is an increased use of LCA as a tool in pavement management decision making to assess environmental impacts in an effort to move towards more sustainable development of roadway materials and maintenance of existing roadway infrastructure. However, there are still many challenges and research needs associated with pavement LCAs that need to be address prior to the routine adoption of LCA in decision making. A review performed by AzariJafari et al. highlighted issues on modeling life cycle environmental impacts of pavements including methodological choices and data set selection [17]. Some examples of issues heighted in the review related to making comparisons of LCA studies was related to the use of inconsistent functional units, system boundaries and background data sets (life cycle inventory).

These observations are further reinforced by current efforts of the Sustainable Pavements Program (SPP) within the Federal Highway Administration (FHWA). SPP has released several documents and technical briefs highlighting the need for compatible data sources and guidelines on conducting LCAs [16], 59-61]. A study by Rangelov et al. in 2021, investigated the use of environmental product declarations (EPD) as data sources, procurement aids and to assess the environmental impacts associated with pavement materials. It was noted that while EPD development is becoming more widespread following product category rules (PCR), a shortcoming exists in that PCR development was largely done separately and often not in coordination among industries and originations [62]. As a result, there may be a lack of harmonization among PRCs leading to questions of consistency and comparability of EPDs developed using one PCR compared to another. Ultimately it was concluded that, “The use of EPDs to inform material procurement can ensure environmental footprint reduction only if EPDs are consistent and comparable, which stems from the PCRs prescriptiveness. PCRs that prescribe background data, provide accurate product description, specify flows represented with foreground

versus background data, have the potential to facilitate environmental improvements and well-informed decisions" [62]. An example of the progression of EPDs from a communication tool to use as a data source in pavement LCA is outlined in Figure 8-1.

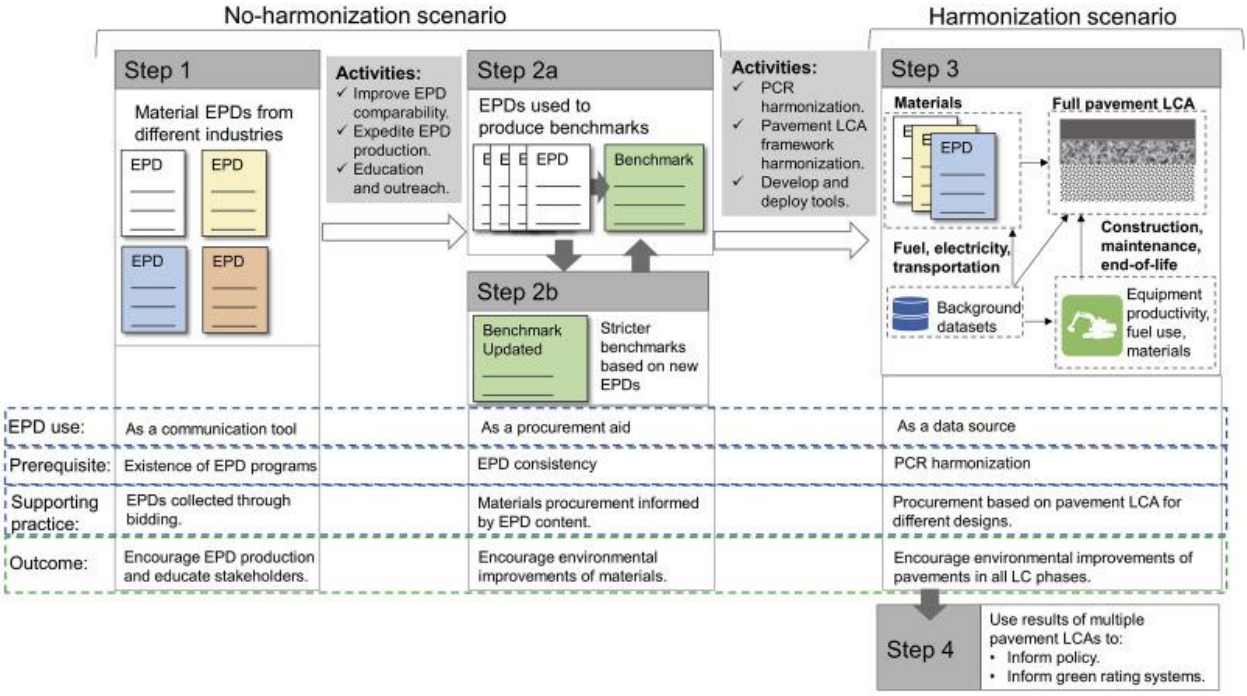

Figure 8-1 Example of potential step-by-step implementation route for use of EPDs in environmental assessment of materials and pavements [62].

Improvements to the LCA framework for pavement maintenance decision making is continuously evolving. Progress has been made by several researchers as described above in identifying key issues, concerns and potential paths forward to ensure transparent, comparable and accurate LCA of pavement materials and systems. The use of EPDs as a public data source over using propriety databases can be beneficial as long as EPDs are developed with prescriptive and harmonized PCRs where all relevant methodological elements (e.g. assessment method, impact categories, data sources etc.) are consistent. It is also important that target data goals and actual data sources used in life cycle inventories be clearly reported.

9. CHAPTER 9

ASPHALT CONCRETE OVERLAY DECISION TREE TOOL DEVELOPMENT

9.1 Chapter Introduction

This chapter is dedicated to the development of a decision tree tool for selection of asphalt mixtures and overlay designs on the basis of outcomes from laboratory, field and predictive modeling performance. A general overview of the developed tool is provided first. Next, decision tree tool inputs and outputs are discussed in greater detailed. A demonstration of the tool is provided in Appendix E.2. Work presented in this chapter directly contributed to the third objective of this dissertation study.

9.2 General Layout and Overview

The proposed decision tree tool is a Microsoft Excel®-based tool comprised of three main modules that the user will interact with and several reference tabs dedicated to intermediate calculations and data sources. The first module is an introduction providing a statement of purpose for the tool, user instructions and a glossary with all relevant terms, assumptions, and system boundaries. The input module will prompt the user to enter information concerning the overlay design they wish to evaluate and pertinent analysis options. The output module will provide the predicted pavement performance curve and agency life cycle cost analysis (LCCA) estimates associated with the given overlay option. Figure 9-1 depicts the general layout of the tool, key features within the three main user modules and the reference and data source sections.

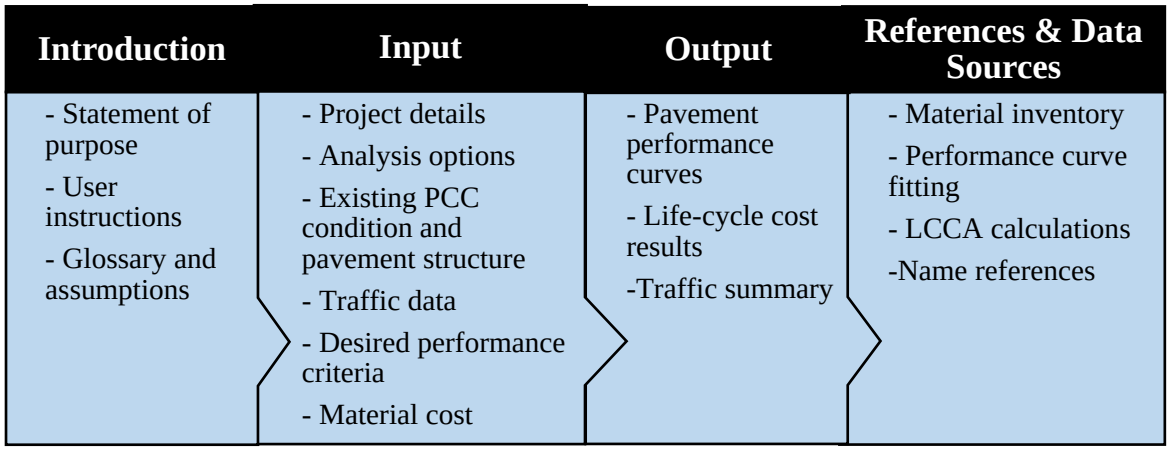

Figure 9-1 Decision tree tool layout.

9.3 Decision Tree Tool Inputs

Decision tree inputs are broken into two categories, (1) required and (2) supplemental information. Examples of required data include geometric properties (e.g. length of overlay section and number of lanes), material properties (e.g. name of asphalt mixture), traffic (e.g. expected average daily traffic in design lane over analysis period) and life cycle cost information (e.g. discount rate). Examples of supplemental information that can be added are the project name, location, and details on the pavement substructure composition. Table 9-1 summarizes the minimum required information to be provided by users to perform the AC overlay analysis within the decision tree tool.

Table 9-1 Required user inputs.

Input	Unit
Total project length	Miles
Discount rate	%
Include shoulder construction	-
Number of lanes	-
Average daily traffic in design lane	# of Vehicles
Truck percentage in design lane	%
Annual traffic growth rate	%
Length of PCC slabs	Feet
Initial load transfer efficiency	Low/Moderate
Analysis period	Years
Threshold for reflective cracking amount (% of underlying joints reflected)	%
Asphalt material type selection (for each individual lift)	-
AC thickness (for each individual lift)	Inches
Average unit price of mixture (for each individual lift)	$/Ton
Construction cost (preparation, placement, striping etc…)	%/Lane Mile

There are many methods to evaluate the existing PCC condition prior to overlay (e.g. LTE, deflections, modulus etc…). In this research study and subsequently the development of the decision tree tool it was chosen to use LTE as the primary means of characterizing the PCC pavement. One reason for this selection was from performing a literature review, a study by Zhou et al. in 2009 investigate the effect of varying input parameters on reflective cracking through a sensitivity analysis [63]. In the case where AC overlays are constructed on jointed plain concrete pavement (JPCP), as is the case with MnROAD test sections included in this study, the influence of 14 different input parameters was considered. Examples of input parameters include, existing PCC slab modulus, slab thickness, LTE, thermal coefficient of expansion, joint spacing, base layer modulus and base layer thickness. It was found that the following input parameters have a significant influence on reflective cracking performance:

- Traffic loading
- Climate

- Asphalt overlay thickness
- Load transfer efficiency
- Asphalt overlay mixture type
- Existing base layer modulus

Furthermore, FWD testing was only available at joint locations (before and after joints) on the MnROAD test sections. Additional FWD testing at mid-span would be required to explore the relationship between deflections and or modulus of the PCC slab with AC reflective cracking performance. Therefore, LTE was chosen as the required user input for characterizing the existing PCC condition.

9.4 Decision Tree Tool Output

9.4.1 Performance Curves

There are two primary outputs from the decision tree tool: (1) predicted pavement performance curves and (2) agency life cycle cost estimates associated with the overlay option in terms of net present value (NPV) and equivalent annual cost (EAC). Performance curves are generated based on a combination of field performance data from the MnROAD test sections and the supplemental finite element model simulations. A Boltzmann sigmoidal function (Figure 9-2, Equation 26) was used to fit reflective cracking field performance data collected from the 12 MnROAD test sections for the driving and passing lanes separately.

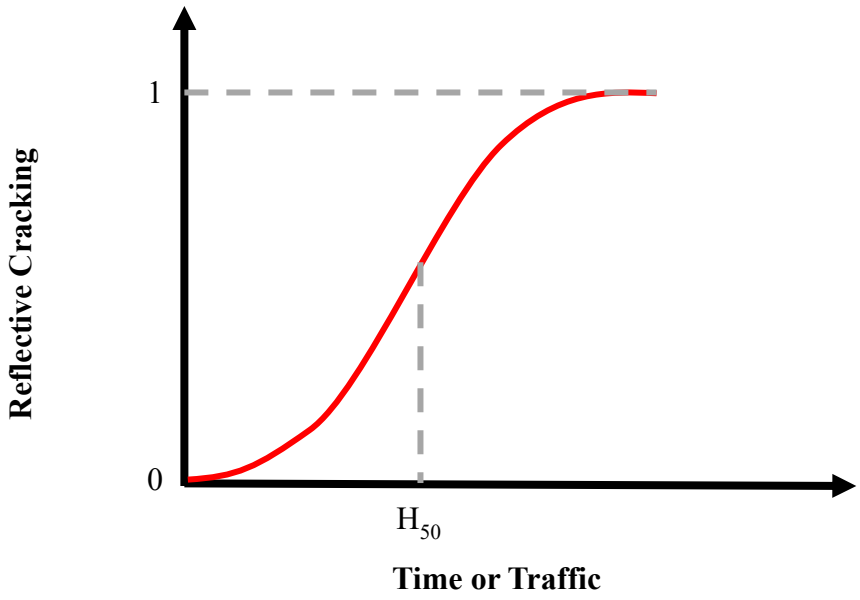

Figure 9-2 Schematic of Boltzmann sigmoidal fitting function.

$$Y = \frac{1}{1+\exp(\frac{H_{50}-x}{S})}$$ Eqn. 26

Where:

Y = predicted reflective cracking amount

H_{50} = half-value, potential at which reflective cracking is halfway between bottom and top asymptotes.

x = in terms or time (months in service) or traffic (number of trucks)

S = slope, steepness of the curve where a larger value denotes a curve with greater slope

This was accomplished by leveraging performance curves presented in section 5.10. Reflective cracking performance (%RC) at the six different distress survey dates for driving and passing lanes separately was plotted against "Truck-Months", which is defined in Equation 27. The reason this unit was chosen was during the field study, it was noted that both traffic and time in service had a

significant impact on reflective cracking performance. Therefore, the combination of both stress inducing loading mechanisms in one unit was assumed to fit the data more realistically as compared to only using traffic or time in service. The truck conversion factor (TCF) was computed separately for the driving and passing lane to take into account differences in truck traffic volume between the two lanes corresponding to low LTE (Driving) and moderate LTE (Passing). TCF was calculated by taking the ratio of cumulative number of truck and number of months in service at the last survey date for MnROAD test sections in each lane respectively.

$$\text{Truck-Months} = m_i + t_i * TCF \qquad \text{Eqn. 27}$$

Where:

i= time in months

m_i = cumulative number of months since construction to time *i*

t_i = cumulative number of trucks since construction to time *i*

TCF = truck conversion factor to time in months. Low LTE TCF = $4.36*10^{-5}$ and Moderate LTE TCF = $7.20*10^{-5}$

An example of a fitted Boltzmann curve for %RC is provided for Cell 988 in the driving lane (Low LTE) in Figure 9-3 and for the passing lane (Moderate LTE) in Figure 9-4. The dashed red line and blue line represent the upper and lower confidence interval assuming a significance level of $\alpha = 0.05$ and 5 degrees of freedom.

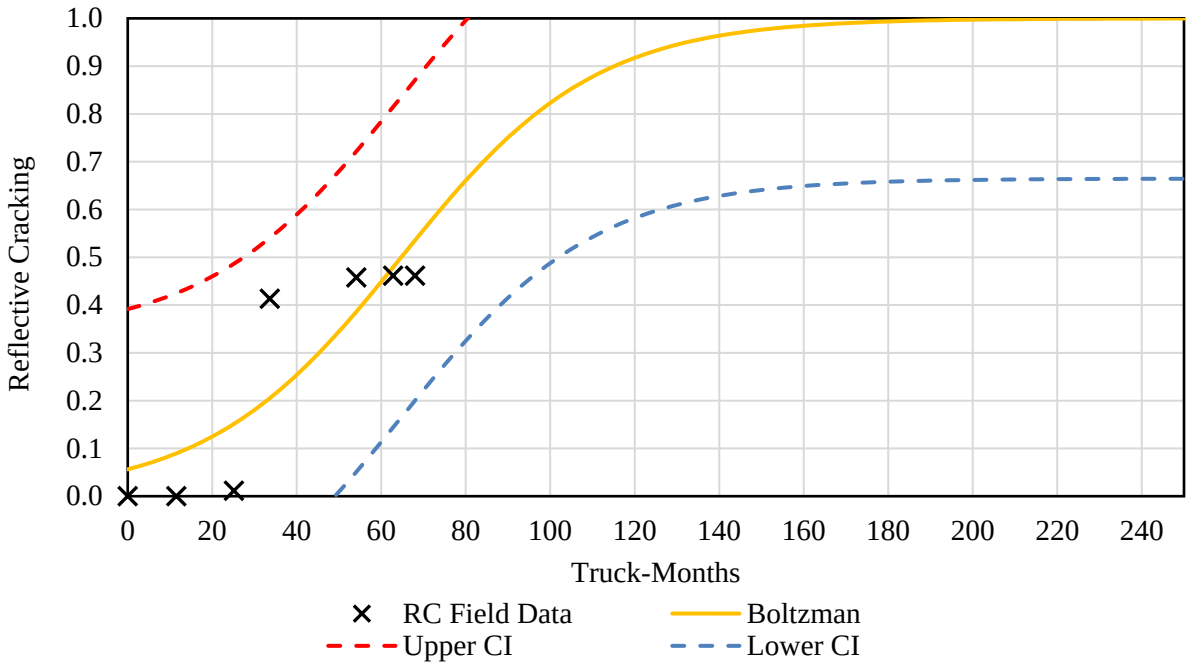

Figure 9-3 Example of fitted %RC performance curve for Cell 988 driving lane.

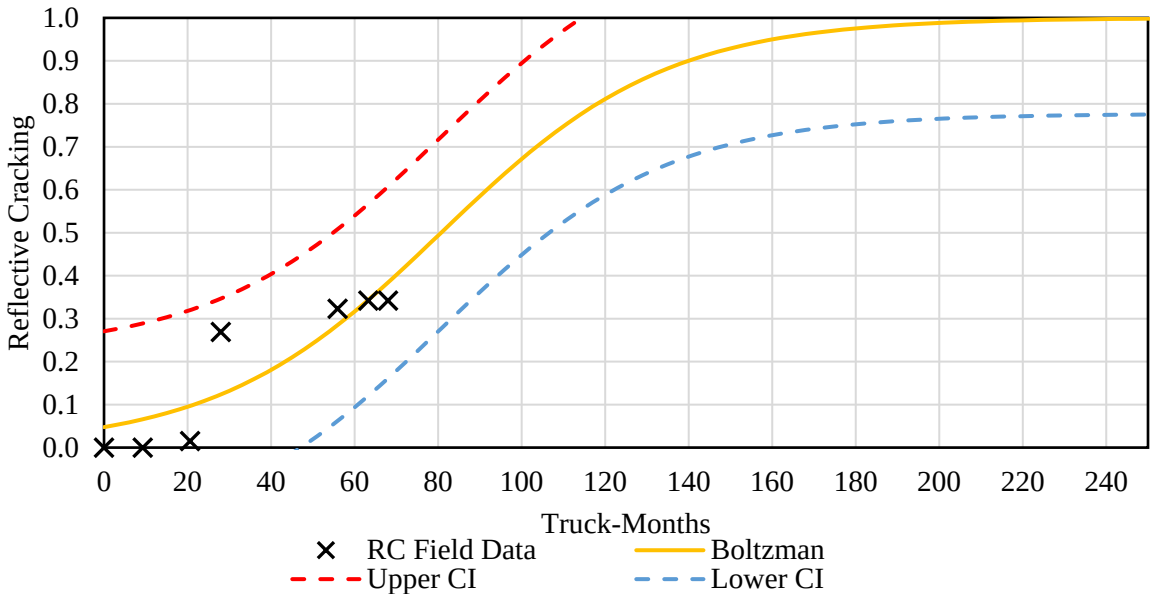

Figure 9-4 Example of fitted %RC performance curve for Cell 988 passing lane.

The process of fitting the collected reflective cracking field performance data versus "Truck-Months" since overlay construction, was repeated for each lane in all 12 MnROAD overlay sections. This provided 24 unique fitting functions for the development of the decision tree tool that cover a variety of overlay pavement structures, material combinations and existing LTE conditions using actual field performance data.

To estimate the Boltzmann sigmoidal fitting coefficients (i.e. half-value and slope) for overlay options that do not have a companion field test sections, an approach was adopted that correlates asphalt mixture fracture properties and overlay structure (thickness and existing PCC LTE) to fitting coefficients. Various cracking performance indices calculated from DCT, SCB and the OT laboratory tests were evaluated to determine the most appropriate values for application in the tool. Table 9-2 summarizes the seven different performance indices evaluated.

Table 9-2 Summary of evaluated laboratory performance indices.

Lab Test	Performance Index Name	Equation	Reference
DCT	Fracture Energy	$G_f = \frac{AREA}{B*(W-a)}$	ASTM D7313-20 [35] and Dave et al. 2019 [56]
	Fracture Strain Tolerance	$FST = \frac{G_f}{S_f}$	Zhu et al. 2017 [36]
	Rate-Dependent Cracking Index	$RDCI = \frac{\int_{t_{peak}}^{t_{0.1peak}} W_c\, dt}{P_{tpeak} \times (t * a)} \times C$	Haslett et al. 2021 [64]
SCB	Flexibility Index	$FI = \frac{G_f}{\lvert m \rvert} * 0.01$	AASHTO TP 124 [31]
	Cracking Resistance Index	$CRI = \frac{G_f}{\lvert P_{max} \rvert}$	Kaseer et al. 2018 [33]
	Rate-Dependent Cracking Index	$RDCI = \frac{\int_{t_{peak}}^{t_{0.1peak}} W_c\, dt}{P_{tpeak} \times (t * a)} \times C$	Nemati et al. 2019 [34]
OT	% Load Reduction @ 1000 Cycles	% Load Reduction @ 1000 cycles	Tex-248-F [28]

For each laboratory test, the average performance index (e.g. fracture energy from DCT testing) was calculated per mixture type and used to calculate a total performance index contribution for the specific overlay construction. Comparisons to overlay field test sections comprised of multiple lifts and asphalt mixture types can then be done using the total performance index contribution. The total performance index contribution was calculated for 10 out of 12 AC overlay pavement cross dedicated to this study at MnROAD. Cell 993 was excluded from the analysis as laboratory testing was not performed on PASSRC material, therefore it was not possible to calculate a representative total performance index for the overlay cross section. Cell 994 was also excluded from the analysis as the pavement structure (thickness and material) was identical to Cell 984 (except for slab stabilization) and did not demonstrate improvement in reflective cracking performance. As only one test section was available for comparison on the use of slab stabilization to mitigate reflective cracking, further research is needed to validate the performance of overlay sections that undergo slab stabilization prior to AC overlay construction.

To illustrate the concept of determining a total performance index, an example calculation for DCT G_f is provided for Cell 988 in Figure 9-5.

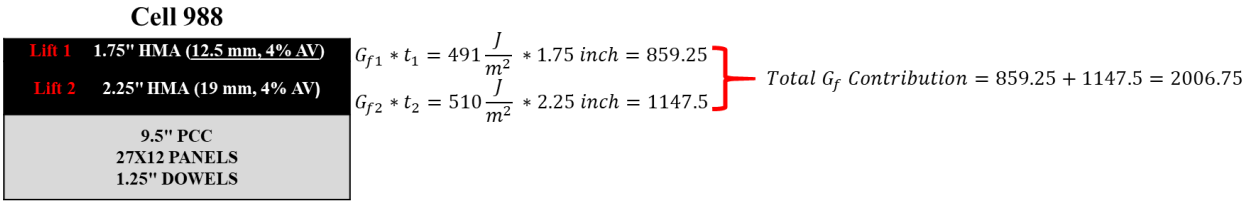

Figure 9-5 Sample calculation of total fracture energy contribution from DCT testing for Cell 987.

To account for pre-overlay condition and differences observed in test section reflective cracking performance in the driving versus passing lane, data was grouped into two categories. Any test sections in the driving or passing lane that had an LTE equal or less than 50% was

considered to be in the low LTE group, while any test section that had initial pre-overlay LTE greater than 50% was considered in the moderate LTE group. It is important to keep in mind that the pre-overlay LTE for MnROAD test sections (Cell 984-995) ranged from approximately 16% to 75%, and no test sections underwent dowel bar retrofitting prior to overlay construction in 2017. Table 9-3 summarizes which sections were classified in the low (L) versus moderate (M) LTE groups.

Table 9-3 Summary of LTE data grouping for driving and passing lanes.

Cell Name	Pre-Overlay LTE (%)	LTE Category
984D	22	L
985D	16	L
986D	22	L
987D	35	L
990D	21	L
991D	21	L
992D	40	L
995D	31	L
984P	59	M
985P	59	M
986P	62	M
987P	74	M
988D	64	M
988P	64	M
989D	56	M
989P	62	M
990P	53	M
991P	61	M
992P	65	M
995P	61	M

Using the two data groups, each of the total performance index contribution values were cross plotted against the fitted half-value or slope (Boltzmann fitting coefficients) corresponding to each test section by lane. Performance index contribution values from DCT, SCB and OT were evaluated. Plots have been generated for the FST and RDCI indices calculated from DCT testing,

as well as FI, CRI and RDCI indices from SCB testing, and the percent load reduction at 1000 cycles from OT testing. All of these parameters have shown promising results with respect to the overlay reflective cracking performance. It should be noted however, that after initial plots were generated, Cell 991 was removed from the data set due to its data point acting as a high leverage point. Recalling from section 5.6 in this dissertation, reflective cracking field performance indices reported that Cell 991 had the highest average reflective cracking rate (AvgRC) after thickness normalization among all test sections during the winter of 2018 (between survey dates November 2018 to April 2019). The impact of the high AvgRC rate causes a sudden jump in reported RC for Cell 991 life curve between 14 months and 19 months in service (Figure 5-31). With Cell 991 being comprised of a relatively thicker overlay design (4 inches total thickness) among the MnROAD test section, this observation was causing the relationship between total laboratory performance indices and Boltzmann fitting coefficients to be skewed. Therefore, the high leverage point was removed from the data set before proceeding with the evaluation of the fit from different laboratory tests.

Figure 9-6 and Figure 9-7 provide an example of the correlation between half-value and slope with DCT total G_f contribution respectively. All other plots for laboratory performance indices from other tests are included in Appendix E.1. The correlation between the half-value and slope were evaluated using R-squared for both the low and moderate LTE data sets for seven different laboratory performance indices. A summary of the R-squared values for fitting the low and moderate LTE data sets is presented in Table 9-4.

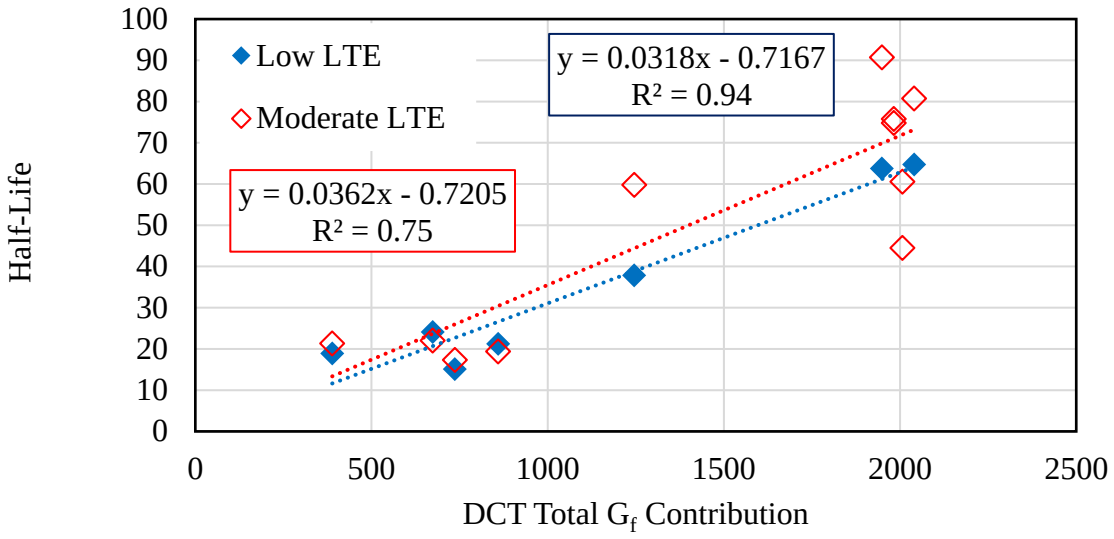

Figure 9-6 Correlation between half-value and DCT total G_f contribution.

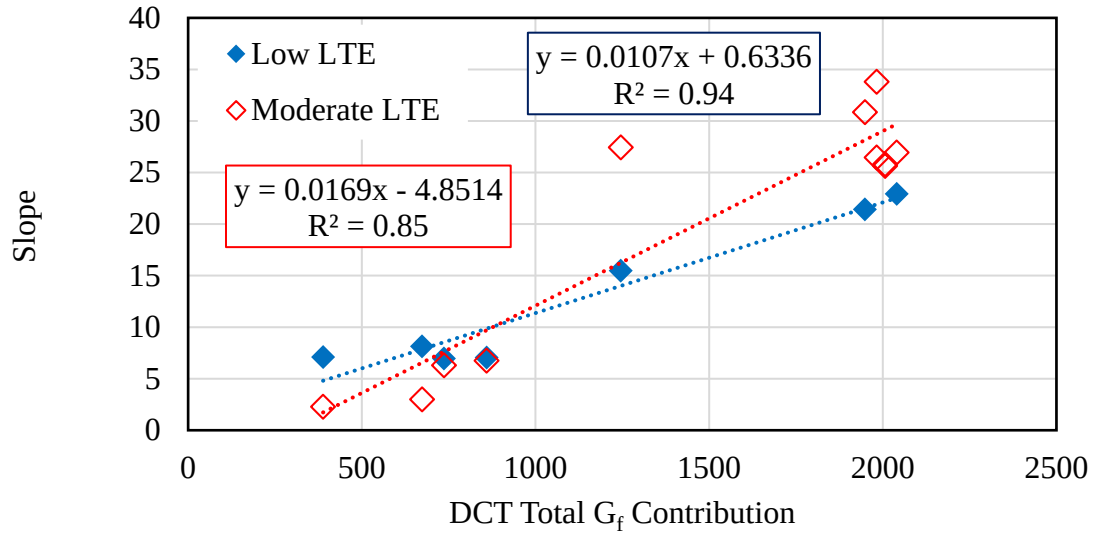

Figure 9-7: Correlation between slope and DCT total G_f contribution.

Table 9-4 Summary of R-squared fitting values for low and moderate LTE data sets.

Lab Test	Performance Index Name	Low LTE		Moderate LTE	
		Half-Value	Slope	Half-Value	Slope
DCT	Fracture Energy	0.94	0.94	0.75	0.85
	Fracture Strain Tolerance	0.96	0.95	0.71	0.79
	Rate-Dependent Cracking Index	0.92	0.90	0.67	0.75
SCB	Flexibility Index	0.87	0.90	0.64	0.83
	Cracking Resistance Index	0.95	0.96	0.71	0.84
	Rate-Dependent Cracking Index	0.86	0.90	0.63	0.82
OT	% Load Reduction @ 1000 Cycles	0.97	0.95	0.71	0.78

Ultimately, DCT total G_f contribution was selected as the most suitable approach to estimate half-value and slope of overlay pavement structures that are not identical to current MnROAD test sections based on the combination of high R-squared values for both low LTE and moderate LTE data sets, and for the ease of implementation (using a single lab test). Furthermore, pervious work by Oshone et al. and Dave et al. have shown DCT G_f contribution to have good correlation to field reflective cracking performance [44], [56]. DCT testing is a popular fracture test performed by state agencies to assess fracture properties of asphalt mixtures. G_f is currently the most commonly used performance index from DCT testing to discriminate cracking resistance of asphalt mixtures. The half-value and slope fitting coefficients for additional overlay pavement structure scenarios (both thickness and material combinations) included within the decision tree tool were determined using the regression equations presented in Figure 9-6 and Figure 9-7, respectively. The fitting coefficients were then used to construct predicted performance curves for a given AC overlay scenario. Prior to implementation of the decision tree tool by state agencies, other performance indices and tests may be adopted, if desired, by using the framework developed here to create similar relationships with Boltzmann fitting coefficients.

9.4.2 Life Cycle Cost (LCC) Analysis

The second major output from the decision tree tool is a LCC estimate. A simplified LCCA was adopted for ease of implementation and to align with the overall goal and scope of the tool. The LCC estimate is meant to provide a starting point for comparison of various AC overlay designs (material type and lift thicknesses) for the rehabilitation of PCC pavements. LCC is calculated using a combination of user inputs and the predicted overlay performance curve. More specifically, the cracking threshold limit selected by the user (e.g. 75% of underlying joints reflected) and the predicted performance curve are used to determine the time at which the threshold is reached, triggering a new overlay construction. The time to the next required overlay construction is then determined. This sequence is repeated until the end of the analysis period (user specified). The cost of overlay construction is based on the user provided AC material unit price and an agency estimate of the all-inclusive construction cost (i.e. for preparation, placement, striping etc.). The total LCC is calculated by discounting all future costs back to present value using Equation 28 summed over the analysis period. The total net present value (NPV) provided in the decision tree tool therefore represents an estimate of the agency's material cost assuming the same overlay structure is constructed throughout the analysis period.

$$Total\ NPV = \ Initial\ Overlay\ Cost + \sum_{k=1}^{N} Future\ Cost_k \left[\frac{1}{(1+i)^{n_k}}\right] - Salvage\ Value \left[\frac{1}{(1+i)^{n_e}}\right] \quad \text{Eqn. 28}$$

Where:

Total NPV = Total net present value, dollars

N = future costs incurred over analysis period, dollars

i = discount rate, percent (user input)

n_k = number of years from initial construction to k^{th} expenditure

n_e = analysis period, year (user input)

Also included in the output section of the decision tree is the estimated equivalent annual cost (EAC). Equation 29 was used to calculate EAC, where all variables are previously described.

$$EAC = \frac{Total\ NPV * i}{[1-(1+i)^{-n_e}]} \quad \text{Eqn. 29}$$

The unit cost of asphalt mixtures is a user input rather than a default value for a given mixture type to allow flexibility for users to enter varying unit prices from year to year and from agency to agency. Similarly, the user input for construction cost (on a per lane mile basis) provides flexibility in use of the tool between different state agencies.

An option to perform crack sealing once the user defined reflective cracking threshold is reached is included in the input module. If the user selects "yes" to performing crack sealing, an estimate of the cost to perform crack sealing on the percentage of joints reflected (in linear feet) is included in the total LCC using MnDOT's 2019 average unit cost for bituminous surface crack and joint repair. This default unit cost value can be manually changed by the user in the input module to more accurately reflect a given agencies expected unit cost. In terms of overlay life extension, a default value of 6 months is applied. The overlay life extension by performing crack sealing is able to be modified by the user to more accurately reflect an agencies knowledge or past experience in observed life extension from crack sealing within their given climatic region.

Ultimately, the LCC estimate presented in the output module of the decision tree tool should be considered as an initial value for the purpose of screening various overlay options. After comparing multiple overlay options (structure and material choice combinations) using the decision tree tool, a more detailed LCCA including both user and agency costs can be performed for a smaller number of overlay options to select the final design. For example, FHWA's RealCost software (Version 2.5) is publicly available for free and provides the ability to compare up to 6 different alternatives using either a deterministic or probabilistic approach [65]. Another more

detailed type of analysis option that could be adopted is the LCCA and LCA framework presented in Chapter 8, where agency and user impacts are included while considering future climate projections. Given the dissertation objective of developing a simple Excel-based decision tree tool, while attempting to limit assumptions and provide user with an estimate of life cycle material costs, the simplified LCC approach was selected. However, it is encouraged to perform a more detailed analysis after screening out overlay design options (both in terms of structure and material choices) for a given traffic level and desired reflective cracking performance threshold.

9.5 Application and Limitations

In development of the decision tree tool, there were restrictions, constraints and assumptions made base on the limited data set. For example, there were only eight different asphalt mixtures used in the construction of 12 overlay test sections at MnROAD with a limited range of initial pre-overly LTE conditions. The following are examples of limitations and applications of the decision tree tool.

- Predicted performance curves and the relationship between total lab performance indices and Boltzmann fitting coefficients were developed using hot mix asphalt that contained RAP percentages from 0% to 25% only (i.e. does not consider high RAP content mixtures, greater than or equal to 30%).
- While there were no SMA mixture used in the MnROAD test sections 984-995, they certainly can be explored and evaluated using the decision tree tool. This can be accomplished by selecting “user defined” mixture when building the overlay cross section to be analyzed. User is then asked to provide the design air void, binder content, mix density and fracture energy.

- Above a certain overlay thickness, thermal loading becomes the driving factor or contributor to reflective cracking in cold regions. Meanwhile, below a certain overlay thickness, traffic is the predominant contributor. It is hypothesized that a balance point between thermal and traffic loading contribution to the formation of reflect cracks in AC overlays exists. Further research is required to explore this relationship and the tradeoff between the two loading mechanisms, while taking into account the composition of the AC overlay (material properties and lift thicknesses)
- The simplified LCCA approach adopted in the current version of the decision tree tool does not consider user costs.
- The LCC estimate should be considered as a preliminary value to screen out overlay design options and followed up with more detailed cost analysis prior to final overlay design selection and construction.
- The application of the decision tree tool is not meant to replace current pavement management tools for maintenance and rehabilitation of pavement infrastructure systems.

10. CHAPTER 10

SUMMARY, CONCLUSIONS, RECOMMENDATIONS AND FUTURE EXTENSIONS

10.1 Summary

Reflective cracking is one of the most common distresses observed in AC overlays and can lead to a decrease in service life and increase in pavement maintenance costs. Ensuring that the most appropriate overlay structure and material choice is selected to withstand both traffic and thermal loading mechanisms is critical. Ultimately, this research aimed to provide guidance on the best materials and techniques to use in rehabilitation of concrete pavements with AC overlays, while creating a user friendly Microsoft Excel®-based tool to screen AC overlay options.

Dissertation research efforts consisted of analysis of laboratory and field performance data from full scale pavement study sections, development of finite element based reflective cracking mechanistic models, and development of life cycle cost analysis as well as life cycle assessment frameworks. One objective of this research was to evaluate the suitability of reflective cracking performance measures for asphalt concrete overlays using laboratory, field and predicted model results (Chapter 4-7). Results and conclusions from these chapters were used to accomplish a second dissertation objective focused on developing a simple decision tree-based tool for selecting suitable asphalt mixtures and overlay designs (Chapter 9). Furthermore, as part of this dissertation work, a third objective was to explore methods to improvement pavement life cycle cost analysis (LCCA) and life cycle assessment (LCA) frameworks by considering realistic traffic conditions and future climate projections in the analysis (Chapter 8). In the following subsections, major conclusions drawn from this dissertation research are highlighted and recommendations for future extension of this research to target relevant knowledge gaps are provided.

10.2 Conclusions

The following is a list of conclusions developed based on research completed as part of this dissertation study. Conclusions are categorized based on the most direct contribution to one of the three principal dissertation objectives.

10.2.1 Dissertation Objective One: Laboratory, Field and Predicted Models

Laboratory Testing

- As part of the laboratory testing campaign carried out on the asphalt mixtures studied in this research, it was observed from complex modulus testing that as the design air void level increases from 3% to 5%, stiffness decreases (SPWEB430E > SPWEB440E > SPWEB450E). This agrees with expected trends from literature. The SPWEB450E mixture exhibits the lowest overall stiffness behavior and had the highest phase angle, corresponding to better expected cracking performance.
- Laboratory testing results from OT, SCB and DCT indicate that the binder rich reflective cracking interlayer mixture (SPWED430I) had superior cracking resistance properties at low and intermediate temperatures compared to other mixtures included in this study.
- A lack of strong correlation was observed between asphalt mixture nominal properties and laboratory cracking tests performed as part of this dissertation work and the limited number of asphalt mixtures. This may indicate that performance testing may not be eliminated completely by use of regression-based models to predict cracking properties. However, when both material properties and pavement structure are considered (e.g. total fracture resistance) a strong relationship was observed with RCTotal field performance index (using a quadratic fit, $R^2 = 0.79$).

- In paper 1, an equivalent performance index approach was adopted to make comparisons of test sections with varying overlay structures in terms of thickness and material properties. Results showed there was relatively good agreement between all equivalent laboratory performance indices derived from DCT testing in identifying the best and worst performing overlay sections according to normalized field performance indices after approximately 3 years of service. In general, the equivalent FST and RDCI laboratory indices rank test sections similarly, while equivalent G_f and DCT_{Index} have comparable ranking. This reinforces the importance of considering both material properties and structure in selecting an overlay design and the impact on field pavement performance. Using such an approach allows for designers to make a trade-off between material costs and overlay thickness to achieve a desired service life at an optimized cost.

Field Performance

- In general, thicker asphalt concrete overlay sections (4 inches total thickness) such as Cell 987 and in-situ density sections (except Cell 991) are the best performers (lower amounts of reflective cracking after 3 years of service). These results reinforce the concept that sufficient overlay structure (along with asphalt mixture cracking resistance) is critical to delay the onset of reflective cracking and to slow its progression.
- To quantitatively compare reflective cracking performance of field sections, it is important to use cracking performance measures that take into account the rate of cracking, onset of cracking early versus later in overlay life, variable pavement cross sections and service life durations. The thickness normalized AvgRC and RCTotal performance indices showed to be an effective method of comparing field test sections comprised of varying overlay structure (number of lifts and thickness), while having the ability to ability to account for

the contribution of each individual mixture or layer in the overall structural performance of the pavement.

- In terms of material selection, the regressed air void (3% AV, Cell 990) and Superpave5 (5% AV, cell 989) design mixtures are the top performers among in-situ density test sections with lower amounts of %RC to date.
- An increase in dielectric constant was observed among all test sections and there does not appear to be any concern of over densification of the in-situ density test sections (Cells 988-991) thus far.
- Discrepancy exists in ranking of test sections based on serviceability measures (e.g. IRI) versus reflective cracking performance (%RC).
- There was no improvement to observed field performance from pre-overlay slab stabilization (Cell 994 compared to Cell 984) in this study. Further research is needed to validate this conclusion further as only one test sections underwent slab stabilization in the overlay test sections included in this study.
- Logistic regression models presented in Chapter 7 (Paper 2) of this dissertation were used to assess the relationship between a binary outcome (event success or failure) with one or more predictor variables. An event success was defined as the formation of a reflective crack and event failure meant no reflective cracking has occurred. Predictive abilities of various models were compared in terms of the percent odds (%odds) of reflective cracking, while assuming varying ability to perform asphalt mixture laboratory performance testing. An example of such a model, where no laboratory performance testing variables are included, showed that a one-unit increase (1-inch) in AC overlay thickness may result in approximately a one-third decrease in the %odds of reflective cracking. A logistic

regression model developed that considers laboratory performance data from DCT, SCB and OT resulted in the most optimal model that balances the best fit and best prediction properties without overfitting.

Performance Prediction

- AASHTOWare® Pavement ME Design™ models are in good agreement with latest field performance (August 2020) ranking of test cells.
- Ranking of FE models were in fair agreement using a historical critical thermal loading event. All FE models simulated using instrumented thermocouple weather data resulted in fully formed macro cracks along the entire overlay thickness due to the relatively quick cooling rate that was simulated based on selecting a critical thermal event.
- In cold climate regions, thermal loading cannot be ignored as it is a major contributor to stress generation with the AC layer. Depending on the overlay lift thickness and material choice (fracture properties), thermal loading may be the driving factor in the formation of reflective cracks as appose to traffic induced stresses at joint locations.
- A tradeoff exists between thermal loading and mechanical loading (tire) on stress generation at joint locations. As a result, both time in service and traffic loading (number of trucks) were incorporated into the development of predicted pavement performance curves.
- A key implication of the findings from the parametric analysis conducted in this dissertation is that for pavement designers and agencies a focus should be placed on increasing ductility (fracture energy) over increasing tensile strength to improve cracking resistance. Additionally, cracking performance properties at low temperatures should not be ignored in the selection of an asphalt mixture for AC overlays in cold climate regions.

10.2.2 Dissertation Objective Two: Pavement LCCA and LCA

- LCA case study results presented in Chapter 8 (Paper 3) showed that the inclusion of realistic traffic conditions into the use phase of the LCA resulted in a 6.4% increase in CED and GWP when compared to baseline conditions simulated for a weeklong operation duration. Results from this case study also showed that optimization of M&R type, material selection and timing may lead to a 2.72% decrease in operations cost and 47.6% decrease in construction/maintenance costs.
- Additionally, from Chapter 8 (Paper 3) it was concluded that cross section type (material characteristics), timing and type of M&R strategy has an impact on IRI, which translates to changes in GWP, CED and LCC.
- Typical pavement LCAs are performed using historical climate data to evaluate pavement performance and provide recommendations for budgeting and planning of M&R strategies in the future. However, due to climate change, this assumption may not be appropriate as flexible pavements' performance is influenced by climate stressors. Case study results presented in Chapter 8 (Paper 4) showed that by incorporating future project climate data and realistic traffic data into an LCA framework can lead to a substantial increase in agency LCA impacts (up to 20% for the presented case-study) as a function of pavement structure and M&R alternative utilized.

10.2.3 Dissertation Objective Three: Decision Tree Tool

- A simple Excel-based decision tree-tool was developed for screening suitable asphalt mixtures and overlay designs in an effort to extend overlay lives by lowering reflective cracking. The framework presented and used in this dissertation to develop a decision tree tool may be applied in future research efforts to move state of practice for other

maintenance and rehabilitation alternatives for deteriorated pavements from policy-based to more of an engineered design approach.

- The flexibility of the developed decision tree tool allows users to adopt other laboratory cracking tests to establish the relationship with Boltzmann sigmoidal fitting functions (required to construct reflective cracking performance curves) following the methodology presented in this dissertation study. Furthermore, the user may choose to enter a "user defined material" to allow the comparison of alternative asphalt mixtures beyond those included in the construction of MnROAD test cells 984-995.

10.3 Recommendations for Future Work

The following is list of possible future extensions of this research study and identification of research needs and recommendations for (1) decision tree tool, and (2) pavement LCA and LCCA frameworks.

10.3.1 Decision Tree Tool

- Validation of decision tree tool using AC overlays on PCC pavements from other MN projects where lab and field performance data is available. Validation may also be done using overlay field sections from other geographical regions across the United States to determine its applicability in both warm and cold climates.
- Expand the decision tree tool data set to consider bituminous over bituminous overlays.
- Expand the decision tree tool data set to consider a wider range of PCC condition prior to overlay construction (e.g. LTE values beyond the MnROAD data set range).
- Explore the impact of thermal loading versus tire loading on reflective cracking further, especially under different climatic conditions (e.g. look at different thermal loading scenarios).

- Further research is needed to determine the impact of reflective cracking performance and life extending benefits of performing dowel bar retrofit.

10.3.2 Pavement LCA and LCCA Frameworks

- LCA frameworks developed as part of this dissertation study including RTD and future climate projections should be considered using more realistic M&R scenarios. For example, rather than holding one M&R treatment option constant throughout the analysis period, a combination of M&R treatments may be used by agency.
- Further research is needed to assess the impact of including RTD under different transportation settings. For example, what is the difference in LCA and LCCA impacts when RTD is included in the analysis of pavement networks within urban versus rural settings.
- Adoption of a probabilistic analysis approach to LCA framework while including RTD and future climate projections data in the operational phase.
- When conducting a LCA for decision making it is paramount that not only a life-cycle thinking approach be utilized (e.g. considers the economic, environmental and social impacts across the complete life cycle of a product, system or service) [66], but that a "system thinking" approach be adopted. System thinking is an approach that emphasizes the understanding of a system by examining the linkages and interactions between the elements that comprise the whole of the system [67]. As an example, when conducting a LCA for pavements within an urban setting, using a system thinking approach that involves relevant stakeholders such as, town planning personnel, roadway managers, and utility companies can help to optimize M&R decision making. The timing of M&R treatments may be selected based on finding a balance between pavement performance, budget

constraints, and other planned or anticipated maintenance work on or near the pavement system being evaluated.

- Consider social impacts in additional to environmental and economic impacts in the decision process to more accurately capture the triple bottom line (People, planet and profit).
- There is currently a knowledge gap in measuring or quantifying social impacts in pavement management practice and further work is needed in order to promote the consideration of social science measures in the decision-making process.
- A gap exists in pavement management systems (PMS) and the monitoring and reporting of data. Climate data should be routinely recorded and integrated into PMS. This type of information is helpful to track seasonal variations and track long term pavement performance with climatic factors such as temperature or precipitation. This can also help decision makers proactively adjust pavement design and material selection to increase pavement resiliency and avoid high costs of premature pavement failures.
- With the growing interest in development and use of product category rules (PCR) and environmental product declarations (EPD) for design and maintenance of pavement infrastructure, an LCA conducted using EPDs for all products and stages of the LCA would be beneficial in combination with RTD and future climate projects.
- A continuous effort should be made towards harmonization of PCRs for use in developing EPDs to be used as datasets for pavement LCAs. Furthermore, there is a need for validation procedures and reliability analysis of data quality and inputs leveraged as part of the life cycle inventory.

11. LIST OF REFERENCES

[1] Lytton, Robert L., et al. “Models for predicting reflection cracking of hot-mix asphalt overlays.” No. Project 01-41, 2010.

[2] Hu, Sheng, Fujie Zhou, and Tom Scullion. “Reflection cracking–based asphalt overlay thickness design and analysis tool.” Transportation research record 2155.1, pp. 12-23, 2010.

[3] Aschenbrener, Tim, et al. “Demonstration project for enhanced durability of asphalt pavements through increased in-place pavement density”. No. 17-05, 2017.

[4] Tran, N., P. Turner, and J. Shambley, “Enhanced compaction to improve durability and extend pavement service life: A Literature Review.” NCAT Report 16-02. National Center for Asphalt Technology at Auburn University, Auburn, Ala., 2016.

[5] U.S. Department of Transportation, Federal Highway Administration - Washington, DC (2021) Innovator Newsletter, July/August 2021, Volume 15(85). https://doi.org/10.21949/1521364

[6] Patel, Harsh. “Implementing the Superpave 5 asphalt mixture design method in Indiana.” Dissertation. Purdue University Graduate School, 2019.

[7] Hekmatfar, A., R. S. McDaniel, A. Shah, and J. E. Haddock, “Optimizing laboratory mixture design as it relates to field compaction in order to improve hot-mix asphalt durability,” Report SPR- 3624. Joint Transportation Research Program, Purdue University, West Lafayette, In., 2013.

[8] Huber, Gerald, et al. “Adjusting design air void levels in Superpave mixtures to enhance durability.” 6th Eurasphalt & Eurobitume Congress, 2016.

[9] West, Randy C., et al. “Regressing air voids for balanced HMA mix design.” No. WHRP 0092-16-06. Wisconsin. Dept. of Transportation, 2018.

[10] Huang, Yue, Roger Bird, and Oliver Heidrich. “Development of a life cycle assessment tool for construction and maintenance of asphalt pavements.” Journal of Cleaner Production 17.2: pp 283-296, 2009.

[11] Lu, Qing, and Chunfu Xin. “Pavement rehabilitation policy for reduced life-cycle cost and environmental impact based on multiple pavement performance measures.” 2018.

[12] Yu, Bin, and Qing Lu. “Life cycle assessment of pavement: Methodology and case study.” Transportation Research Part D: Transport and Environment 17.5: pp 380-388, 2012.

[13] Zhang, H., Lepech, M., Keoleian, G., Qian, S.Z., Li, V., “Dynamic life-cycle modeling of pavement overlay systems: capturing the impacts of users, construction, and roadway deterioration.” Journal of Infrastructure Systems 16, pp 299–309, 2010.

[14] Chan, Arthur, Gregory Keoleian, and Eric Gabler. “Evaluation of life-cycle cost analysis practices used by the Michigan Department of Transportation.” Journal of Transportation Engineering 134.6, pp 236-245, 2008.

[15] Kendall, A. “Life Cycle Assessment for Pavement: Sustainable Pavement Technical Working Group Meeting.” Davis, CA. April 25-26, 2012.

[16] Harvey, John, et al. “Pavement life cycle assessment framework.” No. FHWA-HIF-16-014. United States. Federal Highway Administration, 2016.

[17] AzariJafari, Hessam, Ammar Yahia, and Mourad Ben Amor. “Life cycle assessment of pavements: reviewing research challenges and opportunities.” Journal of Cleaner Production 112, pp 2187-2197, 2016.

[18] Loijos, Alexander, Nicholas Santero, and John Ochsendorf. “Life cycle climate impacts of the US concrete pavement network.” Resources, Conservation and Recycling, pp76-83, 2013.

[19] Santos, J., Ferreira, A., Flintsch, G. “A life cycle assessment model for pavement management: road pavement construction and management in Portugal.” International Journal of Pavement Engineering. 16.4, pp 315-336, 2014.

[20] Wang, Ting, et al. “Life cycle energy consumption and GHG emission from pavement rehabilitation with different rolling resistance.” Journal of Cleaner Production 33, pp 86-96, 2012

[21] Van Deusen, Dave, et al. “Report on 2017 MnROAD construction activities.” Report Number: MN/RC 2018-16, 2018.

[22] AASHTO T 342: Standard method of test for determining dynamic modulus of hot-mix asphalt concrete mixtures, Standard Specifications for Transportation Materials and Methods of Sampling and Testing, 2011.

[23] AASHTO TP 107: Determining the damage characteristic curve of asphalt concrete from direct tension cyclic fatigue tests, American Association of State and Highway Transportation Officials, Washington, D.C., 2004.

[24] Underwood, B. Shane, Cheolmin Baek, and Y. Richard Kim. "Simplified viscoelastic continuum damage model as platform for asphalt concrete fatigue analysis." Transportation research record 2296.1, pp. 36-45, 2012.

[25] Wang, Y. D., and Kim, Y. R. "Development of a pseudo strain energy-based fatigue failure criterion for asphalt mixtures." International Journal of Pavement Engineering 20.10, pp. 1182-1192, 2019.

[26] Zhang, Jun, et al. "Development of a failure criterion for asphalt mixtures under fatigue loading." Road Materials and Pavement Design 14(sup2), pp 1-15, 2013.

[27] Wang, Y. D., Underwood, B. S., and Kim, Y. R. "Development of a fatigue index parameter, Sapp, for asphalt mixes using viscoelastic continuum damage theory." International Journal of Pavement Engineering, pp. 1-15, 2020.

[28] Tex-248-F. "Test procedure for overlay tester." 2014.

[29] Walubita, Lubinda F., et al. "The overlay tester: a sensitivity study to improve repeatability and minimize variability in the test results." No. FHWA/TX-12/0-6607-1. Texas Transportation Institute, 2012.

[30] Garcia, Victor, et al. Improved overlay tester for fatigue cracking resistance of asphalt mixtures. No. TxDOT 0-6815-1. 2017.

[31] AASHTO TP 124-16: Standard method of test for determining the fracture potential of asphalt mixtures using semicircular bend geometry (SCB) at intermediate temperature. American Association of State Highway and Transportation Officials, Washington, DC, 2016.

[32] Al-Qadi, Imad L., et al. "Utilizing lab tests to predict asphalt concrete overlay performance." Illinois Center for Transportation/Illinois Department of Transportation, 2017.

[33] Kaseer, Fawaz, et al. "Development of an index to evaluate the cracking potential of asphalt mixtures using the semi-circular bending test." Construction and Building Materials, 167 pp. 286-298, 2018.

[34] Nemati, R., Haslett, K., Dave, E. V., Sias, J. "Development of a rate-dependent instantaneous power based cracking index parameter for asphalt mixtures." Road Materials and Pavement Design 20.sup1, S315-S331, 2019.

[35] ASTM D7313–20: Standard test method for determining fracture energy of asphalt-aggregate mixtures using the disk-shaped compact tension geometry. ASTM International. Available online: www.astm.org (accessed on 8 April 2021)

[36] Zhu, Yuefeng, et al. "Comprehensive evaluation of low-temperature fracture indices for asphalt mixtures." Road Materials and Pavement Design 18.sup4 pp. 467-490, 2017.

[37] Wagoner MP, Buttlar WG, Paulino GH. "Disk-shaped compact tension test for asphalt concrete fracture." Exp Mech 45, pp. 270–277, 2005a.

[38] Wagoner MP, Buttlar WG, Paulino GH. "Development of a single-edge notched beam test for asphalt concrete mixtures." Journal of Testing and Evaluation 33(6), pp. 452–460, 2005b.

[39] Li X, Marasteanu MO, Iverson N, and Labuz JF. "Observation of crack propagation in asphalt mixtures with acoustic emission," Transportation Research Record, vol 1970, TRB, National Research Council, Washington DC, pp 171–177, 2006.

[40] Song SH, Wagoner MP, Paulino GH, Buttlar WG, "δ25 crack opening displacement parameter in cohesive zone models: experiments and simulations in asphalt concrete," Fatigue and Fracture Engineering Materials and Structures 31(10), pp. 850–856, 2008.

[41] Ahmed, Sarfraz, et al. "Compact tension test for fracture characterization of thin bonded asphalt overlay systems at low temperature." Materials and structures 45.8: pp 1207-1220, 2012.

[42] Pierce, Linda M., et al. "Using falling weight deflectometer data with mechanistic empirical design and analysis." Volume III: Guidelines for Deflection Testing, Analysis, and Interpretation. No. FHWA-HRT-16-011. United States. Federal Highway Administration, 2017.

[43] ASTM D6433-20 Standard Practice for Roads and Parking Lots Pavement Condition Index Surveys. ASTM International. Available online: www.astm.org (accessed on 20 May 2021)

[44] Oshone, Mirkat, Eshan V. Dave, and Jo E. Sias. "Asphalt mix fracture energy based reflective cracking performance criteria for overlay mix selection and design for pavements in cold climates." Construction and Building Materials 211, pp. 1025-1033, 2019.

[45] Saarenketo, Timo. “Measuring electromagnetic properties of asphalt for pavement quality control and defect mapping.” Roadscanners. 2009.

[46] AASHTO T 331: Standard method of test for bulk specific gravity (Gmb) and density of compacted hot mix asphalt (HMA) using automatic vacuum sealing method. American Association of State Highway and Transportation Officials, Washington, DC, 2013.

[47] Paulino, G.H., Buttlar, W.G., and Blankenship, P.B. “GOALI: Reflective Crack Control Treatment and Design Procedures: A New Integrated Approach.” National Science Foundation (NSF) Project 0219566, Final Report, 2006.

[48] Dave, Eshan V. and Buttlar, William G. “Thermal reflective cracking of asphalt concrete overlays.” International Journal of Pavement Engineering, 11: 6, pp.477-488. 2010.

[49] Ahmed, S., et al. “Cracking resistance of thin-bonded overlays using fracture test, numerical simulations and early field performance.” International Journal of Pavement Engineering, 14 (6), pp. 540–552. 2013.

[50] Dave, Eshan V., and Behzad Behnia. “Cohesive zone fracture modelling of asphalt pavements with applications to design of high-performance asphalt overlays.” International Journal of Pavement Engineering 19.3, pp. 319-337. 2018.

[51] Song, S.H., Paulino, G.H. and Buttlar, W.G. “A bilinear cohesive zone model tailored for fracture of asphalt concrete considering rate effects in bulk materials.” Engineering Fracture Mechanics, 73(18), pp. 2829–2848. 2006.

[52] Nemati, Rasool. “Evaluation of structural contribution of asphalt mixtures through improved performance indices.” Dissertation. University of New Hampshire. 2019.

[53] Dave, E.V., S.H. Song, W.G. Buttlar, and G.H. Paulino, “Reflective and thermal cracking modeling of asphalt concrete overlays,” International Conference of Advanced Characterization of Pavement and Soil Engineering Materials, Athens, Greece. Vol. 1, ISBN 978-0-415-44882-6, Taylor & Francis Group, London, pp. 1241-1252. 2007.

[54] Baek, J., Ozer, H., Wang, H., and Al-Qadi, I. “Effects of interface conditions on reflective cracking development in hot-mix asphalt overlays.” Road Materials and Pavement Design, 11 (2), pp. 307–334. 2010.

[55] Dave, E.V., Ahmed, S., Buttlar, W.G., Bausano, J. and Lynn, T. “Investigation of strain tolerant mixture reflective crack relief systems: An integrated approach.” Asphalt Paving Technology-Proceedings Association of Asphalt Technologists, *79*, p.119. 2010.

[56] E.V. Dave, M. Oshone, A. Schokker, C.E. Bennett, “Disc Shaped Compact Tension (DCT) Specifications Development for Asphalt Pavement,” Report Number MN/RC 2019-24, Minnesota Department of Transportation, Research Services Section, 395 John Ireland Boulevard, MS 330, St. Paul, Minnesota 55155, 2019. http://www.dot.state.mn.us/research/reports/2019/201924.pdf

[57] Wang, Ting, et al. “Life cycle energy consumption and GHG emission from pavement rehabilitation with different rolling resistance.” Journal of Cleaner Production 33, pp. 86-96. 2012.

[58] Kang, S., Yang, R., Ozer, H., & Al-Qadi, I. L. “Life-cycle greenhouse gases and energy consumption for material and construction phases of pavement with traffic delay.” Transportation Research Record, 2428(1), 27-34. 2014.

[59] Lu, Qing, Fred L. Mannering, and Chunfu Xin. “A Life Cycle Assessment Framework for Pavement Maintenance and Rehabilitation Technologies: or An Integrated Life Cycle Assessment (LCA)–Life Cycle Cost Analysis (LCCA) Framework for Pavement Maintenance and Rehabilitation.” 2018.

[60] Harvey, John, et al. Environmental Product Declarations: Communicating Environmental Impact for Transportation Products [techbrief]. No. FHWA-HIF-19-087. United States. Federal Highway Administration. Office of Preconstruction, Construction, and Pavements, 2020.

[61] Mukherjee, Amlan, Chaitanya Bhat, and John Harvey. Challenges in Meeting Data Needs for Use of Environmental Product Declarations in Pavement Design and Construction: State of Practice and Future Scope. No. FHWA-HRT-20-022. United States. Federal Highway Administration. Office of Infrastructure Research and Development, 2020.

[62] Rangelov, M., Dylla, H., Mukherjee, A., & Sivaneswaran, N. (2021). Use of environmental product declarations (EPDs) of pavement materials in the United States of America (U.S.A.) to ensure environmental impact reductions. Journal of Cleaner Production, 283, 124619. https://doi.org/10.1016/j.jclepro.2020.124619

[63] Zhou, F., S. Hu, and T. Scullion. (2009). Mechanistic-Empirical Asphalt Overlay Thickness Design And Analysis System, Report FHWA/ TX-09/0-5123-3. FHWA, Texas A&M Transportation Institute, College Station, Texas.

[64] Haslett, K. E., Dave, E. V., & Sias, J. E. (2021). Assessment of Asphalt Mixture Disk-Shaped Compact Tension Test Indices for Reflective Cracking Performance. Journal of Testing and Evaluation.

[65] Federal Highway Administration. RealCost [Computer software]. Version 2.5. Office of Asset Management. https://www.fhwa.dot.gov/infrastructure/asstmgmt/lccasoft.cfm

[66] Federal Highway Administration. "*TECH BRIEF: BUILDING BLOCKS OF LIFE-CYCLE THINKING*." U.S. Department of Transportation Federal Highway Administration. https://www.fhwa.dot.gov/pavement/sustainability/pubs/hif19027.pdf. (accessed on 20 July 2021)

[67] Systems thinking. (2021). Learning for Sustainability. (published on 9 March 2021). https://learningforsustainability.net/systems-thinking/. (accessed on 20 July 2021)

12. APPENDICES

APPENDIX A: Chapter 4 Appendices

Appendix A.1: Paper 1 - Assessment of Asphalt Mixture Disk-Shaped Compact Tension Test Indices for Reflective Cracking Performance

Authors: Katie E. Haslett, Eshan V. Dave and Jo E. Sias

Journal: Journal of Testing and Evaluation

Assessment of Asphalt Mixture Disk-Shaped Compact Tension Test Indices for Reflective Cracking Performance

[1]Katie E. Haslett, [2]*Eshan V. Dave, [3]Jo E. Sias

ABSTRACT

Disk-shaped compact tension (DCT) testing is a commonly used low temperature fracture test to determine the cracking resistance of asphalt mixtures. The current testing specification only considers the fracture energy (G_f) from load-crack mouth opening displacement (CMOD) test data. However, G_f does not directly take into consideration the behavior of the post peak region of the curve, which may indicate the mixture's ability to resist crack propagation and provide insight into fracture processes (e.g., crack growth velocity). It is possible to have two DCT specimens with similar G_f values but dramatically different load-displacement responses. The main focus of this paper is to make a comparative evaluation of various performance indices developed for DCT fracture testing with respect to field reflective cracking performance of 10 full-scale asphalt concrete (AC) overlay test sections. This study evaluates G_f in addition to three other indices; fracture strain tolerance (FST), rate-dependent cracking index (RDCI) and a proposed DCT_{Index} from Minnesota Department of Transportation (MnDOT), that consider the post-peak load-displacement behavior. An equivalent performance index approach is adopted to make

[1] Ph. D. Candidate, Department of Civil and Environmental Engineering, University of New Hampshire, 33 Academic Way, Durham, NH 03824, ORCID: 0000-0002-3494-1066
[2] Associate Professor, Department of Civil and Environmental Engineering, University of New Hampshire, 33 Academic Way, Durham, NH 03824, ORCID: 0000-0001-9788-2246
[3] Professor, Department of Civil and Environmental Engineering, University of New Hampshire, 33 Academic Way, Durham, NH 03824, ORCID: 0000-0001-5284-0392
* Corresponding author

comparisons of test sections with varying overlay structures in terms of thickness and material properties. Results from this study showed there was relatively good agreement between all equivalent laboratory performance indices in identifying the best and worst performing overlay sections according to normalized field performance indices after approximately 3 years of service. In general, the equivalent FST and RDCI laboratory indices rank test sections similarly, while equivalent G_f and DCT_{Index} have comparable ranking.

Keywords: Disk-Shaped Compact Tension, Performance Indices, Equivalent Index, Laboratory Performance, Field Performance, Reflective Cracking

Introduction

Fracture testing along with numerous performance indices derived from fracture tests are often used as a method to evaluate cracking resistance of asphalt mixtures. It is well established that asphalt is a viscoelastic material and follows a quasi-brittle fracture behavior. Fracture energy (G_f), is most commonly used to compare asphalt mixtures cracking performance from load-displacement curves. However, two mixtures with similar fracture energy values may exhibit drastically different post-peak behavior along the load-displacement curve, and result in different cracking resistance performance. Therefore, it is important to take into consideration the rate of crack growth (crack velocity) in comparing asphalt mixtures' performance.

The current research study focused on the comparisons of different cracking performance indices determined from the disk-shaped compact tension (DCT) test with normalized field reflective cracking performance of test sections. Field performance normalization was done to allow for comparisons between laboratory performance indices and field performance based primarily on the material, that is, without the influence of overlay thickness. While overlay thickness has significant effect on reflective cracking performance, the focus of research presented

in this paper was on material scale comparisons between indices. The first objective was to evaluate G_f, fracture strain tolerance (FST), rate-dependent cracking index (RDCI) and DCT_{Index} using an equivalent index approach to normalize contribution coming from different layers and thicknesses in field pavement test sections. The second objective was to compare equivalent laboratory performance indices to normalized field performance data in asphalt concrete (AC) overlays over Portland cement concrete (PCC).

In the following section, a description of the asphalt mixtures and corresponding field sections included in this study is provided. Next, background information on DCT testing, laboratory performance indices, the equivalent index approach and field performance monitoring is described. Then, results and discussion are presented followed by a summary of conclusions from the study.

Materials and Field Sections

This study considered six different mixtures with a variety of nominal maximum aggregate sizes (NMAS), design air void levels, and reclaimed asphalt pavement (RAP) content, as shown in table 1. These six mixtures were used in in constructing 10 full-scale overlay pavement test sections (Cells 984-992 and cell 994) located parallel to the MnROAD mainline on Interstate-94 (I-94) westbound highway. All pavement test sections are AC overlays on 241 mm thick PCC slabs over 127 mm aggregate base material. The original PCC pavement consisted of 8.23 m jointed reinforced slabs with skewed joints containing 31.8 mm dowel bars, and this pavement was constructed in 1973. Table 2 provides a summary of the overlay section designs and corresponding asphalt mixtures. Laboratory testing was performed on asphalt mixtures sampled at the time of construction in September of 2017.

Table 1: Summary of mixtures design properties.

Mix ID *(Design Approach)*	NMAS (mm)	Binder	Des. Air Voids (%)	Des. Total AC (%)	RAP (%)	Des. Gyrations
A440E *(Traditional Superpave 9.5mm)*	9.5	58H-28	4.0	5.8	25	90
B430E *(Regressed Air Void, 3%)*	12.5	58H-28	3.0	5.7	20	90
B440E *(Traditional Superpave 12.5mm)*	12.5	58H-28	4.0	5.4	20	90
B450E *(Superpave 5%)*	12.5	58H-28	5.0	6.6	15	50
C440E *(Traditional Superpave, 19mm)*	19.0	58H-28	4.0	5.6	10	90
D430I *(Binder Rich Reflective Cracking Interlayer)*	4.75	58E-34	2.0-3.0	8.2	0	50

Table 2: Summary of mixtures and corresponding field sections on MnROAD bypass.

Cell	Mixture Type	Comment	Overlay Thickness (mm)
984	A440E	Single lift	38.1
985	B440E	Single lift	38.1
986	B440E	Single lift + spray paver	44.5
987	C440E	Lift 1	63.5
	A440E	Lift 2	38.1
988	C440E	Lift 1	57.2
	B440E	Lift 2	44.5
989	C440E	Lift 1	57.2
	B450E	Lift 2	44.5
990	C440E	Lift 1	57.2
	B430E	Lift 2	44.5
991	C440E	Lift 1	57.2
	A440E	Lift 2	44.5
992	D430I	Lift 1 (interlayer)	25.4
	A440E	Lift 2 (over interlayer)	38.1
994	A440E	Lift 1 (slab stabilization)	38.1

Minimal maintenance had been done on the test sections during previous rehabilitation treatments, with the exception of areas that required full-depth joint replacement or panel replacement as needed. In the most recent rehabilitation project prior to AC overlay construction (2013), diamond grinding in the driving lane was performed[1]. In general, the PCC pavement was reported to be in fair condition with the primary distress being joint faulting with mid-panel cracks and spalling.

Only one test section (Cell 994) was preceded by a polyurethane compaction grouting and void filling prior to overlay construction. The objective behind performing slab stabilization is to reduce the potential for high deflections located at joints and cracks in the underlying PCC pavement, thereby reducing the potential for reflective cracking. A direct comparison can be drawn between the performance of cells 984 and 994, which have the same overall pavement design structure and asphalt mixtures but differ only by the pre-overlay slab stabilization in cell 994.

Falling weight deflectometer (FWD) testing was performed prior to overlay construction to assess the structural capacity of the existing PCC in test cells. Data was recorded for the driving and passing lanes separately, and load transfer efficiency (LTE) calculated. Figure 1 summarizes the pre-overlay LTE results for each test section by lane.

Figure 1: Pre-overlay load transfer efficiency (LTE).

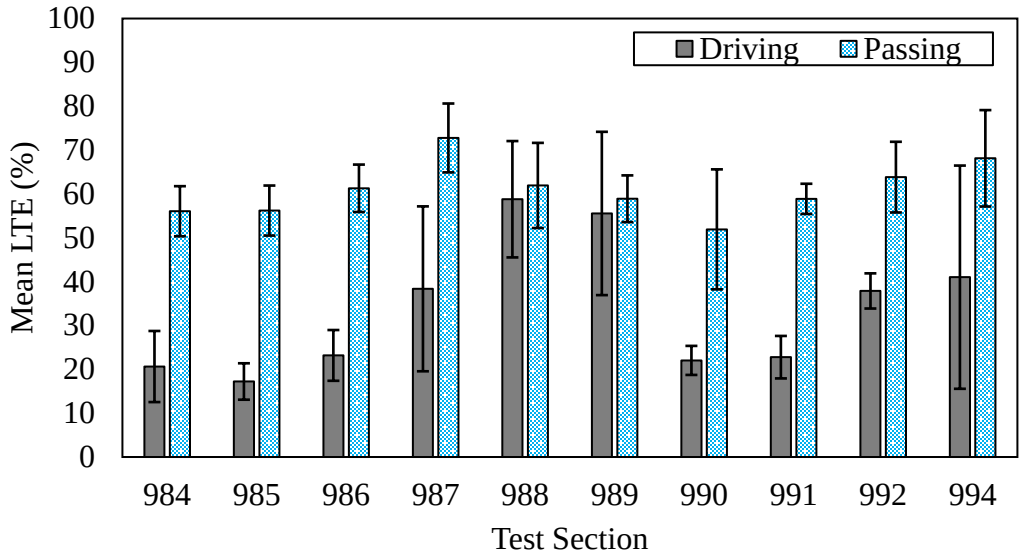

As expected, LTE was higher in the passing lane for all test sections as compared to the driving lane. Among the thicker overlay sections (101.6 mm total thickness) in cells 987-991, lower pre-overlay LTE was observed in cell 990 (3% AV, 12.5 mm surface course) and cell 991 (4% AV surface course, 9.5 mm) as compared to cells 987, 988 and 989. When comparing cell 994 to cell 984 (38.1 mm conventional overlay without slab stabilization) pre-overlay LTE for both driving and passing lanes was higher in cell 994. Cell 985, which also has a 38.1 mm conventional overlay, reported the lowest LTE in the driving lane among all the test sections.

Background and Methodology

Reflective cracking in AC overlays is one of the primary distresses leading to extensive maintenance and rehabilitation costs. Both thermal and traffic loading mechanism will contribute to the generation of stress concentration at location of joints and cracks in the underlying pavement, leading to the formation of reflective cracks. A method to assess the crack resistance of various asphalt mixtures is critical to ensure sufficient mixture performance is achieved in the field. It has

been shown that low temperature cracking performance is not solely based on binder properties but rather a combination of aggregate skeleton, aggregate mineralogy, binder properties and the overall cohesion of the mixture[2]. Therefore, it is important to not only test the individual components (binder and aggregate) but the asphalt concrete mixtures.

There have been several asphalt tests proposed to evaluate low-temperature cracking performance. For example, the Thermal Stress Restrained Specimen Test (TSRST), Asphalt Concrete Cracking Device (ACCD) and the Bending Beam Rheometer (BBR)[3-5]. These laboratory tests are useful to determine the critical cracking temperature of different asphalt mixtures, however the testing protocol requires relatively complex specimen geometry, experimental set-up and or testing conditions. As a result, the development of fracture mechanics-based testing of asphalt mixture gained popularity with testing procedures such as Semi-Circular Bending (SCB), Disk-shaped Compact Tension (DCT), Single Edge Notch Beam (SENB) and Indirect tensile (IDT) tests[6-10]. The current study focuses specifically on the evaluation of cracking performance indices from the DCT test.

The DCT test was developed using similar principles from the ASTM E399 standard for compact tension testing of metals. Wagoner et al. developed the DCT test to obtain fracture energy of asphalt concrete utilizing cylindrical geometry specimens, which are compliant to gyratory compacted or field cored specimens[11]. This is one of the main advantages of the DCT test over the SENB to as the geometry of the test is easily obtained from field cores. Wagoner et al. showed that the variability of fracture energy obtained from the DCT geometry is comparable with the variability associated with other fracture tests such as SENB or SCB test for asphalt concrete[11]. Since the development of the DCT test, there has been extensive research to refine testing procedures (e.g. loading rate, test temperature, replicate numbers) to ensure test repeatability for

asphalt concrete mixtures containing a wide variety of material properties[11-18]. The following subsection provides further details on DCT testing procedure and corresponding performance indices that were investigated as part of the present study.

DCT LABORATORY TESTING

The current state of practice testing procedure is outline in American Society of Testing Materials (ASTM) D7313-20, "Determining Fracture Energy of Asphalt-Aggregate Mixtures Using the Disk-Shaped Compact Tension Geometry."[19] There were 12 replicates tested per asphalt mixture type and an example of a typical load versus crack mouth opening displacement (CMOD) curve is shown in figure 2, highlighting the pre-peak, peak load and post-peak region of the curve.

Figure 2: Typical load versus crack mouth opening displacement (CMOD) curve.

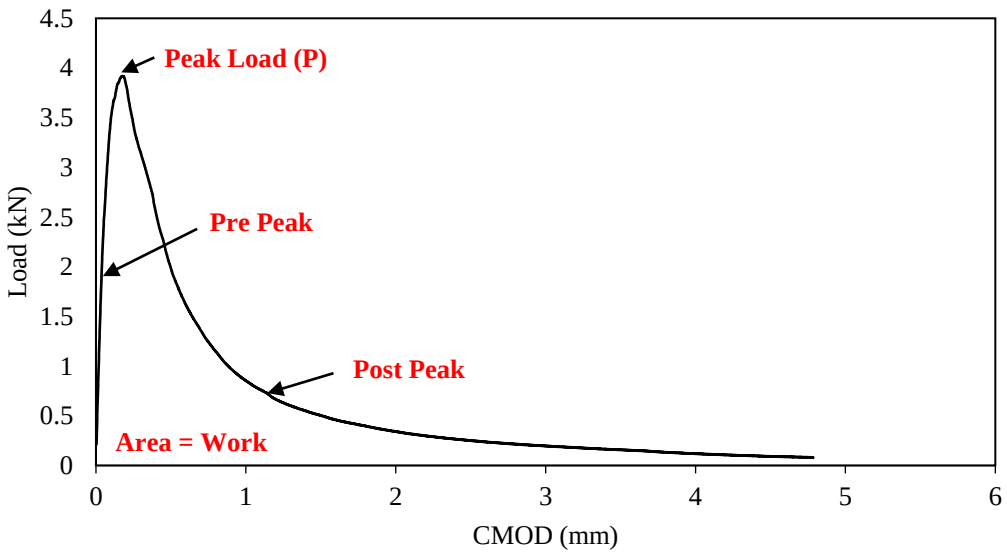

There are several different types of performance indices that can be derived from the DCT load-CMOD curves including energy measures, strength (peak-load) measures and stress-intensity factor measurements. The goal of this study was to compare four performance indices calculated

from DCT test data with reflective cracking field performance data corresponding to 10 AC overlay sections. A brief description of each performance index is provided next.

Fracture Energy (G_f)

DCT testing is most commonly used to determine fracture energy (G_f) of asphalt mix specimens subject to mode I (tensile) loading. Fracture energy is defined as the amount of energy required to create a unit fracture surface and is determined from the area under the load-CMOD curve (fracture work) normalized by the fracture area generated during the test (depends on specimen geometry) (Eqn. 1)[19]. In this equation, "t" is the specimen thickness and "a" represents the initial ligament length.

$$G_f = \frac{Fracture\ work}{t * a} \quad \text{Eqn. 1}$$

A key motivation behind the development of additional performance indices beyond G_f was to differentiate asphalt mixtures that have comparable G_f values, yet have very different fracture behavior (peak load and post-peak region), as demonstrated in figure 3. The difference in rate of crack propagation may not necessarily be capture by G_f alone, therefore additional indices that take into account a second piece of information from the load-CMOD curve can be useful in distinguishing asphalt mixture performance and relating that to field performance.

Figure 3: Example load-CMOD curves for two DCT specimens with similar fracture energy values but different load-displacement responses.

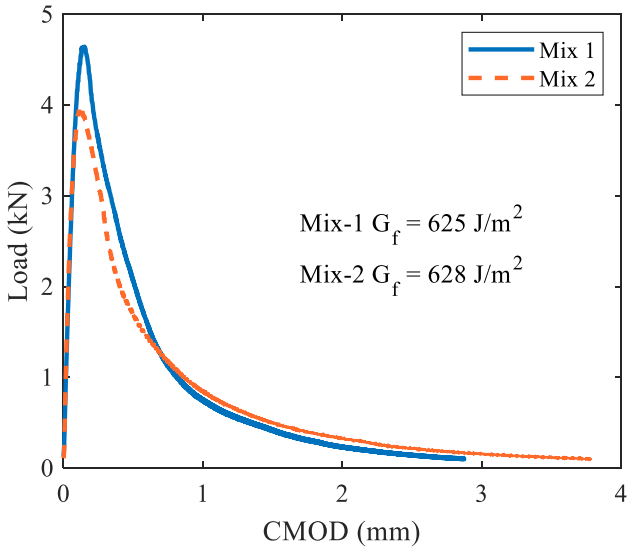

Fracture Strain Tolerance (FST)

Fracture strain tolerance (FST) was proposed as secondary index to distinguish low temperature cracking resistance of mixtures from DCT testing by Zhu et al.[20] The goal of the FST index was to provide the same level of distinction between mixtures as the flexibility and toughness indices while lowering the variability. The main difference in the determination of FST is that the index normalizes fracture energy (G_f) by fracture strength (S_f) as shown in equation 2.

$$FST = \frac{G_f}{S_f} \quad \text{Eqn. 2}$$

S_f can calculated using equation 3, where (P_{max}) represents the maximum load, (t) is the specimens thickness, (L) is the distance from loading location to specimen's boundary, and (a) is ligament length.

$$S_f = \frac{2P_{max}(3L-a)}{t*a^2} \quad \text{Eqn. 3}$$

DCT_{Index}

The Minnesota Department of Transportation (MnDOT) has recently proposed an alternative approach for the interpretation of low-temperature performance test results from DCT test referred to as the DCT_{Index}. The DCT_{Index} calculation is based on the conversion of replicate DCT tests to a single "representative curve" in which points along the representative curve are identified by decreasing percentages of peak load (95%, 85%, 75% etc..) as shown by the red x-markers in figure 4.

Figure 4: Example DCT_{Index} representative curve (dashed line) of post peak region for A400E mixture. (solid line and markers: post peak locations for slope calculations)

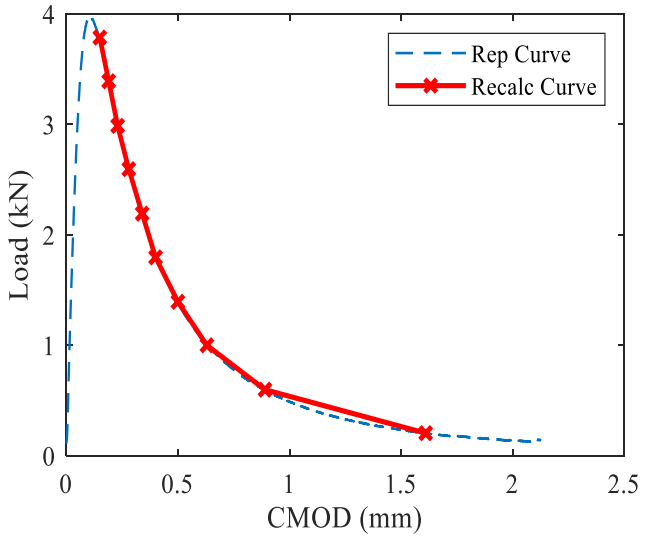

The slope at each of these points is calculated and the DCT_{Index} is calculated using equation 4, where (t) is the specimen thickness, (D) is the specimen diameter, G_f represents fracture energy, m_N is the slope at N% of peak load (absolute value), and l_N is the CMOD at N% of peak load. Initially, different ranges of the DCT_{Index} along the post-peak slope from 95 % to 15% were explored. It was determined that the range from 95-75% of the post-peak slope resulted in the closest ranking to available reflective cracking field performance data for the 10 AC overlay

sections, therefore only the DCT_{Index} from 95-75% is included within this study and from this point on is referred to as simply DCT_{Index}.

$$DCT_{Index} = \frac{t}{95} \times \frac{G_f}{|m_N|} \times \left(\frac{l_N}{D}\right) \quad \text{Eqn. 4}$$

Rate-Dependent Cracking Index

A rate-dependent cracking index (RDCI) originally developed for SCB testing by Nemati et al., was included in this study to assess its ability to differentiate cracking performance of mixtures obtained from DCT testing geometry[21]. RDCI utilizes a cumulative fracture work potential and instantaneous power approach that captures fracture energy and the crack velocity of the material. While all indices discussed prior focus on characteristics of the load-CMOD curve (slope or peak load), RDCI incorporates the loading rate and history of dissipated work during crack growth into the index calculation to discriminate fracture properties of different asphalt mixtures. Figure 5 provides an example of the determination of cumulative work (accumulated area under the load-CMOD curve) as a function of time from peak load (t_{peak}) to 10% of the peak load ($t_{0.1peak}$).

Figure 5: Determination of cumulative work between time at peak load and 10% of peak load for RDCI calculation.

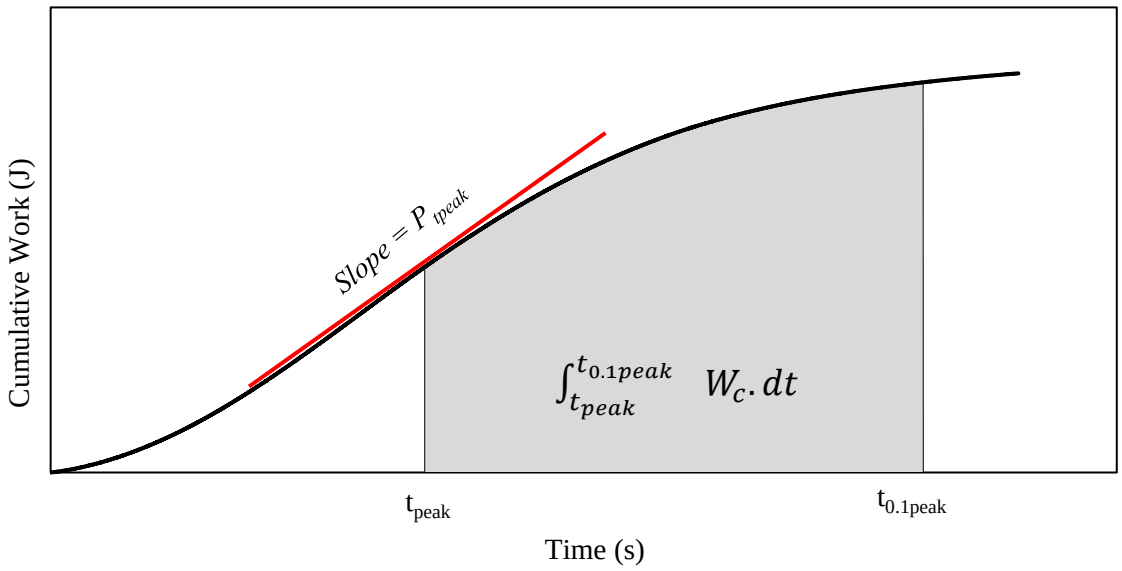

From figure 5, the instantaneous power at peak load is denoted as ($P_{t=peak}$), which is a scalar product of the force applied and velocity at time t_{peak}. The RDCI index calculation incorporates these key points discussed above by taking the area under the cumulative work versus time graph from t_{peak} to $t_{0.1peak}$, normalizing by the product of $P_{t=peak}$ and ligament area, which is the product of specimen thickness (t) and ligament length (a). Finally, a unit correction factor (C) equal to 0.01 is applied (Eqn. 5).

$$RDCI = \frac{\int_{t_{peak}}^{t_{0.1peak}} W_c dt}{P_{tpeak} \times (t * a)} \times C \qquad \text{Eqn. 5}$$

In summary, the calculation of FST, DCT_{Index} and RDCI performance indices in spirit are very similar. They all aim to take into consideration an additional piece of information from the load-CMOD curve response. In the case of FST, it uses fracture strength to normalize fracture energy, DCT_{Index} uses post peak slope and the corresponding CMOD values, and RDCI uses instantaneous power (slope of cumulative work versus time).

EQUIVALENT INDEX APPROACH

To make comparisons between laboratory measured asphalt mixture performance indices and the full-scale pavement test sections located at MnROAD, an equivalency index concept was applied and normalized field performance data (using overlay thickness) used. This is particularly useful when comparing field sections with varying overlay structures (multiple lifts with different asphalt mixtures for each lift), as was the case for 6 of 10 AC overlay sections included in this study. To calculate the equivalent index, the laboratory index value associated with a given mixture (x_i) is multiplied by the contributing layer thickness (t_i) and then normalized by the total overlay thickness (Eqn. 6). The total contribution of varying asphalt mixtures within a given test section can then be compared to thickness normalized reflective cracking field performance.

$$Eqv.Index = \frac{\sum_{i=1}^{n}(x_i * t_i)}{\sum_{i=1}^{n} t_i} \quad \text{Eqn. 6}$$

FIELD PERFORMANCE MONITORING AND INDICES

Field performance data was obtained in the format of distress survey maps from MnDOT. Cracking reported at the location of joints on the distress survey maps was converted into a percentage of cracking at joints and is referred to as reflective cracking percent (%RC) in this study (Eqn. 7).

$$\%RC = \frac{Sum\ of\ crack\ lengths\ reported\ at\ joint\ locations}{Total\ linear\ feet\ of\ joint\ underlying\ pavement} * 100 \quad \text{Eqn.7}$$

To evaluate the %RC reported in each overlay field section, it is important to use field cracking performance measures that consider variable pavement cross section structures and their service life durations. A study by Oshone et al., in 2019 proposed several different field cracking performance measures[22]. Field cracking measures considered in this study included average reflective cracking rate (AvgRC) per month of service, and the total reflective cracking

performance index (RCTotal). RCTotal is similar in nature to the concept of fracture work where RCTotal utilizes the total area under a plot of percent reflective cracking versus pavement service life duration normalized with respect to the time of the last survey. Equations 8 and 9 provide further detail on the calculation of the respective field performance indices.

$$AvgRC = \frac{Refelctive\ cracking\ at\ latest\ survey}{Life\ at\ latest\ survey} \quad \text{Eqn. 8}$$

$$RCTotal = \frac{Reflective\ cracking\ work}{Life\ at\ latest\ survey^2} \quad \text{Eqn. 9}$$

Where:

AvgRC = average reflective cracking rate, % reflective cracking per month

RCTotal = total reflective cracking performance index, % reflective cracking per month

Next, to compare equivalent laboratory performance indices in terms of asphalt mixture contribution to cracking resistance, field performance indices were adjusted with respect to overlay thickness (by multiplying the cracking performance measure by overlay thickness in meters). The intent behind normalizing AvgRC and RCTotal using overlay thickness was to more readily compare the asphalt mixture performance to field performance by accounting for the varying pavement structures. The resulting units for normalized AvgRc and RCTotal are then in terms of percent reflective cracking per meter of overlay thickness per month (%*m/month).

Results and Discussion

LAB PERFORMANCE

First, the six study mixtures were compared using the average mixture performance index values from DCT testing. Average G_f, FST, RDCI and DCT_{Index} from 95-75% of post peak region of representative curve were calculated and are summarized in figure 6. Error bars represent one

standard deviation interval. The B450E mixtures is ranked as the best (highest index value) according to the FST and RDCI, while the D430I mixture is the best according to G_f and DCT_{Index}. All performance indices ranked the A440E mixture as the worst (lowest index value).

Figure 6: Lab performance indices results for (a) fracture energy (G_f), (b) fracture strain tolerance (FST), (c) DCT_{Index} from 95-75% post-peak and (d) rate-dependent cracking index (RDCI).

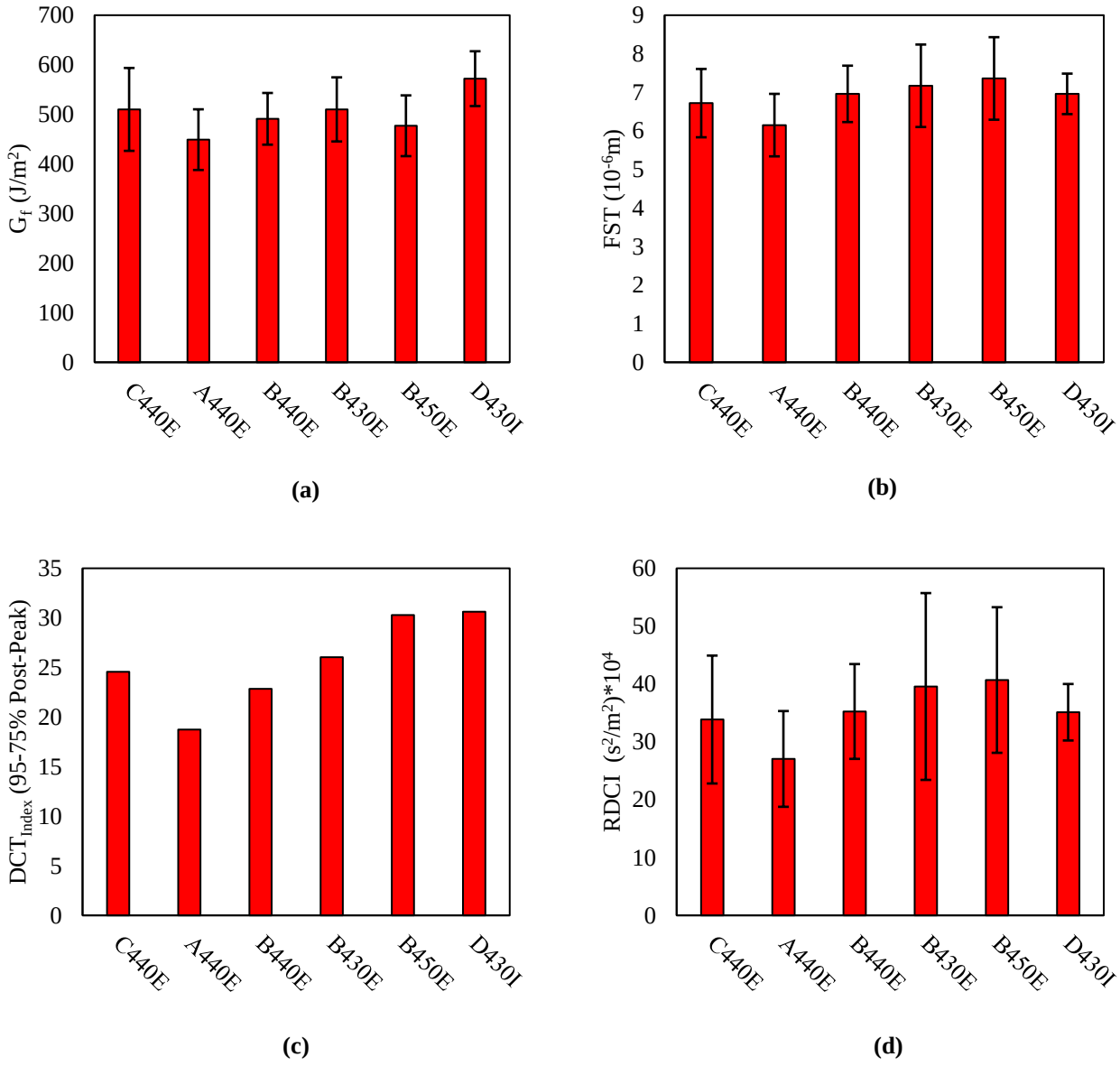

To illustrate the equivalent index approach, a sample calculation is provided for cell 987 using G_f. Cell 987 was constructed in two lifts containing a 63.5 mm base course (C440E mixture

with G_f of 510 J/m^2) and 38.1 mm surface course (A440E mixture with G_f of 449 J/m^2). The equivalent G_f index is calculated first by summing the products of G_f by layer thickness contribution (63.5*510 + 38.1*449 = 4949) then normalizing by the total thickness of the overlay (4949/101.6 = 487 J/m^2).

Figure 7 summarizes the equivalent performance indices for (a) G_f, (b) FST, (c) DCT_{Index} from 95-75% post-peak, and (d) RDCI respectively. Within figure 7, the top four equivalent indices are denoted in green, middle three in orange and bottom three in red. In general, the ranking or grouping of test sections is comparable when using equivalent G_f and equivalent DCT_{Index}. The equivalent FST and RDCI indices also rank test sections similarly. Based on the equivalent lab performance indices, it is anticipated that test cells 984 and 994 will have the worst thickness normalized field performance as all equivalent indices ranked these sections in red. The top performing test sections are expected to be cells 989 and 990, which had the highest equivalent index values for all four equivalent indices as shown in green.

The equivalent index ranking of test sections is influenced by the material type and combination of asphalt mixtures within an overlay structure. For example, cell 992 is constructed in two lifts, where the first lift is a 25.4 mm binder rich reflective cracking interlayer mixture (D430I) with relatively high DCT indices (better crack resistance properties), and the second lift contains a 38.1 mm surface mixture (A440E) with lower DCT indices (lower crack resistance properties). As a result, equivalent laboratory performance indices for cell 992 are not as high as some of the other tests sections where both lifts contain asphalt mixtures with moderate cracking resistance performance. This can be observed by the ranking of cell 992 in red according to the equivalent FST and RDCI indices.

Figure 7: Equivalent overlay test section performance indices for (a) fracture energy (G_f), (b) fracture strain tolerance (FST), (c) DCT_{Index} from 95-75% post-peak and (d) rate-dependent cracking index (RDCI).

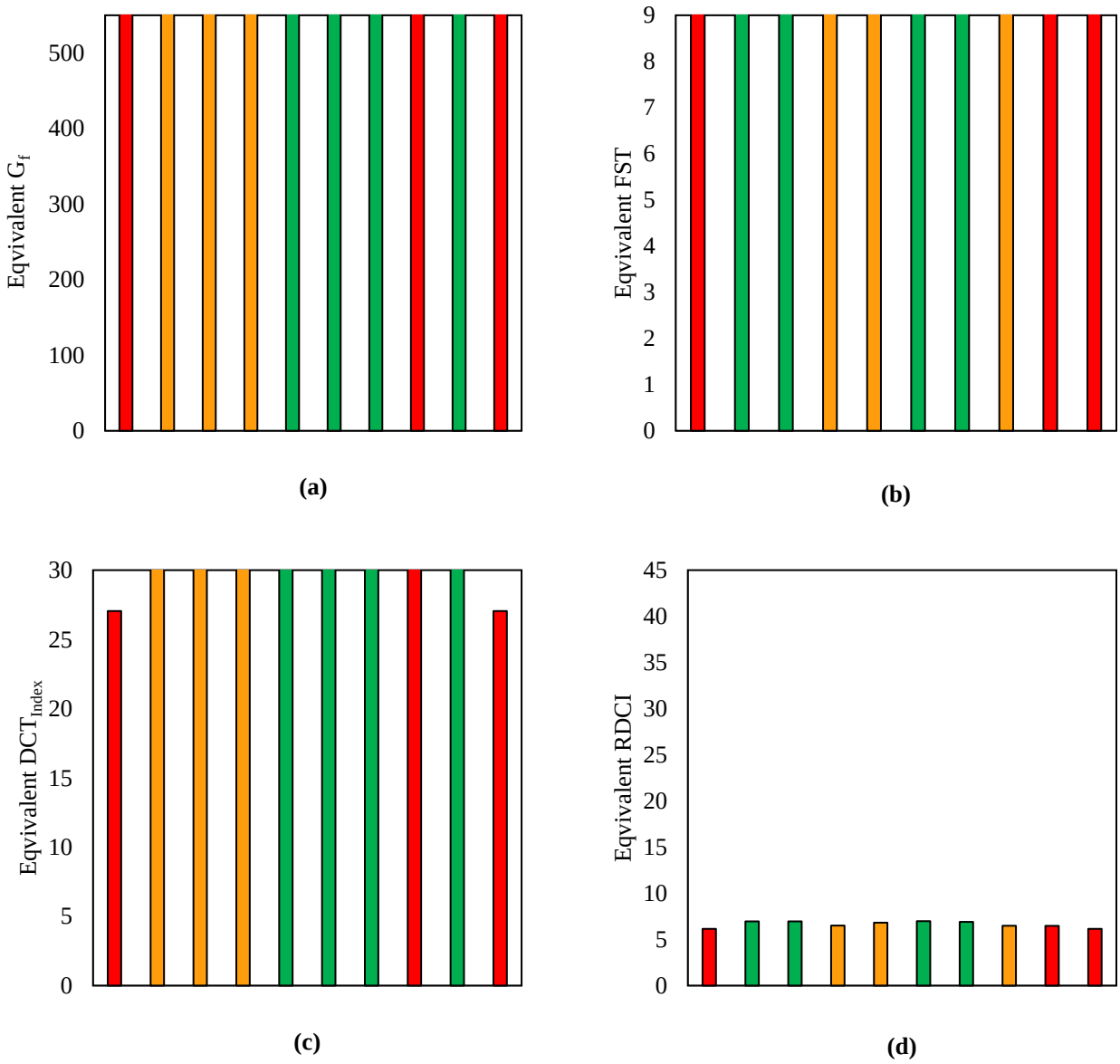

FIELD PERFORMANCE

Distress surveys collected at six different dates post construction were used to quantify the amount of reflective cracking in each test section. Figure 8 summarizes the %RC after approximately 3 years (35 months) of service. In general, the thicker overlay sections (101.6 mm),

except for cell 991, appear to be performing better over time. The section that reported the highest reflective cracking (worst performance) was cell 985.

Figure 8: Reflective cracking performance with time in service.

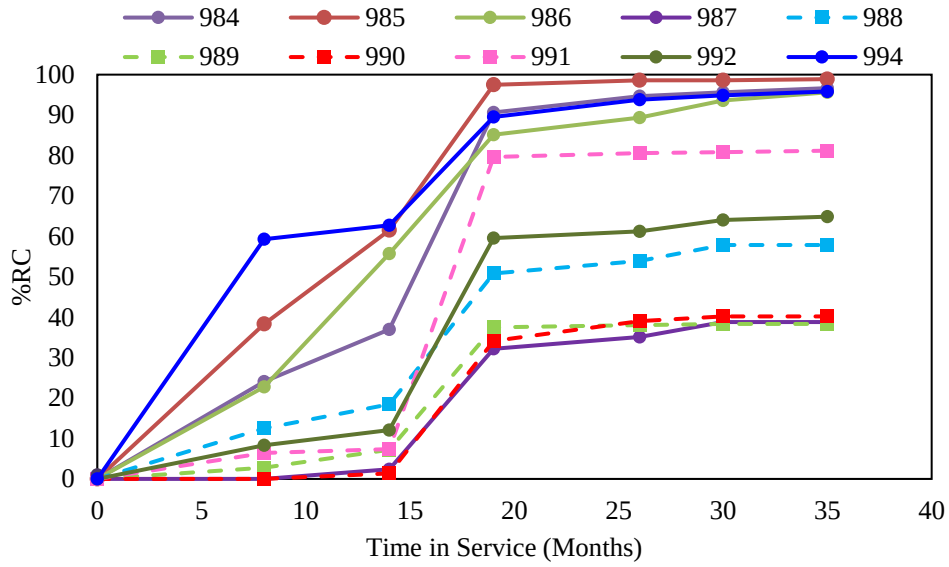

To quantitatively compare reflective cracking performance of field sections, it is important to use cracking performance measures that take into account the rate of cracking, onset of cracking (early versus later in overlay life), variable pavement cross sections materials and service life. Figure 9 and 10 present the normalized AvgRC and RCTotal field performance indices using overlay thickness to account variable overlay thicknesses. The field performance indices are calculated at the six different distress survey dates providing multiple points of comparison with time in service.

Figure 9: Normalized average reflective cracking (AvgRC) rate for field test sections between survey dates.

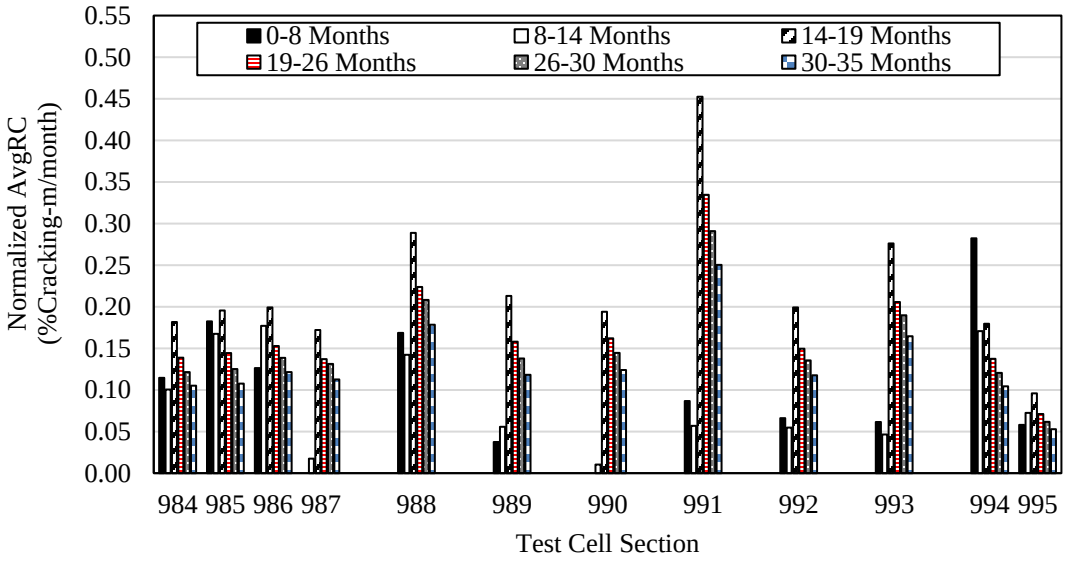

Figure 10: Normalized total reflective cracking (RCTotal) rate for field test sections at time of survey.

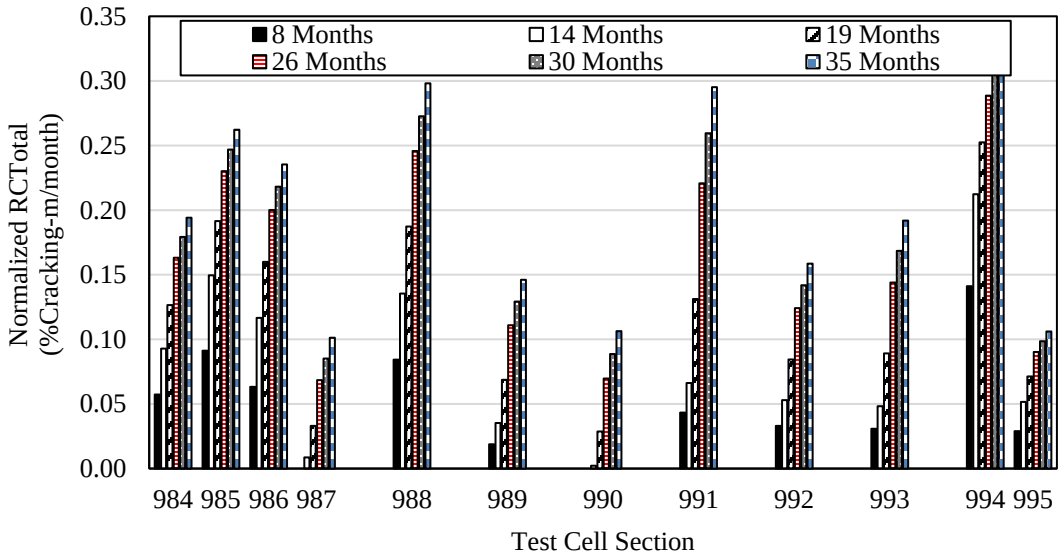

From figure 9, observations can be made regarding which field sections have relatively low or high early rate of reflective cracking. For example, cell 994, which was anticipated to have lower crack resistance based on lab equivalent performance indices, showed poor early reflective cracking performance with relatively higher normalized AvgRC values in the first year of service.

In contrast, cells 987 and 990 had relatively good early performance in terms of normalized AvgRC with minimal reflective cracking reported during the first year of service. Cell 991 can clearly be identified as having the overall highest normalized AvgRC value among all test section between 14 and 19 months in service. Climatic data from weather station located at the site of field test sections confirms that this high AvgRC rate corresponds to a high cooling rate weather event. The impact of several relatively cold thermal loading events in 2018 can also be observed in figure 8 by the steep increases in %RC between the 14 and 19 month surveys.

The best performing tests sections in terms of normalized RCTotal were cells 987 and 990. The worst performing test section out of all 10 overlay sections was cell 994. After normalizing using thickness to account for pavement structure, cells 988 and 991 (thicker overlay sections) were ranked worst compared to conventional 38.1 mm thick AC overlay test sections such as cells 984 or 985. Recalling that cell 985 had the lowest pre-overlay LTE in the driving lane among all test sections indicates that this section outperformed cell 991. Readers are reminded that actual field reflective cracking performance of overlays is function of both asphalt mixture performance and overlay thickness, however, since this paper is focusing on asphalt mixture performance indices from laboratory tests, thickness normalized field performance measures are used for comparison purposes.

It should also be emphasized that it is equally as important when interpreting results in figure 10 to consider the progression of the index values from each survey date. For example, cell 985 and 994 have comparable normalized AvgRC rate values for all survey date intervals except for the first time period between construction and 8 months of service. Cell 994 had higher normalized AvgRC rate initially compared to Cell 985. When comparing the normalized RCTotal index for these two test sections, they are different due to the time effect (early versus late cracking)

being captured. Unlike AvgRC, the RCTotal index encompasses cracking performance over the life of the pavement and gives credit to test sections that crack later and have good early performance. This example reinforces the importance of monitoring pavement performance periodically rather than at a single point in time and the benefit of using performance indices that take into account time in service.

Comparing cells 984 and 994 reveals that slab stabilization (cell 994) was not an effective method to reduce reflective cracking in this case. Both normalized AvgRC and RCTotal performance indices show that cell 994 performed worse than cell 984. This conclusion is based on only one comparison and it is recommended that further evaluation of the use of slab stabilization to mitigate reflective cracking be explored.

RANKING COMPARISON

A comparison of the ranking of field test sections after 35 months in service based on normalized RCTotal field performance index and the equivalent laboratory performance indices is provided in table 3. The top four test sections are highlighted in green, followed by the middle three in orange and the bottom three in red.

Table3: Ranking comparison of asphalt mixture equivalent laboratory performance indices to thickness normalized reflective cracking field performance (normalized RCTotal after 35 months in service).

Cell	Normalized RCTotal	Eqv. G_f	Eqv. FST	Eqv. RDCI	Eqv. DCT_{Index} 95-75%
984	5	9/10	9/10	9/10	9/10
985	7	5/6	2/3	3/4	5/6
986	6	5/6	2/3	3/4	5/6
987	**1**	7	6	6	7
988	9	2	5	5	3
989	3	4	**1**	**1**	**1**
990	2	**1**	4	2	2
991	8	8	7	7	8
992	4	3	8	8	4
994	10	9/10	9/10	9/10	9/10

Overall, there is fair agreement among all laboratory performance indices that cells 989 and 990 are expected to have the best performance, which agrees with the early %RC performance of those test sections and the ranking based on normalized RCTotal. All laboratory equivalent indices identify cell 994 as one of the worst performing test section. This inference is in good agreement with the reported %RC and the normalized RCTotal field index thus far.

There was one test section that had some discrepancy in ranking based on the laboratory equivalent indices and normalized RCTotal field performance index. Cell 988 was ranked among the worst field test sections according to normalized RCTotal (9^{th}), however was ranked among the top performing test sections using equivalent G_f (2^{nd}) and equivalent DCT_{Index} (3^{rd}). Recalling from figure 1, cell 988 had the highest pre-overlay LTE in the driving and 4^{th} highest in the passing lane prior to overlay construction. Based on the relatively high pre-overlay LTE and high ranking from equivalent laboratory indices, it was anticipated that this test section would be among the top performers. After 35 months of service, cell 988 is ranked 4^{th} with approximately 60% reflective cracking reported.

In general, there is similar ranking of test sections using either the equivalent FST or RDCI index. Likewise, there is similar ranking of test sections using equivalent G_f and DCT_{Index}. It is hypothesized that this similarly may be due to the fact that DCT_{Index} was considered from 95-75% of the post-peak slope in this study. Authors originally considered using ranges of DCT_{Index} along the post-peak curve beyond 75%, however larger discrepancies in the ranking of test sections was observed with respect to %RC ranking. Therefore, the range of 95-75% of the post-peak was selected for this study.

Summary and Conclusions

This study focused specifically on evaluating four different performance indices derived from DCT fracture testing with respect to field reflective cracking performance. There were two primary objectives of this study, first to evaluate G_f, FST, RDCI and DCT_{Index} using an equivalent index approach in order to take into consideration differences in overlay structures. The second objective was to compare equivalent lab performance indices to normalized field performance of 10 full-scale AC overlay test sections. Laboratory testing results were presented first by mixture type, and then by an equivalent index to make comparisons to field test sections. The following conclusions are made based on the results of this study:

- Performance indices such as FST, DCT_{Index} and RDCI can be useful methods to evaluate crack resistance of asphalt mixtures by taking into consideration a secondary piece of information (e.g. peak load, fracture strength, instantaneous power) beyond G_f obtained from the load-CMOD curve. Results from this study showed that equivalent FST, DCT_{Index} and RDCI were equally as able to distinguished asphalt mixture as equivalent G_f.

- There was relatively good agreement between all equivalent laboratory performance indices in identify the best and worst performing test sections according to normalized RCTotal. In general, the equivalent FST and RDCI laboratory indices rank test sections similarly, while equivalent G_f and DCT_{Index} have similar ranking. The ranking provided by equivalent G_f and DCT_{Index} has marginally better comparison with thickness normalized field reflective cracking performance as compared to FST and RDCI.
- Results in this study illustrated the importance of monitoring field performance with time as ranking of test sections can vary in terms of short and long-term performance. Normalized field performance indices such as AvgRC and RCTotal, which consider time in service, can be an effective method to compare different mixture combinations in overlays.
- After approximately 3 years (35 months) in service, the best performing overlay sections are the thicker test sections including cells 987, 989 and 990. These test sections were all constructed in two lifts and contain the same base lift material (C440E) and have varying surface course mixtures (A440E, B450E or B430E). Out of these top performing sections, cell 990 had lowest pre-overlay LTE in both the driving and passing lanes. This demonstrates that importance of overlay structure cannot be entirely ignored while making performance comparisons.
-

FUTURE WORK AND RECOMMENDATIONS

Authors recommend that continued monitoring and evaluation of these test sections occur in order to assess and make conclusions on the long-term reflective cracking performance and ranking of test sections. In present work, effect of aging is not considered, asphalt mixture cracking

performance evolves significantly with aging, future effort should consider aging effects in laboratory performance assessment. Furthermore, the equivalent index approach for comparing indices derived from DCT fracture testing can be applied to other AC mixtures with varying material properties and corresponding field sections in different climatic regions.

Acknowledgements

The authors would like to acknowledge the National Road Research Alliance for supporting research presented in this paper. Acknowledgments are also extended to the Minnesota Department of Transportation and MnROAD facility staff for their contributions and assistance in collecting field performance data and performing the disk-shaped compact tension testing. Conclusions and findings presented are those of authors and do not necessarily indicate preference of opinion of project sponsors.

References

1. Van Deusen, David A., et al. Report on 2017 MnROAD Construction Activities. No. MN/RC 2018-16. Minnesota Dept. of Transportation. Research Services & Library, 2018.

2. Judycki, J., Jaskula, P., Dolzycki, B., Pszewski, M., Rys, D., & Stienss, M. (2015). Investigation of low-temperature cracking in newly constructed high-modulus asphalt concrete base course of a motorway pavement. Road Materials and Pavement Design, 16(Suppl.1), 362-288, https://doi.org/10.1080/14680629.2015.1029674

3. Monismith, C. L., Secor, G. A., & Secor, K. E. (1965). Temperature induced stresses and deformation in asphalt concrete. Proceedings, American Association of Asphalt Paving Technologists, 34, 248-285.

4. Kim, S., Sargand, S., & Wargo, A. (2009). A simple test procedure for evaluating low temperature crack resistance of asphalt concrete (report no. FHWA/OH-2009/5). Columbus, OH: Ohio Department of Transportation.

5. Velasquez, R., Zofka, A. Marasteanu, M., & Turos, M. (2011). Bending beam rheometer testing of asphalt mixtures. International Journal of Pavement Engineering, 12(5), 461-474, https://doi.org/10.1080/10298430903289956

6. Li, X., & Marasteanu, M. O. (2004). Evaluation of the low temperature fracture resistance of asphalt mixtures using the semi-circular bend test. Journal of the Association of Asphalt Paving Technologist, 73, 401-426.

7. Wagoner, M. P., Buttlar, W. G., & Paulino, G. H. (2005a). Development of a single-edge notched beam test for asphalt concrete mixtures. ASTM Journal of Testing and Evaluation, 33(6), 452-460.

8. Wagoner, M. P., Buttlar, W. G., & Paulino, G. H. (2005b). Development of a single-edge notched beam test for the study of asphalt concrete fracture. Geotechnical Special Publication No. 130: Advances in Pavement Engineering, Proceedings of Sessions of the GeoFrontiers 2005 Congress, Austin, TX, https://doi.org/10.1061/40776(155)11
9. Marasteanu, M., et al. Investigation of Low Temperature Cracking in Asphalt Pavements- A Transportation Pooled Fund Study. No. 776, MN/RC 2007-43. Minnesota, Dept. of Transportation, 2007.
10. Marasteanu, M. O., W. Buttlar, H Bahia, C. Williams, et al. (2012). Investigation of Low Temperature Cracking in Asphalt Pavements: National Pooled Fund Study Phase II, Minnesota Department of Transportation, MN/RC 2012-23.
11. Wagoner, M. P., W.G. Buttlar, and G. H. Paulino. "Disk-shaped compact tension test for asphalt concrete fracture." Experimental mechanics 45.3 (2005): 270-277, https://doi.org/10.1007/BF02427951
12. Braham, Andrew F. William G. Buttlar, and Mihai O. Marasteanu. “Effect of binder type, aggregate and mixture composition on fracture energy of hot-mix asphalt in cold climates.” Transportation Research Record 2001.1 (2007): 102-109, https://doi.org/10.3141%2F2001-12
13. Dave, Eshan V., et al. “Low temperature fracture evaluation of asphalt mixtures using mechanical testing and acoustic emissions techniques.” Journal of the Association of Asphalt Paving Technologists, 80 (2011).
14. Dave Eshan V. and Chelsea Hoplin. “Flexible pavement thermal cracking performance sensitivity to fracture energy variation of asphalt mixtures.” Road Materials and

Pavement Design 16.sup1 (2015): 423-441, https://doi.org/10.1080/14680629.2015.1029697

15. Li, Xinjun et al. “Effect of factors affecting fracture energy of asphalt concrete at low temperature.” Road materials and pavement design 9. Sup 1 (2008): 397-416, https://doi.org/10.1080/14680629.2008.9690176
16. Wagoner, M. P. Fracture tests for bituminous-aggregate mixtures: laboratory and field investigation. Diss. University of Illinois at Urbana-Champaign, 2006, http://hdl.handle.net/2142/83316
17. Zhou, Fujie, et al. “Experimental design for field validation of laboratory tests to assess cracking resistance of asphalt mixtures.” NCRP Project (2016): 9-57.
18. Zhou, Fujie, et al. “Selection and preliminary evaluation of laboratory cracking tests for routine asphalt mix designs.” Road Materials and Pavement Design 18.sup1 (2017): 62-86, https://doi.org/10.1080/14680629.2016.1266741
19. ASTM D7313-20: Standard Test Method for Determining Fracture Energy of Asphalt-Aggregate Mixtures Using the Disk-Shaped Compact Tension Geometry.
20. Zhu, Yuefeng, et al. "Comprehensive evaluation of low-temperature fracture indices for asphalt mixtures." Road Materials and Pavement Design 18.sup4 (2017): 467-490, https://doi.org/10.1080/14680629.2017.1389085
21. Nemati, Rasool, et al. "Development of a rate-dependent cumulative work and instantaneous power-based asphalt cracking performance index." Road Materials and Pavement Design (2019): 1-17, https://doi.org/10.1080/14680629.2019.1586753
22. Oshone, Mirkat, Eshan V. Dave, and Jo E. Sias. "Asphalt mix fracture energy based reflective cracking performance criteria for overlay mix selection and design for

pavements in cold climates." Construction and Building Materials 211 (2019): 1025-1033, https://doi.org/10.1016/j.conbuildmat.2019.03.27

APPENDIX B: Chapter 6 Appendices

Appendix B.1: Modeling inputs

Table B.1-1 provides the prony series shear modulus, bulk modulus and tau values by mixture type and Table B.1-2 provides WLF shift factors used to model viscoelastic properties of asphalt concrete overlays at reference temperature of 21.1 ˚C for all mixtures except the UTBWC which had a reference temperature of 24 ℃.

Table B.1-1 Prony series inputs for Abaqus models by mixture type.

Mixture Name	gi prony	ki prony	tau i prony
SPWEA440E	1.20E-01	2.59E-01	3.10E-05
	1.00E-01	2.18E-01	2.46E-04
	9.04E-02	1.96E-01	1.69E-03
	6.85E-02	1.48E-01	1.16E-02
	4.35E-02	9.42E-02	8.32E-02
	1.98E-02	4.30E-02	5.11E-01
	9.09E-03	1.97E-02	3.30E+00
	4.18E-03	9.06E-03	2.32E+01
	4.85E-03	1.05E-02	4.01E+02
SPWEB440E	1.28E-01	2.78E-01	2.44E-05
	9.67E-02	2.09E-01	2.04E-04
	8.78E-02	1.90E-01	1.49E-03
	6.70E-02	1.45E-01	1.07E-02
	4.36E-02	9.44E-02	7.75E-02
	1.92E-02	4.16E-02	5.15E-01
	8.67E-03	1.88E-02	3.35E+00
	4.20E-03	9.11E-03	2.30E+01
	4.90E-03	1.06E-02	3.28E+02
SPWEB430E	1.24E-01	2.70E-01	3.13E-05
	9.89E-02	2.14E-01	2.45E-04
	8.98E-02	1.95E-01	1.70E-03
	6.80E-02	1.47E-01	1.18E-02
	4.25E-02	9.21E-02	8.43E-02
	1.90E-02	4.13E-02	5.43E-01
	8.71E-03	1.89E-02	3.57E+00

	4.18E-03	9.05E-03	2.50E+01
	4.75E-03	1.03E-02	3.79E+02
SPWEB450E	1.68E-01	3.65E-01	1.88E-05
	9.52E-02	2.06E-01	1.78E-04
	7.77E-02	1.68E-01	1.30E-03
	5.68E-02	1.23E-01	9.08E-03
	3.50E-02	7.59E-02	6.32E-02
	1.45E-02	3.15E-02	4.58E-01
	6.25E-03	1.35E-02	3.27E+00
	2.86E-03	6.20E-03	2.45E+01
	3.75E-03	8.12E-03	4.95E+02
SPWEC440E	1.38E-01	2.99E-01	2.18E-05
	9.72E-02	2.11E-01	1.91E-04
	8.48E-02	1.84E-01	1.39E-03
	6.44E-02	1.39E-01	9.77E-03
	4.09E-02	8.85E-02	6.95E-02
	1.84E-02	3.98E-02	4.65E-01
	8.01E-03	1.74E-02	3.19E+00
	3.73E-03	8.08E-03	2.33E+01
	4.79E-03	1.04E-02	4.07E+02
SPWED430I	1.16E-01	2.52E-01	3.24E-05
	1.10E-01	2.37E-01	2.60E-04
	9.28E-02	2.01E-01	1.85E-03
	6.44E-02	1.40E-01	1.27E-02
	4.21E-02	9.12E-02	9.29E-02
	1.76E-02	3.81E-02	6.12E-01
	8.27E-03	1.79E-02	3.84E+00
	4.17E-03	9.04E-03	2.56E+01
	4.95E-03	1.07E-02	3.55E+02
SPWED440E	1.56E-01	3.37E-01	2.16E-05
	9.98E-02	2.16E-01	1.91E-04
	8.31E-02	1.80E-01	1.36E-03
	5.97E-02	1.29E-01	9.25E-03
	3.56E-02	7.71E-02	6.37E-02
	1.42E-02	3.08E-02	4.39E-01
	6.02E-03	1.30E-02	3.02E+00
	2.91E-03	6.31E-03	2.21E+01
	3.99E-03	8.64E-03	3.43E+02

UTBWC	1.58E-01	0.00E+00	1.54E+01
	1.98E-01	0.00E+00	2.54E+02
	1.36E-01	0.00E+00	4.82E+03
	2.98E-01	0.00E+00	4.62E+04
	2.11E-01	0.00E+00	1.94E+06

Table B.1-2 WLF shift factors by mixture type at reference temperature of 21.1 ˚C for all mixtures except UTBWC which was at reference temperature of -24 ˚C.

Mix Name	C1	C2
SPWEA440E	15.1	122.8
SPWEB440E	14.8	118.9
SPWEB430E	20.2	164.2
SPWEB450E	16.8	135.4
SPWEC440E	15.0	119.3
SPWED430I	16.5	131.0
SPWED440E	15.8	127.3
UTBWC	17.0	98.07

EICM thermal data for asphalt concrete and PCC layers for 6 different simulated pavement structures is shown in Tables B.1-3 to B.1-8 where the maximum low temperature is highlighted in bold font.

Table B.1-3 EICM surface AC and PCC temperature data for cells 984, 985 and 994.

Cell 984, 985, 994		
Time (hrs)	AC Surface Temp (˚C)	PCC Surface Temp (˚C)
1	-27.2	-26.5
2	-27.3	-26.4
3	-28	-26.4
4	-29.4	-26.7
5	-30.6	-27.4
6	-31.1	-27.8
7	-31.4	-28.2
8	-31.8	-28.5
9	-32.2	-28.8
10	-32.4	-29
11	-32.7	-29.3
12	-32.9	-29.5
13	-33.2	-29.7
14	-33.4	-29.9
15	-33.6	-30.1
16	-33.7	-30.3
17	**-33.8**	-30.4
18	**-33.8**	**-30.5**
19	-33.5	**-30.5**
20	-32.9	**-30.5**
21	-31.7	-30.1
22	-30.6	-29.6
23	-29.9	-29.1
24	-29.5	-28.7

Table B.1-4 EICM surface AC and PCC temperature data for cells 986.

Cell 986		
Time (hrs)	AC Surface Temp (˚C)	PCC Surface Temp (˚C)
1	-27.1	-26.3
2	-27.3	-26.2
3	-28	-26.2
4	-29.5	-26.5
5	-30.6	-27
6	-31	-27.3
7	-31.4	-27.6
8	-31.7	-27.9
9	-32.1	-28.1
10	-32.3	-28.4
11	-32.6	-28.6
12	-32.8	-28.8
13	-33.1	-29
14	-33.2	-29.2
15	-33.4	-29.3
16	-33.5	-29.5
17	-33.6	-29.6
18	**-33.7**	-29.7
19	-33.4	**-29.8**
20	-32.8	-29.7
21	-31.5	-29.5
22	-30.5	-29.1
23	-29.8	-28.7
24	-29.4	-28.4

Table B.1-5 EICM surface AC and PCC temperature data for cells 987.

Cell 987		
Time (hrs)	AC Surface Temp (˚C)	PCC Surface Temp (˚C)
1	-27.2	-25.7
2	-27.3	-25.5
3	-27.4	-25.3
4	-28.1	-25.2
5	-29.7	-25.3
6	-31	-25.5
7	-31.5	-25.7
8	-31.9	-26
9	-32.3	-26.2
10	-32.6	-26.4
11	-32.9	-26.5
12	-33.2	-26.7
13	-33.4	-26.9
14	-33.7	-27
15	-33.9	-27.2
16	-34.1	-27.3
17	-34.2	-27.5
18	**-34.3**	-27.6
19	**-34.3**	-27.7
20	-34	-27.8
21	-33.3	**-27.9**
22	-32	-27.8
23	-30.8	-27.6
24	-30	-27.4

Table B.1-6 EICM surface AC and PCC temperature data for cells 988, 989, 990 and 991.

Cell 988, 989, 990, 991		
Time (hrs)	AC Surface Temp (˚C)	PCC Surface Temp (˚C)
1	-26.4	-21.7
2	-26.6	-21.6
3	-27.4	-21.6
4	-29	-21.6
5	-30.3	-21.8
6	-30.8	-22.1
7	-31.2	-22.3
8	-31.5	-22.5
9	-31.9	-22.7
10	-32.1	-22.8
11	-32.5	-23
12	-32.7	-23.2
13	-32.9	-23.3
14	-33.1	-23.5
15	-33.3	-23.6
16	-33.3	-23.7
17	**-33.4**	-23.8
18	**-33.4**	-24
19	-33.2	-24
20	-32.5	**-24.1**
21	-31.1	**-24.1**
22	-30	-23.9
23	-29.3	-23.7
24	-28.9	-23.5

Table B.1-7 EICM surface AC and PCC temperature data for cells 992 and 993.

Cell 992, 993		
Time (hrs)	AC Surface Temp (˚C)	PCC Surface Temp (˚C)
1	-27.5	-27.4
2	-27.5	-27.2
3	-27.6	-27
4	-28.3	-26.9
5	-29.8	-27.1
6	-31.1	-27.5
7	-31.6	-27.9
8	-31.9	-28.2
9	-32.3	-28.4
10	-32.6	-28.7
11	-32.9	-28.9
12	-33.2	-29.1
13	-33.4	-29.3
14	-33.7	-29.5
15	-33.8	-29.7
16	-34.1	-29.9
17	-34.2	-30.1
18	**-34.3**	-30.2
19	**-34.3**	-30.3
20	-34	**-30.4**
21	-33.4	**-30.4**
22	-32.1	-30.2
23	-30.9	-29.9
24	-30.2	-29.5

Table B.1-8 EICM surface AC and PCC temperature data for cells 995.

Cell 995		
Time (hrs)	AC Surface Temp (˚C)	PCC Surface Temp (˚C)
1	-20.1	-20.8
2	-20.3	-20.6
3	-21.1	-20.8
4	-22.6	-21.3
5	-24	-22.1
6	-24.5	-22.6
7	-24.9	-23
8	-25.3	-23.4
9	-25.7	-23.7
10	-26	-24
11	-26.2	-24.2
12	-26.5	-24.5
13	-26.8	-24.7
14	-27	-24.9
15	-27.2	-25.1
16	-27.4	-25.3
17	-27.4	-25.5
18	**-27.5**	**-25.6**
19	-27.3	**-25.6**
20	-26.8	-25.5
21	-25.9	-25.2
22	-24.8	-24.7
23	-23.7	-24
24	-22.8	-23.4

Table B.1-9 to Table B.1-11 summarize the AC surface temperature corresponding to each hour of the critical thermal cooling event recorded from instrumented thermocouples at MnROAD test facility. The lowest temperature reached for each pavement cross section type is highlighted in bold font.

Table B.1-9 Asphalt concrete surface temperature data for Cell 984, 985 and 994.

Cell 984, 985, 994	
Time (hrs)	AC Surface Temp (˚C)
1	-12.3
2	-14.2
3	-16.7
4	-18.3
5	-20.4
6	-21.9
7	-23.0
8	-23.9
9	-24.7
10	-25.3
11	-25.6
12	-25.8
13	-25.7
14	-25.8
15	-25.8
16	-26.0
17	-26.0
18	**-26.2**
19	**-26.2**
20	-25.5
21	-23.5

Table B.1-10 Asphalt concrete surface temperature data for Cell 987 to Cell 991.

Cell 987, 988, 989, 990, 991	
Time (hrs)	AC Surface Temp (˚C)
1	-17.6
2	-20.0
3	-22.0
4	-22.4
5	-23.1
6	-23.5
7	-23.8
8	-24.4
9	-24.6
10	-24.9
11	-25.3
12	-25.3
13	-25.3
14	**-25.4**
15	**-25.4**
16	-25.3
17	**-25.4**
18	-24.4
19	-22.9
20	-21.7
21	-19.6

Table B.1-11 Asphalt concrete surface temperature data for Cell 992.

Cell 992	
Time (hrs)	AC Surface Temp (˚C)
1	-10.7
2	-14.5
3	-17.8
4	-20.4
5	-22.7
6	-24.6
7	-25.4
8	-26.3
9	-27.2
10	-27.6
11	-27.8
12	-27.7
13	-27.6
14	-27.7
15	-27.8
16	-28.0
17	**-28.1**
18	-28.0
19	**-28.1**
20	-26.6
21	-23.4

Appendix B.2: Finite Element Simulation Results

Table B.2-1 and Table B.2-2 summarize detailed damage ratio results for thermal loading and the combination of thermal and tire loading for each MnROAD model test section under EICM historical thermal loading conditions.

Table B.2-1 Damage ratio detailed results table for thermal loading from EICM.

Thermal Loading									
Cell #	Layer	Thickness		Δmax	ΔS	ΔC	Damage Area (A)	Total Damage Area (B)	Damage Ratio (%)
		(in)	(mm)						
984	Wearing	1.5	38.1	9.48E-01	1.60E-11	1.53E-01	34.98	5.83	100
985	Wearing	1.5	38.1	9.84E-01	1.55E-11	1.73E-01	36.30	6.61	100
986	Wearing	1.75	44.45	3.38E-02	1.55E-11	1.73E-01	0.478	7.71	6.20
987	Wearing	1.5	38.1	1.71E+00	1.60E-11	1.53E-01	64.45	16.54	100.00
	Base	2.5	63.5	1.79E+00	1.65E-11	1.69E-01	111.29		
988	Wearing	1.75	44.45	2.09E-08	1.55E-11	1.73E-01	0.00	17.35	0.50
	Base	2.25	57.15	1.12E-02	1.65E-11	1.69E-01	0.09		
989	Wearing	1.75	44.45	1.85E-08	1.42E-11	1.84E-01	0.00	17.82	0.33
	Base	2.25	57.15	8.71E-03	1.65E-11	1.69E-01	0.06		
990	Wearing	1.75	44.45	1.64E-08	1.57E-11	1.78E-01	0.00	17.55	0.48
	Base	2.25	57.15	1.10E-02	1.65E-11	1.69E-01	0.08		
991	Wearing	1.75	44.45	1.86E-08	1.60E-11	1.53E-01	0.00	16.44	0.37
	Base	2.25	57.15	8.94E-03	1.65E-11	1.69E-01	0.06		
992	Wearing	1.5	38.1	1.73E+00	1.60E-11	1.53E-01	1.74	10.33	100.00
	Base	1	25.4	6.57E+01	1.77E-11	1.77E-01	44.16		
993	Wearing	1.5	38.1	-	-	-	-	-	-
	Base	1	25.4	-	-	-	-		
994	Wearing	1.5	38.1	9.48E-01	1.60E-11	1.53E-01	34.98	5.83	100
995	Wearing	0.75	19.05	1.33E+00	5.05E-12	5.61E-01	25.23	10.69	100

Table B.2-2 Damage ratio detailed results table for thermal and tire loading from EICM.

Thermal and Tire Loading									
Cell #	**Layer**	**Thickness**		**Δmax**	**ΔS**	**ΔC**	**Damage Area (A)**	**Total Damage Area (B)**	**Damage Ratio (%)**
		(in)	**(mm)**						
984	Wearing	1.5	38.1	-	-	-	-	-	-
985	Wearing	1.5	38.1	-	-	-	-	-	-
986	Wearing	1.75	44.45	9.93E-02	1.55E-11	1.73E-01	1.338	7.71	17.35
987	Wearing	1.5	38.1	-	-	-	-	-	-
	Base	2.5	63.5	-	-	-	-		
988	Wearing	1.75	44.45	5.75E-02	1.55E-11	1.73E-01	0.57	17.35	56.2
	Base	2.25	57.15	2.57E-01	1.65E-11	1.69E-01	9.18		
989	Wearing	1.75	44.45	5.07E-02	1.42E-11	1.84E-01	0.48	17.82	51.2
	Base	2.25	57.15	2.47E-01	1.65E-11	1.69E-01	8.64		
990	Wearing	1.75	44.45	4.77E-02	1.57E-11	1.78E-01	0.40	17.55	51.9
	Base	2.25	57.15	2.51E-01	1.65E-11	1.69E-01	8.71		
991	Wearing	1.75	44.45	4.62E-02	1.60E-11	1.53E-01	0.38	16.44	53.9
	Base	2.25	57.15	2.45E-01	1.65E-11	1.69E-01	8.47		
992	Wearing	1.5	38.1	-	-	-	-	-	-
	Base	1	25.4	-	-	-	-		
993	Wearing	1.5	38.1	-	-	-	-	-	-
	Base	1	25.4	-	-	-	-		
994	Wearing	1.5	38.1	-	-	-	-	-	-
995	Wearing	0.75	19.05	-	-	-	-	-	-

Table B.2-3 summarizes the detailed damage ratio results for applicable FE models simulated with thermal loading conditions from instrumented MnROAD test section.

Table B.2-3 Damage ratio detailed results table for thermal loading from instrumented MnROAD test sections.

Thermal Loading									
Cell #	**Layer**	**Thickness**		**Δmax**	**ΔS**	**ΔC**	**Damage Area (A)**	**Total Damage Area (B)**	**Damage Ratio (%)**
		(in)	**(mm)**						
984	Wearing	1.5	38.1	2.54E-01	1.60E-11	1.53E-01	9.48	5.83	100
985	Wearing	1.5	38.1	3.14E-01	1.55E-11	1.73E-01	11.55	6.61	100
986	Wearing	1.75	44.45	-	-	-	-	-	-
987	Wearing	1.5	38.1	1.54E+00	1.60E-11	1.53E-01	57.59	16.54	100
	Base	2.5	63.5	1.48E+00	1.65E-11	1.69E-01	90.63		
988	Wearing	1.75	44.45	3.52E-01	1.55E-11	1.73E-01	15.38	17.35	100
	Base	2.25	57.15	3.80E-01	1.65E-11	1.69E-01	20.72		
989	Wearing	1.75	44.45	1.73E+00	1.42E-11	1.84E-01	75.32	17.82	100
	Base	2.25	57.15	1.66E+00	1.65E-11	1.69E-01	91.97		
990	Wearing	1.75	44.45	4.72E-01	1.57E-11	1.78E-01	20.68	17.55	100
	Base	2.25	57.15	5.08E-01	1.65E-11	1.69E-01	27.93		
991	Wearing	1.75	44.45	1.80E+00	1.60E-11	1.53E-01	79.18	16.44	100
	Base	2.25	57.15	1.76E+00	1.65E-11	1.69E-01	98.78		
992	Wearing	1.5	38.1	3.51E+00	1.60E-11	1.53E-01	127.54	10.94	100
	Base	1	25.4	3.18E+00	1.55E-11	2.01E-01	78.07		
993	Wearing	1.5	38.1	-	-	-	-	-	-
	Base	1	25.4	-	-	-	-		
994	Wearing	1.5	38.1	-	-	-	-	-	-
995	Wearing	0.75	19.05	-	-	-	-	-	-

Appendix B.3: AASHTOWare Pavement ME Design Inputs

Dynamic modulus data by mixture type is shown in Tables B.3-1 to B.3-6 where units are in terms of pounds per square inch (psi).

Table B.3-1 SPWEA440E dynamic modulus data.

Temp (°F)	Frequency (Hz)			
	0.1	1	10	25
10	2306846	2629246	2834267	2891076
40	759097	1235965	1779488	2048980
70	121598	286481	608972	779836
100	34766.1	63187.7	148078	212177
130	17930.2	27773.7	52019.8	70204

Table B.3-2 SPWEB440E dynamic modulus data.

Temp (°F)	Frequency (Hz)			
	0.1	1	10	25
10	2371748	2678600	2870310	2922845
40	784103	1277479	1838311	2054427
70	127485	296811	625809	799681
100	38807.3	68407.7	154466	218822
130	21126.3	31657.7	57144.7	76047.7

Table B.3-3 SPWEB430E dynamic modulus data.

Temp (°F)	Frequency (Hz)			
	0.1	1	10	25
10	2093736	2416686	2618607	2673550
40	711068	1179141	1693250	1908876
70	121533	282441	600205	776276
100	36139.6	62664.2	141621	201514
130	19170.2	26955.1	45602.5	59445.8

Table B.3-4 SPWEB450E dynamic modulus data.

Temp (°F)	Frequency (Hz)			
	0.1	1	10	25
10	1963675	2290150	2499082	2556794
40	558071	985064	1485435	1696409
70	85254.8	200740	455412	601960
100	26857.7	46204.8	99822.9	144324
130	15366.6	21515.3	36114.2	46919.3

Table B.3-5 SPWED430I dynamic modulus data.

Temp (°F)	Frequency (Hz)			
	0.1	1	10	25
10	1773125	2016571	2168429	2209888
40	595199	958836	1379414	1557064
70	92220.5	209373	445833	572004
100	28370.9	48449	106836	152009
130	15744.7	22425.4	38308.6	50017.9

Table B.3-6 SPWEC440E dynamic modulus data.

Temp (°F)	Frequency (Hz)			
	0.1	1	10	25
10	2466337	2775668	2965323	3016596
40	782869	1310828	1888543	2126683
70	125270	292881	631183	818047
100	39360.4	66152.8	148588	212170
130	22014.7	31807.6	55400.8	72923.6

Shear modulus and phase angle data collected using the 4 mm DSR test for typical PG 58-28 (Table B.3-7) and PG 58-34 (Table B.3-8) binders was used as default values for level 1 binder data input as there was no available binder data on the actual binder used in test section 984-995. Units for shear modulus are in terms of psi and phase angle in terms of degrees.

Table B.3-7 PG 58-28 level 1 binder input data at 10 rad/sec frequency.

Temp (°F)	G* (Pa)	Phase Angle
75	12952100	41.7
86	4927900	48.4
97	3245990	51.3

Table B.3-8 PG 58-34 level 1 binder input data at 10 rad/sec frequency.

Temp (°F)	G* (Pa)	Phase Angle
75	5681290	54.3
86	2296100	58.9
97	806572	62.2

PCC material property inputs are provided in Table B.3-9.

Table B.3-9 Detailed PCC Pavement ME design and material properties inputs.

PCC Pavement ME Default Values		
PCC	Thickness (in)	9.5
	Poisson Ratio	0.2
	Unit Weigh (pcf)	150
Mix	Aggregate Type	Limestone
	Cement Content (lb/yd^3)	600
	Cement Type	Type 2
	W/C Ratio	0.42
	Curing Method	curing compound
	Reversible shrinkage (%)	50
	PCC zero-stress temperature (deg F)	Calculated
	Time to develop 50% ultimate shrinkage (day)	35
	Ultimate shrinkage (microstrain)	537.5 (calculated)
Strength (Level 3)	28-day PCC Modulus of rupture (psi)	690
	28-day elastic modulus (psi)	3000000
Thermal	Coefficient of expansion (in/in/deg F)	5.56E-06
	PCC heat capacity (BTU/lb-deg F)	0.28
	Thermal conductivity (BTU-hr-ft-deg F)	1.25

Appendix B.4: Three-Way Comparison of Predicted Model Results

Historical Climate Results

Table B.4.1 Summary of predicted distress levels assuming default weather station data from Champaign, Illinois. Green cells passed the specified design criteria while red cells failed.

Cell Number	Field Performance (%RC)	Pavement ME (ACTR, ft/mile)	FE Thermal (Damage Ratio)	FE thermal and Tire (Damage Ratio)
984	96.7	5558	100	N.A.
985	98.9	4610	100	N.A.
986	95.6	4374	6.2	17.4
987	38.8	3640	100	N.A.
988	57.9	3989	0.5	56.2
989	38.3	1843	0.33	51.2
990	40.2	2443	0.48	51.9
991	81.2	3936	0.37	53.9
992	64.9	5061	100	N.A.
993	90.8	5061	N.A.	N.A.
994	95.8	5558	100	N.A.
995	97.1	N.A.	100	N.A.

Minnesota Climate Results

Table B.4.2 Summary of predicted distress levels using MnROAD weather station data. Green cells passed the specified design criteria while red cells failed.

Cell Number	Field Performance (%RC)	Pavement ME (ACTR ft/mile)	FE Thermal (Damage Ratio)	FE thermal and Tire (Damage Ratio)
984	96.7	3787	100	N.A.
985	98.9	3796	100	N.A.
986	95.6	3437	100	N.A.
987	38.8	3129	100	N.A.
988	57.9	3108	100	N.A.
989	38.3	3535	100	N.A.
990	40.2	3135	100	N.A.
991	81.2	3192	100	N.A.
992	64.9	3149	100	N.A.
993	90.8	3149	N.A.	N.A.
994	95.8	3787	100	N.A.
995	97.1	N.A.	N.A.	N.A.

APPENDIX C: Chapter 7 Appendices

Appendix C.1: Paper 2 - A Statistical Analysis Framework to Evaluate Asphalt Concrete Overlay Reflective Cracking Performance

Authors: Katie E. Haslett, Eshan V. Dave, Jo E. Sias and Ernst Linder

Journal: Transportation Research Record Special Collection of the 2021 AAPT Annual Meeting

A Statistical Analysis Framework to Evaluate Asphalt Concrete Overlay Reflective Cracking Performance

Katie E. Haslett (ORCID ID: 0000-0002-3494-1066)
Department of Civil and Environmental Engineering
University of New Hampshire, Durham, NH, USA, 03824
Tel: 978-494-3105; Email: keh11@wildcats.unh.edu

Eshan V. Dave (ORCID ID: 0000-0001-9788-2246)
Associate Professor
Department of Civil and Environmental Engineering
University of New Hampshire, Durham, NH, USA, 03824
Tel: 603-862-5268; Email: Eshan.Dave@unh.edu

Jo E. Sias (ORCID ID: 0000-0001-5284-0392)
Professor
Department of Civil and Environmental Engineering
University of New Hampshire, Durham, NH, USA, 03824
Tel: 603-862-3277; Email: Jo.Sias@unh.edu

Ernst Linder (ORCID ID: 0000-0002-9658-2329)
Professor
Department of Mathematics and Statistics
University of New Hampshire, Durham, NH, USA, 03824
Tel: 603-862-2687; Email: Ernst.Linder@unh.edu

ABSTRACT

The purpose of this paper is to provide a robust process to statistically analyze reflective cracking field performance data. There is often a lack of consistency and transparency in performing statistical analysis of pavement field performance data, which may not satisfy ANOVA or regression modeling assumptions. A total of 12 full-scale asphalt concrete (AC) overlay pavement test sections located at the MnROAD test facility are used to demonstrate the statistical framework. The percentage of cracking reported at joint locations (%RC) is used to represent reflective cracking performance, and its relationship to pre-overlay load transfer efficiency (LTE), truck traffic, overlay thickness and common performance indices determined from laboratory tests are investigated. The three laboratory tests considered in this study are the disk-shaped compact tension (DCT), semi-circular bend (SCB) and overlay tester (OT). Logistic regression models were used for estimation. Predictive abilities of various models are compared in terms of the percent odds (%odds) of reflective cracking. This is done while assuming varying ability to perform asphalt mixture laboratory performance testing. An example of such a model, where no laboratory performance testing variables are included, showed that a one-unit increase (1-inch) in AC overlay thickness may result in approximately a one-third decrease in the %odds of reflective cracking. A logistic regression model developed that considers laboratory performance data from DCT, SCB and OT resulted in the most optimal model that balances the best fit and best prediction properties without overfitting.

Keywords: Asphalt Concrete Overlays, Reflective Cracking, Field Performance, Laboratory Performance, Statistical Analysis, Generalized Linear Models

INTRODUCTION

Asphalt concrete (AC) overlays are a commonly used as maintenance and rehabilitation (M&R) treatment for deteriorated Portland Cement Concrete (PCC) pavements. Reflective cracking continues to be one of the most prominent distresses in AC overlays over PCC, leading to a shortened service life of the M&R treatment. Ensuring that a sufficient overlay thickness and appropriate asphalt material selection is used to meet a target service life is critical. Often, laboratory performance tests are used to discriminate between good and poor asphalt mixtures using cracking performance indices. Equally as important in the overlay selection process is determining the effects of existing PCC pavement condition and the expected traffic level. A step towards gaining a better understanding on what variables may significantly affect reflective cracking performance is to perform statistical analyses with laboratory performance test results, pavement structure and field performance.

This study uses disk-shaped compact tension (DCT), Illinois flexibility index semi-circular bend (SCB) and overlay tester (OT) results from mixtures corresponding to 12 full-scale overlay pavement test sections located at the MnROAD test facility. A systematic process of how to analyze field performance data that is inherently non-linear and how to overcome this challenge is discussed. The three main objectives of this study are:

1) Determine if the properties/performance indices of the asphalt mixtures determined from various laboratory tests are statistically different.
2) Explore if any significant relationship exists between field reflective cracking performance (%RC) and pre-overlay load transfer efficiency (LTE), overlay thickness, truck traffic and laboratory measured performance indices.
3) Provide a simple exploratory data analysis framework to statistically analyze laboratory and field reflective cracking performance while illustrating best practices.

The scope of this paper consists of a brief background on reflective cracking, followed by a section introducing the methodology undertaken in this study to accomplish the research objectives. A summary of materials and corresponding field test sections is then given, followed by results and discussion demonstrating the exploratory data analysis framework, and finally by a summary of key findings.

BACKGROUND

Reflective cracking is a common distress in AC overlays on PCC pavement due to the combinations of thermal and mechanically driven movements at underlying joints and cracks that reflect through the asphalt surface layer. The most common modes of fracture failure associated with reflective cracking are mode I (opening), mode II (sliding) and mixed mode. Cracks typically form above joint locations due to horizontal tensile or shear stresses generated within the asphalt overlay from traffic loading and temperature variations [1-2]. Contraction and expansion due to cyclic temperature variations as well as warping due to temperature gradients throughout the thickness of the AC layer and underlying PCC slab can lead to the formation of reflective cracks. A major concern with the formation of reflective cracks is that it can lead to premature failure of the overlay and result in further deterioration of underlying pavement layers when water is allowed to infiltrate into the pavement structure. Furthermore, it reduces the structural and functional service life of the composite pavement. Therefore, it is imperative to establish a connection between asphalt mixture fracture performance determined from laboratory testing with field reflective cracking performance. By developing a better understanding of the link between laboratory and field performance, designers and engineers can select the most appropriate overlay design (material choice and thickness) to mitigate reflective cracking potential and achieve longer service life of the overlay.

Several researchers have attempted to correlate laboratory performance to field reflective cracking performance. For example, a study by Walubita et al. in 2020 aimed to correlate laboratory monotonic-loading overlay tester (OT) to field crack performance of six in-service highway sections from four different climatic regions within Texas. It was shown that the OT test was able to statistically differentiate the AC mixtures and also correlated well (coefficient of determination [R^2]>60%) with the measured field cracking performance [3]. Another study by Bennert et al.(2009) sought to determine the cause of premature reflective cracking on I-495 in Massachusetts by using the combination of field falling weight deflectomer (FWD) testing and laboratory testing to simulate horizontal and vertical movements. Flexural beam fatigue testing was used to simulate vertical movements while the OT simulated horizontal joint movements. It was concluded that for the vertical deflection mode, the deflection spectra approach predicted levels of reflective cracking in agreement with measured field performance; for the horizontal deflection mode, OT test results were in agreement with the general trend of reflective cracking performance in the field [4]. However, there still remains a need for further research to validate the correlation of other laboratory testing methods to field reflective cracking performance [5].

In a study by Zhou et al. in 2009, a sensitivity analysis was performed to investigate the effect of varying input parameters on reflective cracking [6]. In the case where AC overlays are constructed on jointed plain concrete pavement (JPCP), as is the case with MnROAD test sections included in this study, the influence of 14 different input parameters were considered. Examples of input parameters include, existing PCC slab modulus, slab thickness, LTE, thermal coefficient of expansion, joint spacing, base layer modulus and base layer thickness. It was found that the following input parameters have a significant influence on reflective cracking performance:

- Traffic loading
- Climate
- Asphalt overlay thickness
- Load transfer efficiency
- Asphalt overlay mixture type
- Existing base layer modulus

In the present study, the first research objective seeks to identify if indices calculated from cracking performance tests are statistically different, and how well the three different laboratory tests discriminate the mixture performance. The second research objective directly targets the input parameters identified by Zhou et al., in addition to laboratory equivalent performance indices, and provides a means to validate the significance of the effect of these parameters on reflective cracking performance. Finally, the third research objective aims to provide a simple step-by-step exploratory data analysis framework that can be followed and applied to laboratory and field reflective cracking performance data.

METHODOLOGY

The following subsections provide a brief description of materials and field test sections considered, lab testing conducted, and an overview of the proposed statistical framework with a brief description of statistical analysis techniques used in this study.

Materials and Field Test Sections

This paper leverages 12 full-scale overlay pavement test sections (Cells 984-995) and one control section (Cell 983) located at the Minnesota Department of Transportation's MnROAD test facility on the original alignment of westbound Interstate 94 [7]. All pavement test sections are AC overlays on 9.5-inch thick PCC slabs (27-ft × 12-ft panels and 1.25-inch diameter dowel bars) over 5-inch MnDOT Class 5 aggregate base material. Each test section is 500-ft in length with a 100-ft transition zone between test sections. A summary of the field test sections along with the corresponding asphalt mixtures properties are provided in Tables 1 and 2, respectively.

Climate and the existing base layer modulus are assumed to be constant among test sections as overlays are constructed adjacent to one another. Furthermore, field test sections have been subject to approximately 816,000 flexible equivalent single axle loads (ESALs) and 1,165,000 rigid ESALs from the time of construction (September 2017) to May 2020. Traffic occurs on test sections typically for a week duration within a given month. The sum of traffic loading from all vehicle classes on both driving and passing lanes was approximately 7.2 million vehicles during this time period, with approximately 17% of the total traffic contribution coming from trucks.

An effort was made to follow the three basic principles of design of experiments. In accordance with the first basic principle, control, there was one test section (Cell 983) without any AC overlay. In terms of randomization (the second principle), materials from all AC overlay test sections were randomly sampled at the time of construction. The third principle is repetition, which was accounted for by taking multiple field performance measurements periodically throughout the service life of each overlay test section. However, it should be noted that a major limitation of field studies is that often times it is unfeasible, due to time and cost constraints, to develop a full factorial design or even a fractional factorial design. This makes it challenging to study main effects with some degree of plausibility without having confounding of higher order interactions in the statistical analysis.

TABLE 1 Summary of field test sections and corresponding asphalt concrete mixtures.

Cell	Description	Mixture ID	Comment	Overlay Thickness (inch)
983	Control	-	-	-
984	AC over concrete (1 lift)	A440E	Single lift	1.5
985		B440E	Single lift	1.5
986		B440E	Single lift (spray paver)	1.75
987	AC over concrete (2 lift)	C440E	Lift 1	2.5
		A440E	Lift 2	1.5
988	AC over concrete, Density Sections (2 lift)	C440E	Lift 1	2.25
		B440E	Lift 2	1.75
989		C440E	Lift 1	2.25
		B450E	Lift 2	1.75
990		C440E	Lift 1	2.25
		B430E	Lift 2	1.75
991		C440E	Lift 1	2.25
		A440E	Lift 2	1.75
992	AC over concrete with interlayer	D430I	Lift 1 (interlayer)	1
		A440E	Lift 2 (over interlayer)	1.5
993	AC over concrete with PASSRC[a]	PASSRC[a]	Lift 1	1
		A440E	Lift 2	1.5
994	AC over concrete (1 lift) with slab stabilization	A440E	Lift 1	1.5
995	AC over concrete (1 lift)	UTBWC[b]	Lift 1, (spray paver)	0.75

[a] Permeable Asphalt Stabilized Stress Relief Course; [b] Ultra-Thin Bonded Wear Course

TABLE 2 Summary of mixture properties.

Mix ID (Design Approach)	NMAS	Binder	Des. Air Void (%)	Des. Total AC (%)	RAP (%)
A440E (Traditional Superpave)	9.5	58H-28	4.0	5.8	25
B430E (Regressed Air Void, 3%)	12.5	58H-28	3.0	5.7	20
B440E (Traditional Superpave)	12.5	58H-28	4.0	5.4	20
B450E (Superpave5)	12.5	58H-28	5.0	6.6	15
C440E (Traditional Superpave)	19.0	58H-28	4.0	5.6	10
D430I (Binder Rich Reflective Cracking Interlayer)	4.75	58E-34	2.0-3.0	8.2	0
PASSRC[a] (Permeable Stress-Absorbing Reflective Cracking Interlayer)	9.5	64S-22	-	3.6	0
UTBWC[b] (Ultra-thin bonded open-graded wear course)	9.5	58V-34	-	5.3	0

Field Performance

Manual crack surveys of each test section were used to quantify reflective cracking performance. Crack distress maps were converted into a percentage of joints cracked within each test cell (excluding the transition zones between the sections). This was accomplished by first taking an inventory of all crack maps and quantifying the total crack length at each joint location. The percent of reflective cracking (% RC) within a test cell was calculated by taking the sum of crack lengths (at underlying joints) within a test cell and normalizing by the total length of PCC joints within the test cell. Figure 1 summarizes the %RC reported by driving and passing lanes for the 12 AC overlay test sections as of August 2020 (35 months in service). In general, less reflective cracking is observed in the thicker overlays (4-inches). Furthermore, LTE percentages prior to overlay construction are provided by lane. As expected, higher LTE was observed in the passing lane compared to the driving lane for all test sections.

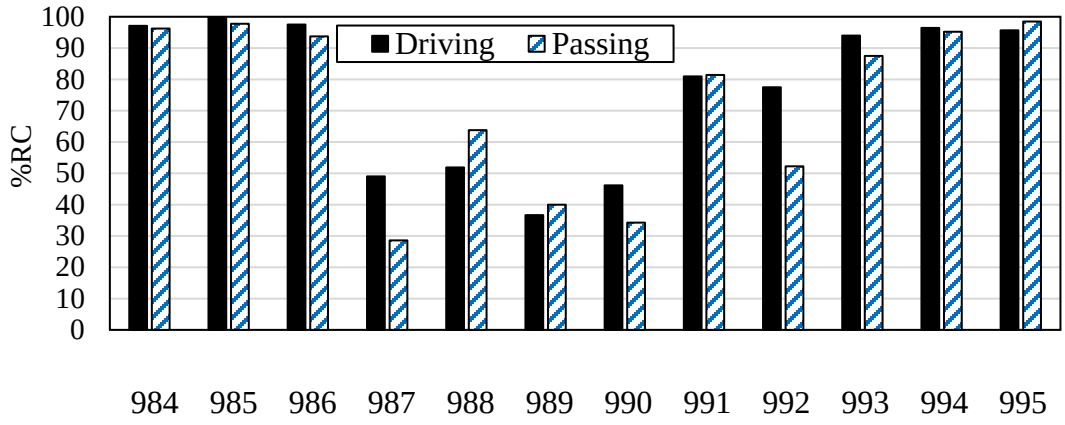

Driving LTE (%)	21	17	23	38	59	56	22	23	38	29	41	32
Passing LTE (%)	56	56	61	73	62	59	52	59	64	59	68	59

FIGURE 1 Reflective cracking (%RC) performance for driving and passing lane after 35 months in service. Numbers within table represent the load transfer efficiency prior to overlay construction.

Lab Performance Testing

Three different laboratory cracking tests were included to evaluate cracking resistance of the asphalt mixtures by means of commonly determined performance indices. Disk-shaped compact tension (DCT) testing was conducted on 12 replicates per mixture type following the MnDOT modified version of the ASTM D7313 procedure. Illinois flexibility index semi-circular bend (SCB) testing was conducted on 24 replicates per mixture type following AASHTO TP 124. Finally, the overlay tester (OT) was performed on five replicates per mixture type following the TX-248-F procedure. All asphalt material was collected at the time of construction in September 2017. A summary of the laboratory performance test values for the mixtures to construct the field test sections is provided in Table 3. The coefficient of variation (COV) for DCT results ranged from 3.3% - 17.1% for all mixtures, while the COV for SCB performance indices ranged from 4.8% - 26.9% and for OT performance indices from 1.3% - 4.3%.

TABLE 3 Summary of average laboratory performance indices by asphalt mixture type.

Lab Test	Performance Index	Mixture Name						
		A440E	B430E	B440E	B450E	C440E	D430I	UTBWC
DCT	Fracture Energy (J/m^2)	449	510	491	477	510	572	518*
	Peak Load (kN)	4.04	3.94	3.89	3.57	4.16	4.44	1.27*
	Time at Peak Load (sec)	6.19	6.84	6.13	6.36	6.69	9.05	-
SCB	Fracture Energy (J/m^2)	2162	1758	1762	1886	1665	1962	-
	Flexibility Index	18.6	14.8	21.8	25.8	15.8	26.4	-
	Cracking Resistance Index	929	835	1001	1073	837	1105	-
	Rate-Dependent Cracking Index ($s^2/m^2 \times 10^4$)	32.8	26.7	39.9	45.6	28.0	46.4	-
OT	Percent Load Reduction at 1000 Cycles	80.7	78.9	83.2	77.6	80.7	72.3	-
*Measured using compact tension (CT) testing instead of DCT.								

To make comparisons between laboratory measured asphalt mixture performance and pavement test sections comprised of multiple lifts and materials, an equivalent index approach was adopted. The equivalent index was calculated using Equation 1 where (x_i) is the laboratory index value associated with a given mixture, (t_i) is the contributing layer thickness and (n) is the number of lifts within a test section. The equivalent performance index value therefore represents an average contribution for a given pavement structure. This provides a necessary link to pair reflective cracking field performance data of test sections with laboratory performance of different asphalt mixtures that make up each overlay structure.

$$Equivalent\ index = \frac{\sum_{i=1}^{n}(x_i * t_i)}{\sum_{i=1}^{n}(t_i)} \quad \text{Eqn. 1}$$

Proposed Statistical Analysis Framework

Figure 2 depicts the proposed statistical analysis framework to evaluate laboratory and field reflective cracking performance data to identify significant variables and/or relationships. There are five key steps to the framework that should be followed in chronological order. In this study, the JMP® statistical software package was utilized to conduct the analysis [8].

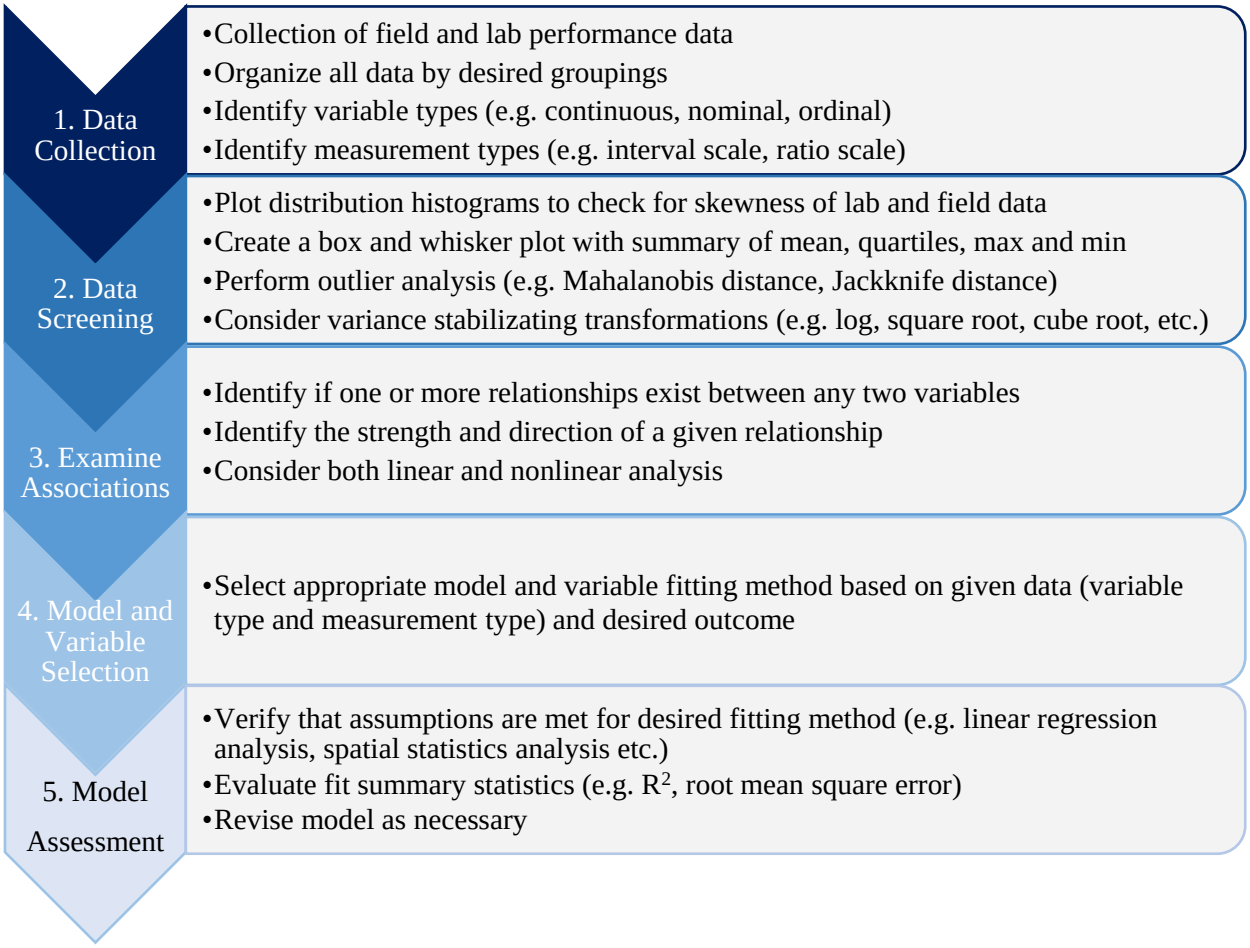

FIGURE 2 Steps in the proposed statistical analysis framework.

ANOVA and Tukey's HSD Test

The one-way analysis of variance (ANOVA) is used to determine whether there are any statistically significant differences between the means of three or more independent (unrelated) groups. The null hypothesis (H_o) generally assumes that all means are equal. Upon determining if one or more group means are statistically different, ANOVA itself cannot identify which particular differences between pairs of means are significant. Post-hoc tests such as individual student t-tests or Tukey's Honest Significant Difference tests (Tukey's HSD), can be used to identify where those specific group means differ by comparing all possible pairs of means. A connecting letters report can be generated to summarize which means are significantly different. In context of this study, ANOVA is used in combination with Tukey's HSD test to answer the first study objective focused on determining if different AC mixtures cracking performance from DCT, SCB and OT laboratory performance indices are significantly different. For all laboratory performance indices with the same letter, the difference between means is not statistically significant. If two performance indices have different letters, they are significantly different. Tukey's HSD test adjusts the significance level to account for the fact that several tests are conducted simultaneously, and an error occurs if at least one of the individual tests is erroneously deemed significant.

Generalized Linear Models

Logistic regression is a specific type of generalized linear model (GLM) for response variables where regular multiple regression does not apply [9]. To analyze reflective cracking field performance, which has an output variable bound from 0 to 100 percent of joints cracked and typically relates to

independent predictor variables in a sigmoidal shape, logistic regression should be utilized instead of linear regression. Furthermore, logistic regression is generally used to describe data and to explain the relationship between one dependent binary variable (e.g. reflective crack formed or not formed) and one or more nominal, ordinal, interval or ratio-level independent variables. The functional form of a logistic regression model is shown in Equation 2, where the probability of reflective cracking occurring (P_i) relates to the predictors $x_{1,i}$, $x_{2,i}$, …, $x_{k,i}$. A common transformation for P_i is the logit ("log odds ratio") transformation, which may be written as shown in Equation 3. Rewriting the equation relating %RC to its predictors using the logit transformation of P_i produces Equation 4 [10], which is linear in the predictors.

$$P_i = \frac{1}{1+e^{-(\beta_0+\beta_1 x_{1,i}+\beta_2 x_{2,i}+\cdots+\beta_k x_{k,i})}} \quad \text{Eqn. 2}$$

$$logit(P_i) = \ln(\frac{P_i}{1-P_i}) \quad \text{Eqn. 3}$$

$$\ln\left(\frac{P_i}{1-P_i}\right) = \beta_0 + \beta_1 x_{1,i} + \beta_2 x_{2,i} + \cdots + \beta_k x_{k,i} \quad \text{Eqn. 4}$$

Using the logit to predict outcomes can be a useful tool, serving as a connection to the probability of an event occurring (i.e. reflective crack will form or not). The logit transformation is the link between a logistic outcome and a linear model. The $\beta_{n\ (n=1,2,\ldots k)}$ estimates do not reflect estimates of probability, but rather reflect estimates that relate to the odds ratio when exponentiated. From there, the conversion from odds to probability can be computed using Equation 5.

$$P_i = \frac{odds}{1+odds} \quad \text{Eqn. 5}$$

RESULTS AND DISCUSSION

A case study utilizing reflective cracking field performance from MnROAD AC overlay test sections (Cell 984-995) was used to demonstrate the proposed statistical analysis framework. The following subsections provide step-by-step results and discussion using the MnROAD AC overlay data set while illustrating best practices in performing statistical analysis of laboratory and field performance data.

Step 1: Data Collection

The first step of the framework focused on collecting and organizing data, as shown in Table 4. This study investigated the influence of design or field variables such as travel lane, truck traffic, AC overlay thickness and pre-overlay LTE (as measure of existing PCC slab condition prior to overlay) on reflective cracking performance. Asphalt mixture cracking resistance was evaluated using DCT, SCB and OT laboratory performance tests. It is acknowledged that the behavior of underlying slabs due to existing PCC condition and combination of mechanical and environmental loading will have an impact on overlay reflective cracking performance. For the case study presented herein leveraging MnROAD test sections, the same traffic and environmental loading history can be assumed to be the same for all test sections. The primary input for slab characterization was selected as pre-overlay LTE as this is a common metric to evaluate the existing PCC condition prior to overlay and for design of AC overlays and was shown to be a significant influence on overlay reflective cracking performance [6]. The use of other criteria to characterize existing PCC condition, additional laboratory performance tests to characterize asphalt mixtures cracking resistance, or effect of different climate conditions can be used with the five-step statistical analysis framework presented in this study.

Manual distress surveys of each test cell were performed by MnDOT staff at six dates since the time of construction. Distress survey data can be further examined on a per lane basis (driving or passing) for each test section, resulting in 144 field data observation points.

TABLE 4 Summary of variables used in the statistical analysis.

Data Source	Variable Name	Notation	Variable Range	Variable Type	Measurement Type
Field	Reflective Cracking (%)	%RC	0 to 100	Continuous	Numeric, Ratio
	Travel Lane	Lane	Driving or Passing	Nominal	Character
	Number of Truck Passes	Traffic	0 to 3.37×10^6	Discrete	Numeric
	AC Overlay Thickness (inches)	Thickness	0.75 to 4	Continuous	Numeric, Ratio
	Pre-Overlay Load Transfer Efficiency (%)	Pre-Overlay LTE	17.2 to 72.8	Continuous	Numeric, Ratio
Lab - DCT	Fracture Energy (J/m^2)	G_f	350 to 729	Continuous	Numeric, Ratio
	Peak Load (kN)	P_{max}	3.18 to 4.74	Continuous	Numeric, Ratio
	Time at Peak Load (sec)	t_{max}	4.6 to 10.0	Continuous	Numeric, Ratio
Lab - SCB	Fracture Energy (J/m^2)	G_f	1,156 to 2,461	Continuous	Numeric, Ratio
	Flexibility Index	FI	10.1 to 41.8	Continuous	Numeric, Ratio
	Cracking Resistance Index	CRI	698 to 1,323	Continuous	Numeric, Ratio
	Rate-Dependent Cracking Index ($s^2/m^2\times10^4$)	RDCI	19.4 to 69.0	Continuous	Numeric, Ratio
Lab - OT	Percent Load Reduction at 1000 Cycles	%Red. @ 1000 Cycles	70.7 to 88.0	Continuous	Numeric, Ratio

Step 2: Data Screening

Exploration and removal of outliers was performed in order to avoid any bias in the conclusions drawn from the statistical analysis. In this study, a preliminary visual check for outliers was performed using standard box plots to visualize data distributions, skewness and spread. Next, outlier analysis was performed using JMP® software following the Mahalanobis distance approach, which has been successfully employed by other researchers to identify and remove outliers [11-12]. Three outlier replicates were identified in the SCB data set and removed prior to performing further statistical analysis. There were no outliers identified in the DCT or OT data sets.

Prior to conducting ANOVA or regression analysis, all data should be screened to determine if variance stabilizing transformations are required (e.g. log, square root, cube root etc.) for either the response variable or for any of the predictor variables. Extremely skewed distributions in the predictors can lead to highly influential points and/or outliers, while in the response variables it may produce violations of the constant variance assumption. Therefore, as a good general practice it can be helpful to plot distributions of all variables to determine if variance stabilizing transformation should be applied. As an example, Figure 3a shows the distribution of truck traffic recorded on MnROAD test sections at the time of the six different distress survey dates. Due to the observed highly skewed distribution (skewedness = 2.71 and variance = 7.54×10^{11}), a natural logarithm transformation was applied to truck traffic data and resulted in the distribution shown in Figure 3b (skewedness = -0.00195 and variance = 0.251).

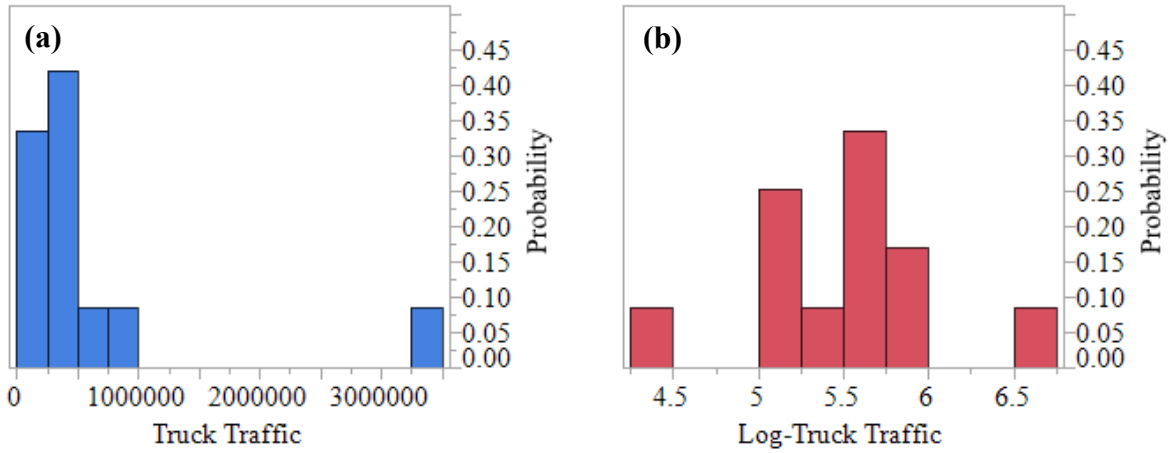

FIGURE 3 Distribution of (a) truck traffic and variable transformed (b) log-truck traffic.

Step 3: Examining Associations

The third step in the framework involved performing ANOVA testing of laboratory test data to determine if there are any statistically significant differences between the groups of means, and subsequently using the Tukey's HSD test to determine where those differences exist. Table 5 summarizes the connecting letter reports for the three different lab performance tests and their respective performance indices, which had significant differences between groups of means. For all performance indices except fracture energy determined from SCB testing, the D430I interlayer mixture was statistically the best performing mixture. This conclusion is based on assigning the letter "A" to the mean group of mixtures with the highest performance index values. For all performance indices except for % load reduction at 1000 cycles from OT testing, a higher value is desirable. In the case of the OT performance index, the letter "A" was assigned to the mean group of mixtures with the lowest % load reduction at 1000 cycles. From Table 5, comparisons of performance indices from the three different laboratory tests can be made on the ability to statistically differentiate cracking performance of the eight mixtures. For example, the OT grouped the B430E mixture as B/C (i.e. not being statistically different from mixtures containing either letter B or C, but significantly different than mixtures containing only letter A). Meanwhile, the results from DCT testing indicate that B430E mixture is not statistically different from any of the mixtures as the letter B appears in the connected letter report for all three performance indices.

TABLE 5 Summary of Tukey's HSD connecting letter report for DCT, SCB and OT laboratory performance tests.

Lab Test	Performance Index	Mixture					
		A440E	B430E	B440E	B450E	C440E	D430I
DCT	Fracture Energy	B	A/B	B	B	A/B	A
	Peak Load	B/C	B/C	C	D	B	A
	Time at Peak Load	B	B	B	B	B	A
SCB	Fracture Energy	A	C/D	C/D	B/C	D	B
	Flexibility Index	B/C	D	B	A	C/D	A
	CRI	C	D	B	A	D	A
	RDCI	C	D	B	A	C/D	A
OT	% Load Reduction at 1000 cycles	B/C	B/C	C	B	B/C	A

Next, Pearson correlation coefficient estimates were examined to identify the strength and direction of linear relationships between mix design variables and lab performance indices. In general, there were only mild to weak relationships observed between volumetric properties and lab performance indices. However, with a limited data set of mixtures and limited range of variable inputs, no formal hypothesis tests about the correlations were performed. This is simply an exploratory exercise and is not meant to provide strong conclusions on the impact of mixture variables on performance indices. An example of a more confirmatory correlation analysis was done in a recent study by Oshone et al., where the effect of mix design variables on thermal cracking performance parameters of mixtures from fracture energy derived from DCT testing and black space location from complex modulus testing [12].

Step 4: Model and Variable Selection

The fourth step in the statistical analysis framework is model and variable selection. Logistic regression was selected as a suitable model for reflective cracking field performance due to its sigmoidal shape and ability to predict a non-normal dependent variable. Several logistic regression models were constructed and estimated using various selections of explanatory (or "independent") variables when attempting to predict reflective cracking performance. Models were constructed using equivalent performance indices from DCT, SCB and OT individually as well as the combination of laboratory tests. Initial models considering only data sources from the field categories in Table 4 (i.e. assumes no access to laboratory testing data) revealed that the effect of log-traffic, adjusted for the effect of other variables, resulted in the sigmoidal pattern shown in the leverage plot (Figure 4).

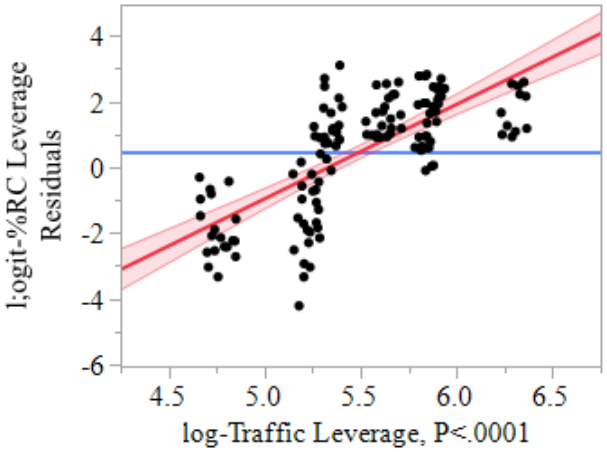

FIGURE 4 Leverage plot of log-traffic and logit %RC.

Therefore, a third degree polynomial could be considered to model the variable effect of log-traffic; however, a simpler model with only a linear term log-traffic which is equal to the natural log of truck traffic divided by 10000 [ln(Traffic/10000)] was chosen. This simpler model resulted in the same R^2 value, however allows for easier interpretation of the effect of traffic on reflective cracking. Table 6 summarizes the eight different models evaluated as part of this study and the statistically significant variables included in each model.

TABLE 6 Summary of logistic regression models evaluated in study.

Model #	Lab Test	Variables Included
1	None	Lane, Pre-Overlay LTE, Thickness, ln(Traffic)
2	DCT	Lane, Pre-Overlay LTE, Thickness, ln(Traffic), G_f
3	SCB	Lane, Pre-Overlay LTE, Thickness, ln(Traffic), FI
4	OT	Lane, Pre-Overlay LTE, Thickness, ln(Traffic), %Red. @ 1000 Cycles
5	DCT, SCB	Lane, Pre-Overlay LTE, Thickness, ln(Traffic), G_f, FI
6	DCT, OT	Lane, Pre-Overlay LTE, Thickness, ln(Traffic), G_f, %Red. @ 1000 Cycles
7	SCB , OT	Lane, Pre-Overlay LTE, Thickness, ln(Traffic), FI, %Red. @ 1000 Cycles
8	DCT, SCB, OT	Lane, Pre-Overlay LTE, Thickness, ln(Traffic), G_f, FI, %Red. @ 1000 Cycles

Step 5: Model Assessment

The first model considered was a baseline model to predict the %odds of reflective cracking when no information is available from laboratory performance testing. Figure 5 shows a plot of the actual versus predicted logit-%RC for the model and a summary table of the regression estimates, standard error, t-ratio and the significance for each variable included in the model. As part of the final step in the statistical analysis framework, model assessment and refinement was carried out by verifying that assumptions are met for logistic regression, and by evaluating the fit of the model. Metrics such as R^2, root mean square error (RMSE), t-test and p-values from model variables were used to examine the overall model fit. Model 1 resulted in an R^2 of 0.68 and RMSE of 1.206. For the given variables included in Model 1, t-test results and corresponding p-values indicate that all variables resulted in a significant relationship except for pre-overlay LTE (p-value=0.1049). This means that for the given model, there is strong evidence that all variables except pre-overlay LTE have a statistically significant relationship with reflective cracking adjusted for the presence of the other variable terms. However, this observation may be misleading due to the limited spread in pre-overlay LTE data for the 24 test sections (driving and passing lanes) considered in this study. It is recommended that further test sections with varying LTE values prior to overlay construction be considered to refine this conclusion. As a result, the pre-overlay LTE variable was left in as a term in subsequent models.

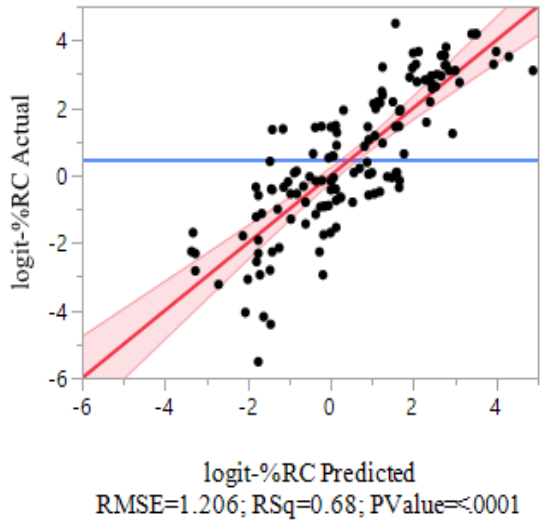

Term/ Variable	Estimate Coefficient	Std. Error	t Ratio	Prob >|t|
Intercept	-0.228	0.618	-0.37	0.7127
Lane [Driving]	-0.792	0.191	-4.14	<.0001
Pre-Overlay LTE (%)	-0.018	0.011	-1.63	0.1049
Thickness (inch)	-1.045	0.089	-11.69	<.0001
ln-Traffic	1.248	0.104	12.01	<.0001

FIGURE 5 Actual versus predicted plot of logit-%RC for Model 1 (left), and parameter estimates from logistic regression model (right).

Interpretation of regression coefficients can provide useful information for decision makers about the impact of model variables on reflective cracking potential. Using overlay thickness as an example, the regression coefficient value is -1.045. Therefore, one unit increase in overlay thickness represents the mean multiplicative change of exp(-1.045)=0.35 in the %odds of RC. In other words, the %odds are reduced to about one-third when increasing overlay thickness by one inch, adjusted for the other variables in the model. To illustrate this example further, Figure 6 , which is a prediction profiler – an interactive feature of the JMP software - shows the predicted logit(%RC) in red and 95% confidence interval values in blue for a 3-inch total overlay thickness (top panel) compared to a 4-inch total overlay thickness (bottom panel) while holding all other model variable terms constant. For the 3-inch overlay, the predicted %odds of RC are approximately 50% [exp(-0.697)=0.5], while for the 4-inch overlay the %odds are reduced by approximately a third to 17.5% [exp(-1.742)=0.175].

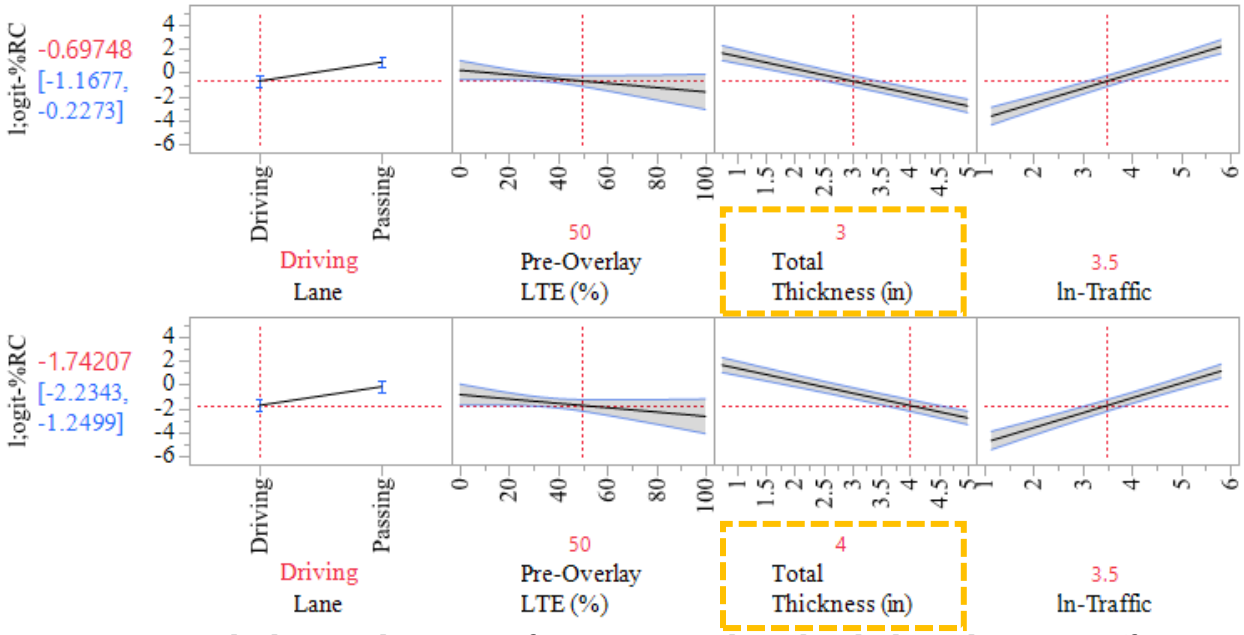

FIGURE 6 Example showing the impact of increasing total overlay thickness by one unit (from 3 to 4 inches) while holding all other variables constant.

For models 2 through 8, varying degrees of laboratory performance data from DCT, SCB or OT were assumed to be available and utilized in model development. The equivalent performance index associated with the 12 different AC overlay structures was utilized in this step to take into account mixture cracking resistance contribution from multi-lift overlays and link it to field reflective cracking performance. Figure 7 shows the results for model 8, which included performance indices (variable terms) from all three laboratory tests. Model 8 produced the highest R^2 of 0.72 and had a RMSE of 1.1033. By observing the t-test results and corresponding p-values, it can be concluded that lane, ln-traffic, and equivalent OT load reduction have significant relationships (p-value < 0.0001) with reflective cracking, while total thickness and equivalent fracture energy from DCT testing have fair relationships (0.0001 < p-value < 0.005) with reflective cracking. Both equivalent flexibility index and pre-overlay LTE reported no significant relationship.

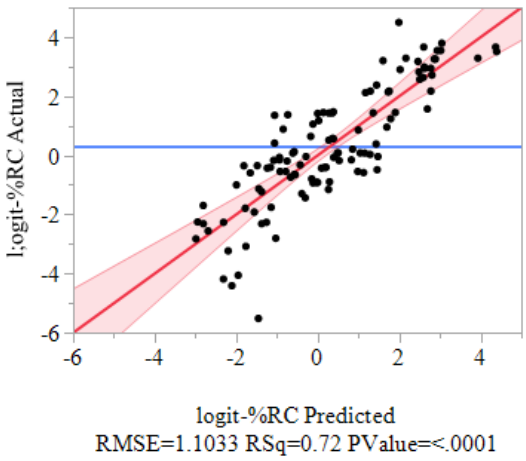

Term/ Variable	Estimate Coefficient	Std. Error	t Ratio	Prob>|t|
Intercept	-15.008	6.150	-2.44	0.0164
Lane[Driving]	-0.806	0.195	-4.13	<.0001
Pre-Overlay LTE (%)	-0.023	0.012	-1.97	0.052
Total Thickness (in)	-0.507	0.234	-2.17	0.0325
ln-Traffic	1.176	0.106	11.08	<.0001
Eqv. OT Load Reduction	0.285	0.068	4.18	<.0001
Eqv. FI	0.160	0.092	1.73	0.0866
Eqv. Fracture Energy	-0.025	0.010	-2.55	0.0121

FIGURE 7 Actual versus predicted plot of logit-%RC for Model 8 (left), and parameter estimates from logistic regression model (right).

One method to perform comparisons of all models relative to each other is to use forwards or backwards elimination techniques. Assessment of model fit may be performed using a penalized-likelihood criteria such as the Bayesian information criterion (BIC) or the Akaike information criterion (AIC), where the model with the lowest BIC or AIC is preferred. Another method to consider is using the R^2-adjusted term rather than simply looking at R^2 to assess model fit. R^2-adjusted is also considered a complexity penalizing selection criterion, which often gives similar results to the AIC criterion. When fitting models, it is possible to increase the likelihood by adding parameters, but in doing so, it may result in overfitting. AIC, BIC and R^2-adjusted attempt to resolve this problem by introducing a penalty term for the number of parameters within the model. Generally, the penalty term is larger in BIC than in AIC, thus BIC favors models with fewer predictor variables. However, it can be useful to look at both criteria simultaneously when making decisions on model selection and the tradeoff in required laboratory performance testing necessary to improve the model fit and the associated time and cost with performing the testing. Table 7 shows the fit of all models considered using these criteria.

TABLE 7 Summary of logistic regression models fits.

Model #	Description	R-square	R-square adjusted	RMSE	AIC	BIC
1	No performance testing	0.681	0.671	1.21	444.5	461.3
2	DCT G_f	0.693	0.680	1.19	403.7	422.5
3	SCB FI	0.667	0.652	1.20	366.9	384.9
4	OT Load Reduction	0.705	0.691	1.13	353.5	371.4
5	DCT G_f & SCB FI	0.676	0.657	1.19	366.4	386.7
6	DCT G_f & OT Load Reduction	0.715	0.698	1.11	352.1	372.5
7	SCB FI & OT Load Reduction	0.705	0.688	1.13	355.8	376.1
8	DCT G_f & SCB FI & OT Load Reduction	0.723	0.704	1.10	351.3	374.0

An "optimal" model balances the best fit and best prediction properties without overfitting. It can be observed that model 8 has the highest R^2 value, lowest AIC and third lowest BIC value. A general trend exists whereas the number of performance tests included in the model increases, the model fit also increases. An exception to this trend is model 4, which leverages only laboratory performance test results from OT to predict the percent odds of reflective cracking occurring as it reported a relatively good model fit (R^2 = 7.05; AIC 353.5; BIC 371.4).

Application of Logistic Regression Models

Three different overlay pavement structures were selected out of the 12 MnROAD test sections to provide an example of the application of logistic regression models to predict the probability of reflective cracking. A 1.5-inch conventional single lift overlay (Cell 984), a 2.5-inch overlay constructed in two lifts with a 1-inch interlayer (Cell 992), and a thicker overlay section (4-inch) constructed in two lifts (Cell 989). Table 8 summarizes the model variables assumed corresponding to each test section's existing PCC LTE and equivalent performance indices. For comparison purposes, the lane (Driving) was held constant, and the traffic (number of trucks) associated with just over 1 year of service was selected as reference point. The number of trucks was acquired from MnDOT's traffic monitoring system, which reported that at 14 months in service there were 278,276 trucks that drove over test sections in the driving lane. Since the traffic variable in the logistic model is in terms of natural logarithm per 10,000 trucks, the number of trucks after 14 months in service was converted accordingly [ln(278276/10,000) = 3.3].

TABLE 8 Model variable inputs for three different overlay structures.

Model Variable	Cell 984	Cell 992	Cell 989
Lane	Driving	Driving	Driving
Pre-Overlay LTE (%)	20.6	37.9	55.5
Total Thickness (in.)	1.5	2.5	4
ln-Traffic	3.3	3.3	3.3
Eqv. OT Load Reduction	80.7	77.3	79.4
Eqv. FI	18.6	21.7	19.9
Eqv. Fracture Energy	449	498	496

Figure 8 shows the percent change of reflective cracking occurring within each of the three overlay pavement cross sections with the same level of truck traffic. This probability was calculated by converting odds to probability using Equation 5. There is no consistent trend among models in ranking of the predicted probability of reflective cracking occurring across the three overlay structures. It is hypothesized this is due to the difference in asphalt mixtures and overlay designs for the three overlay sections and the influence of laboratory performance testing (i.e equivalent performance indices are included in model and influence the outcome). Overall, Cell 989 reported the lowest percent chance of reflective cracking from all eight models with probabilities ranging from 10.3% (model 6) to 12.8% (model 5). Meanwhile, for Cell 992 the probabilities ranged from 22.7% (model 6) to 46.9% (model 3) and Cell 984 from 75.3% (model 4) to 82.7% (model 5). It can be observed that the range in probabilities was narrower for Cell 989 (thicker overlay section) compared to Cell 992 (2.5 inches) or Cell 984 (1.5 inches). This highlights the variability in predicting whether a reflective crack will form or not depends not only on the model selected but also the thickness of the overlay itself. In reality, all three of these test sections have experienced some level of reflective cracking after a year in service. Cell 984 reported the highest amount of cracking reported at joints with 38%, while Cell 992 had 15% and Cell 989 had 2%. As expected, this trend in observed %RC field performance corresponds well with the predicted probability of cracking among these three test sections since models were developed using all MnROAD overlay sections. In general, it can be concluded that there is a consistent trend in Cell 984 predicting the highest probabilities (irrespective of model) and Cell 989 the lowest probabilities of reflective cracking.

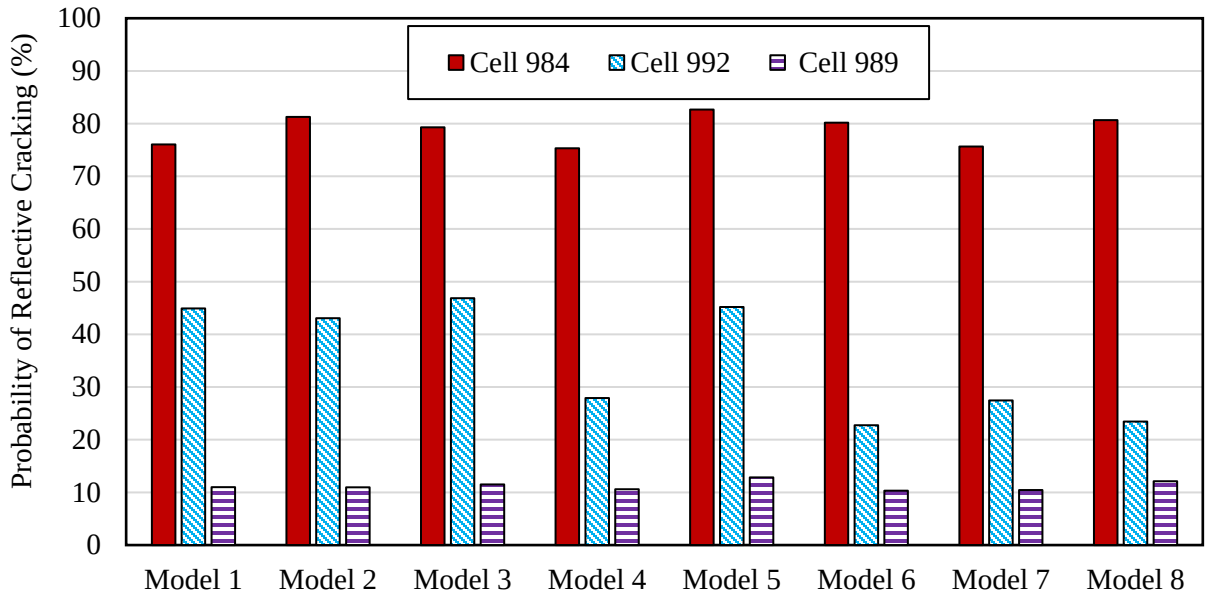

FIGURE 8 Summary of predicted probability of reflective crack occurring after 14 months of service.

A similar type of analysis could be performed on any of the remaining MnROAD test sections or a new alternative overlay section where the asphalt mixture cracking resistance is characterized in the laboratory and subsequently the equivalent performance indices determined given the AC overlay structure. Implementation of models presented herein can be useful in linking laboratory performance testing with field reflective cracking performance. Given the common constraints of time and money associated with constructing field test sections, performing statistical analysis following the framework presented in this study and utilizing predictive models can be advantageous to gain an estimate of field performance. Depending on an agency's or contractor's ability to perform different laboratory performance tests, the corresponding model can be selected and used to predicted the chance of reflective cracking occurring.

Limitations and Assumptions

It is important to acknowledge limitations and assumptions of any model to ensure the proper application and conclusions are drawn. The logistic regression model is used to assess the relationship between a binary outcome (event success or failure) with one or more predictor variables. In this study, an event success was defined as the formation of a reflective crack and event failure meant no reflective cracking has occurred. A major key to regression modeling is to ensure that the correct predictor variables are included in the model. In this study, pre-overlay LTE was used as the sole indicator of the existing PCC slab condition. Furthermore, there were only 12 test sections used in the model development with a limited LTE range of 17% - 73%. Therefore, careful consideration regarding the implementation of models presented in this study should be taken when considering LTE levels outside of this range (or any other model variable term beyond the ranges listed in Table 4). Through previous research efforts, LTE was identified as a significant influence on AC overlay performance. Zhou et al. found that reflective cracking will quickly occur when the load transfer efficiency is below 70%, and no reflective cracking when the LTE is 90% or above [6]. Therefore, the logistic regression models presented in this paper would benefit from including additional overlay field test section performance data with LTE conditions above 70%.

Another limitation of using logistic regression is the sensitivity of using highly correlated explanatory (or predictor) variables (multicollinearity), causing the effect of each variable on the regression model to become less precise [13]. For example, this may be the case when including multiple equivalent performance indices from different laboratory tests. In the models presented in this study, multicolinearity

was not deemed a significant factor. The percentage of variable pairs with a correlation greater than 0.5 (absolute value) was 18% (8 out of 45 pairs). Another method to detect multicollinearity is to use a variance inflation factor (VIF), which is "A measure of how much the standard error of the estimate of the coefficient is inflated due to multicollinearity" [14]. A lower VIF is desirable and in general, a VIF of 5 to 10 may indicate that multicollinearity exists and might be problematic. A VIF greater than 10 indicates multuicollineary exists and is indeed an issue. In the case of the eight different models presented in this study, the highest VIF was reported in models 5 and 8 for the total thickness parameter estimate with VIF values of 6.2 and 6.7 respectively. All other parameter estimates in each model were below a VIF of 5.

SUMMARY AND CONCLUSIONS

In summary, a five-step exploratory statistical analysis framework to analyze laboratory and field reflective cracking performance data was presented. Results from ANOVA and Tukey's HSD testing showed that all three performance tests were able to discriminate the various asphalt mixture cracking performance. For all performance indices considered in this study, except fracture energy determined from SCB testing, the D430I interlayer mixture was ranked statistically as the best performing mixture.

A case study applying the framework to investigate relationships between DCT, SCB, OT laboratory tests and reflective cracking performance of 12 AC overlay pavement test sections was used to illustrate the statistical analysis framework. Logistic regression models were developed and results were presented for a scenario where decision makers do not have access to laboratory testing data on AC overlay materials as well as a scenario where DCT, SCB and OT results are available. It was established for the model where no laboratory testing is conducted, that a one-unit increase (1-inch) in AC overlay thickness may result in approximately a reduction to a third of the %odds of reflective cracking. The best-fit model included laboratory performance data from DCT, SCB and OT tests.

Future extension of this work may be performed by incorporating additional asphalt mixtures and other laboratory performance measured properties through the same statistical analysis framework to investigate if any significant relationships exist. Expanding the data set to include AC overlay test sections from different climatic regions can also help to develop a more comprehensive logistic regression model. Lastly, the five-step exploratory statistical analysis approach presented in this study may also be used for other applications beyond reflective cracking of AC on PCC pavements. For example, the evaluation and or modeling of other common pavement distresses such as fatigue or rutting.

ACKNOWLEDGMENTS

The authors would like to acknowledge the National Road Research Alliance for supporting the research presented in this paper. Furthermore, authors would like to express their sincere gratitude to Minnesota department of Transportation and MnROAD facility staff for their contributions and assistance in collecting field performance data. Conclusions and findings presented are those of authors and do not necessarily indicate preference or opinion of project sponsors.

AUTHOR CONTRIBUTION STATEMENT

The authors confirm contribution to the paper as follows: study conception and design: Katie Haslett (KEH), Eshan V. Dave (EVD), Jo E. Sias (JES); data collection: KEH; analysis and interpretation of results: KEH, EVD, JES, Ernst Linder (EL); draft manuscript preparation: KEH, EVD, JES, EL. All authors reviewed the results and approved the final version of the manuscript.

REFERENCES

1. C. Chen. (2014). Evaluation of Iowa asphalt pavement joint cracking. Graduate Theses and Dissertations. Report Number 13925. Iowa State University, Ames, Iowa.

2. Bennert, Thomas. (2009). A rational approach to the prediction of reflective cracking in bituminous overlays for concrete pavements. Diss. Rutgers University-Graduate School-New Brunswick.

3. Walubita, Lubinda F., et al. (2021). "Correlations and preliminary validation of the laboratory monotonic overlay test (OT) data to reflective cracking performance of in-service field highway sections." Construction and Building Materials 267: 121029.

4. Bennert, T., Worden, M., & Turo, M. (2009). Field and laboratory forensic analysis of reflective cracking on Massachusetts Interstate 495. Transportation research record, 2126(1), 27-38.

5. Loría-Salazar, L. G. (2008). Reflective cracking of flexible pavements: Literature review, analysis models, and testing methods. University of Nevada, Reno.

6. Zhou, F., S. Hu, and T. Scullion. (2009). Mechanistic-Empirical Asphalt Overlay Thickness Design And Analysis System, Report FHWA/ TX-09/0-5123-3. FHWA, Texas A&M Transportation Institute, College Station, Texas.

7. Van Deusen, Dave, et al. (2018). Report on 2017 MnROAD Construction Activities. Report Number: MN/RC 2018-16.

8. JMP®, Version JMP Pro 15. SAS Institute Inc., Cary, NC, 1989-2019.

9. Myers, R. H., & Montgomery, D. C. (1997). A tutorial on generalized linear models. Journal of Quality Technology, 29(3), 274-291.

10. Diez, D., Cetinkaya-Rundel, M., & Barr, C. D. (2019). *Open Intro Statistics* (4th ed.). https://www.openintro.org/book/os/

11. Nemati, R. and Dave, E. (2017). Nominal property based predictive models for asphalt mixture complex modulus (dynamic modulus and phase angle). *Construction and Building Materials, 158:308-319.*

12. Oshone, M., Ghosh, D., Dave, E. V., Daniel, J. S., Voels, J. M., & Dai, S. (2018). Effect of mix design variables on thermal cracking performance parameters of asphalt mixtures. Transportation Research Record, 2672(28), 471-480.

13. Ranganathan, P., Pramesh, C. S., & Aggarwal, R. (2017). Common pitfalls in statistical analysis: logistic regression. Perspectives in clinical research, 8(3), 148.

14. Statistical Analysis System (SAS) Institute Inc. Statistics Knowledge Portal - Multicollinearity. Retrieved May 12, 2021, from https://www.jmp.com/en_in/statistics-knowledge-portal/what-is-multiple-regression/multicollinearity.html

APPENDIX D: Chapter 8 Appendices

Appendix D.1: Paper 3 – Realistic Traffic Condition Informed Life Cycle Assessment: Interstate 495 Maintenance and Rehabilitation Case Study

Authors: Katie E. Haslett, Eshan V. Dave and Weiwei Mo

Journal: Sustainability

Article

Realistic Traffic Condition Informed Life Cycle Assessment: Interstate 495 Maintenance and Rehabilitation Case Study

Katie E. Haslett [1], Eshan V. Dave [1]* and Weiwei Mo [1]

[1] University of New Hampshire; keh11@wildcats.unh.edu ; eshan.dave@unh.edu ; weiwei.mo@unh.edu
* Correspondence: eshan.dave@unh.edu; Tel.: +1-603-862-5268

Received: date; Accepted: date; Published: date

Abstract: As construction costs continue to rise and adequate amounts of funding continues to be a challenge, the allocation of resources is of critical importance when it comes to the maintenance and rehabilitation (M&R) of highway infrastructure. A Life Cycle Assessment (LCA) methodology is presented here that integrates realistic traffic conditions in the operational phase to compare M&R scenarios over the analysis period of a 26-km stretch of Interstate-495. Pavement International Roughness Index (IRI) were determined using AASHTO's PavementME System. Meanwhile, vehicle fuel consumption and emission factors were calculated using a combination of Google Maps®, the U.S. EPA's Motor Vehicle Emission Simulator, the SHRP2 Naturalistic Driving Study, and MassDOT's Transportation Data Management System. The evaluation of pavement performance with realistic traffic conditions, varying M&R strategies and material characteristics was quantified in terms of Life Cycle Cost (LCC), Global Warming Potential (GWP) and Cumulative Energy Demand (CED) for both agencies and users. The inclusion of realistic traffic conditions into the use phase of the LCA resulted in a 6.4% increase in CED and GWP when compared to baseline conditions simulated for a week long operation duration. Results from this study show that optimization of M&R type, material selection and timing may lead to a 2.72% decrease in operations cost and 47.6% decrease in construction/maintenance costs.

Keywords: Pavement, LCA; LCCA; Asphalt; Realistic Traffic Conditions; Rehabilitation

1. Introduction

America's road infrastructure received a report card grade of a D from the American Society of Civil Engineers (ASCE) in 2017 [1]. ASCE reported 6.9 billion hours of delay in traffic, equating to an average of 42 hours of delay per driver [1]. In addition to traffic delays, TRIP (a private nonprofit organization that researches, evaluates and distributes economic and technical data on surface transportation issues) reported that 44% of the nation's highways were in poor or mediocre condition in 2018 causing U.S. road users $130 billion ($599 per driver) in extra vehicle repairs and operating costs [2]. In general, current practice of pavement design and maintenance and rehabilitation (M&R) plans are based on performance and economic factors while neglecting environmental impacts. Furthermore, the majority of cost impacts of the roadway M&R decisions are driven by agency costs only, neglecting the impacts incurred by road users. There is a growing need for performing life cycle assessment (LCA) and life cycle cost analysis (LCCA) as part of decision process to ensure that resources, time, and money is being allocated efficiently to maintain highway infrastructure systems.

Incorporating an LCA-LCCA approach into the pavement design and M&R process will help to improve the pavement management of highway infrastructure systems [3 (pp. 86-96), 4 (pp.27-34), 5]. It will also help to identify explicit and implicit costs incurred by both agencies and users. To date there has been an extensive amount of recent research focused on the development of LCA frameworks for pavements, which can be attested by a series of Pavement LCA symposia (2010, 2012, 2014 and 2017) and the corresponding compilation of proceedings [6, 7, 8, 9]. Transportation agencies are also increasingly becoming aware and involved in the development of LCA tools for pavements. For example, the US Department of Transportation and Federal Highway Administration (FHWA) recently released a pavement LCA framework document in an effort to aid the implementation and adoption of LCA principles in the pavement design process [10]. In addition to the LCA framework, this report also provided guidance on the overall approach, methodology, system boundaries and identified current knowledge gaps in pavement LCA. The report also identified current research gaps in LCA framework including topics such as, traffic delay, rolling resistance, pavement albedo, and end of life allocation.

A study in 2018 focused on the development of an integrated LCA-LCCA framework to aid in the decision making process for pavement M&R activities during the entire pavement life cycle [5]. It was concluded in the study that material, construction-related traffic congestion, and pavement surface roughness effects are three major contributors to energy consumption and greenhouse gas (GHG) emissions for pavement M&R activities [5]. When considering a high-traffic-volume highway, such as Interstate 495 which was selected as the case study location, energy and GHG savings accumulated during the use phase of the LCA due to rolling resistance can become even more significant compared to the energy use and GHG emissions from material production and construction in pavement M&R activities. It has been shown through several other studies the effect of pavement roughness on vehicle operation costs in terms of extra fuel consumption, vehicle repairs and maintenance, and tire wear during the use phase of the LCA [3 (pp. 86-96), 11 (pp. 105-116), 12, 13, 14 (pp.424-436)].

The motivation of this study is to use a LCA-LCCA approach to evaluate pavement performance over the design life with the inclusion of realistic traffic conditions, different pavement M&R alternatives, and pavement material characteristics. Building upon a study performed by DeCarlo et al. in 2017, where a section of interstate highway in the New England region was selected to investigate the impact pavement structure and M&R treatment timing, the present study aims to include realistic traffic conditions in the operational phase of a pavement LCA [15]. The study presented herein has three primary objectives: (1) to perform a LCA on an interstate highway with the implementation of real time traffic data (RTTD) and M&R strategy decisions to optimize performance over a given pavement analysis life; (2) to evaluate pavement performance with realistic traffic conditions, varying M&R strategies and material characteristics in terms of Life Cycle Cost (LCC), Global Warming Potential (GWP) and Cumulative Energy Demand (CED) for both agencies and users; and (3) to quantify the increase in fuel consumption and resulting emissions due to decrease in ride quality (as expressed by the International Roughness Index, IRI) caused by accumulated distresses and pavement degradation over the analysis period. Ultimately, when an LCA-LCCA approach is utilized, pavement performance over a given analysis period can be optimized to determine a cost-effective and eco-friendly pavement M&R plan [5].

In the subsequent sections a brief summary of the materials and methods utilized in this study are presented. Information regarding the selection of the case study location, details relating to the construction, use, and M&R phase of the LCA are discussed followed by key results and a sensitivity analysis of select variables. Lastly, a discussion of the LCA results is presented and the importance of incorporating realistic traffic conditions into the LCA framework is demonstrated.

2. Materials and Methods

2.1. Case Study Location

A 26 km section of Interstate I-495 in Massachusetts was analyzed, from Chelmsford to Methuen as shown in Figure 1. This section of interstate was selected as it consists of a high volume of commuter traffic. Temporal traffic volume data on this interstate section were collected from the Massachusetts Department of Transportation (MASSDOT) data management system [16]. Interstate I-495 consists of 3 lanes in each direction with a distributional factor of 50% (of 24-hour peak volume). The annual average daily traffic (AADT) was approximately 121,000 vehicles. Of this volume, the business commercial vehicles (FHWA Class 4 and above) consisted of 9,243 (8%) vehicles (detailed traffic distribution is provided in Appendix A.3).

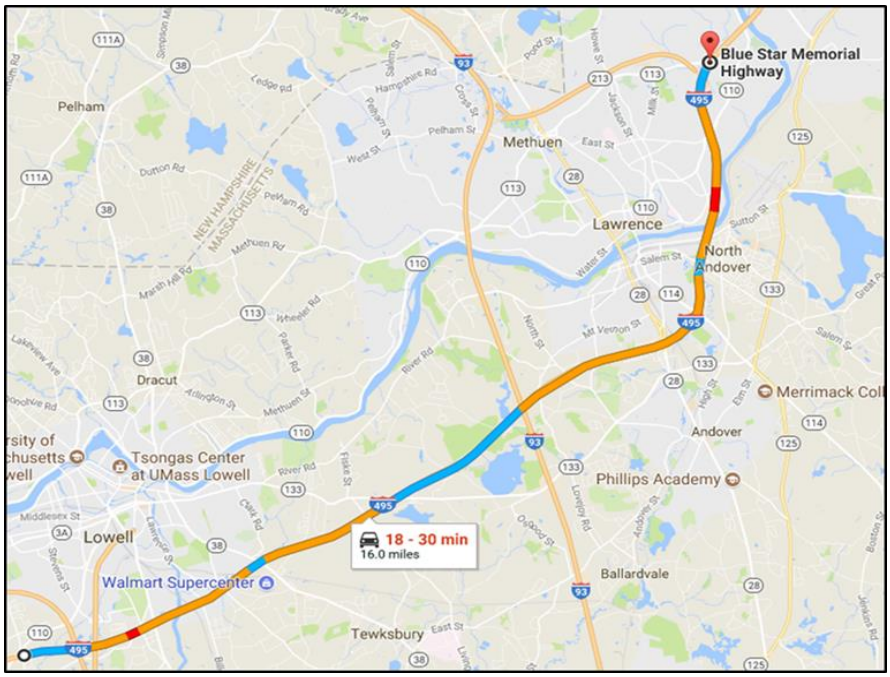

Figure 1: Map of 25.7 km roadway on I-495 from Chelmsford to Methuen, MA [17].

2.2. General Methodology

A typical pavement LCA system boundary includes raw materials and excavation, material transportation, construction, operation and maintenance, and end-of-life. In this study, a focus was placed on the initial construction, use, and maintenance phases from both an agency and user perspective. The end-of-life phase was neglected because of the challenges associated with accurately accounting for reclaimed asphalt pavement (RAP) material and its impacts beyond the analysis period of the given section of I-495 being investigated as part of this study. Three types of impacts were investigated: life cycle cost, cumulative energy demand (CED), and global warming potential (GWP). Figure 2 describes the general process of the LCA-LCCA approach that was followed. In the subsequent sections, the construction phase, use phase and the M&R strategies are described in greater detail.

As shown in Figure 2, once the case-study location was identified the first step in the process involved collection of various spatial and temporal data that are necessary to capture various facets of LCA process. The analysis was divided into two primary phases of activities for pavements: (1) Construction (initial, M&R) and (2) Operation. Construction activities included in the analysis are initial construction, maintenance, rehabilitation and reconstruction. The operational phase analysis was conducted using both

steady-state and realistic traffic conditions. Impacts of pavement roughness on various life time impacts and costs were included in the analysis. Lastly, a sensitivity analysis was conducted to assess effects of changing traffic volume, vehicle fuel efficiencies and fuel prices over the course of analysis duration.

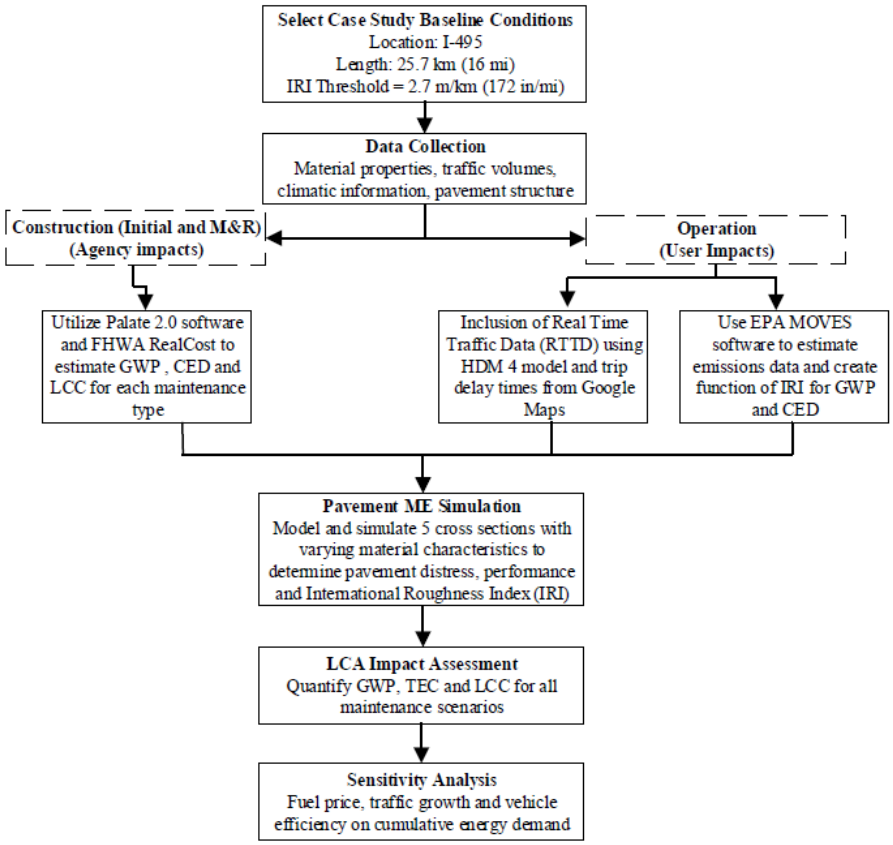

Figure 2: Flow chart of LCA case study.

2.2.1. Construction Phase: Materials and Pavement Cross-Sections

An inventory of raw materials required to construct the 26-km stretch of road was developed based upon typical New England mixture characteristics. The various cross sections are comprised of a combination of a wearing or surface course, binder course, base course, granular base and subgrade. Base and subbase layer designs were held constant while five different surface courses with varying material properties were evaluated as part of this study (Table 1). Therefore, each simulated cross section had the same overall thickness on top of the existing subgrade (105 cm), what varied was the surface course material properties. The materials chosen for surface course are represent typical asphalt mixtures and binder used in the New England region [18].

Table 1: Summary of materials used in simulated pavement cross-sections.

Mixture Name	Course Description	Layer Thickness (cm)	Asphalt Binder Type	Amount of Recycled Asphalt Pavement in the

				Mix (% by total weight of mix)
ARGG-1	Surface	5	PG 58-28	10
ARGG-2	Surface	5	PG 58-28	0
T-1	Surface	5	PG 64-28	19.3
THS-1	Surface	5	PG 76-28	19.3
SHM-1	Surface	5	PG 70-34	0
B-1	Binder	20	PG 64-28	25
BB-1	Base	20	PG 64-28	25
GB	Granular Base	60	-	-

Each cross-section design will present its own unique degradation trajectory, which is further modeled through Pavement ME by altering the material properties of the asphalt layer. The baseline unit raw material and construction impacts and costs associated with each process were obtained from two LCA software programs, Simapro 8.3 and the Pavement Life-Cycle Assessment Tool (PaLATE 2.0) [19, 20]. Further detailed information on the inventory unit impacts is provided in Appendix A.1. Transportation distances of the materials were quantified based upon the manufacturers' locations contracted out by the Massachusetts Department of Transportation (MassDOT) for previous pavement projects. It was assumed that the transportation distance from plant to the job site location was 10 miles.

2.2.2. Construction Phase: Maintenance and Rehabilitation

A total of 6 M&R strategies were compared in this study using a combination of Pavement ME design software and existing literature on the impacts of M&R strategies on IRI. Typical surface treatments such as crack seal and microsurfacing were included as pavement preservation or pavement maintenance strategies, while common pavement rehabilitation strategies including cold-in-place recycling and mill and overlay were explored.

Initial and terminal IRI values were set based on Pavement ME default values of 1 m/km and 2.7 m/km, respectively. As it is commonly recommended for pavement life cycle cost analysis (such as, [21 p. 158]), a minimum of 3 full maintenance cycles for each type M&R be used in the analysis prior to selecting the terminal year of the analysis period. This was done to ensure that sufficiently long analysis period was used to make a relative fair comparison among different M&R strategies, specifically when converting various costs to net present value (NPV) and equivalent annual costs (EAC). The analysis periods vary from 92 to 135 years depending on the type of M&R and cross section material properties. A brief description of each M&R alternative is listed below.

- **Do nothing and reconstruct (DNR):** The first M&R scenario is simply the choice to perform no maintenance or rehabilitation and to reconstruct at the end of the pavement systems service life (reached the terminal IRI). The pavement performance curves in terms of IRI and time for this scenario is determined using Pavement ME.
- **Crack sealant (CS):** The next M&R alternative evaluated the use of crack sealant every two years during the service life of the pavement until the terminal IRI value was reached and the pavement system was reconstructed. Crack sealant is a common preventative maintenance treatment to fill cracks at the surface of the pavement structure to prevent water from infiltrating. It was found in literature that the overall pavement service life is extended by 2 years when applying crack sealant as a pavement preservation technique [22]. For simplicity, it was assumed that pavement continues to deteriorate at the same rate after applying the crack sealant treatment but a two-year extension of the service life was applied

before reaching the terminal IRI trigger value. It should also be noted that crack sealant is a preservation treatment and does not address structural issues as a M&R strategy.

- **Microsurfacing (MS 2.2 m/km):** Microsurfacing applied when an IRI trigger value of 2.2 m/km was reached. Microsurfacing is a common M&R treatment type that applies a mixture of water, asphalt emulsion, aggregate and chemical additives to an existing asphalt pavement surface in order to preserve the underlying pavement structure. It provides a new pavement driving surface and according to a study by MnDOT it resets the IRI by approximately 0.7 m/km [23]. A type III microsurface was molded in this study. It should be highlighted that microsurfacing is a pavement preservation treatment and does not address underlying structural issues.
- **Microsurfacing (MS 2.5 m/km):** Microsurfacing was applied when an IRI trigger value of 2.5 m/km was reached. Once again, IRI was reset by approximately 0.7 m/km. [23].
- **Cold-In-Place (CIR) Recycling**: CIR is a pavement rehabilitation technique that involves reclaiming 50 mm to 100 mm of the existing pavement structure. It is a similar process to cold plant mix recycling except that it is performed directly in the field typically by a paving train of equipment. Once the terminal IRI value has been triggered, the CIR treatment is performed and the IRI decreases by approximately 1.1 m/km. [24, 25]. The simulated cross section after CIR was performed consisted of a 5-cm asphalt concrete (AC) surface course, 5-cm AC base course, 10-cm of cold recycled asphalt pulverized in place, and 60-cm granular base. CIR is generally accepted as a pavement rehabilitation strategy that has the ability to address structural distresses. Pavement ME was used to determine the pavement performance curves when CIR was used as a M&R strategy.
- **Mill and Overlay (MO):** Mill and overlay of approximately 50 mm was performed once the terminal IRI value was reached. On average the IRI is reset by (0.95 to 1.26 m/km), therefore this M&R alternative scenario reset the IRI to the initial value of 1 m/km and then allows the pavement cross section to reach the terminal IRI value of 2.7 m/km before reconstructing [26, 27]. Reconstruction was performed after one MO treatment to avoid the impractical scenario of constantly MO highway pavement systems. MO often falls in the gray area as a mix between a surface treatment or a rehabilitation strategy. For the purpose of this study, MO is considered as a rehabilitation treatment capable of addressing structural distresses. Pavement ME simulations were conducted for each cross-section with use of MO treatment to determine the pavement performance curves.

Figure 3 provides an example of the M&R timing sequence over the analysis period for the ARGG-1 cross section. The terminal year of year 135 from the present time was determined when a minimum of 3 full cycles of each M&R strategy was completed. The M&R timing sequences for other pavement cross sections are provided in Appendix A.2.

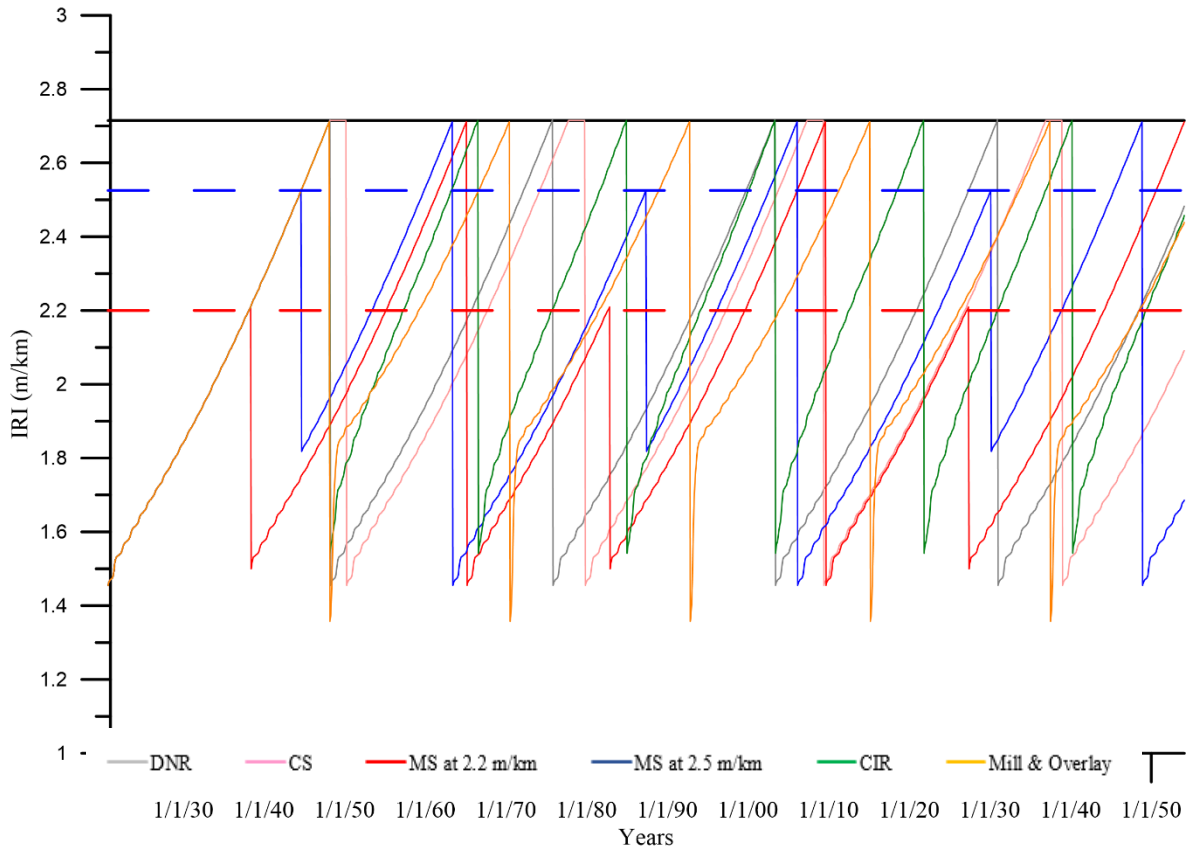

Figure 3: Example of M&R timing sequence for ARGG-1 cross section over analysis period with a terminal year of 2154.

2.2.3. Use Phase

In order to incorporate realistic traffic conditions into the use phase of the LCA, hourly traffic congestion patterns over the course of a week on the target pavement segment from Google Maps® were obtained. A representative week of hourly congestion patterns was then repeated to form a year (52 weeks) of realistic traffic conditions. MassDOT's Transportation Data Management System was used to collect information regarding daily traffic volume for each vehicle type on the target pavement segment.

Next, acceleration/deceleration rates obtained from the SHRP 2 NDS databases were assigned to all vehicles based on the congestion condition and the expected vehicle speeds under each traffic congestion condition (Appendix A.3, Table A.3.1) [28]. Note that same acceleration and deceleration rates were used for different vehicle classes, however the vehicle specific power for each of these classes differ and are accounted in the emissions calculations. The MOVES software was used to convert the volume and pattern of traffic (i.e., vehicle type, speed, and acceleration) to GWP and CED estimates [29]. However, it should be noted that MOVES assumes constant pavement performance (highest smoothness), while the influence of pavement degradation on vehicle fuel consumption and emissions is neglected. To address this gap, pavement distresses over the design life were modelled using the Pavement ME design software for the 5 different pavement cross section types [30]. The International Roughness Index (IRI) was used to assess pavement degradation and ride roughness. IRI measures the simulated transient vertical movement of a generic motor vehicle to the roughness in a single wheel path of the road surface and is typically reported

in meters per kilometer [31]. IRI correlates with vehicle fuel usage and the associated costs and emissions [12].

It is important to note that while M&R is being performed on the roadway it often requires lane closures. Traffic congestion may arise resulting in an increase in emissions. These delays were not included in this study at present time, however, the inclusion of idle time and traffic congestion from daily traffic was included. Idle time was incorporated into the results by assuming on average vehicles idle for 10 minutes per km for the 130 km of mildly congested (typically shown as red on Google Maps®) roadways per week and for 30 minutes per km for the 6.6 km of highly congested (typically shown as dark red on Google Maps®) roads on I-495. By incorporating realistic traffic conditions into the use phase of the LCA, the increase in emissions due to traffic delays without consideration of lane closures was accounted for. It is recommended that the impact of lane closures be investigated further to determine the significance of M&R lane closure times associated with each strategy (i.e. lane closure time to perform crack seal versus time to perform mill and overlay) may have on the overall LCA impacts.

The inclusion of realistic traffic conditions followed a six step process. The first step used vehicle characteristics from Chatti and Zabaar [12]. Some examples of these characteristics include mass, drag coefficient, frontal area, and rolling resistance tire factors. They were then utilized in HDM-4 tractive force model equations to solve for aerodynamic forces and rolling resistances [32]. The tractive forces were used to determine the vehicle specific power. Vehicle Specific Power (VSP) is a measure of a vehicles instantaneous power per mass. VSP reveals how driving conditions affect emissions. It is a function of speed, roadway grade, acceleration, IRI, and many other variables. Since MOVES is not set-up to directly incorporate effects of IRI change on fuel usage, the results from Chatti and Zabaar were used to calibrate VSP bins for each vehicle class with respect to different pavement IRI. Once VSP bins were compiled for each variation in vehicle type, speed, and acceleration, these vehicle specific powers were used as input to the MOVES software.

Next, MOVES simulations were performed to obtain values of CED and GWP per length traveled. It is necessary to obtain emissions per length so they can be applied to varying traffic conditions. The MOVES outputs were then altered to allow the incorporation of the International Roughness Index (IRI). Due to the generalization of VSP Bins in MOVES software, a change in IRI does not produce a significant change in the output from MOVES for acceleration, deceleration or idle phases. This is not unexpected, since during acceleration and deceleration the power demands associated with those activities are substantially higher than that coming directly from change in pavement roughness. Similarly, during idle stage, there is no motion and thus pavement surface characteristics have no impact on fuel consumption.

Lastly, the altered MOVES outputs were then combined with vehicle counts and classifications from MassDOT's Transportation Data Management System and traffic conditions from Google Maps®. This was only completed for one week of hourly traffic data because Google Maps® generalizes each week day and weekend day to have the same traffic conditions throughout the entire year. In other words, a Friday in July will have the same results as a Friday in January in terms of traffic delay estimates. Therefore, in total 168 traffic conditions were evaluated for a single week's worth of traffic on an hourly basis. The process outlined above to obtain a week's worth of traffic data was then scale to represent the traffic conditions over a course of a year, and ultimately over the entire LCA analysis period. The implementation of RTTD was completed for both southbound and northbound directions over the 26 km stretch of roadway on I-495.

2.3. Life Cycle Cost Analysis

LCC was estimated using a discount rate of 4% and converted to net present value (NPV). A 4% discount rate was assumed in this study base on guidance from FHWA Life-Cycle Cost Analysis in Pavement Design report that stated long-term trends for real discount rates hover around 4% and a

discount rate between 3 to 5% is an acceptable range as it is consistent with historical values in Appendix A of Office of Management and Budget (OMB) Circular A-94 [33]. Costs were converted to net present value (NPV) using Equation 1, where FV is the future value, r represents the discount rate (4%) and n is the number of years in the future the price must be brought back to present value.

$$\mathrm{NPV} = \frac{\mathrm{FV}}{(1+\mathrm{r})^{\mathrm{n}}} \quad (1)$$

2.4. Sensitivity Analysis

A sensitivity analysis on the price of fuel, traffic growth rate, and vehicle energy efficiency was performed to assess their influence on the economic performance of the LCCA. Table 2 summarizes the price of gasoline and diesel considered in the sensitivity analysis.

Table 2: Gasoline and diesel prices used for three scenarios used in sensitivity analysis from US EIA 2017 Report [34].

Scenario	Gasoline Price ($)	Diesel Price ($)
Low	1.64	1.71
Current	2.80	3.00
High	4.04	4.66

Traffic growth rate varied by 1%, 2% and 3% with respect to the baseline conditions, which assumed no traffic growth. To account for the improvement in motor vehicle technology, cumulative energy demand (CED) was reduced every decade by 1%, 2% and 3%. All pavement section and M&R strategy combinations (24 total) were evaluated using low, current and high fuel price values for a total of 84 scenarios.

3. Results

3.1. Effect of Realistic Traffic as Compared to Steady Speed

First to validate the importance of including realistic traffic conditions in the use phase of the LCA, a comparison to baseline traffic conditions was conducted. LCA results showed that using real time traffic data resulted in a 6.4% increase in CED and GWP, in comparison to baseline conditions during a given week. These percentages were based on a daily traffic count of approximately 133,000 vehicles. Therefore, the inclusion of RTTD is equivalent to accounting for the impact of an additional 8,512 vehicles per day. Figure 4 highlights the difference in CED when realistic traffic conditions are included. Similar trend in GWP is observed when RTTD is included in the operations phase of the LCA.

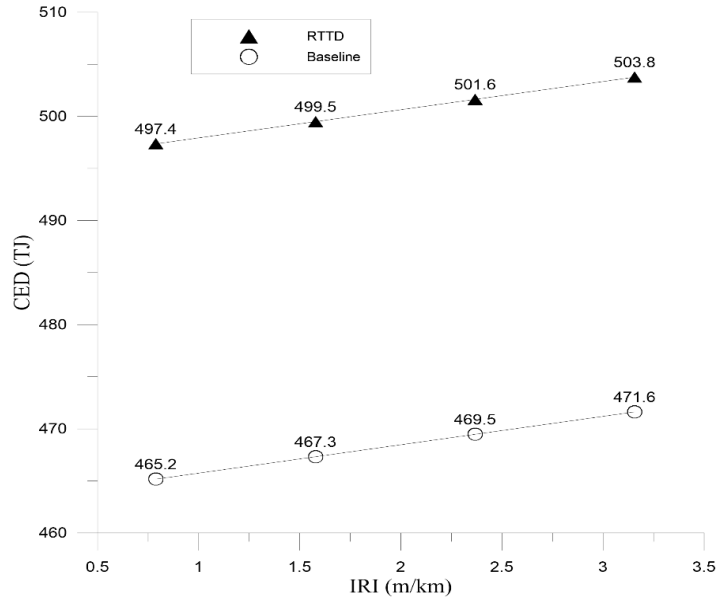

Figure 4: Comparison of baseline traffic scenario and the inclusion of realistic traffic conditions (indicated by RTTD).

3.2. Overall LCA Results

3.2.1. Global Warming Potential (GWP)

From this point on all results are presented with the inclusion of RTTD. Figures 5a and 5b show the two most contrasting cross sections (ARGG-1 and T-1) in terms of percent difference in GWP. User impact is represented by the solid black bars while agency impact is shown by the grey hashed bars. Table 3 includes the results for all five cross sections for comparison of GWP impact in terms of Gigagrams of CO_2 equivalent.

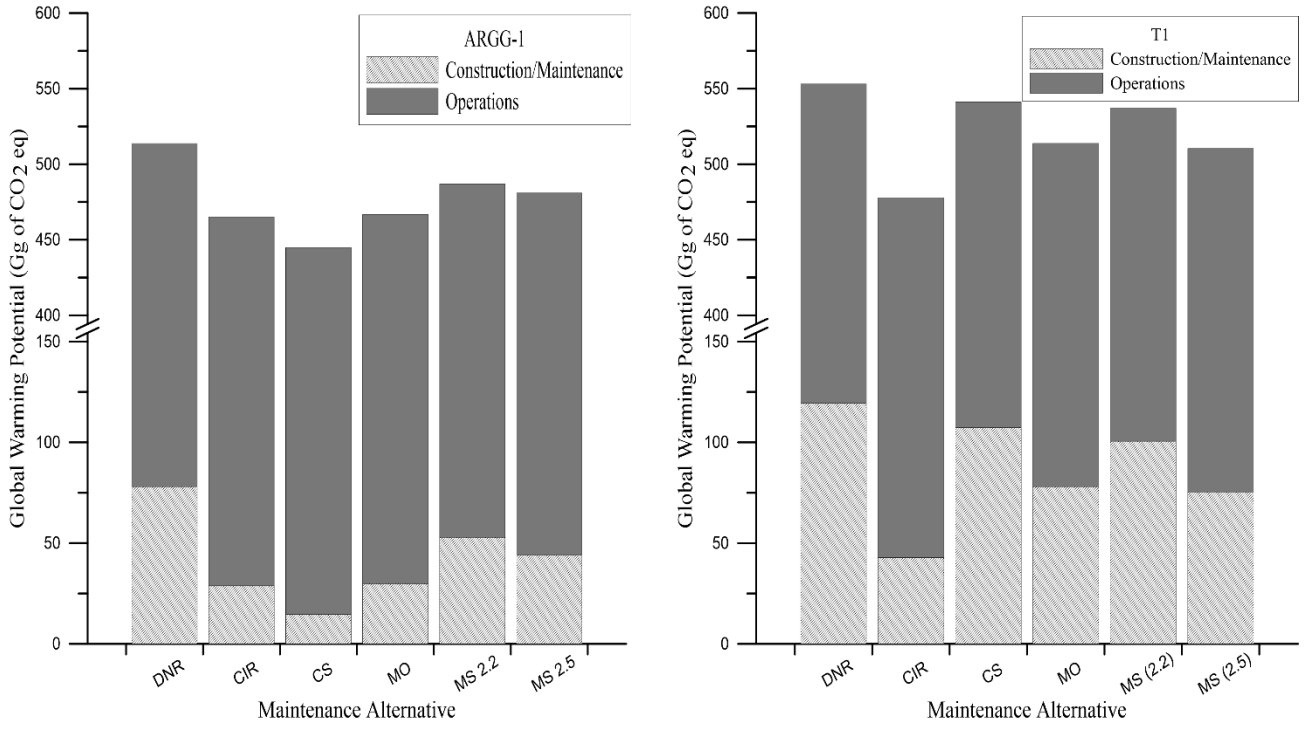

(a) **(b)**

Figure 5: GWP impact broken down into construction and M&R, and operations of vehicles over LCA analysis period for **(a)** ARGG-1 and **(b)** T-1 pavement cross section.

Table 3: Summary of M&R alternative scenario results in terms of GWP impact incurred by agencies and users for all 5 cross sections.

Cross Section	Maintenance Alternative											
	DNR		CIR		CS		MO		MS 2.2 m/km		MS 2.5 m/km	
	C/M	O	C/M	O	C/M	O	C/M	O	C/M	O	C/M	O
	Gg CO_2 eq											
ARGG-1	78	436	29	436	15	430	30	437	53	434	44	437
ARGG-2	77	435	26	435	72	436	29	435	52	435	55	438
SHM-1	73	430	27	436	52	435	-	-	54	436	26	437
T-1	119	434	43	435	107	434	78	436	101	436	75	435
THS-1	83	435	34	437	91	435	-	-	75	436	61	435

Note: C/M = Construction and maintenance (agencies)
O = Operations (users)
DNR = Do nothing reconstruct
CIR = Cold in-place recycling
MO = Mill and overlay

MS = Microsurface

It can be inferred from both Figure 5 and Table 3 that while the type of pavement cross section and the use of different asphalt mixtures have an impact of the life cycle costs and impacts, this is not as significant as the type and timing of M&R performed over the design life of a pavement structure. All GWP user impacts are relatively similar, ranging from 430 to 438 Gg of CO_2 equivalent. In contrast, the agency impact ranges from 15 to 119 Gg of CO_2 equivalent depending on the type and timing of M&R.

The cross section and M&R alternative that had the lowest operational impact in terms of GWP for both users and agencies is associated with the ARGG-1 cross section combined with CS. By simply maintaining the pavement system using crack sealant to prevent water infiltration and rapid degradation of the pavement surface it benefits not only the users of the roadway but the agency in which is responsible for maintaining the pavement infrastructure. In terms of policy or practical implications, these findings support the need for implementing pavement preservation treatments. Whereby if a highway network is routinely treated with preventative maintained using a preservation treatment such as CS, the need for pavement reconstruction could be avoided resulting in a lower operational costs for users and agencies. Furthermore, the asphalt rubber gap-graded mixture without inclusion of recycled asphalt pavement appears to have better performance and lower life cycle impacts.

In comparison, the highest user (operational) GWP impact is associated with the ARGG-2 cross section using MS 2.5. The highest construction and M&R GWP impact resulted from the combination of the using SHM-1 cross section and the DNR alternative. For all cross sections the M&R alternative to do nothing and reconstruct (DNR) had the highest total impact including both agency and user impacts with T-1 cross section performing the worst with 553 Gg of CO_2 equivalent.

3.2.2. Life Cycle Cost (LCC)

The last comparison of cross section and M&R alternatives considered in this study was in terms of LCC. All LCC are presented below are in terms of NPV. Figure 6a and 6b show results for cross section ARGG-1 and T-1 to be consistent with GWP comparison in section 3.2.1. However, Table 4 may be referenced for further comparison of all 5 cross sections, broken into user and agency LCC impacts.

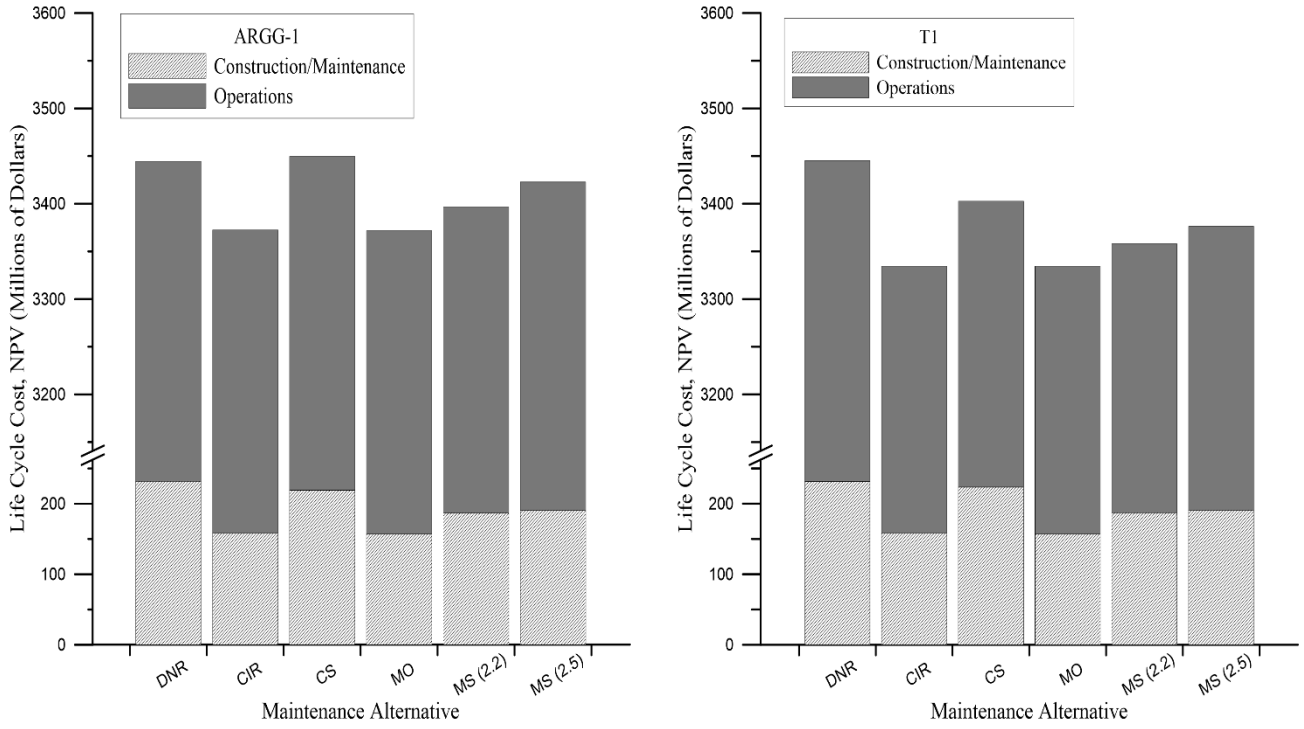

Figure 6: LCC impact broken down into construction and maintenance, and operations of vehicles over LCA analysis period for **(a)** ARGG-1 and **(b)** T-1 pavement cross section.

Table 4: Summary of M&R alternative scenario results in terms of LCC impact incurred by agencies and users for all 5 cross sections.

Cross Section	Maintenance Alternative											
	DNR		CIR		CS		MO		MS 2.2 m/km		MS 2.5 m/km	
	C/M	O	C/M	O	C/M	O	C/M	O	C/M	O	C/M	O
	Millions of Dollars											
ARGG-1	232	3213	158	3214	219	3231	157	3215	187	3209	191	3232
ARGG-2	231	3213	158	3215	219	3219	157	3216	187	3210	156	3224
SHM-1	299	3145	160	3147	277	3146	-	-	253	3144	215	3145
T-1	232	3213	158	3177	224	3179	157	3178	187	3171	191	3186
THS-1	267	3209	159	3203	252	3196	-	-	219	3200	199	3193

Note: C/M = Construction and maintenance (agencies)
O = Operations (users)
DNR = Do nothing reconstruct
CIR = Cold in-place recycling
MO = Mill and overlay
MS = Microsurface

LCC impact is not constant among five cross sections and depends on material properties, M&R treatment and the application timing over the service life. For example, comparing Figure 6a (ARRG-1) and Figure 6b (T-1) crack sealant every two years followed by reconstruction once terminal IRI is reached resulted in the overall highest total LCC for ARGG-1 cross section but for the T-1 cross section it was from the DNR scenario. It is important to note that while total LCC is highest for this case, depending on the cross-section the distributions of user and agency LCC is different. In other words, the total bar height is comprised of different user (black portion) and agency (gray portion) costs.

The overall lowest total LCC impact between these two cross sections was the MO scenario. The lowering of LCC with mill and overlay is resulting from greater structural contribution from an overlay and having the IRI of the pavement return to new pavement condition with each application of overlay. It should be highlighted again that these results are made with realistic traffic conditions without consideration to lane closure time associated with the varying M&R strategies during the use phase. With the realistic traffic conditions and assumptions made in this study, it can be concluded that by optimizing M&R type, material selection and timing of treatment, decision makers can achieve a 2.72% difference in operations cost (users) and 47.6% difference in construction/maintenance cost (agency).

The varied LCC from agencies and users' perspective may lead to substantial economic and environmental tradeoffs for agencies and users. In comparing the GWP results to the LCC results, the most environmental conscious decision may not appear as the most economical decision, assuming that economics is only assessed in terms of the construction and operational costs. Depending on whether decisions are being made from a user's perspective, agency perspective or an overall combination of the two, the most economical and environmental alternative varies. Furthermore, future studies necessitate inclusion of GWP and LCC in a combined manner to optimize the costs as well as financial impacts associated with unit GWP. Implementing a LCA-LCCA approach can help to identify those tradeoffs and identify both a cost-effective and eco-friendly pavement M&R plan.

3.2 Sensitivity Analysis

A comparison for all M&R options was performed as part of the sensitivity analysis however, only results for the ARGG-1 cross section is included for demonstration purposes. Figure 7 shows the percent different from baseline conditions (0% traffic growth and current fuel price) in terms of NPV when assuming low versus high fuel price scenario as defined in Table 2.

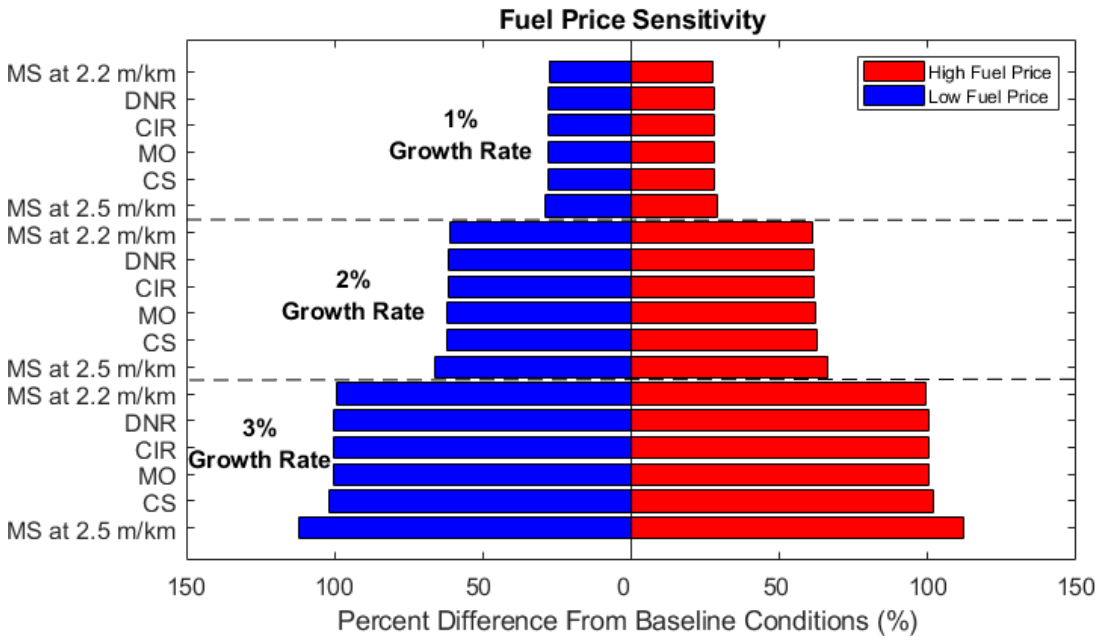

Figure 7: Fuel price sensitivity analysis example for ARGG-1 cross section showing comparison of low fuel price scenario (blue) and high fuel price scenario (red) at three levels of traffic growth (1, 2 and 3%).

There is minimal difference in terms of NPV over the analysis period when using either low or high fuel prices as seen in Figures 7 with respect to baseline conditions. In general, this trend was consistent among all cross sections considered in this case study. However, it should be noted that as traffic growth rate increases from 1 to 3 percent, the timing of microsurfacing becomes more critical as the impact on NPV increases.

The SHM-1 cross section, which consisted of a surface course that was a highly polymer modified mixture, had the same fuel consumption cost regardless of the M&R treatment alternative while holing all other parameters constant. In comparison, results for the other four cross sections showed that microsurfacing at a trigger value of 2.5 m/km consistently had a higher cost of fuel consumption as the traffic growth rate increased.

The cost of fuel consumption was not only dependent on traffic growth rate, but the combination of traffic growth and CED reduction with the improvement of vehicle efficiency each decade. As the percentage of CED improvement and traffic growth rate increased, greater distinction in fuel consumption costs between the different M&R alternatives was observed. Overall, the MS at 2.5 m/km M&R alternative was the most sensitive to variations in traffic growth and CED improvement.

4. Discussion, Conclusions and Recommendations

Results from this study emphasis the importance of utilizing a holistic approach to decision and policy making regarding the M&R of highway infrastructure systems. Economic and environmental tradeoffs for agencies and users exist and vary depending on the stakeholders considered or prioritized during the decision process. It is recommended that life cycle LCC, GWP and CED be considered in the decision process. This recommendation is supported by the results presented in this paper, where use of only construction or only use phases LCA impacts may not yield optimality.

The inclusion of realistic traffic conditions was shown to have an impact on the use phase of the LCA. This finding agreed with the literature review from other studies that have shown pavement surface

roughness to affect vehicle fuel consumption and emissions during the use phase of the LCA. The framework presented in this study is unique in providing guidance on how to consider realistic traffic conditions using publicly available data sources. This contribution helps bridge the gap of moving from traditional pavement management to an LCA-LCCA informed approach. It also provided a method to consider not only agency cost but also user costs in the decision process.

From a user's perspective, the results from this study indicated that the most economical decision overall was to perform a microsurface when 2.2 m/km IRI was reached (SHM-1 cross section). The most carbon/energy efficient alternative was to perform crack sealant treatment every two years followed by reconstruction once the terminal IRI was reached (ARRGG-1 cross section). Similarly, from an agency based perspective the results showed that the most economical decision was microsurfacing at 2.5 m/km scenario (ARGG-2 cross section) and the lowest environmental impact was achieved by the crack sealant M&R scenario (ARGG-1 cross section). While this study only considered two different trigger values on when to apply the MS treatment, it is recommended that other IRI trigger times be evaluated to truly optimize the proper timing of M&R strategies. It has been shown by Ogwang et al in 2019 that agency-wide cracking-threshold policies affect the magnitude of future emissions and costs significantly [35]. It is an essential step to developing a cost-effective and environmentally friendly M&R plan to determine not only the correct type of M&R strategy to apply but the optimal timing of that treatment for a given pavement condition.

This study also showed that material characteristics matter and what may be optimal for one highway will vary for a different highway. As an example, when considering ARGG-1 cross section only, the optimal M&R strategy selection is different. The M&R alternative to perform microsurfacing at 2.5 m/km trigger value results in the highest user cost, while allowing the road to degrade and reconstruct after reaching the terminal IRI value (DNR scenario) is the most expensive for agencies. When comparing all cross sections together, SHM-1 is the worst overall from an agency's perspective and ARGG-1 is the worst overall from a user's perspective.

Meanwhile, from an environmental impact perspective, the highest agency impact for the ARGG-1 cross section is observed for the DNR M&R scenario and the highest environmental impact from users is seen with the MO M&R scenario. Comparing all cross sections reveals the highest environmental impacts for agencies with the T-1 cross section following the DNR M&R scenario and from user's perspective the ARGG-2 cross section following the MS 2.5 M&R scenario. Therefore, it can be concluded that decision makers must give attention to the pavement structure and its material characteristics, the type of M&R options that are available within an agency, budget constraints and potential environmental impacts that are associated with each when developing a long term M&R plan for highway pavement infrastructure systems. This paper provides a methodology to develop that M&R plan with the inclusion of realistic traffic conditions to evaluate LCA and LCCA impacts that can be applied to other highways and be implemented within infrastructure asset management systems with varying material properties, traffic conditions and available M&R strategies.

This study highlighted the importance of including realistic traffic conditions into the operations phase of a pavement LCA. A 6.4% difference in CED and GWP was observed with the inclusion of realistic traffic compared to steady state constant speed conditions. Results from this study also provided valuable insight into the trade-off between GWP, CED and LCC impacts resulting from performing and LCA on varying pavement cross sections and M&R alternatives for both agencies and users. Cross section type in addition to the timing and type of M&R strategy has an impact on IRI which translates to changes in GWP, CED and LCC. In terms of NPV, the mill and overlay M&R strategy had the lowest LCC for agencies and users. Results from this study also showed that optimization of M&R type, material selection and timing may lead to a 2.72% difference in operations cost (users) and 47.6% difference in construction/maintenance cost (agency). Lastly, a sensitivity analysis was performed to assess the robustness of input assumptions such as traffic growth, fuel price and vehicle efficiency over the analysis period. Fuel price had minimal

impact on LCA results, however traffic growth and CED improvements had impact on results depending on type of pavement cross section and the M&R strategy applied.

It is recommended that further analysis be performed to investigate the effect of the number of cycles performed for each M&R alternative during the analysis period has on the overall LCA results. Since fuel consumption is directly related to CED and ultimately the IRI performance curve, a greater understanding of the effect each M&R alternative has on the IRI performance is critical. For example, when applying a microsurface treatment at 2.2 m/km IRI or 2.5 m/km IRI, is it an accurate estimation to reset both IRI values by 0.7 m/km, or does it vary depending on the IRI value at the time of treatment. It is also recommended that a similar analysis be conducted on other M&R alternatives such as chip seal, fog seal or full depth reclamation to evaluate other practical M&R techniques that may be used over the pavement design life. The M&R scenarios presented in this study were held constant throughout the analysis period. However, in reality a combination of M&R alternatives would be performed on a given cross section during its service life. A third recommendation would be to include lane closer and traffic delays related to the time to perform each M&R strategy during the use phase of the LCA.

The framework presented in this study may be applied to performing an LCA on a combination of M&R techniques over the design life of a given pavement section. It is critical to include RTTD in the operation phase of a pavement LCA and to carefully consider the impacts of both users and agencies when making management decisions in order to optimize social, environmental and economic impacts. The adoption of an LCA and LCCA approach in the pavement design and M&R decision process can help to identify the most cost effective and environmental friendly option benefiting all stakeholders.

Author Contributions: Conceptualization, EVD and WM; methodology, KEH, EVD and WM; formal analysis, KEH; writing—original draft preparation, KEH; writing—review and editing, EVD, KEH and WM; visualization, KEH; supervision, EVD and WM; project administration, EVD and WM.

Funding: This research was partly funded by the University of New Hampshire Center for Infrastructure Resiliency to Climate.

Acknowledgments:

Acknowledgement is extended to Shane Majenski for his contributions to the implementation of real time traffic data into the operations phase of the LCA. Thank you to Rasool Nemati for supply material characteristics information and testing results for typical New Hampshire asphalt materials used in this study. Support provided by Prof. Jo E. Sias and the UNH Center for Infrastructure Resiliency to Climate is much appreciated by researchers.

Conflicts of Interest:

The funders had no role in the design of the study; in the collection, analyses, or interpretation of data; in the writing of the manuscript, or in the decision to publish the results

Appendix A

A.1 Life Cycle Inventory

Impact Unit	Units	Value	Source
Production			
Asphalt Concrete	MJ/ton	641	SimaPro
Asphalt Concrete	kg CO_2 eq/ton	84.7	SimaPro
Gravel	MJ/ton	265	SimaPro
Gravel	kg CO_2 eq/ton	14.1	SimaPro
Sand	MJ/ton	61.8	SimaPro
Sand	kg CO_2 eq/ton	4.25	SimaPro
Transportation			
Dump Truck transportation	MJ/ton*mile	5.134	SimaPro
Dump Truck transportation	kg CO_2 eq/ton*mile	0.321	SimaPro
Construction			
Asphalt Paver (Productivity)	ton/hr	10	PaLATE
Asphalt Rolling - TandemIngersol Rand DD90HF (productivity)	ton/hr	395	PaLATE
Asphlat Roller - Pheumatic Dynapac CP134	ton/hr	884	PaLATE
Unbound Material Placement - Caterpillar 120H	ton/hr	300	PaLATE
Unbound Material Compaction (productivity)	ton/hr	1832	PaLATE
Construction Machine Operation	MJ/ton	10816	SimaPro
Construction Machine Operation	kg CO_2 eq/hr	72	SimaPro
Maintenance			
Asphalt Milling	ton/hr	6.23	SimaPro
Asphalt Milling	kg CO_2 eq/yd^3	0.409	SimaPro
CIR Recycler 800hp (Productivity)	ton/hr	1713	PaLATE
CIR Recycler 800hp (Productivity)	kg CO_2 eq/yd^3	0.99	PaLATE
Crack Seal Treatment	MJ/ft^2	0.92	Chehovits et al., 2010
Crack Seal Treatment	kg CO_2 eq/ft^2	0.000067	Chehovits et al., 2010
Operation			
Gasoline	MJ/gal	132	EPA
Gasoline	lb CO_2 eq/gal	19.6	EPA
Diesel	MJ/gal	137.7	EPA
Diesel	lb CO_2 eq/gal	22.4	EPA

A.2 Life Cycle Analysis Period

Table A.2.1 summarize how many cycles of each M&R type were completed during the analysis period by cross section type. In Table A.2.1, highlighted values in bold denote the M&R type which controlled the terminal year (i.e complete 3 full cycles in the longest period of time).

Table A.1: Summary of M&R cycles by cross section over the course of the analysis period.

M&R Alternative	Cross Section				
	ARGG-1	ARGG-2	SHM-1	T-1	THS-1
DNR	5	5	6	5	6
CS	5	5	5	5	5
MS @ 2.2 m/km	**3**	**3**	4	**3**	4
MS @ 2.5 m/km	4	4	**3**	4	**3**
CIR	7	6	9	6	9
M&O	6	6		6	

Figures A.2.1 though A.2.5 show the M&R timing sequences for all cross sections considered in this study.

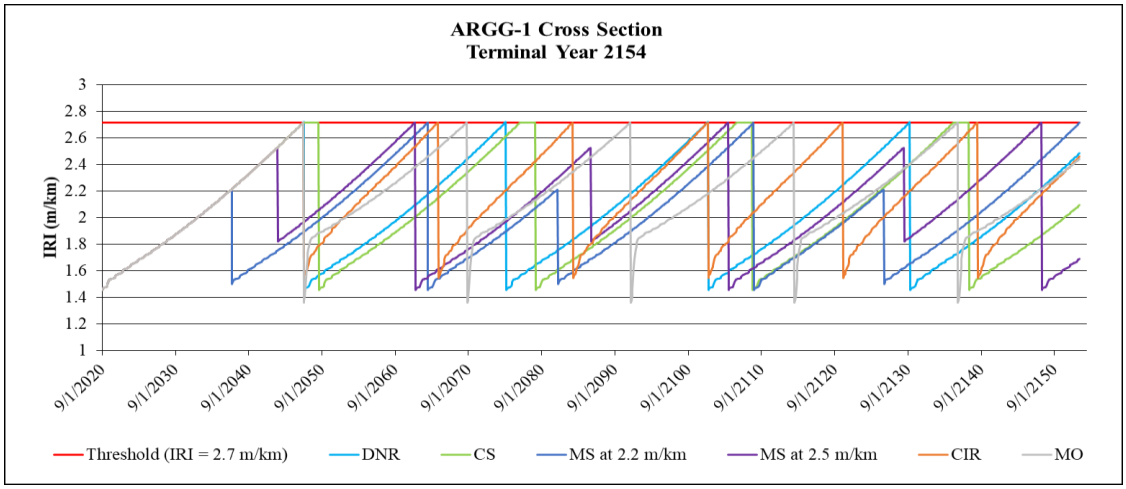

Figure A.2.1: ARGG-1 cross section M&R activity timing.

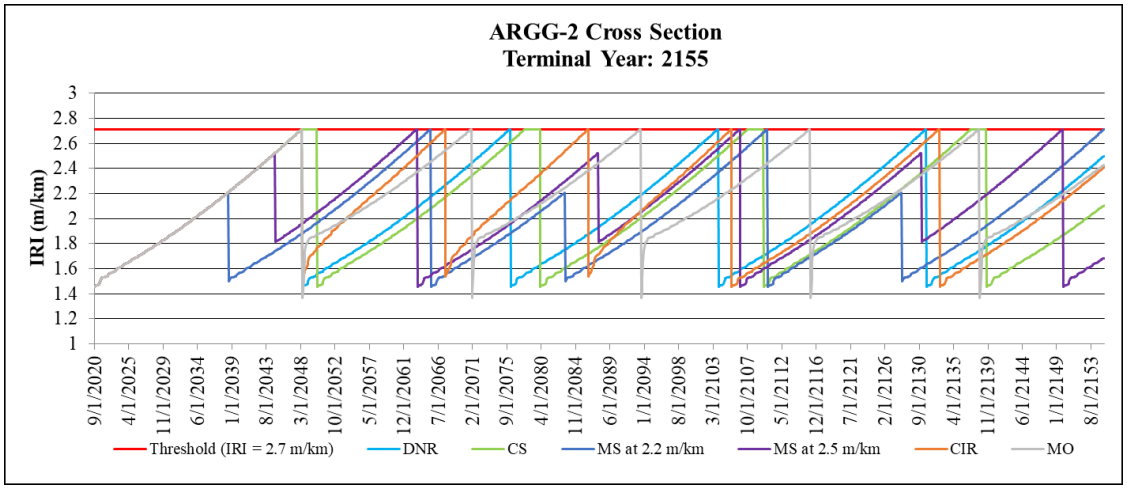

Figure A.2.2: ARGG-2 cross section M&R activity timing.

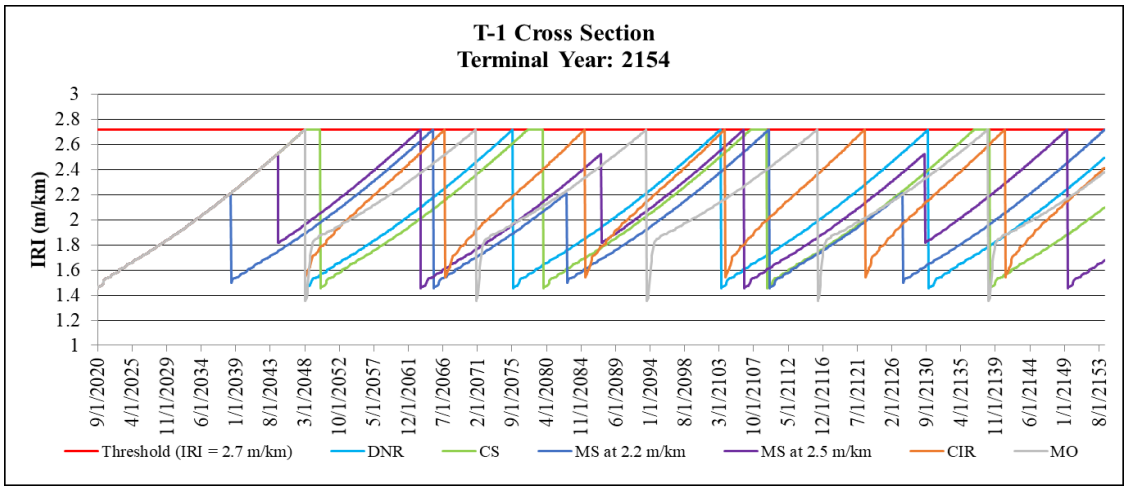

Figure A.2.3: T-1 cross section M&R activity timing.

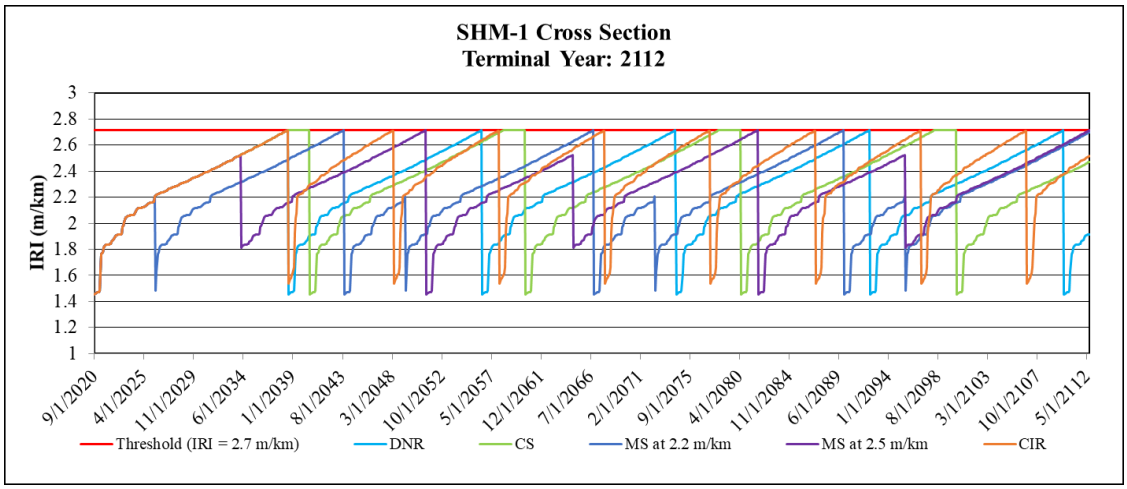

Figure A.2.4: SHM-1 cross section M&R activity timing.

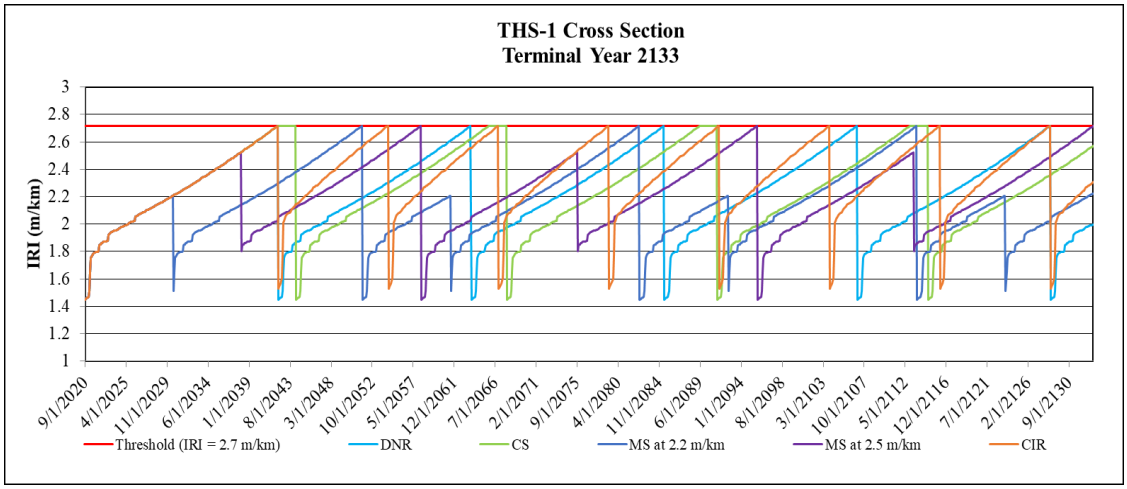

Figure A.2.5: THS-1 cross section M&R activity timing.

A.3 Implementation of RTTD

Step 1

Table 4-12. HDM 4 new default values—vehicle and tire characteristics.

Vehicle Class	Number of Axles	*Nw*	M (tons)	*Kcr*2	CD	AF (m^2)	WD	Tire Type	*CR*1	*b*11	*b*12	*b*13	C_{0tc} (dm^3/1000 km)	C_{tcte} (dm^3/MNm)	VOL (dm^3)	VEHF AC
Small car	2	4	1.9	0.5	0.42	1.9	0.62	Radial	1	22.2	0.11	0.13	0.01747	0.001	1.4	2
Medium car	2	4	1.9	0.5	0.42	1.9	0.62	Radial	1	22.2	0.11	0.13	0.01747	0.001	1.4	2
Large car	2	4	1.9	0.5	0.42	1.9	0.62	Radial	1	22.2	0.11	0.13	0.01747	0.001	1.4	2
Van	2	4	2.54	0.67	0.5	2.9	0.7	Radial	1	25.9	0.09	0.10	0.01602	0.00092	1.6	2
Four-wheel drive	2	4	2.5	0.58	0.5	2.8	0.7	Radial	1	25.9	0.09	0.10	0.01602	0.00092	1.6	2
Light truck	2	4	4.5	0.99	0.6	5	0.8	Radial	1	29.6	0.08	0.08	0.01602	0.00092	1.6	2
Medium truck	2	6	6.5	0.99	0.6	5	0.8	Bias	1.3	29.6	0.08	0.11	0.02999	0.00099	6	1
Heavy truck	3	10	13	1.1	0.7	8.5	1.05	Bias	1.3	38.85	0.06	0.11	0.03829	0.00135	8	1
Articulated truck	5	18	13.6	1.1	0.8	9	1.05	Bias	1.3	38.85	0.06	0.20	0.04328	0.00153	8	1
Mini bus	2	4	2.16	0.67	0.5	2.9	0.7	Radial	1	25.9	0.09	0.10	0.01747	0.00092	1.6	2
Light bus	2	4	2.5	0.99	0.5	4	0.8	Radial	1	29.6	0.08	0.08	0.01747	0.00092	1.6	2
Medium bus	2	6	4.5	0.99	0.6	5	1.05	Bias	1.3	38.85	0.06	0.07	0.02999	0.00099	6	1
Heavy bus	3	10	13	1.1	0.7	6.5	1.05	Bias	1.3	38.85	0.06	0.11	0.03829	0.00135	8	1
Coach	3	10	13.6	1.1	0.7	6.5	1.05	Bias	1.3	38.85	0.06	0.11	0.03829	0.00135	8	1

Figure A.3.1: Step 1, NCHRP-720 vehicle characteristics [8].

Table 4-9. HDM 4 tractive forces model.

Name	Description	Unit
Aerodynamic forces (*Fa*)	$Fa = 0.5 * \rho * CD * AF * \upsilon^2$	N
CD	Drag coefficient (Table 4-12)	dimensionless
AF	Frontal area (Table 4-12)	m^2
ρ	Mass density of the air (default = 1.2)	kg/m^3
υ	Vehicle speed	m/s
Gradient forces (*Fg*)	$Fg = M * GR * g$	N
M	Vehicle weight (Table 4-12)	kg
GR	Gradient	radians
g	Gravity	m/s^2
Curvature forces (*Fc*)	$Fc = \max\left(0, \frac{\left(\frac{M*\upsilon^2}{R} - M*g*e\right)^2}{Nw*Cs} * 10^{-3}\right)$	N
R	Curvature radius (Default = 3000)	m
Superelevation (*e*)	$e = \max(,0.045 - 0.68 * Ln(R))$	m/m
Nw	Number of wheels (Table 4-12)	dimensionless
Tire stiffness (*Cs*)	$Cs = a0 + a1 * \frac{M}{Nw} + a2 * \left(\frac{M}{Nw}\right)^2$	kN/rad
*a*0 to *a*2	Model parameter (Table 4-10)	dimensionless
Rolling resistance (F_r)	$Fr = CR2 * (b11 * Nw + CR1 * (b12 * M + b13 * \upsilon^2))$	N
*CR*1	Rolling resistance tire factor (Table 4-12)	factor
Rolling resistance parameters (*b*11, *b*12, *b*13)	$b11 = 37 * Dw$ $b12 = 0.064 / Dw$ $b13 = 0.012 * Nw / Dw^2$	factors
Dw	Diameter of wheel	
Rolling resistance surface factor (*CR*2)	$= Kcr2[a0 + a1 * Tdsp + a2 * IRI + a3 * DEF]$	factor
*Kcr*2	Calibration factor (Table 4-12)	factor
*a*0 to *a*3	Model coefficient (Table 4-11)	dimensionless
Texture depth using sand patch method (*Tdsp*)	$Tdsp = 1.02 * MPD + 0.28$	mm
MPD	Mean Profile Depth	mm
IRI	International roughness index	m/km
DEF	Benkelman Beam rebound deflection	mm

Figure A.3.2: Step 1, NCHRP-720 vehicle characteristic formulas [8].

Table A.3.1: Acceleration rates corresponding to Google Maps predicted congestion level orange, red and dark red using SHRP 2 NDS databases.

	Car Acceleration (m/s^2)	**Truck Acceleration (m/s^2)**
Orange	2.94	1.47
Red	2.94	1.47
Dark Red	2.9	1.45

Step 2

$$VSP = \frac{Power}{Mass} = \frac{\frac{d}{dt}(E_{Kinetic} + E_{Potential}) + F_{Rolling} \cdot v + F_{Aerodynamic} \cdot v + F_{int\,ernal\,friction} \cdot v}{m} =$$

$$\approx v \cdot a \cdot (1 + \varepsilon_i) + g \cdot grade \cdot v + g \cdot C_R \cdot v + \frac{1}{2}\rho_a C_D \frac{A}{m}(v + v_w)^2 \cdot v + C_{if} \cdot v$$

Figure A.3.3: Step 2, Vehicle specific power formula [17].

Where; v= vehicle speed, m= vehicle mass, a= vehicle acceleration, ε_i= Mass factor, C_D= drag coefficient,C_R= coefficient of rolling resistance, A= frontal area of the vehicle, ρ_a= ambient air density, v_w = headwind into the vehicle

Step 3

VSP Bin	Characteristics
0	Braking
1	Idling
11	Low Speed Coasting; VSP< 0; 1<=Speed<25
12	Cruise/Acceleration; 0<=VSP< 3; 1<= Speed<25
13	Cruise/Acceleration; 3<=VSP< 6; 1<=Speed<25
14	Cruise/Acceleration; 6<=VSP< 9; 1<=Speed<25
15	Cruise/Acceleration; 9<=VSP<12; 1<=Speed<25
16	Cruise/Acceleration; 12<=VSP; 1<=Speed<25
21	Moderate Speed Coasting; VSP< 0; 25<=Speed<50
22	Cruise/Acceleration; 0<=VSP< 3; 25<=Speed<50
23	Cruise/Acceleration; 3<=VSP< 6; 25<=Speed<50
24	Cruise/Acceleration; 6<=VSP< 9; 25<=Speed<50
25	Cruise/Acceleration; 9<=VSP<12; 25<=Speed<50
26	Cruise/Acceleration; 12<=VSP; 25<=Speed<50
27	Cruise/Acceleration; 12<=VSP<18; 25<=Speed<50
28	Cruise/Acceleration; 18<=VSP<24; 25<=Speed<50
29	Cruise/Acceleration; 24<=VSP<30; 25<=Speed<50
30	Cruise/Acceleration; 30<=VSP; 25<=Speed<50
33	Cruise/Acceleration; VSP< 6; 50<=Speed
35	Cruise/Acceleration; 6<=VSP<12; 50<=Speed
36	Cruise/Acceleration; 12 <= VSP; 50<=Speed
37	Cruise/Acceleration; 12<=VSP<18; 50<=Speed
38	Cruise/Acceleration; 18<=VSP<24; 50<=Speed
39	Cruise/Acceleration; 24<=VSP<30; 50<=Speed
40	Cruise/Acceleration; 30<=VSP; 50<=Speed

Figure A.3.4: Step 3, MOVES VSP Bins examples.

Step 4

Run	Header Item:	Item Value
	Report Description:	Summary Report
	Report Date/Time:	2017-10-30 17:47:0
	MOVES Output Database:	VehicleClass_Out
	Emission Process:	All
33	Run Date/Time:	2017-10-26 01:09:46.0
33	Run Specification:	C:\Users\Shane Majenski\Documents\Fall 2017\Senior Project\Vehicle Cl
33	Run Spec File Date/Time:	2017-10-26 01:09:18.0
33	Run Spec Description:	Vehicle Classification Run .
33	Mass Units:	g
33	Energy Units:	KJ
33	Distance Units:	mi
33	Time Units:	hour

Figure A.3.5: Step 4, MOVES Run Specification output information.

Run	TotalEnergy	CO2_Equiv
33	82416	6072

Figure A.3.6: Step 4, MOVES output.

Step 5

MOTORCYCLE (NCHRP 720 Classification: Car, MOVES: Motorcycle) Gas														
Length (Miles)	Grade (%)	v(mph)	v (m/s)	a(m/s^2)	IRI (m/km)	Faero (kW/ton)	Froll (kW/ton)	VSP (kW/Tonne)	VSP Bin	Condition	SourceTypeID	Run	Total Energy Consumption (MJ)	GWP Unit (kg CO2 eq)
1	0	60	26.8224	0	0	0.000252	0.059	6.448402596	35	Good	11	3	2.689	0.194
1	0	60	26.8224	0	0.25	0.000252	0.062	6.520946694	35	Good	11	3	2.689	0.194
1	0	60	26.8224	0	0.5	0.000252	0.065	6.593490792	35	Good	11	3	2.689	0.194
1	0	60	26.8224	0	0.75	0.000252	0.067	6.66603489	35	Good	11	3	2.689	0.194
1	0	60	26.8224	0	1	0.000252	0.070	6.738578987	35	Good	11	3	2.689	0.194
1	0	60	26.8224	0	1.25	0.000252	0.073	6.811123085	35	Good	11	3	2.689	0.194
1	0	60	26.8224	0	1.5	0.000252	0.075	6.883667183	35	Good	11	3	2.689	0.194
1	0	60	26.8224	0	1.75	0.000252	0.078	6.956211281	35	Acceptable	11	3	2.689	0.194
1	0	60	26.8224	0	2	0.000252	0.081	7.028755378	35	Acceptable	11	3	2.689	0.194
1	0	60	26.8224	0	2.25	0.000252	0.083	7.101299476	35	Acceptable	11	3	2.689	0.194
1	0	60	26.8224	0	2.5	0.000252	0.086	7.173843574	35	Acceptable	11	3	2.689	0.194
1	0	60	26.8224	0	2.75	0.000252	0.089	7.246387672	35	Bad	11	3	2.689	0.194
1	0	60	26.8224	0	3	0.000252	0.092	7.318931769	35	Bad	11	3	2.689	0.194
1	0	60	26.8224	0	3.25	0.000252	0.094	7.391475867	35	Bad	11	3	2.689	0.194
1	0	60	26.8224	0	3.5	0.000252	0.097	7.464019965	35	Bad	11	3	2.689	0.194
1	0	60	26.8224	0	19.1	0.000252	0.266	11.99077166	35	Bad	11	3	2.689	0.194
1	0	60	26.8224	0	19.2	0.000252	0.267	12.0197893	37	Bad	11	35	3.44	0.248

Figure A.3.7: Step 5, MOVES interpolation- no change in MOVES output from 0m/km IRI to 19.1m/km IRI.

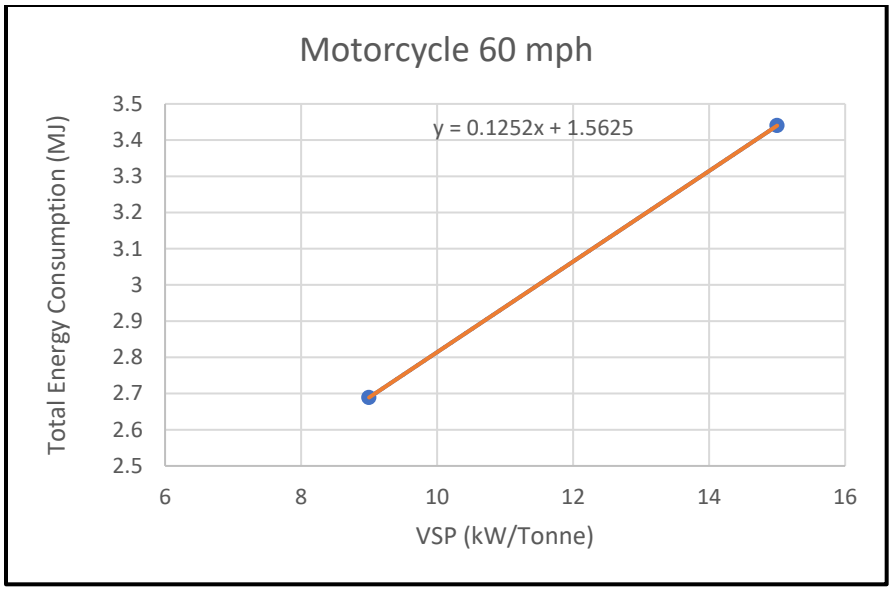

Figure A.3.8: Step 5, MOVES interpolation for total energy consumption.

Step 6

			Total Energy Consumption (MJ)/ 1 Mile												
Color	Acceleration/Deceleration	Speed (mph)	Motorcycle	Car	Light Truck	Bus	2A SU	3A SU	>3A SU	<5A 2U	5A 2U	>5A 2U	<6A >2A	6A >2A	>6A >2A
Green	None	60	2.370	2.823	3.483	55.351	32.963	45.902	34.629	82.416	82.416	82.552	82.552	82.552	82.552
Green	Deceleration	60	2.689	2.023	2.374	24.605	5.269	20.848	6.615	82.416	82.416	82.552	82.552	82.552	82.552
Orange	None	40	3.011	2.600	2.824	46.748	26.751	44.902	30.535	123.787	123.787	123.992	123.992	123.992	123.992
Orange	Deceleration	40	2.590	2.101	2.436	19.818	6.310	17.810	2.406	157.131	157.131	157.389	157.389	157.389	157.389
Orange	Acceleration	40	4.339	7.671	8.930	104.757	72.103	99.465	66.715	123.787	123.787	123.992	123.992	123.992	123.992
Red	None	20	3.229	3.829	4.126	42.795	24.344	42.045	28.862	95.475	95.475	95.633	95.633	95.633	95.633
Red	Deceleration	20	3.446	3.123	3.674	20.755	3.083	19.807	5.965	95.475	95.475	95.633	95.633	95.633	95.633
Red	Acceleration	20	4.846	8.287	9.300	79.295	76.308	79.466	72.208	95.475	95.475	95.633	95.633	95.633	95.633
Dark Red	None	10	6.117	7.172	7.567	50.880	31.609	50.384	38.325	145.543	145.543	145.782	145.782	145.782	145.782
Dark Red	Deceleration	10	6.542	6.246	7.349	29.312	5.941	28.622	11.928	118.315	118.315	118.511	118.511	118.511	118.511
Dark Red	Acceleration	10	7.986	11.849	13.149	89.985	66.780	87.226	74.648	190.950	190.950	191.265	191.265	191.265	191.265

Figure A.3.9: Step 6, MOVES interpolation output for varying vehicle classifications and traffic conditions.

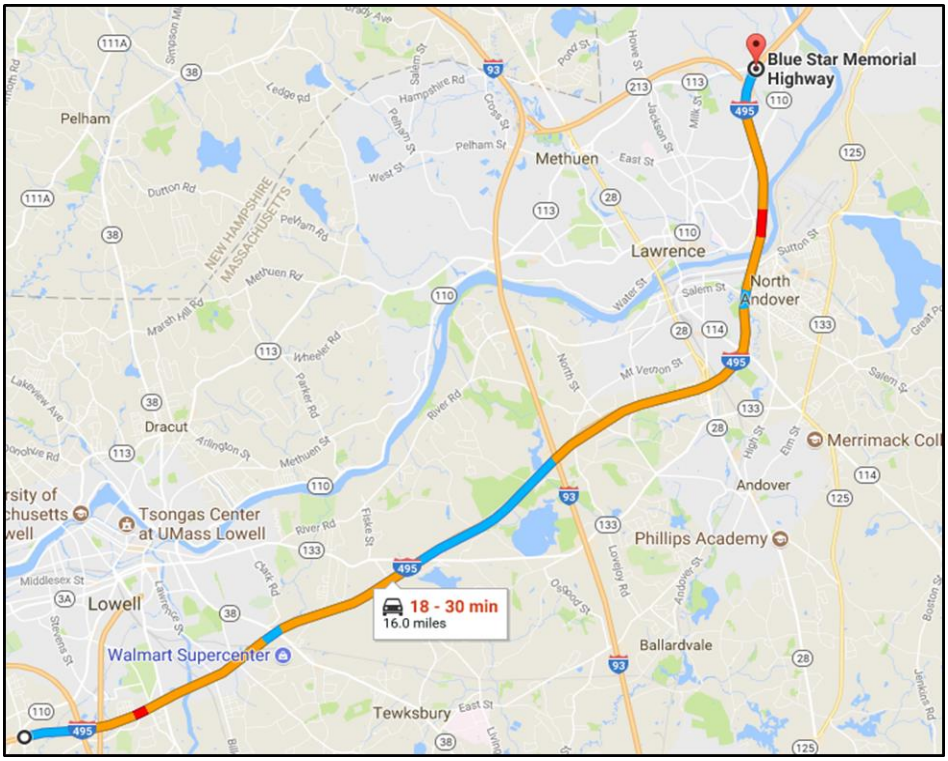

Figure A.3.10: Step 6, Google Maps® traffic conditions for Interstate I-495 [13].

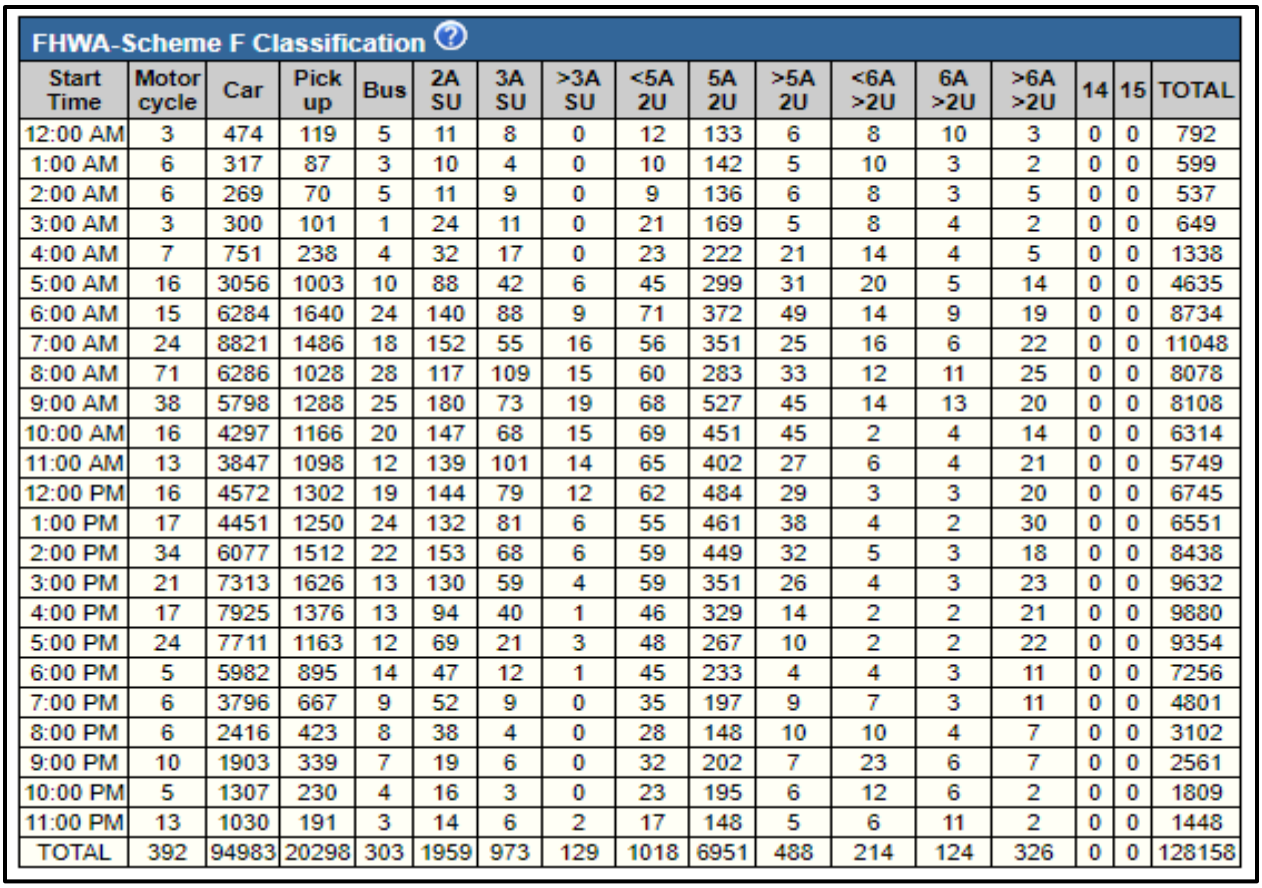

FHWA-Scheme F Classification

Start Time	Motor cycle	Car	Pick up	Bus	2A SU	3A SU	>3A SU	<5A 2U	5A 2U	>5A 2U	<6A >2U	6A >2U	>6A >2U	14	15	TOTAL
12:00 AM	3	474	119	5	11	8	0	12	133	6	8	10	3	0	0	792
1:00 AM	6	317	87	3	10	4	0	10	142	5	10	3	2	0	0	599
2:00 AM	6	269	70	5	11	9	0	9	136	6	8	3	5	0	0	537
3:00 AM	3	300	101	1	24	11	0	21	169	5	8	4	2	0	0	649
4:00 AM	7	751	238	4	32	17	0	23	222	21	14	4	5	0	0	1338
5:00 AM	16	3056	1003	10	88	42	6	45	299	31	20	5	14	0	0	4635
6:00 AM	15	6284	1640	24	140	88	9	71	372	49	14	9	19	0	0	8734
7:00 AM	24	8821	1486	18	152	55	16	56	351	25	16	6	22	0	0	11048
8:00 AM	71	6286	1028	28	117	109	15	60	283	33	12	11	25	0	0	8078
9:00 AM	38	5798	1288	25	180	73	19	68	527	45	14	13	20	0	0	8108
10:00 AM	16	4297	1166	20	147	68	15	69	451	45	2	4	14	0	0	6314
11:00 AM	13	3847	1098	12	139	101	14	65	402	27	6	4	21	0	0	5749
12:00 PM	16	4572	1302	19	144	79	12	62	484	29	3	3	20	0	0	6745
1:00 PM	17	4451	1250	24	132	81	6	55	461	38	4	2	30	0	0	6551
2:00 PM	34	6077	1512	22	153	68	6	59	449	32	5	3	18	0	0	8438
3:00 PM	21	7313	1626	13	130	59	4	59	351	26	4	3	23	0	0	9632
4:00 PM	17	7925	1376	13	94	40	1	46	329	14	2	2	21	0	0	9880
5:00 PM	24	7711	1163	12	69	21	3	48	267	10	2	2	22	0	0	9354
6:00 PM	5	5982	895	14	47	12	1	45	233	4	4	3	11	0	0	7256
7:00 PM	6	3796	667	9	52	9	0	35	197	9	7	3	11	0	0	4801
8:00 PM	6	2416	423	8	38	4	0	28	148	10	10	4	7	0	0	3102
9:00 PM	10	1903	339	7	19	6	0	32	202	7	23	6	7	0	0	2561
10:00 PM	5	1307	230	4	16	3	0	23	195	6	12	6	2	0	0	1809
11:00 PM	13	1030	191	3	14	6	2	17	148	5	6	11	2	0	0	1448
TOTAL	392	94983	20298	303	1959	973	129	1018	6951	488	214	124	326	0	0	128158

Figure A.3.11: Step 6, Example of MassDOT's Transportation Data Management System information database on vehicle classification [12].

Vehicle Classifications

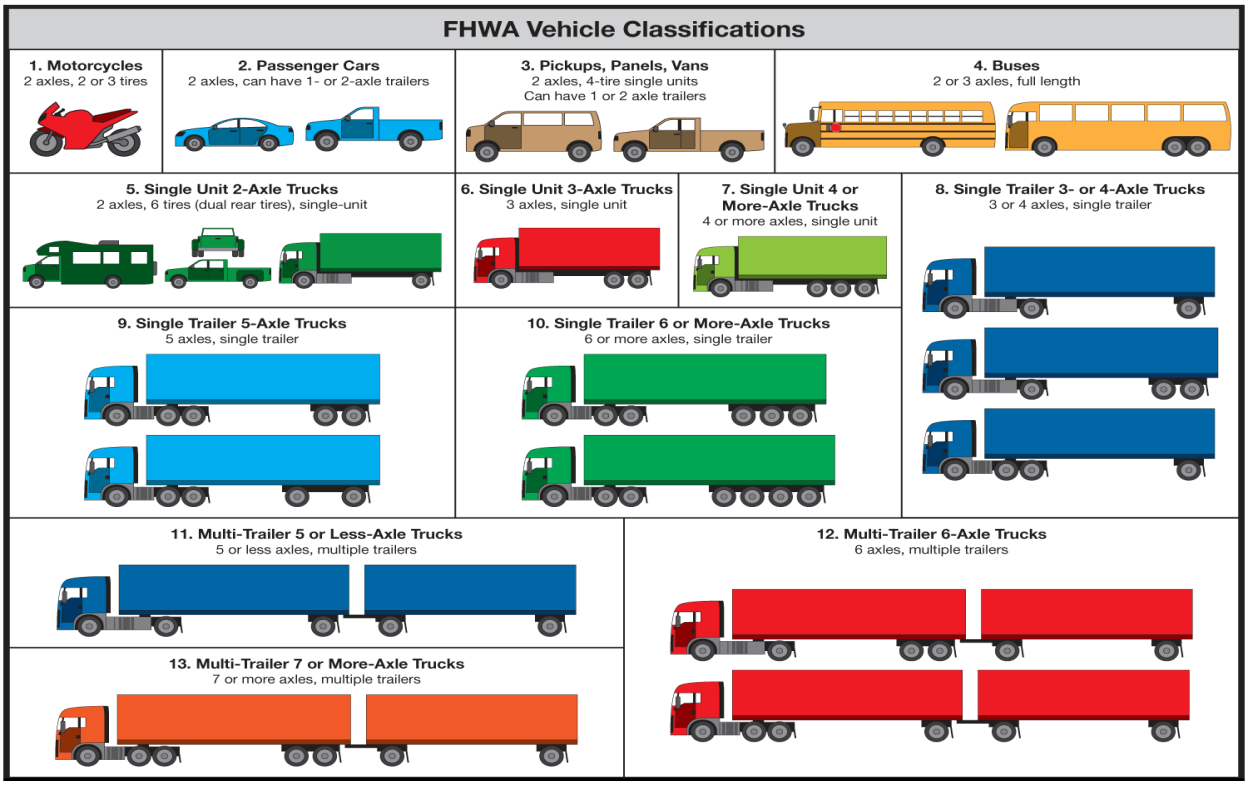

Figure A.3.12: MassDOT's Transportation Data Management System information vehicle classification chart [12].

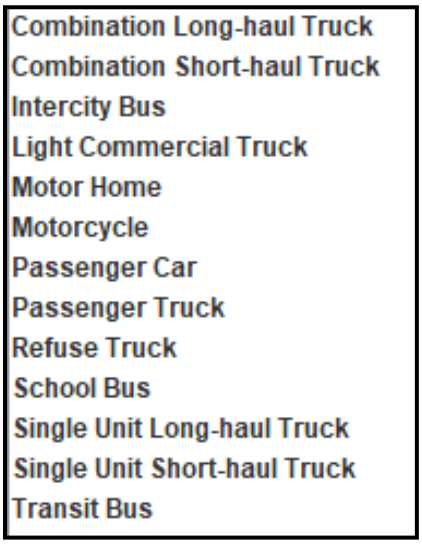

Figure A.3.13: MOVES vehicle classifications.

Table 4-12. HDM 4 new default values—vehicle and tire characteristics.

Vehicle Class	Number of Axles	*Nw*	M (tons)	*Kcr*2	CD	AF (m^2)	WD	Tire Type	*CR*1	*b*11	*b*12	*b*13	C_{0kc} (dm^3/1000 km)	C_{kcw} (dm^3/MNm)	VOL (dm^3)	VEHF AC
Small car	2	4	1.9	0.5	0.42	1.9	0.62	Radial	1	22.2	0.11	0.13	0.01747	0.001	1.4	2
Medium car	2	4	1.9	0.5	0.42	1.9	0.62	Radial	1	22.2	0.11	0.13	0.01747	0.001	1.4	2
Large car	2	4	1.9	0.5	0.42	1.9	0.62	Radial	1	22.2	0.11	0.13	0.01747	0.001	1.4	2
Van	2	4	2.54	0.67	0.5	2.9	0.7	Radial	1	25.9	0.09	0.10	0.01602	0.00092	1.6	2
Four-wheel drive	2	4	2.5	0.58	0.5	2.8	0.7	Radial	1	25.9	0.09	0.10	0.01602	0.00092	1.6	2
Light truck	2	4	4.5	0.99	0.6	5	0.8	Radial	1	29.6	0.08	0.08	0.01602	0.00092	1.6	2
Medium truck	2	6	6.5	0.99	0.6	5	0.8	Bias	1.3	29.6	0.08	0.11	0.02999	0.00099	6	1
Heavy truck	3	10	13	1.1	0.7	8.5	1.05	Bias	1.3	38.85	0.06	0.11	0.03829	0.00135	8	1
Articulated truck	5	18	13.6	1.1	0.8	9	1.05	Bias	1.3	38.85	0.06	0.20	0.04328	0.00153	8	1
Mini bus	2	4	2.16	0.67	0.5	2.9	0.7	Radial	1	25.9	0.09	0.10	0.01747	0.00092	1.6	2
Light bus	2	4	2.5	0.99	0.5	4	0.8	Radial	1	29.6	0.08	0.08	0.01747	0.00092	1.6	2
Medium bus	2	6	4.5	0.99	0.6	5	1.05	Bias	1.3	38.85	0.06	0.07	0.02999	0.00099	6	1
Heavy bus	3	10	13	1.1	0.7	6.5	1.05	Bias	1.3	38.85	0.06	0.11	0.03829	0.00135	8	1
Coach	3	10	13.6	1.1	0.7	6.5	1.05	Bias	1.3	38.85	0.06	0.11	0.03829	0.00135	8	1

Figure A.3.14: NCHRP-720 vehicle classifications [8].

Vehicle Classifications			
FHWA Traffic Count	NCHRP 720	MOVES	Distribution (%)
Car	Car	Car	100
Motorcycle	Motorcycle	Motorcycle	100
Pick Up	Four-wheel Drive	Passenger Truck	100
Bus	Light Bus	School Bus	15
	Medium Bus	Transit Bus	80
	Coach	Intercity Bus	5
2A SU	Light Truck	Single-Unit Long Haul Truck	100
3A SU	Medium Truck	Single-Unit Long Haul Truck	100
>3A SU	Heavy Truck	Single-Unit Long Haul Truck	90
		Refuse Truck	10
<5A SU and 5A SU	Articulated Truck	Combination Short Haul Truck	100
>5A 2U and higher	Articulated Truck	Combination Long Haul Truck	100

Figure A.3.15: Vehicle classification combinations and distributions.

Trips by Maximum Acceleration and % Rur Frwy < 4 Lns

% Rur Frwy < 4 Lns

	0.0 - 20.0	20.0 - 40.0	40.0 - 60.0	60.0 - 80.0	80.0 - 100.0	>= 100.0	NULL (no value)	Total
< 0.0	0	0	0	0	0	0	0	0
0.0 - 0.1	0	0	0	0	7.6	0	0	7.6
0.1 - 0.2	0	0	0	0	22.5	0	0	22.5
0.2 - 0.3	0	0	0	0	40.7	0	0	40.7
0.3 - 0.4	0	0	0	0	25.1	0	0	25.1
0.4 - 0.5	0	0	0	0	3.5	0	0	3.5
0.5 - 0.6	0	0	0	0	0.2	0	0	0.2
0.6 - 0.7	0	0	0	0	0	0	0	0
>= 0.7	0	0	0	0	0.2	0	0	0.2
NULL (no value)	0	0	0	0	0.3	0	0	0.3
Total	0	0	0	0	100.0	0	0	100.0

Figure A.3.16: SHRP 2 NDS acceleration data [16]

A.4 Pavement ME Inputs

A.4.1 Material Characteristic Inputs

Table A.4.1: Pavement ME material characteristics for each layer.

Asphlt material properties		**Mixture Name**						
		ARGG-1	**ARGG-2**	**T-1**	**THS-1**	**SHM-1**	**B-1**	**BB-1**
Aggregate gradation	Cum % rt. 3/4 in sieve	100	100	100	100	100	99	88
	Cum % rt. 3/8 in sieve	84	85	81	84	86	74	56
	Cum % rt. #4 sieve	40	37	57	57	59	46	36
	% Passing #200 sieve	3.5	3.5	3.8	4	3.7	3.5	3.5
Aspahlt Binder	Superpave (PG)	58-28	58-28	64-28	76-28	70-34 PMA	64-28	64-28
Asphalt General	Reference temp (F)	70	70	70	70	70	70	70
	Poisson's ratio	0.36	0.35	0.36	0.36	0.35	0.36	0.36
	Effective binder %	6.68	6.32	4.9	4.9		4.39	4.35
	Air voids %	5.36	3.01	3.5	6.21	4	5.18	4.38
	Total Unit weight (pcf)	144.8	146.9	158.7	155.6	151.5	149.5	151.3
	Thermal conductivity AC	0.67	0.67	0.67	0.67	0.67	0.67	0.67
	Heat capcity aspahlt	0.23	0.23	0.23	0.23	0.23	0.23	0.23

A.4.2 Dynamic Modulus (E*) Pavement ME Input

ARGG -1				
	Frequency (Hz)			
Temp (F)	0.1	1	10	25
10	1688550.19	1966960.96	2175448.5	2240515.8
40	687552.7197	979985.536	1331318.2	1476540
70	169907.9615	304180.895	522202.28	636736.3
100	56526.39519	96813.0315	179173.21	231341.41
130	29662.06475	43677.4749	71655.429	89572.235

Figure A.4.2.1: Dynamic modulus input for ARGG-1 cross section.

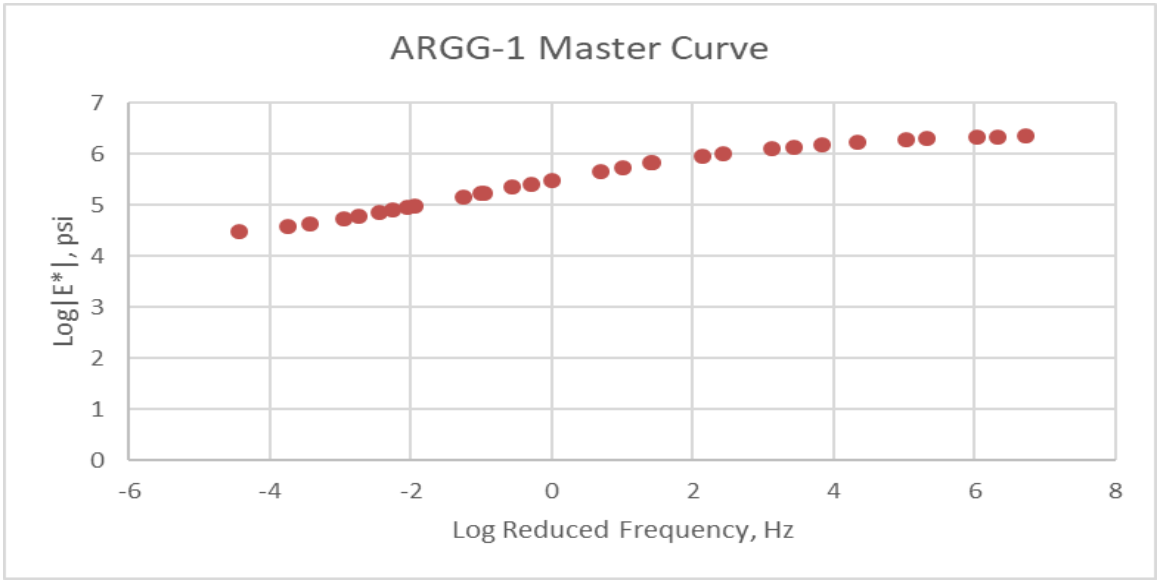

Figure A.4.2.2: ARGG-1 cross section master curve.

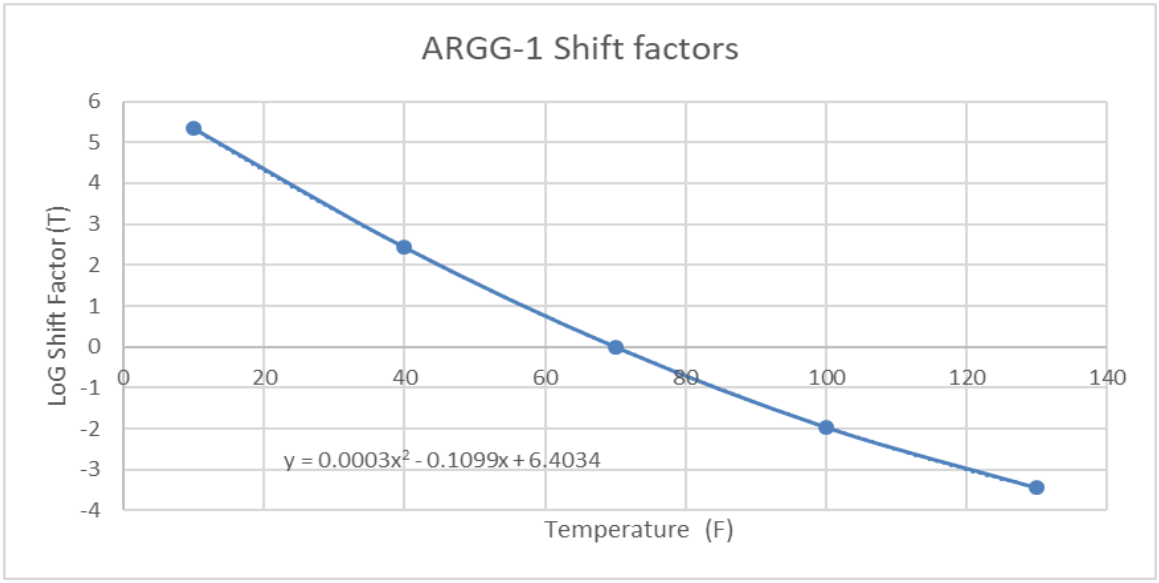

Figure A.4.2.3: ARGG-1 cross section shift factors.

ARGG -2				
	Frequency (Hz)			
Temp (F)	0.1	1	10	25
10	2014657.96	2300848	2516240	2584199
40	804896.3419	1132508	1517460	1673494
70	191077.648	350222.3	596736.8	723122.5
100	58660.58927	106064	203032.5	261578.6
130	28301.08178	46310.03	83084.46	106713.7

Figure A.4.2.4: Dynamic modulus input for ARGG-2 cross section.

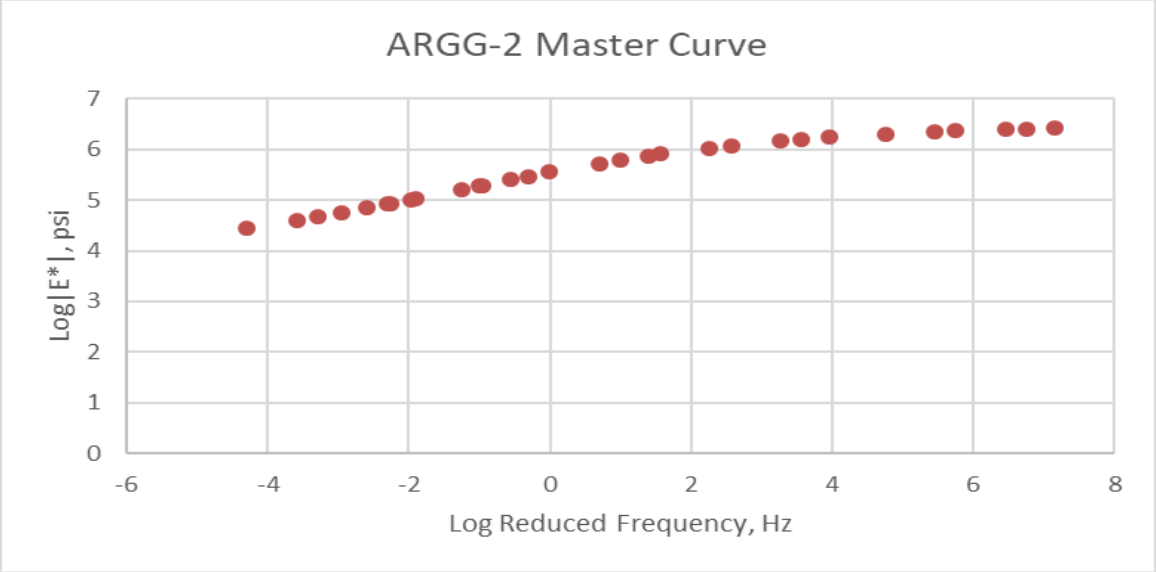

Figure A.4.2.5: ARGG-2 cross section master curve.

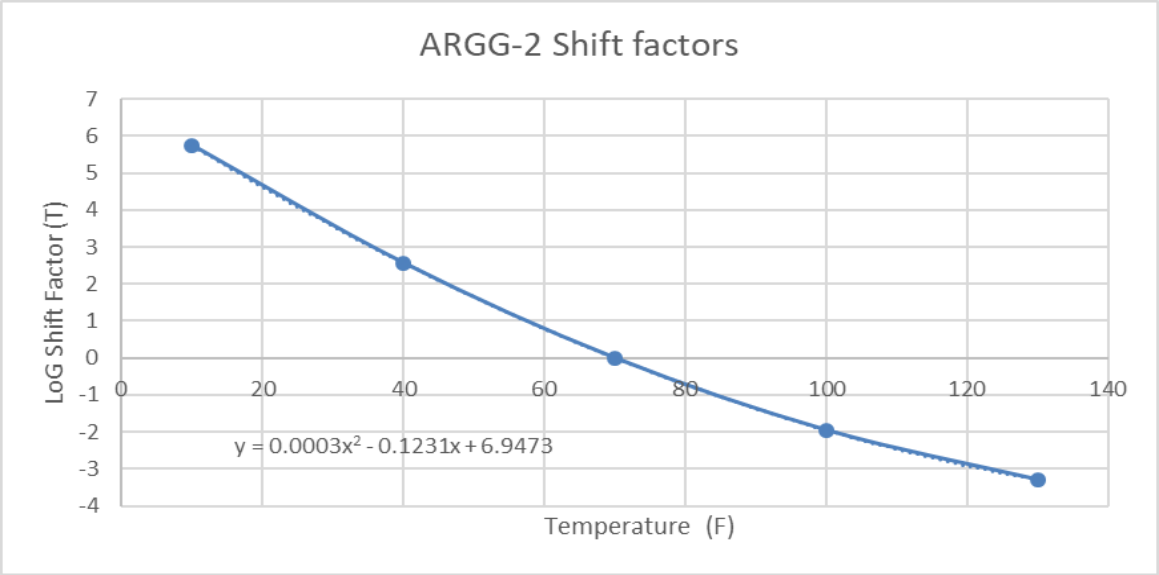

Figure A.4.2.6: ARGG-2 cross section shift factors.

T -1				
	Frequency (Hz)			
Temp (F)	0.1	1	10	25
10	1671717.47	2057179	2315221	2387669
40	655208.6218	1081775	1568820	1770225
70	111555.0371	262359.1	558316.2	716218.8
100	32156.70826	57201.74	131883.5	188498.1
130	14663.03545	19164.5	29545.46	37104.88

Figure A.4.2.7: Dynamic modulus input for T-1 cross section.

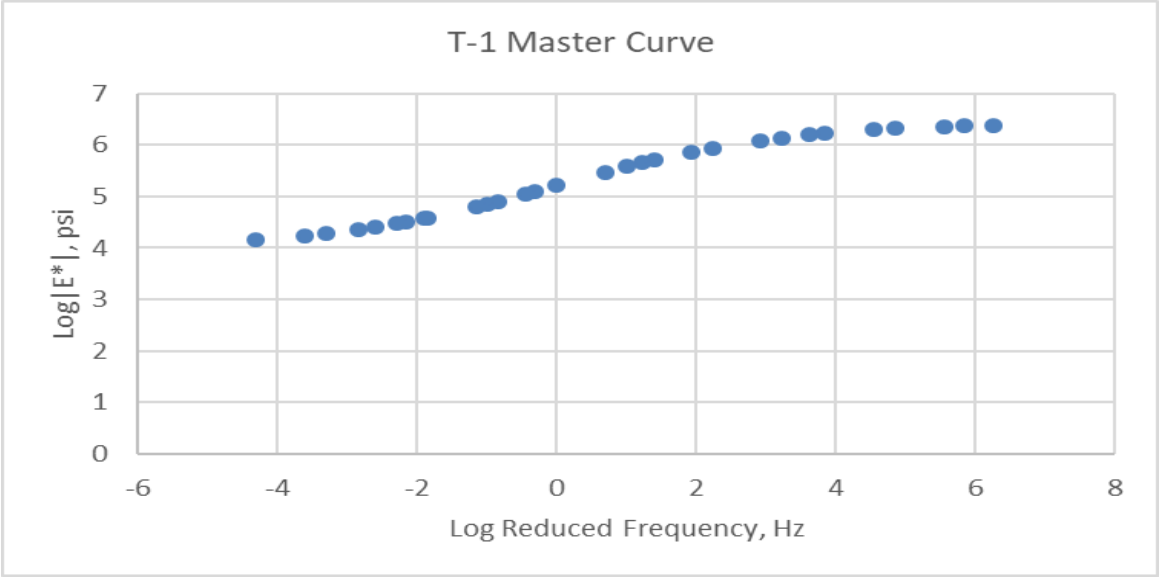

Figure A.4.2.8: T-1 cross section master curve.

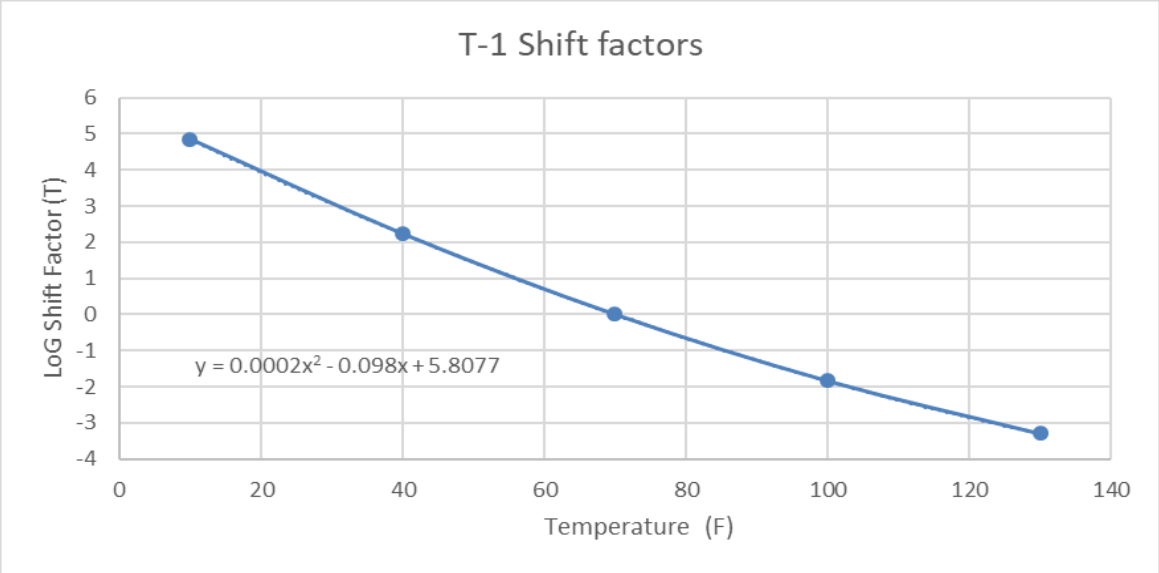

Figure A.4.2.9: T-1 cross section shift factors.

THS -1				
	Frequency (Hz)			
Temp (F)	0.1	1	10	25
10	2468122.901	2773966	2962146	3013166
40	1060744.307	1530931	2067423	2278389
70	198413.424	427556.5	820621.8	1016861
100	55629.35472	102580.4	233180.4	324235.4
130	27789.83053	41829.18	75808.53	100861

Figure A.4.2.10: Dynamic modulus input for THS-1 cross section.

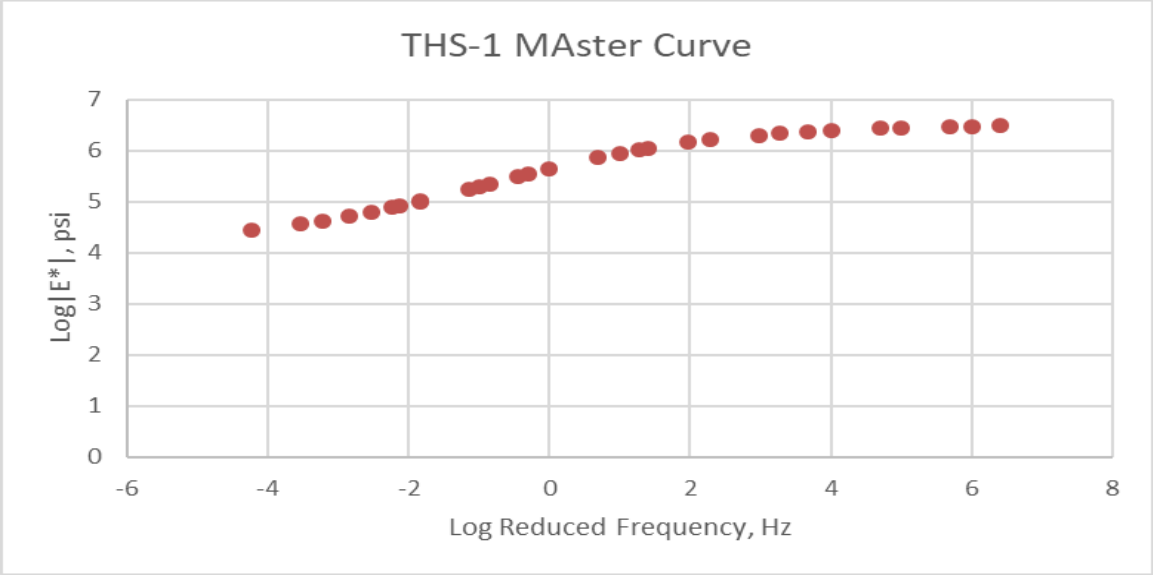

Figure A.4.2.11: THS-1 cross section master curve.

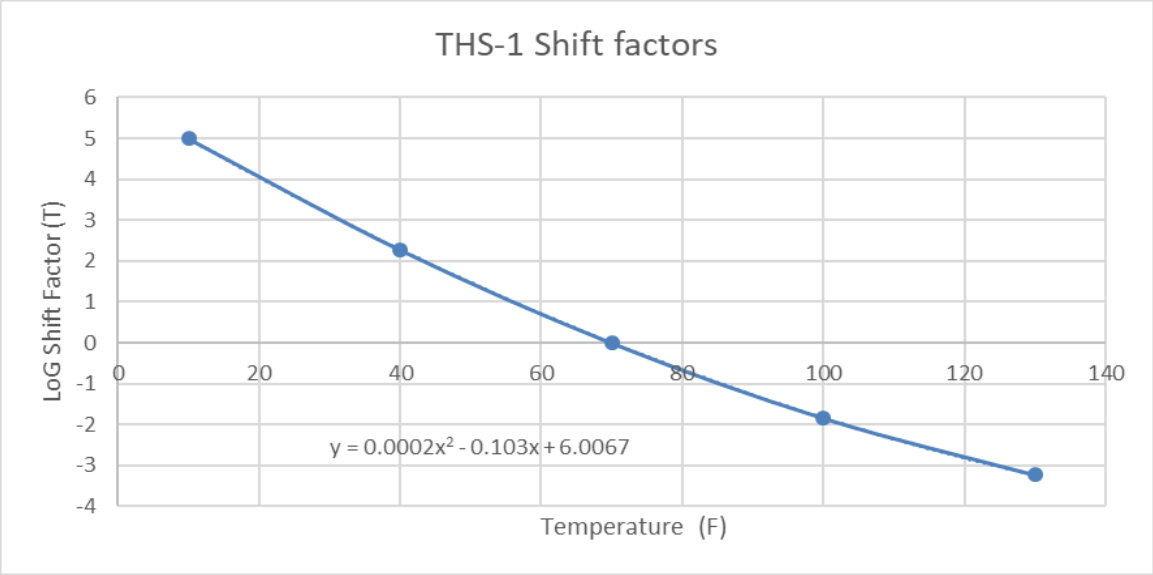

Figure A.4.2.12: THS-1 cross section shift factors.

SHM -1				
	Frequency (Hz)			
Temp (F)	0.1	1	10	25
10	1334184.018	1721320	1987313	2061850
40	323538.2494	648593.7	1092120	1273953
70	70265.07206	135411.7	289778.7	390499.8
100	34666.43581	48370.83	81156.58	105082.9
130	27227.06839	31853	41968.07	48997.99

Figure A.4.2.13: Dynamic modulus input for SHM-1 cross section.

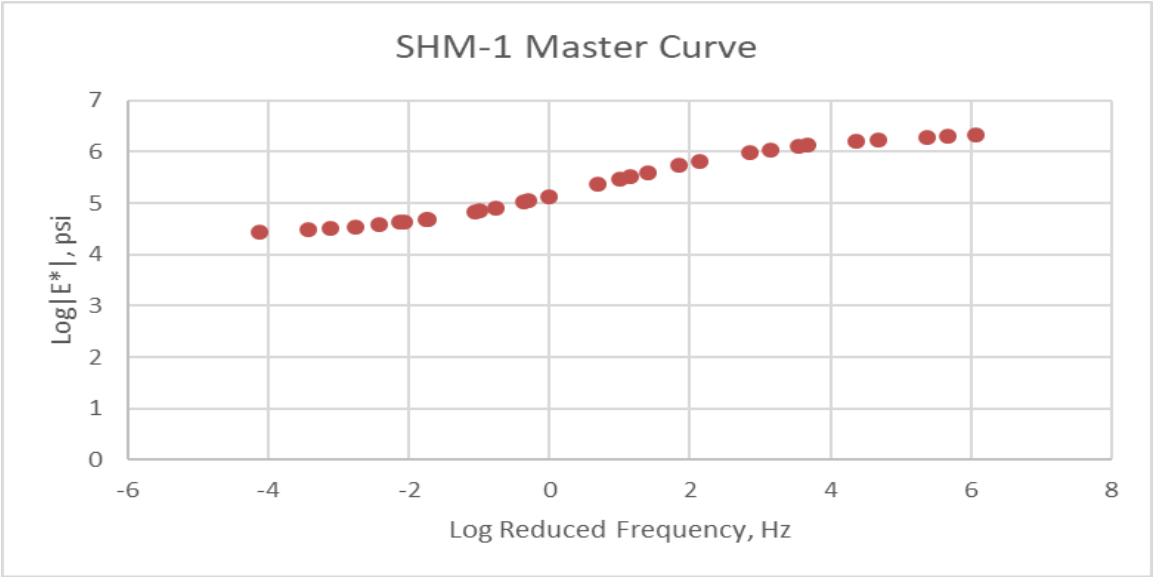

Figure A.4.2.14: SHM-1 cross section master curve.

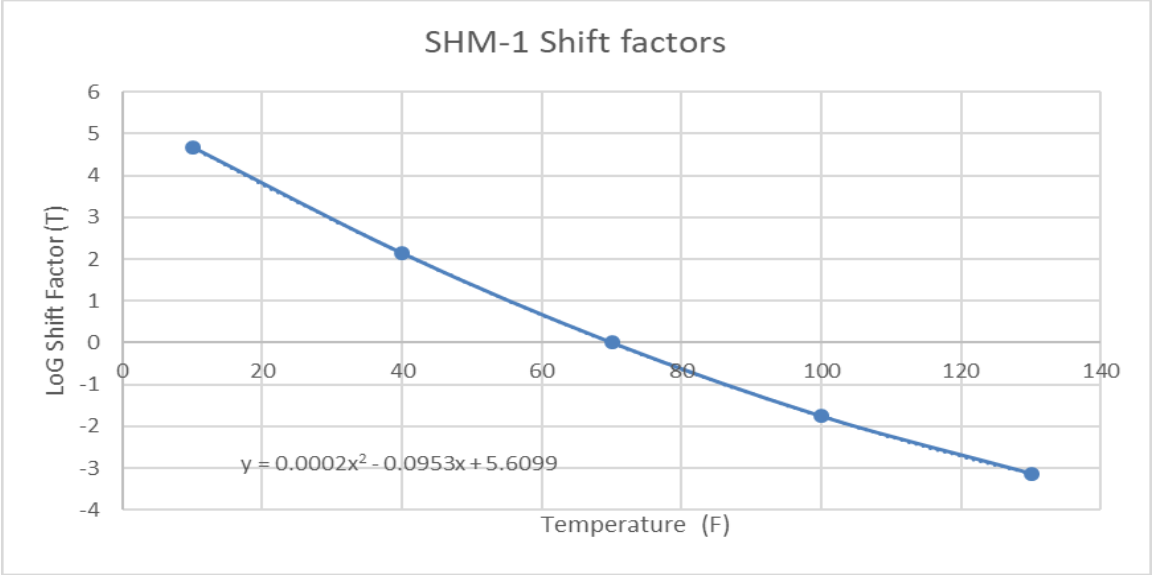

Figure A.4.2.15: SHM-1 cross section shift factors.

B-1				
	Frequency (Hz)			
Temp (F)	0.1	1	10	25
10	2389826	2739077	2977744	3047586
40	1022230	1482512	1986847	2187285
70	222885.2	461931.6	853728.2	1047307
100	53774.47	112214.4	255679	350569.3
130	21303.35	37603.73	77110.14	105669.7

Figure A.4.2.16: Dynamic modulus input for B-1 cross section.

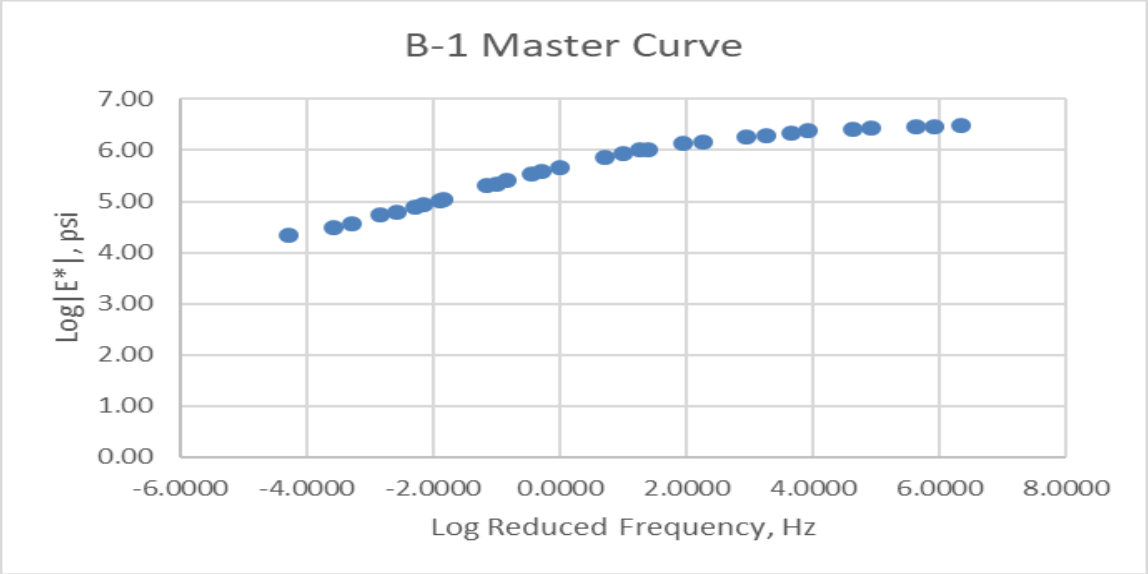

Figure A.4.2.17: B-1 cross section master curve.

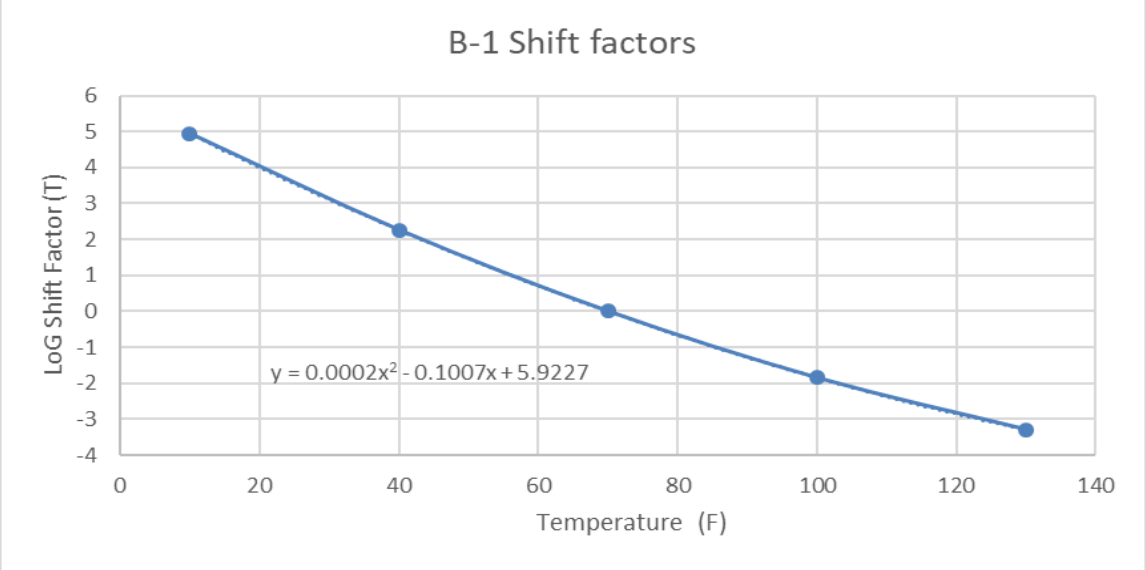

Figure A.4.2.18: B-1 cross section shift factors.

BB-1				
	Frequency (Hz)			
Temp (F)	0.1	1	10	25
10	2442356.456	2576548	2662972	2687742
40	948857.5471	1360029	1820795	2000413
70	159373.9746	363308.6	678359	835859.2
100	41299.4409	81029.95	185399.2	256839.6
130	23343.24016	46724.3	102701.4	141528.8

Figure A.4.2.19: Dynamic modulus input for BB-1 cross section.

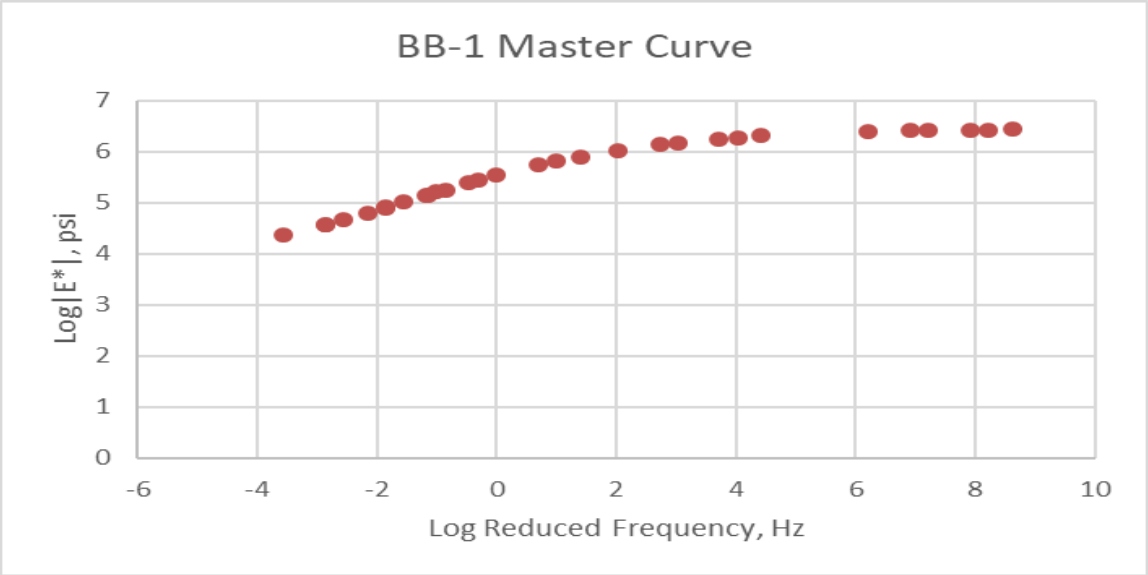

Figure A.4.2.20: BB-1 cross section master curve.

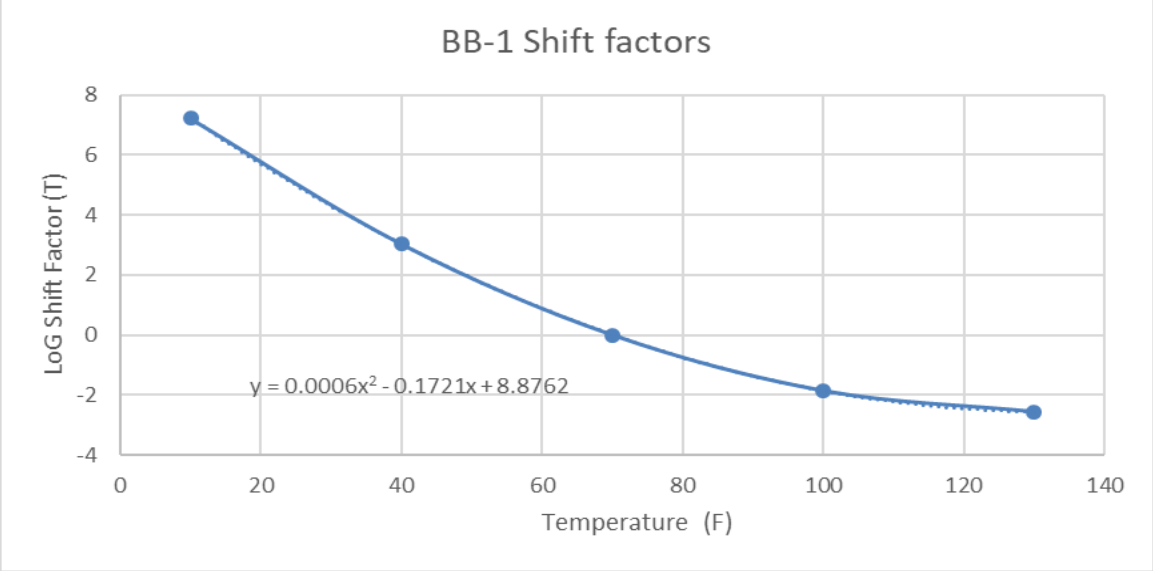

Figure A.4.2.21: BB-1 cross section shift factors.

A.4.3 Complex Shear Modulus (G*) Pavement ME Binder Input

Table A.4.3.1: Summary of PG grade information for each mix.

B-1	Temp (C)	Temp (F)	G* (Pa)	Phase angle
PG 64-28	64	147.2	1193	86
	70	158	300	87.5
	76	168.8	250	89

BB-1	Temp (C)	Temp (F)	G* (Pa)	Phase angle
PG 64-28	64	147.2	1107	82.93
	70	158	300	85.97
	76	168.8	250	89

ARGG-1	Temp (C)	Temp (F)	G* (Pa)	Phase angle
PG 58-28	58	136.4	1505	85.93
	64	147.2	700	87.47
	70	158	300	89

ARGG-2	Temp (C)	Temp (F)	G* (Pa)	Phase angle
PG 58-28	58	136.4	1479	86.18
	64	147.2	700	87.59
	70	158	300	89

T-1	Temp (C)	Temp (F)	G* (Pa)	Phase angle
PG 64-28	64	147.2	1100	82.76
	70	158	300	85.88
	76	168.8	250	89

THS-1	Temp (C)	Temp (F)	G* (Pa)	Phase angle
PG 76-28	76	168.8	1301	67.83
	82	179.6	200	78.42
	88	190.4	100	89

SHM-1	Temp (C)	Temp (F)	G* (Pa)	Phase angle
PG 70-34	70	158	1245	54.21
	76	168.8	250	71.61
	82	179.6	200	89

A.5 Maintenance and Rehabilitation Alternative Emission Results

Table A.5.1: ARGG-1 M&R alternative emissions from Palate 2.0 software.

ARGG-1 Cross Section			
Baseline		**Energy [MJ]**	**CO_2 [Mg] = GWP**
Initial Construction	**Materials Production**	37,972,888,683	2,004,224
	Materials Transportation	2,003,300,632	149,765
	Processes (Equipment)	193,655,431	14,535
	SUM	40,169,844,745	2,168,524
Mill and Fill		**Energy [MJ]**	**CO_2 [Mg] = GWP**
Maintenance	**Materials Production**	6,865,339,512	368,288
	Materials Transportation	405,995,727	30,352
	Processes (Equipment)	54,425,489	4,085
	SUM	7,325,760,728	402,725
CIR		**Energy [MJ]**	**CO_2 [Mg] = GWP**
Maintenance	**Materials Production**	5,149,004,634	276,216
	Materials Transportation	340,644,743	25,466
	Processes (Equipment)	49,098,146	3,685
	SUM	5,538,747,523	305,368
Microsurface		**Energy [MJ]**	**CO_2 [Mg] = GWP**
Maintenance	**Materials Production**	3,432,669,756	184,144
	Materials Transportation	275,293,760	20,581
	Processes (Equipment)	41,779,821	3,136
	SUM	3,749,743,337	207,861

Table A.5.2: ARGG-1 M&R alternative emissions from Palate 2.0 software.

ARGG-2 Cross Section			
Baseline		Energy [MJ]	CO_2 [Mg] = GWP
Initial Construction	Materials Production	37,972,888,683	2,004,224
	Materials Transportation	2,003,300,632	149,765
	Processes (Equipment)	193,655,431	14,535
	SUM	40,169,844,745	2,168,524
Mill and Fill		Energy [MJ]	CO_2 [Mg] = GWP
Maintenance	Materials Production	6,795,577,992	363,862
	Materials Transportation	412,709,701	30,854
	Processes (Equipment)	55,053,496	4,132
	SUM	7,263,341,189	398,848
CIR		Energy [MJ]	CO_2 [Mg] = GWP
Maintenance	Materials Production	5,096,683,494	272,897
	Materials Transportation	345,680,224	25,843
	Processes (Equipment)	49,569,152	3,720
	SUM	5,491,932,870	302,460
Microsurface		Energy [MJ]	CO_2 [Mg] = GWP
Maintenance	Materials Production	3,397,788,996	181,931
	Materials Transportation	278,650,747	20,832
	Processes (Equipment)	42,093,825	3,159
	SUM	3,718,533,568	205,922

Table A.5.3: THS - 1 M&R alternative emissions from Palate 2.0.

THS-1 Cross Section			
Baseline		**Energy [MJ]**	**CO_2 [Mg] = GWP**
Initial Construction	**Materials Production**	37,972,888,683	2,004,224
	Materials Transportation	2,003,300,632	149,765
	Processes (Equipment)	193,655,431	14,535
	SUM	40,169,844,745	2,168,524
Mill and Fill		**Energy [MJ]**	**CO_2 [Mg] = GWP**
Maintenance	**Materials Production**	5,381,887,465	284,662
	Materials Transportation	404,968,158	30,275
	Processes (Equipment)	54,198,337	4,068
	SUM	5,841,053,960	319,005
CIR		**Energy [MJ]**	**CO_2 [Mg] = GWP**
Maintenance	**Materials Production**	4,036,415,599	213,497
	Materials Transportation	339,874,066	25,409
	Processes (Equipment)	48,927,782	3,672
	SUM	4,425,217,448	242,578
Microsurface		**Energy [MJ]**	**CO_2 [Mg] = GWP**
Maintenance	**Materials Production**	2,690,943,733	142,331
	Materials Transportation	274,779,975	20,542
	Processes (Equipment)	41,666,245	3,127
	SUM	3,007,389,953	166,001

Table A.5.4: T - 1 M&R alternative emissions from Palate 2.0 software.

T-1 Cross Section			
Baseline		**Energy [MJ]**	**CO_2 [Mg] = GWP**
Initial Construction	**Materials Production**	37,972,888,683	2,004,224
	Materials Transportation	2,003,300,632	149,765
	Processes (Equipment)	193,655,431	14,535
	SUM	40,169,844,745	2,168,524
Mill and Fill		**Energy [MJ]**	**CO_2 [Mg] = GWP**
Maintenance	**Materials Production**	5,442,180,423	287,509
	Materials Transportation	412,579,971	30,844
	Processes (Equipment)	54,922,550	4,122
	SUM	5,909,682,943	322,475
CIR		**Energy [MJ]**	**CO_2 [Mg] = GWP**
Maintenance	**Materials Production**	4,081,635,317	215,631
	Materials Transportation	345,582,926	25,835
	Processes (Equipment)	49,470,942	3,713
	SUM	4,476,689,185	245,180
Microsurface		**Energy [MJ]**	**CO_2 [Mg] = GWP**
Maintenance	**Materials Production**	2,721,090,211	143,754
	Materials Transportation	278,585,882	20,827
	Processes (Equipment)	42,028,352	3,154
	SUM	3,041,704,445	167,736

Table A.5.5: SHM - 1 M&R alternative emissions from Palate 2.0 software.

SHM-1 Cross Section			
Baseline		**Energy [MJ]**	**CO_2 [Mg] = GWP**
Initial Construction	**Materials Production**	37,972,888,683	2,004,224
	Materials Transportation	2,003,300,632	149,765
	Processes (Equipment)	193,655,431	14,535
	SUM	40,169,844,745	2,168,524
Mill and Fill		**Energy [MJ]**	**CO_2 [Mg] = GWP**
Maintenance	**Materials Production**	5,492,078,801	290,431
	Materials Transportation	411,118,915	30,735
	Processes (Equipment)	54,788,931	4,112
	SUM	5,957,986,647	325,278
CIR		**Energy [MJ]**	**CO_2 [Mg] = GWP**
Maintenance	**Materials Production**	4,119,059,101	217,823
	Materials Transportation	344,487,134	25,754
	Processes (Equipment)	49,370,728	3,706
	SUM	4,512,916,963	247,282
Microsurface		**Energy [MJ]**	**CO_2 [Mg] = GWP**
Maintenance	**Materials Production**	2,746,039,401	145,215
	Materials Transportation	277,855,354	20,772
	Processes (Equipment)	41,961,542	3,149
	SUM	3,065,856,297	169,137

References

2017 Infrastructure Report Card - Roads. American Society of Civil Engineers (ASCE), 2017, www.infrastructurereportcard.org/wp-content/uploads/2017/01/Roads-Final.pdf.

TRIP, National Fact Sheet. September 2018. http://www.tripnet.org/docs/Fact_Sheet_National.pdf

Wang, Ting, et al. "Life cycle energy consumption and GHG emission from pavement rehabilitation with different rolling resistance." Journal of Cleaner Production 33 (2012): 86-96.

Kang, S., Yang, R., Ozer, H., & Al-Qadi, I. L. (2014). Life-cycle greenhouse gases and energy consumption for material and construction phases of pavement with traffic delay. Transportation Research Record, 2428(1), 27-34.

Lu, Qing, Fred L. Mannering, and Chunfu Xin. "A Life Cycle Assessment Framework for Pavement Maintenance and Rehabilitation Technologies: or An Integrated Life Cycle Assessment (LCA)–Life Cycle Cost Analysis (LCCA) Framework for Pavement Maintenance and Rehabilitation." (2018).

Pavement Life Cycle Assessment Workshop, University of California, Davis, May 2010, www.ucprc.ucdavis.edu/p-lca/presentations.html.

Ventura, A, and C De la Roche. International Symposium on Life Cycle Assessment and Construction – Civil Engineering and Buildings, 2012. ISBN: 978-2-35158-127-8

"International Symposium on Pavement LCA 2014." Pavement LCA 2014, 2014. www.ucprc.ucdavis.edu/p-lca2014/Papers.aspx.

Al-Qadi, Imad, et al. Pavement LCA Symposium 2017, University of Illinois at Urbana-Champaign, Apr. 2017, lcasymposium.ict.illinois.edu/proceedings/.

Harvey, John T, et al. Pavement Life Cycle Assessment Framework. Federal Highway Administration, July 2016. www.fhwa.dot.gov/pavement/sustainability/hif16014.pdf.

Zaabar, Imen, and Karim Chatti. "Calibration of HDM-4 models for estimating the effect of pavement roughness on fuel consumption for US conditions." Transportation Research Record: Journal of the Transportation Research Board 2155 (2010): 105-116.

Chatti, Karim, and Imen Zaabar. (2012). Estimating the effects of pavement condition on vehicle operating costs. Vol. 720. Transportation Research Board.

Robbins, Mary M., and Nam Tran. "Literature review: the effect of pavement roughness on vehicle operating costs." National Center for Asphalt Technology Report 15 2 (2015): 15-02.

Ziyadi, Mojtaba, et al. "Vehicle energy consumption and an environmental impact calculation model for the transportation infrastructure systems." Journal of cleaner production 174 (2018): 424-436.

DeCarlo, C, et al. "Sustainable Pavement Rehabilitation Strategy Using Consequential Life Cycle Assessment." Bearing Capacity of Roads, Railways and Airfields, 2017, doi:10.1201/9781315100333-311.

MassDOT. (2018). Transportation data management system (MS2). Retrieved from http://mhd.ms2soft.com/tcds/tsearch.asp?loc=Mhd&mod=

Google. Google maps. Retrieved from www.google.com/maps/dir/42.7323361,-71.1411406/42.6010 946,-71.3603337/@42.6764548,-71.2893349, 37709m/data =!3m1!1e3!4m2!4m1!3e0

Nemati, R. Dave, E. V., Daniel, J. S., "Statistical Evaluation of Effect of Mix Design Properties on Performance Indices of Asphalt Mixtures." ASTM Journal of Testing and Evaluation. 2019. (article in press)

SimaPro 8.0.0 (2013). PRÉ.

Consortium on Green Design and Manufacturing from the University of California-Berkeley. (2013). Pavement life-cycle assessment tool for environmental and economic effects (PaLATE).

CalTrans, 2013, LIFE-CYCLE COST ANALYSIS PROCEDURES MANUAL, California Department of Transportation, Sacramento, CA, p. 158.

Mousa, M., Elseifi, M. A., Bashar, M., Zhang, Z., & Gaspard, K. (2018). Field Evaluation and Cost Effectiveness of Crack Sealing in Flexible and Composite Pavements. Transportation Research Record, 0361198118767417

Cole, M., & Geib, J. (2016). MnDOT's Experience: Efforts to Improve Micro Surfacing Performance. Retrieved from https://www.dot.state.mn.us/materials/pavementpreservation/mndotexperiences/documents/EffortstoImproveMicroSurfacingPerformance.pdf

Damp, Stephen. "Cold In-Place Recycling: Southeast Pavement Preservation Partnership." www.pavementpreservation.org/wp-content/uploads/presentations/Cold%20In-Place%20Recycling.pdf

Lane, Becca, and Tom Kazmierowski. "Short Term Performance of an Innovative Cold In-Place Recycling Technology in Ontario." 2005 Annual Conference of the Transportation Association of Canada, 2005, conf.tac-atc.ca/english/resourcecentre/readingroom/conference/conf2005/docs/s15/lane.pdf

Fitts, Gary L. "Thin Overlays for Pavement Preservation and Functional Rehabilitation." www.ltrc.lsu.edu/ltc_09/pdf/Fitts,%20Gary.pdf.

Harikrishnan Nair, et al. "Assessment of an Incentive Only Ride Specification for Asphalt Pavements." Virginia Center for Transportation Innovation and Research, Final Report VCTIR 16-R2, Sept. 2015.

Transportation Research Board (TRB). (2018). InSight Data access website - SHRP2 naturalistic driving study. Retrieved from https://insight.shrp2nds.us/

Environmental Protection Agency (EPA). (2014). MOtor vehicles emissions simulator (MOVES) (MOVES2014a ed.) EPA.

AASHTOWare. (2015). Pavement ME design. (Version 2.3).

Wilde, J. W. (2007). Implementation of an international roughness index for mn/DOT pavement construction and rehabilitation. (No. MN/RC-2007-09). 395 John Ireland Boulevard, MS 330 St. Paul, Minnesota 55155-1899: Minnesota Department of Transportation. Retrieved from ttp://www.lrrb.org/PDF/200709.pdf

Kerali, H. (2000). HDM-4: Highway development and management: Volume one: Overview of HDM-4.

Walls, James, and Michael R. Smith. "Life-cycle cost analysis in pavement design: in search of better investment decisions." Federal Highway Administration. (1998).

"New England (PADD 1A) Regular All Formulations Retail Gasoline Prices." Petroleum and Other Liquids, US Energy Information Administration, Apr. 2017. www.eia.gov/petroleum/gasdiesel/

Ogwang, Allan, Samer Madanat, and Arpad Horvath. "Optimal Cracking Threshold Resurfacing Policies in Asphalt Pavement Management to Minimize Costs and Emissions." Journal of Infrastructure Systems 25.2 (2019): 04019003.

Chehovits, Jim, and Larry Galehouse. "Energy usage and greenhouse gas emissions of pavement preservation processes for asphalt concrete pavements." Proceedings on the 1st International Conference of Pavement Preservation. 2010.

Appendix D.2: Paper 4 – Impacts of climate-change and realistic traffic conditions on asphalt pavement and rehabilitation decisions using life cycle assessment

Authors: Katie E. Haslett, Eshan V. Dave and Weiwei Mo

Conference Paper: Pavement, Roadway, and Bridge Life Cycle Assessment 2020: Proceedings of the International Symposium on Pavement.

Impacts of Climate-Change and Realistic Traffic Conditions on Asphalt Pavement and Rehabilitation Decisions using Life Cycle Assessment

K. Haslett, E. Dave & W. Mo
Department of Civil and Environmental Engineering, University of New Hampshire, Durham, New Hampshire, USA

ABSTRACT: Typical pavement Life Cycle Assessment (LCA) are performed using historical climate data to evaluate pavement performance and provide recommendations for budgeting and planning of M&R strategies in the future. However, due to climate change, this assumption may not be appropriate as flexible pavements' performance is influenced by climate stressors. This study explores the impacts of future climate data and realistic traffic data (RTD) in the pavement M&R evaluation process. A 26-km stretch of Interstate-495 was used to evaluate costs and environmental impacts with varying M&R scenarios and pavement structures. Predicted performance using historical and future projected climate data in combination with RTD is used for life cycle cost and global warming potential estimation. Results show that incorporating future project climate data and RTD can lead to a substantial increase in agency LCA impacts (up to 20% for the presented case-study), the increase is function of pavement structure and M&R alternative

1. INTRODUCTION AND BACKGROUND

Since the late 19th century, climate change has consisted of a global temperature rise (0.9 degrees Celsius), global sea level rise (203 mm) and an increase in extreme weather events, among others (Climate Change: Vital Signs of the Planet, 2019). While these changes alone are of concern, the implications to human life, infrastructure systems and the economy is grave. Climate change poses a serious threat to both natural and built systems including transportation infrastructure systems (i.e. bridges, rail, road networks, airports etc.). In context of the road network, future increases in very hot days and heat waves pose a concern with pavement integrity and permanent deformation (Gudipudi et al. 2017). Accelerated sea level rise and increased extreme precipitation events will cause changes in subgrade moisture level, water table depth and flooding susceptibility; alter bearing capacity of the pavement system; and in turn, degrade the performance of the road infrastructure system (Daniel et al. 2014, Knott et al. 2017 and Knott et al. 2019).

This may result in serious implications to freight movement, which is multimodal and moves approximately 50 million tons of freight across the US every day. For example, truck freight, which relies on the efficient and safe transportation of goods via the road network reported a movement of 11.5 billion tons of freight in 2015 and is expected to increase by 44% to move 16.5 billion tons by 2045 (USDOT, 2015). Meanwhile, traffic congestion, road closures and delays affect citizens daily where on average a road-user spends 42 hours waiting in traffic each year, and the annual cost of truck congestion is 28 billion dollars (USDOT, 2015).

The use of life cycle assessment (LCA) and life cycle cost analysis (LCCA) are increasing in pavement management due to the growing need to consider sustainable, cost and environmentally effective maintenance and rehabilitation (M&R) plans. Future planning incorporating the effects of a changing climate and realistic traffic conditions is critical. Typically, pavement LCA are

performed using historical climate data to plan pavement life expectancy and inform M&R plans. However, pavements systems are constantly exposed to the natural environment and impacts of climate change, therefore it may not be applicable to use historical climate data to inform decisions about future pavement performance.

In recent years, there have been several studies conducted that explore the impacts on pavement performance using future projected climate data in the form of temperature (Meagher et al., 2012), precipitation and the combination of both (Heitzman et al. 2011 and Mndawe et al. 2015). In 2017, Gudipudi et al. conducted a study with the primary object to predict performance of freeway sections in different climatic regions across the US using different climate models. Performance predicted using historical climate data compared to incorporating projected climate data was performed focusing on various pavement distresses such as fatigue cracking, asphalt concrete (AC) rutting and total rutting. However, an LCA approach was not used to make comparisons among various M&R treatments and the timing of those treatments using historical versus projected climate data in combination with realistic traffic data (RTD).

The study herein explores the use of incorporating future projected climate data and RTD into a pavement LCA analysis. Building upon a LCA framework that includes real time traffic data and considers both user and agency costs (Haslett et al. 2019), the addition of future climate data (temperature and precipitation) in the pavement performance analysis is demonstrated in this paper using a case study for two flexible pavement cross sections and three M&R alternatives. The primary study objective of this study was to use an LCA framework to investigate impacts in terms of global warming potential (GWP) and life cycle cost (LCC) when using historical climate data compared to projected future climate data in combination with realistic traffic conditions.

2. METHODOLOGY

2.1 Life Cycle Assessment Framework

A pavement LCA framework that included raw materials and excavation, material transportation, operational and maintenance impacts and end-of-life was used in this study. A 30-year analysis period was considered and all impacts (GWP and LCC) were quantified in terms of agency, user and total impact. LCA software programs including SimaPro 8.3 and the Pavement-Life-Cycle Assessment Tool (PaLATE2.0) were used to collect unit impact information on raw materials, transportation and construction impacts. Pavement performance curve information was generated using the American Association of State Highway and Transportation Officials (AASHTO) PavementME design software and then used to determine fuel consumption and carbon emission factors for different vehicle classes under various International Roughness Index (IRI) and speeds. Scenarios were calculated using a combination of Google Maps®, the U.S. Environmental Protection Agency (EPA) Motor Vehicle Emission Simulator (MOVES), the SHRP2 Naturalistic Driving Study, and Massachusetts Department of Transportation (MassDOT) Data Management System. Further detail on the incorporation of RTD into an LCA framework is discussed in a prior study (Haslett et al. 2019). Lastly, end-of-life was account for by discounting salvage value (remaining life) of each pavement M&R scenario at the end of the 30-year analysis period.

2.2 Case Study Location and Pavement Cross Sections

This case study utilized a 26-km section of Interstate 495 (I-495) in Massachusetts, from Chelmsford to Methuen. This highway is comprised of 3 lanes in each direction with a distributional factor of 50% (of 24 hr. peak volume). Traffic volume information for this section was collected from MassDOT's traffic data management system. To be conservative, all simulations assumed no annual change in total traffic volume, i.e. annual growth rate of 0%.

Two different pavement cross sections were simulated, a "thick pavement" and "thin pavement" section. Simulating two different cross section allows for comparisons to be drawn on the role of pavement structure on performance under future climate conditions with respect to the different M&R strategies explored in this study. Table 1 summarizes the pavement cross section information used in this study for three different M&R scenarios; do nothing and reconstruct (DNR), mill and overlay (MO) and cold-in-place recycling (CIR).

Table 1: Pavement cross-sections and AASHTO PavementME design software input parameters used for given case study location.

Input Type	Variable	DNR[b]	MO[d]	CIR[f]
Thick Cross Section	Layer 1	50.8 mm AC[c]	50.8 mm OL[e]	50.8 mm AC
	Layer 2	101.6 mm AC	101.6 mm AC	101.6 mm CIR
	Layer 3	203.2 mm Crushed Stone Base		
	Layer 4	609.6 mm Prepared Subgrade (A-2-6)		
	Layer 5	Natural Subgrade (A-2-6) Semi-infinite		
Thin Cross Section	Layer 1	50.8 mm AC	50.8 mm OL	25.4 mm OL
	Layer 2	50.8 mm AC	50.8 mm AC	76.2 mm CIR
	Layer 3	101.6 mm Crushed Stone Base		
	Layer 4	Prepared Subgrade (A-2-6) 609.6 mm		
	Layer 5	Natural Subgrade (A-2-6) Semi-infinite		
Traffic	AADTT[a]	12,175		
	Lanes	3		
	Speed (km/hr)	105		
Climate	Elevation (m)	5.8		
	Location	Boston, MA		

[a] AADTT = Two way annual average daily truck traffic.

[b] DNR = Do nothing and reconstruct

[c] AC= Flexible Asphalt concrete

[d] MO = Mill and Overlay

[e] OL = Flexible Overlay

[f] CIR = Cold-In-Place Recycling

2.3 Maintenance and Rehabilitation Scenarios

For both the thick and thin pavement cross section, three different M&R strategies (DNR, MO and CIR) were consider using historical climate data and future projected climate data following the RCP 8.5 emission pathway resulting in a total of 12 scenarios. Initial IRI values for each cross section were determined using a 90% reliability factor in PavementME design software. The thick pavement cross section required an initial IRI value of 1.55 m/km, meanwhile the thin pavement section required an initial IRI of 1.66 m/km. While the initial IRI values are similar when using either historical or future climate projection data, the performance curve slopes vary due to the rate of accumulated pavement distresses. Figure 1 provides an example of the predicted performance curves from PavementME design software for both the thick and thin pavement section. The analysis period of 30 years from 2020-2050 was held constant among all scenarios. The dashed lines represent the respective M&R scenario performance curves assuming historical climate data, while the solid lines represent the same M&R scenarios but assuming future projected climate data.

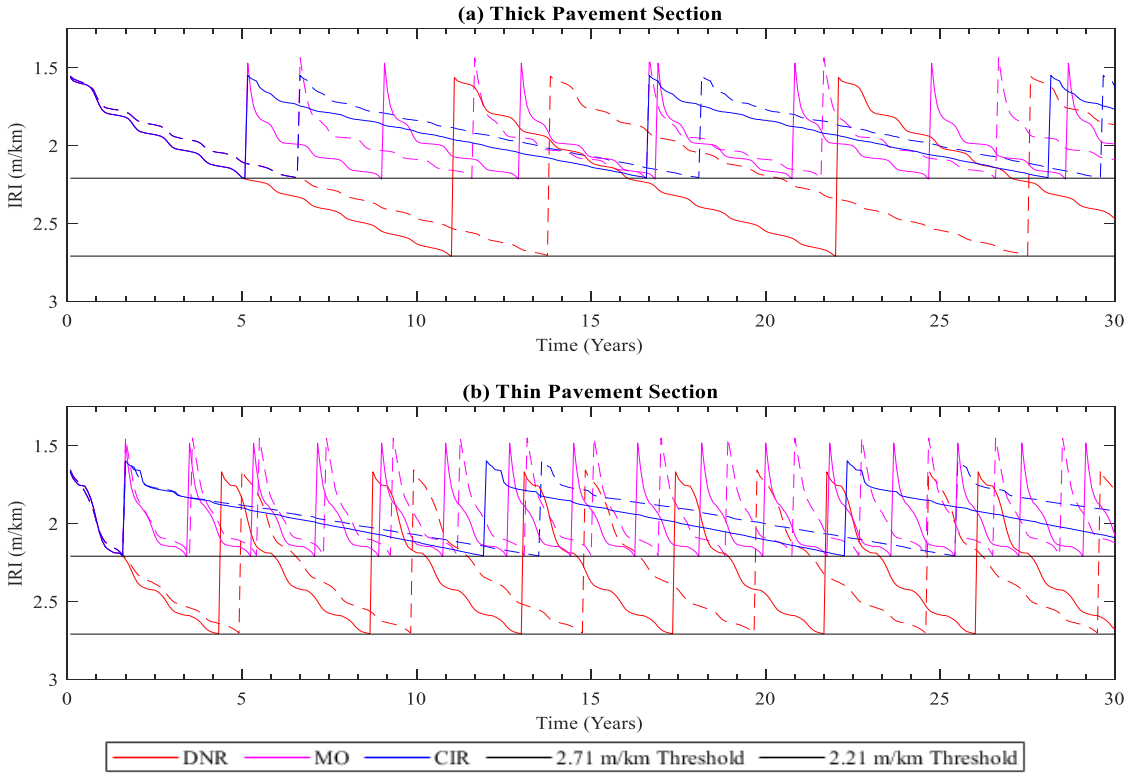

Figure 1: Performance curves for (a) thick pavement section and (b) thin pavement section comparing maintenance and rehabilitation timing for historical climate data (dashed line) and future climate data (solid line) scenarios.

The DNR scenario assumes that no M&R activity is conducted over the analysis period except for reconstruction when a terminal IRI value of 2.71 m/km is reached. The MO scenario begins with the same initial IRI values as the DNR scenario, however when the pavement degrades to an IRI of 2.21 m/km a MO treatment is triggered (the milling depth and overlay thickness are equal and assumed to be constant in each MO application). The MO treatment is repeated until the end of the 30-year analysis period. Similarly, the CIR scenario begins with the same initial IRI curve as the DNR scenario but when an IRI threshold of 2.21 m/km is reached it triggers the CIR treatment, at which point the CIR performance curve is repeated until the end of the analysis period. Please note that as with typical CIR practice, the CIR layer is surfaces with an asphalt concrete overlay.

2.4 Climate Data Integration

Climate data averaged from 21 models assuming RCP 8.5 (highest emission pathway) and RCP 4.5 (intermediate emission pathway) was integrated into AASHTO's PavementME design system to evaluate pavement performance using pavement IRI. This paper presents only the comparison of historical climate data to RCP 8.5 future climate projection data for brevity and due to early findings in the study that there was not a significant difference in performance curves using average RCP 4.5 or RCP 8.5 emission scenarios, therefore the timing of M&R treatments being triggered would be comparable. It is also acknowledged that future research efforts should undertake a probabilistic approach with the use of 21 different global circulation models as opposed to taking the average of them.

Climate data was procured from Coupled Model Intercomparison Project Phase 5 (CMIP5) for a 12 km square grid near the case study location (latitude 42° 30' 58.68"N and longitude 71° 44' 44.88"W). Daily precipitation and daily maximum and minimum temperature were obtained for the years 2020-2050. To incorporate climate date in to PavementME, further processing is required to convert temperature and

precipitation to hourly climatic data. Daily precipitation values were divided into 24 equal increments and spaced over the course of a given day. Converting daily maximum and minimum temperatures into hourly data was slightly more computationally intensive. A method adapted by Valle et al. in 2017 was followed in this study where the minimum daily temperature (t_{min}) occurs at sunrise and the maximum temperature (t_{max}) occurs at 2 p.m. Equations 1-4 are used to calculate intervening temperatures:

for 0:00 < h < rise and 14:00 < h < 24:00, $T(h) = t_{ave} + amp(\cos(\pi \times h')/(10+rise))$ (1)
for rise < h < 14:00, $T(h) = t_{ave} - amp(\cos(\pi (h'-rise)/(14)))$ (2)
where
$h' = h + 10$ if h < rise (3)
$h' = 14$ if h > 14 (4)

where rise = time of sunrise in hours; T(h) = temperature at any hour; h = time in hours, h' = h+10 if h < rise, h' = 14:00 if h> 14:00; $t_{ave} = (t_{min} + t_{max})/2$; $amp = (t_{max} - t_{min})/2$.

In addition to hourly temperature and precipitation data, PavementME also requires wind speed, percent sunshine, percent humidity and water table depth as climatic input factors. For wind, sunshine and humidity inputs the last year of historical climate data available was repeated for subsequent years until the end of the analysis period. This input assumption is deemed appropriate as the effect on pavement performance (in terms of IRI) is not considered dominate, therefore effects are negligible (Qiao et al. 2013). For water table depth, it was assumed to remain at a constant depth of 3.05 m. Change in groundwater level due to climate change is of concern and may have considerable implications on pavement performance and service life depending on the location as demonstrated by Knott et al. in 2017 and 2019. However, due to groundwater projection not being available in the CMIP5 dataset researchers verified groundwater level trends provided by the United States Geological Survey (USGS) and determined that groundwater level may not be of major concern for the current case study location, therefore it was not considered in this analysis.

2.5 Life Cycle Cost Determination

To make fair comparisons among all M&R scenarios over the 30 year analysis period, all life cycle costs for both users and agencies were converted to net present value (NPV) using Equation 5:

$$NPV = \frac{Future\ Cost}{(1+i)^n} \quad (5)$$

where i = discount rate (percent); n = number of years from initial construction.

If a pavement alternative had any remaining life determined from its respective IRI performance curve, its salvage was accounted for in the calculation of LCC. This was accomplished by taking the percentage of remaining months in service and discounting that percent of remaining life to present value. For example, if a given M&R alternative had 15 months of service life remaining based on the its IRI performance curve and it was expected to have 60 months of total service life, then 25% of the M&R treatment cost was discounted back to present value.

3. RESULTS AND DISCUSSION

LCA impacts for all scenarios explored in this case were quantified in terms of GWP (CO_2 eq) and LCC (dollars). Comparisons are drawn on the impacts of using historical climate data or future climate projection data in the LCA framework for operations (user impact), construction and maintenance (agency impact) and total impact (combination of user and agency).

3.1 Global Warming Potential (GWP)

The GWP of a greenhouse gas (GHG) indicates the amount of warming a gas can cause over a given period (typically 100 years). GWP is an index, where CO_2 has an index value of 1 and for all other GHG (methane, nitrous oxides, hydrofluorocarbons etc.) the index value is the number of times more warming they cause compared to CO_2 (Brander et al. 2012). For this study, carbon dioxide equivalent (CO_2 eq) was used, which signifies the amount of CO_2 that would have the equivalent global warming impact. Table 2 summarizes the GWP impact for all scenarios using historical, future projected climate data and the percent difference with respect to using historical climate data. Results are tabulated for the thick pavement section and for the thin pavement section separately.

Table 2: Global warming potential impact summary table for all maintenance and rehabilitation scenarios during historical and future projected climate data.

Global Warming Potential (Gg CO_2eq)								
M&R Scenario	**Thick Pavement Section**				**Thin Pavement Section**			
	Impact	Historical	8.5 RCP[f]	%Diff[g]	Impact	Historical	8.5 RCP	%Diff
DNR[a]	C/M[d]	4.57	5.71	20.00	C/M	12.76	14.48	11.86
	Ops[e]	13.22	13.22	0.00	Ops	13.23	13.23	0.00
	Total	17.79	18.93	6.03	Total	25.99	27.71	6.20
MO[b]	C/M	3.92	4.57	14.34	C/M	7.88	8.14	3.23
	Ops	13.21	13.21	0.00	Ops	13.21	13.21	0.01
	Total	17.13	17.78	3.69	Total	21.09	21.35	1.24
CIR[c]	C/M	2.90	2.93	0.95	C/M	2.58	2.65	2.84
	Ops	13.205	13.204	-0.01	Ops	13.21	13.21	0.00
	Total	16.11	16.13	0.17	Total	15.78	15.86	0.48

[a] DNR = Do nothing and reconstruct
[b] MO = Mill and overlay
[c] CIR = Cold-in-place recycling
[d] C/M = Construction and maintenance (agency impact)
[e] Ops = Operations (user impact)
[g] RCP = Representative concentration pathway
[f] %Diff = Percent difference with respect to impacts using historical climate data

It can be observed that there is a larger difference in GWP impact when using future climate data as compared to historical due to construction and maintenance (C/M) activities as oppose to operational impacts from roadway users, regardless of cross section type. For the thick pavement cross section, the total difference in impact is highest for the DNR scenario (6.03%) followed by the MO (3.69%) and CIR treatment (0.17%). The same trend is observed for the thin pavement cross section. The direct implication for pavement designers and policymakers is the potential underestimation of GWP impact over the lifetime of pavement system. The magnitude of the underestimation is dependent on pavement structure, as well as the type of M&R undertaken over the pavement service life (i.e. no maintenance, MO only or use of CIR). One reason why the percent difference is higher for thicker pavements compared to thin pavements while holding all traffic, material characteristics and climate scenarios constant is the critical role of having a sufficient pavement structure to withstand the current traffic level. From Figure 1a and Figure 1b the increase in frequency of M&R treatments is clearly shown for two different pavement structures. There is a higher frequency of M&R activity for the thin pavement section under the given traffic loading over the 30-year analysis period. This trend holds true when comparing performance curves generated with historical climate data and future projected climate data.

The operational impact (Ops) compared for each scenario includes the impact from all vehicles traveling on the 26 km stretch of interstate for 30 years (entire analysis period). Operational impact considers

pavement roughness as well as realistic traffic condition (daily traffic congestion) based on average travel patterns from Google Maps® to quantify the user impact over the analysis period.

Another interesting observation is when comparing all M&R scenarios (historical and future climate data together), the maximum percent difference with respect to the highest impact scenario in terms of CO_2 eq for agency impact was 49.2% and 82.2% for the thick and thin pavement respectively. Similarly, the maximum percent difference from a road user perspective was 0.13% and 0.19% for the thick and thin pavement section. While the difference in impact is higher for agencies due to construction and maintenance costs, it is important to note that the 0.13% and 0.19% is based on the current traffic volume with assumption of no traffic growth over the 30-year analysis period. It is recommended that further analysis be performed to verify the user impact while assuming varying traffic growth percentages. Other variables that may influence operational impact include vehicle fuel efficiency and future fuel costs (Haslett et al. 2019). In practice, when selecting a M&R treatment plan, it is recommended that varying traffic growth levels, vehicle efficiencies and fuel costs be assessed using either a probabilistic approach or sensitivity analysis to ensure uncertainty associated with user impacts can be accounted for.

3.2 Life Cycle Cost Analysis (LCCA)

All life cycle costs (LCC) were calculated in terms of NPV in billions of dollars, while taking into account salvage value at the end of the analysis period. Table 3 summarizes the LCC impacts for all M&R scenarios using historical and future projected climate data and the percent difference with respect to historical climate data.

Table 3: Life cycle cost impact summary table for all maintenance and rehabilitation scenarios during historical and future projected climate data.

Life Cycle Cost (Billions of Dollars)								
M&R Scenario	**Thick Pavement Section**				**Thin Pavement Section**			
	Impact	Historical	8.5 RCP	(%diff)	Impact	Historical	8.5 RCP	(%diff)
DNR	C/M	0.26	0.31	16.55	C/M	0.62	0.70	11.62
	Ops	2.33	2.33	0.01	Ops	2.33	2.29	-1.69
	Total	2.59	2.64	1.97	Total	2.94	2.99	1.41
MO	C/M	0.16	0.16	0.74	C/M	0.17	0.17	0.27
	Ops	2.32	2.32	0.01	Ops	2.29	2.29	0.01
	Total	2.48	2.49	0.05	Total	2.45	2.45	0.03
CIR	C/M	0.16	0.16	0.22	C/M	0.16	0.16	0.38
	Ops	2.32	2.32	0.00	Ops	2.29	2.29	0.00
	Total	2.48	2.49	0.01	Total	2.45	2.45	0.03

[a] DNR = Do nothing and reconstruct
[b] MO = Mill and overlay
[c] CIR = Cold-in-place recycling
[d] C/M = Construction and maintenance (agency impact)
[e] Ops = Operations (user impact)
[g] RCP = Representative concentration pathway
[f] %Diff = Percent difference with respect to impacts using historical climate data

The percent difference by incorporating future project climate data into the LCA framework resulted in a total percent increase of 1.97% and 1.41% in LCC for the DNR scenario for thick and thin pavement section respectively. Once again, a larger difference is observed for agency costs as compared to user costs and most notably for the DNR scenario followed by MO and CIR. The maximum percent difference in LCC for agencies (C/M impact) was 48.8% for the thick pavement cross section and 76.8% for the thin pavement cross section. While results will depend substantially on the highway section of choice, location

and other case specific inputs, the difference in impacts (both GWP and LCC) when using future projected climate data can result in a potential for significant savings over the service life of a roadway.

Meanwhile, the users (ops impact) maximum percent difference in LCC for thick and thin pavement was 0.13% and 1.86% respectively. The slight increase in operational impact when the total pavement structure thickness decrease emphasizes the need to consider operational impact for varying pavement sections as the rate of deterioration (quicker drop in IRI) may impact road user's fuel consumption and in turn increase GWP.

3.3 Impact of Incorporating Future Climate Data

The assumption of using historical climate data to design and predict pavement performance in the future where the climate is changing may lead to under designed pavements and lack of budgeting for M&R over the service life of the road. Pavements are constantly exposed to the natural environment and design to perform under given temperature ranges and environmental conditions. However, if those design criteria do not consider an accurate representation of what the pavement will be exposed to over the course of its service life, it can lead to increased user and agency life-cycle impacts.

Incorporation of future climate data projections within PavementME design software showed that for this evaluated case-study location and all M&R scenarios, pavements will experience a higher distress accumulation and early failure. As a result, the frequency of M&R activity increased for all scenario regardless of pavement structure. There is a need to consider future climate projections when conducting a pavement LCA to ensure that appropriate user and agency impacts are correctly accounted. Results from this case study are in agreement with literature that have incorporated future projected climate (temperature and or precipitation data) showing the increase impacts on pavement distresses (Mills et al. 2009, Heitzman et al. 2011, Daniel et al. 2014, Gudipudi et al. 2017, Mallick et al. 2018, Stoner et al. 2019).

In this study, agency GWP impacts increase by as high as 20% and as low as 0.97% depending on the M&R scenario and pavement structure. Similarly, agency LCC impacts may increase by as much as 16.6% and as low as 0.22%. While this is a fairly high range of increase in agency impact, it reiterates the need to properly predict pavement performance in a changing climate as an opportunity to optimize M&R treatments and long-term budgeting. From a user perspective, the difference in GWP and LCC impacts were not as significant (less than a percent) across all M&R scenarios and pavement section when comparing historical and future climate data. It is important to note the constraints of the case study presented and the possible causation it has on agency and user impacts. By holding the M&R treatment IRI trigger values constant for both the thick and thin pavement section over the entire analysis period, what is observed is an increase in M&R activity as pavement structure decreases and with the incorporation of future projected climate data. The pavement roughness is allowed only to reach an IRI value of 2.71 or 2.21 m/km depending on the M&R scenario before a given M&R treatment is applied and pavement condition restored. However, if M&R activity was held constant (i.e. every 5 or 10 years) and pavement condition allowed to continue to degrade (i.e. IRI continues to increase) it is suspected that operational impact would increase with the incorporation of future projected climate data.

4. SUMMARY

A primary objective of this study was to first illustrate the need to consider future climate data when performing a pavement LCA, this driven by the changing climatic conditions and its impacts on performance and longevity of pavement infrastructure. A method to incorporate future projected climate data an LCA framework that considers realistic traffic conditions was presented along with results from a case study consisting of two different pavement structures and three M&R alternatives. Results from this study show that in general LCA impacts in terms of GWP and LCC increase when using future projected climate data. A higher percent difference in GWP and LCC from use of historical to future projected climate data is observed for agencies due to increased number of construction activities in the future climate conditions. Whereas, since this study limited the pavement performance within a close range of roughness (in terms of IRI), the road user's operational impacts were consistent between historic and future climate. Agency GWP impacts may increase by as much as 20% and as little as 0.97% depending on pavement

structure and the M&R scenario while LCC impacts increase by as much as 16.6% and as little as 0.22%. It should be clear that for this study M&R timing was based on set IRI trigger values, however if M&R timing was held to a consistent schedule (i.e. every 5 or 10 years) and pavement roughness allowed to continue to degrade it is expected that operational impact would increase with the incorporation of future projected climate data. Further analysis is required to verify the assumption regarding the constraint of M&R timing activity and the effect on operational impacts.

Another recommendation for future work or extension of this study would be to perform a probabilistic analysis with the use of 21 different global circulation models available from CMIP5 rather than taking the average of them. However, as demonstrated in this study by simply incorporating future projected climate data into the pavement LCA framework there is a substantial opportunity to improve reliability of the planning and budgeting process for pavement management over the infrastructure life, while minimizing the environmental impact from agencies and users. RCP emission pathways 4.5 (intermediate) and 8.5 (high) were evaluated initially, however it was determined that there was minimal difference on the timing of M&R activities, therefore results from only RCP 8.5 were presented. The implication for agencies is that there is a difference in LCA impacts when using historical compared to future projected climate data regardless of which concentration pathway is assumed. Therefore, it is important to consider future rather than historical climate data when performing a pavement LCA to accurately capture the timing of M&R activities and change in operational impacts due to the higher rate of pavement distress accumulation.

5. REFERENCES

Brander, M., Davis, G. (2012) Greenhouse Gases, CO2, CO2e, and Carbon: What Do All These Terms Mean? Ecometrica. [online] Available at: https://ecometrica.com/assets/GHGs-CO2-CO2e-and-Carbon-What-Do-These-Mean-v2.1.pdf. [Accessed 11 Sep. 2019].

Climate Change: Vital Signs of the Planet. (2019). *Climate Change Evidence: How Do We Know?* National Aeronautics and Space Administration (NASA). [online] Available at: https://climate.nasa.gov/evidence/ [Accessed 11 Sep. 2019].

Daniel, Jo Sias, et al. "Impact of climate change on pavement performance: Preliminary lessons learned through the infrastructure and climate network (ICNet)." *Climatic Effects on Pavement and Geotechnical Infrastructure*. 2014. 1-9.

Gudipudi, Padmini P., B. Shane Underwood, and Ali Zalghout. "Impact of climate change on pavement structural performance in the United States." Transportation Research Part D: Transport and Environment 57 (2017): 172-184.

Haslett, Katie E., Eshan V. Dave, and Weiwei Mo. "Realistic Traffic Condition Informed Life Cycle Assessment: Interstate 495 Maintenance and Rehabilitation Case Study." Sustainability 11.12 (2019): 3245.

Heitzman, Michael, et al. Developing MEPDG Climate Data Input Files for Mississippi. No. FHWA/MS-DOT-RD-11-232. 2011.

Knott, Jayne F., et al. "Assessing the effects of rising groundwater from sea level rise on the service life of pavements in coastal road infrastructure." Transportation Research Record 2639.1 (2017): 1-10. https://doi.org/10.3141/2639-01

Knott, Jayne F., et al., "A Framework for Introducing Climate-Change Adaptation for Pavement Management," Sustainability, 11(16), p. 4382, 2019. https://doi.org/10.3390/su11164382

Mallick, Rajib B., et al. "Understanding the impact of climate change on pavements with CMIP5, system dynamics and simulation." International Journal of Pavement Engineering 19.8 (2018): 697-705.

Meagher, William, et al. "Method for evaluating implications of climate change for design and

performance of flexible pavements." Transportation Research Record 2305.1 (2012): 111-120.

Mills, Brian N., et al. "Climate change implications for flexible pavement design and performance in southern Canada." Journal of Transportation Engineering 135.10 (2009): 773-782.

Mndawe, M. B., et al. "Assessment of the effects of climate change on the performance of pavement subgrade." African Journal of Science, Technology, Innovation and Development 7.2 (2015): 111-115.

Qiao, Y., Flintsch, G. W., Dawson, A. R., & Parry, T. (2013). Examining Effects of Climatic Factors on Flexible Pavement Performance and Service Life. Transportation Research Record, 2349(1), 100–107. https://doi.org/10.3141/2349-12

Stoner, A. M. K., Daniel, J. S., Jacobs, J. M., Hayhoe, K., & Scott-Fleming, I. (2019). Quantifying the Impact of Climate Change on Flexible Pavement Performance and Lifetime in the United States. Transportation Research Record, 2673(1), 110–122. https://doi.org/10.1177/0361198118821877

US Department of Transportation, 2015. Beyond Traffic 2045: Trends and Choices. DOT, US.

APPENDIX E: Chapter 9 Appendices

Appendix E.1: Overlay Performance Curves

In the following subsections, correlations between Boltzmann fitting coefficient (half-value and slope) and laboratory performance indices from DCT, DCB and OT test are presented. Performance data from MnROAD sections is split based on the pre-overlay LTE values into two groups, moderate (>50% LTE) or low LTE (<=50%) and fit separately. A linear fit was applied and the equation of the line used to predict the half value or slope for any given total performance index contribution beyond MnROAD test sections.

DCT Performance Indices

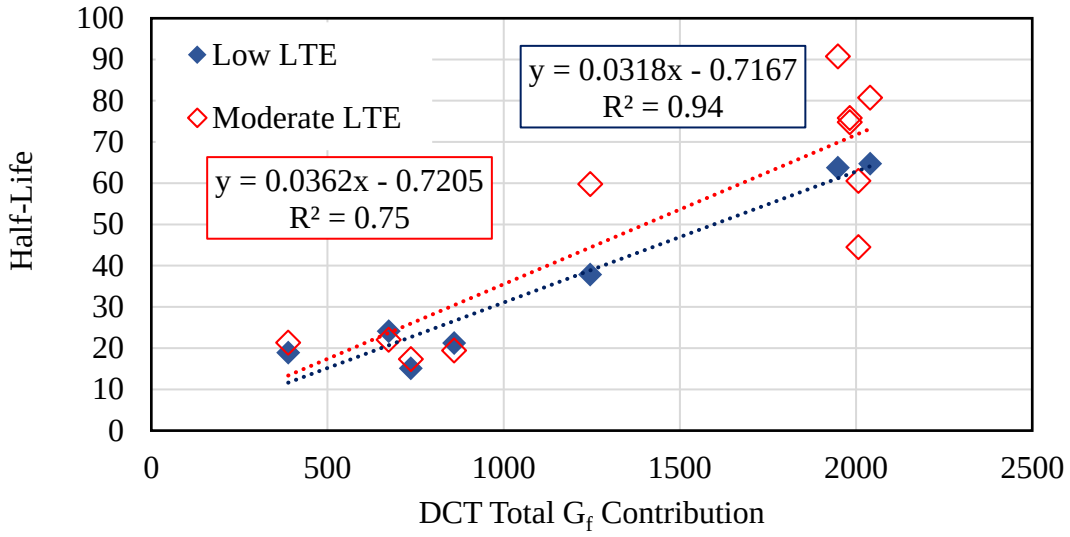

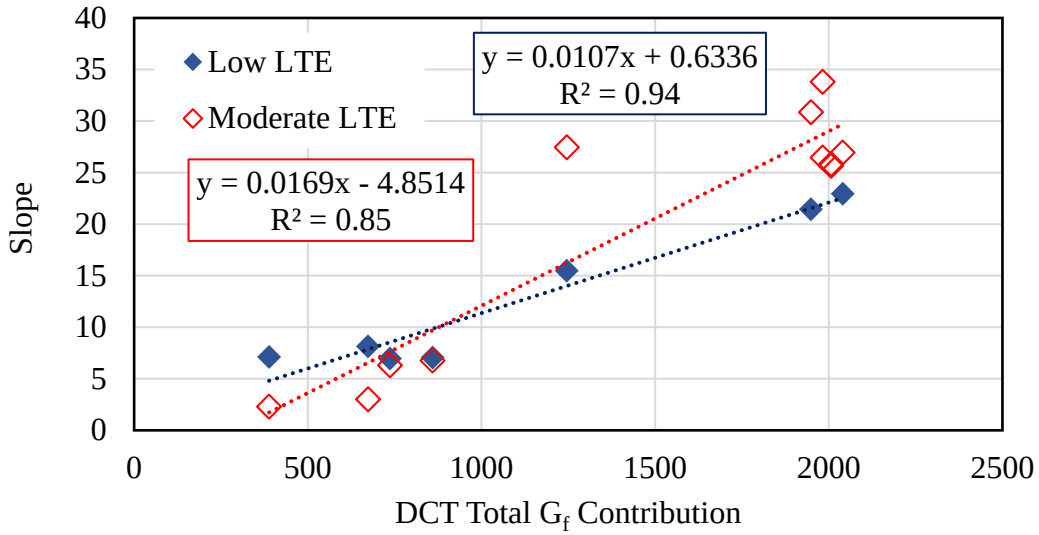

DCT Performance Indices

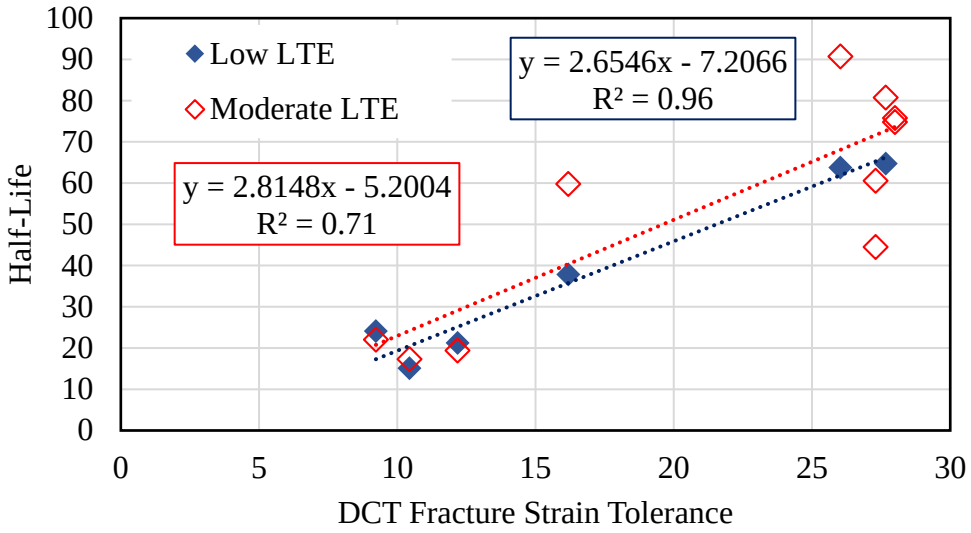

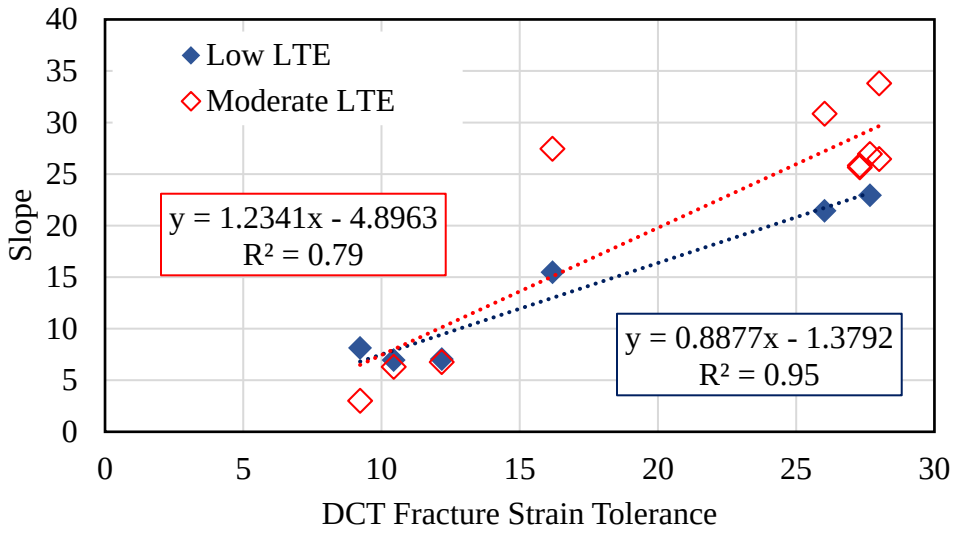

DCT Performance Indices

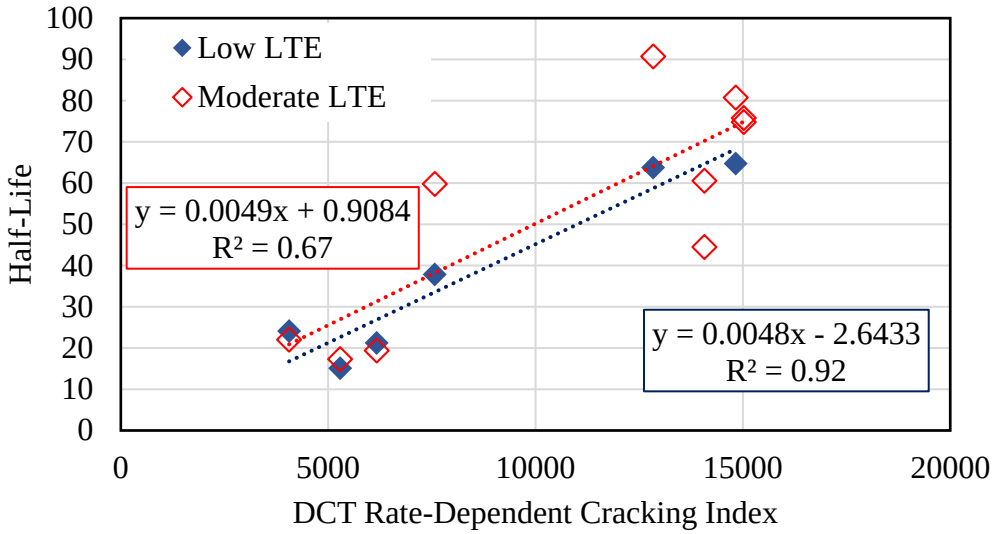

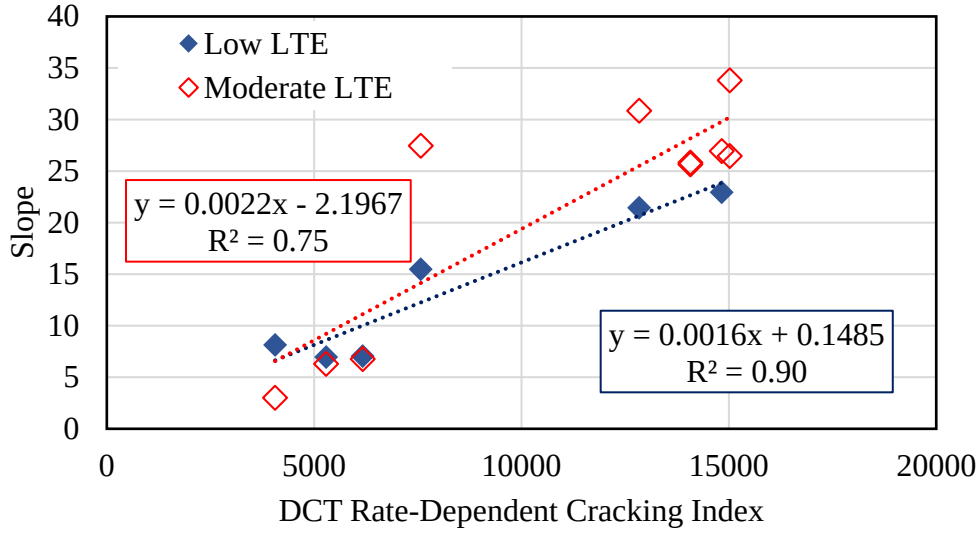

SCB Performance Indices

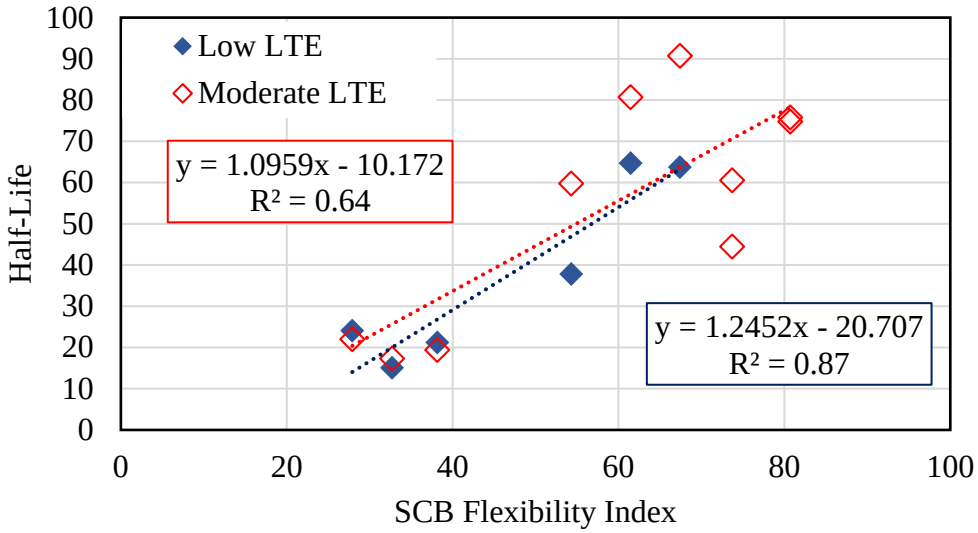

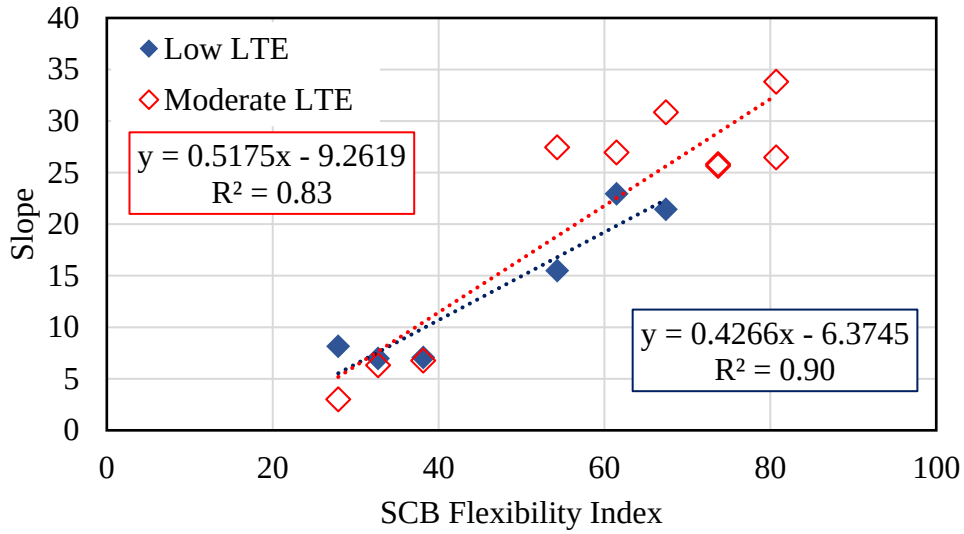

SCB Performance Indices

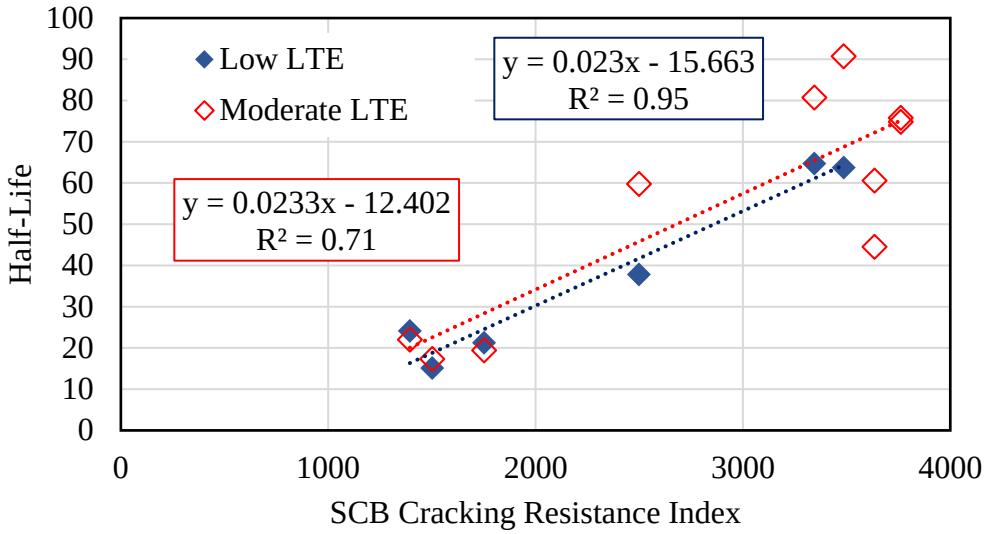

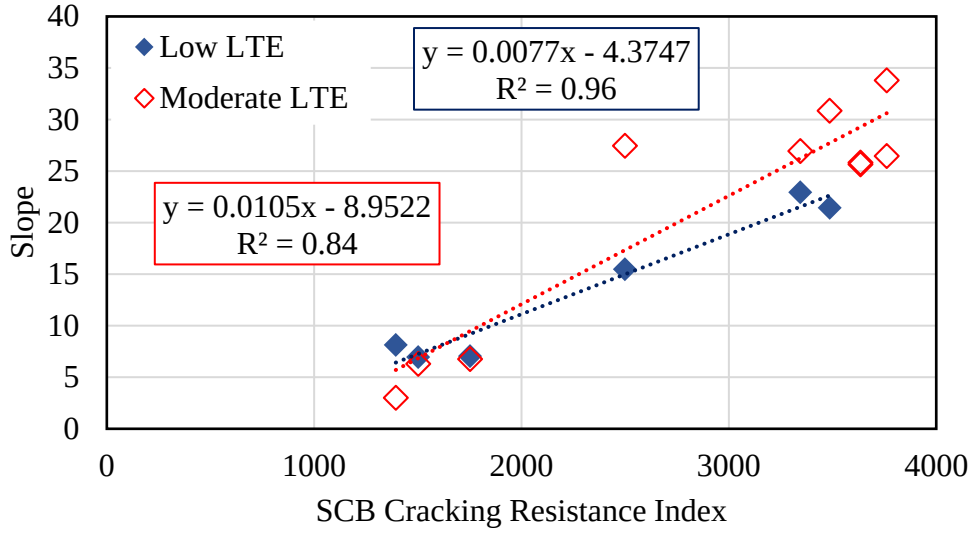

SCB Performance Indices

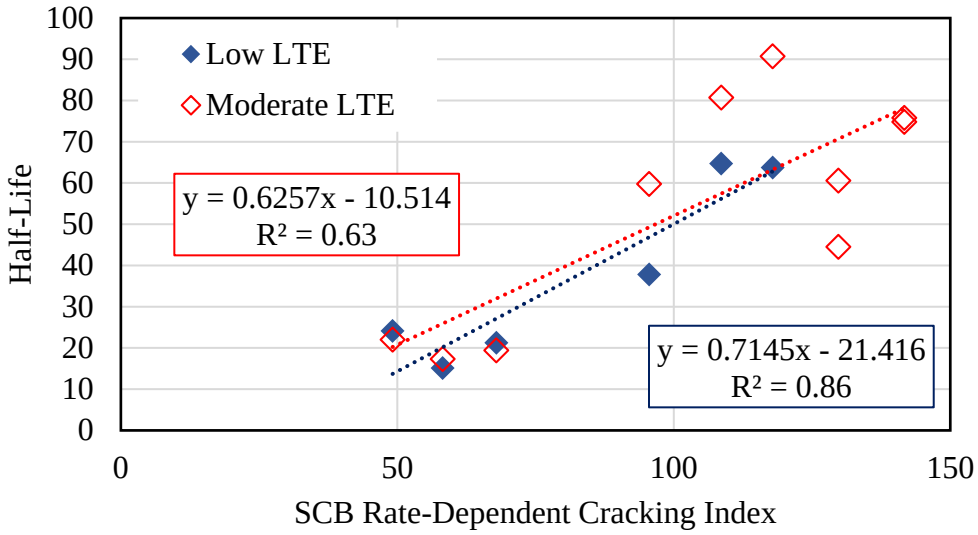

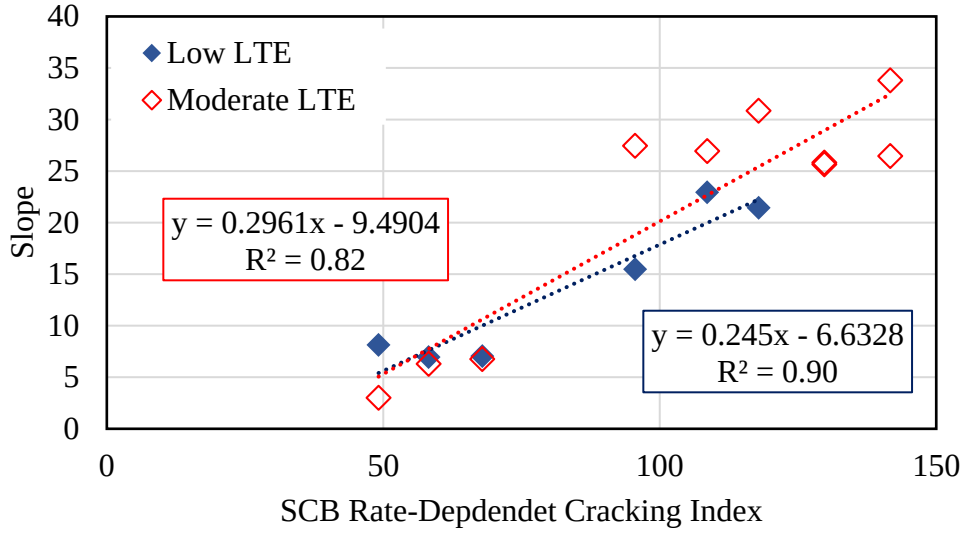

OT Performance Indices

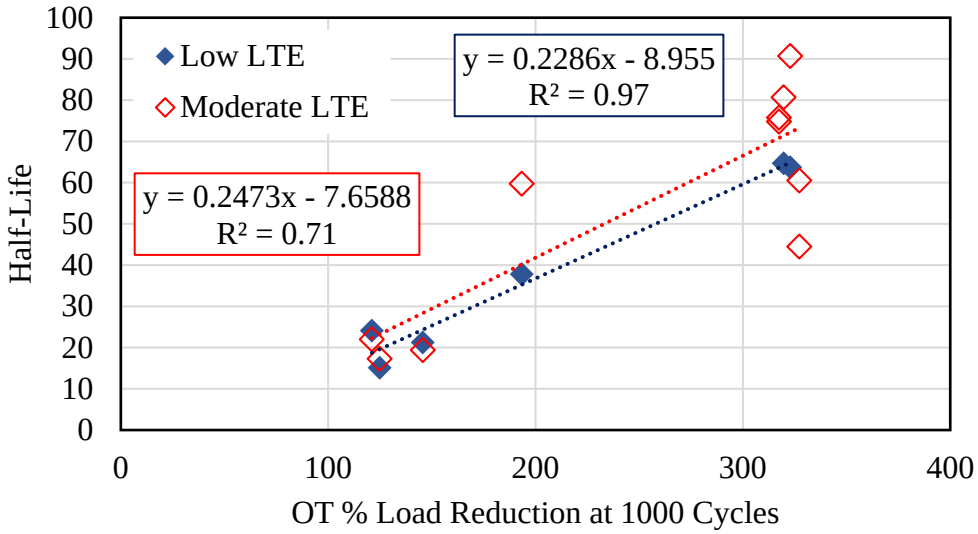

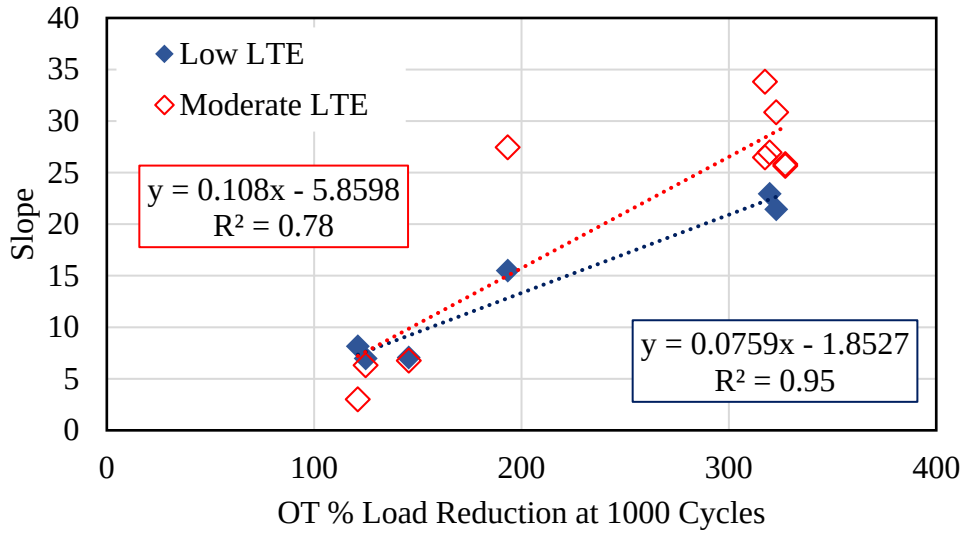

Appendix E.2: Demonstration of Decision Tree Tool

An example is presented herein using the decision tree tool to evaluate the predicted performance and life cycle material cost for Cell 990.Figure E.2-1shows a screenshot of part of the instruction module, providing the user with an overview of the tool and its purpose.

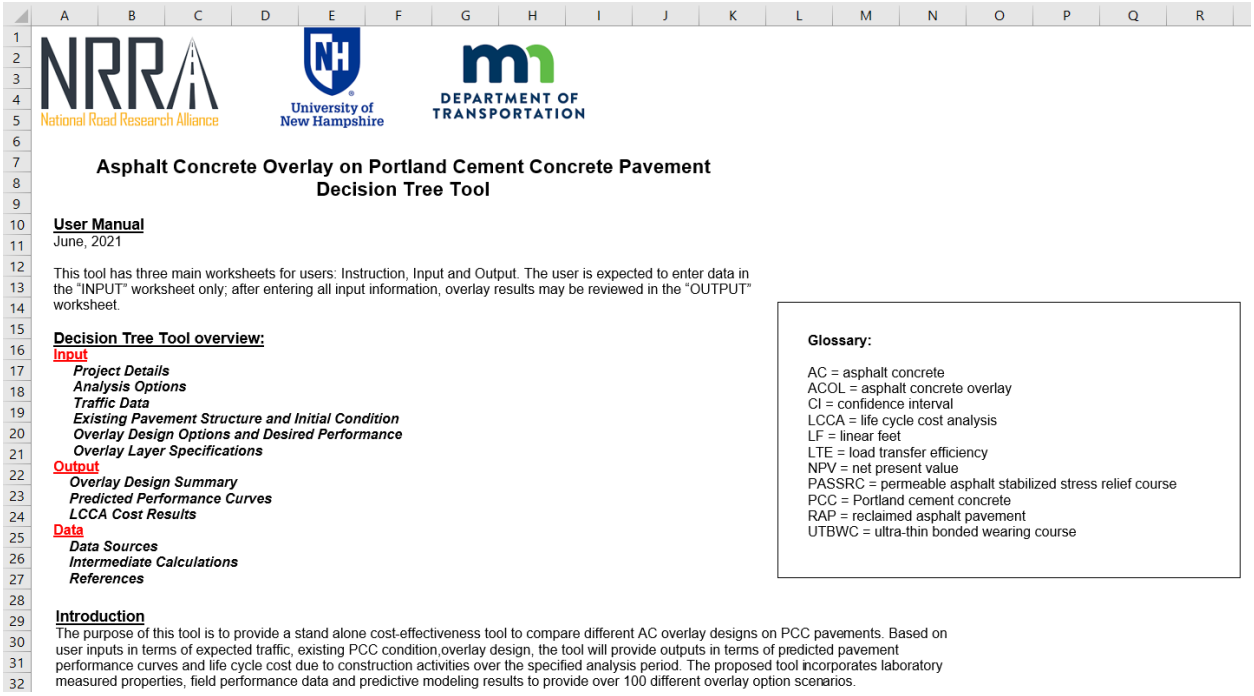

Figure E.2-1 Screenshot of the instruction module in decision tree tool.

Next, a screenshot of the input module is provided with corresponding input information for the demonstration of Cell 990 (Figure E.2-2). As a reminder, cells highlighted in green are required user inputs, while cells highlighted in orange are supplemental information.

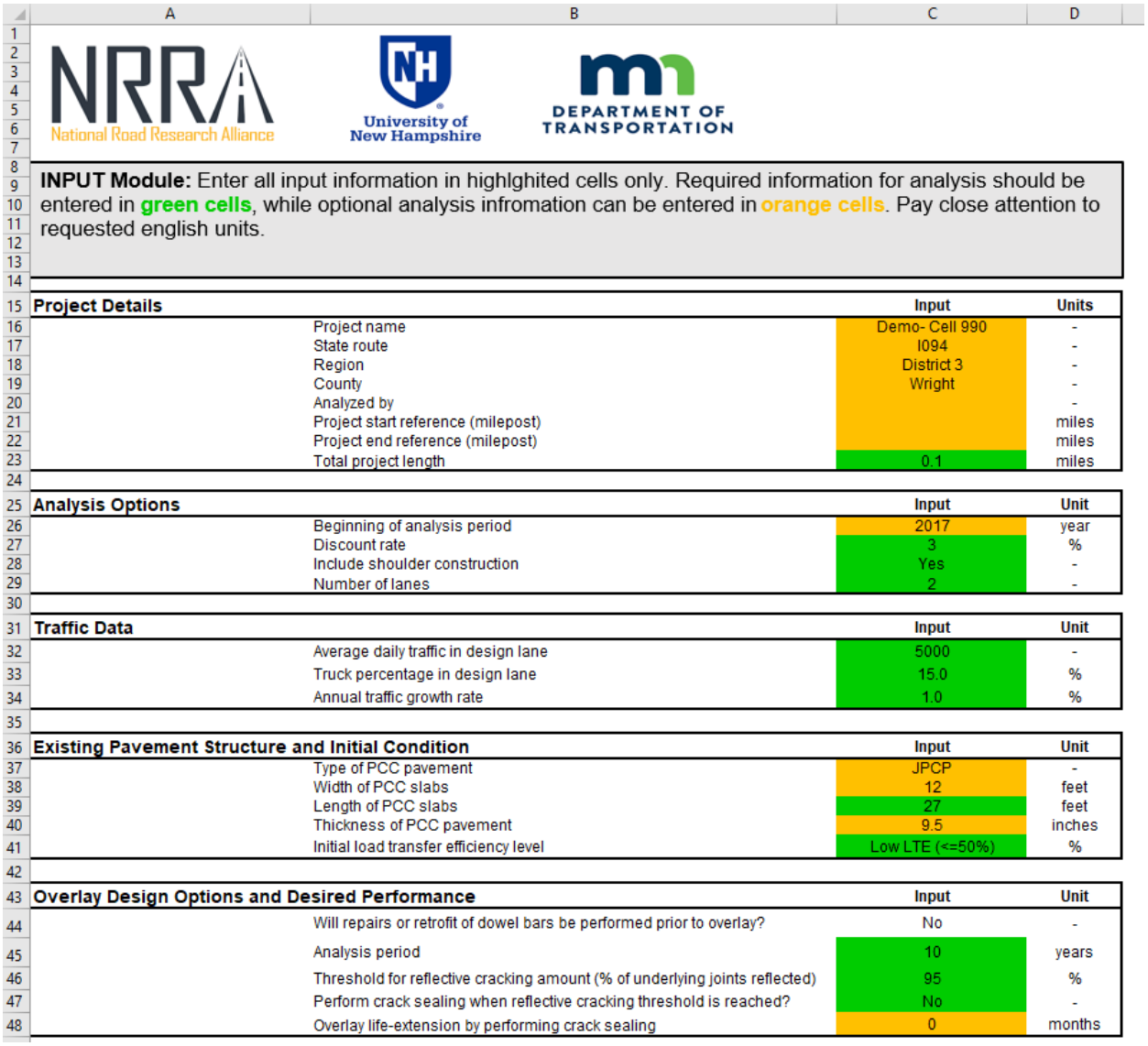

INPUT Module: Enter all input information in highlghited cells only. Required information for analysis should be entered in **green cells**, while optional analysis infromation can be entered in **orange cells**. Pay close attention to requested english units.

Project Details		Input	Units
	Project name	Demo- Cell 990	-
	State route	I094	-
	Region	District 3	-
	County	Wright	-
	Analyzed by		-
	Project start reference (milepost)		miles
	Project end reference (milepost)		miles
	Total project length	0.1	miles

Analysis Options		Input	Unit
	Beginning of analysis period	2017	year
	Discount rate	3	%
	Include shoulder construction	Yes	-
	Number of lanes	2	-

Traffic Data		Input	Unit
	Average daily traffic in design lane	5000	-
	Truck percentage in design lane	15.0	%
	Annual traffic growth rate	1.0	%

Existing Pavement Structure and Initial Condition		Input	Unit
	Type of PCC pavement	JPCP	-
	Width of PCC slabs	12	feet
	Length of PCC slabs	27	feet
	Thickness of PCC pavement	9.5	inches
	Initial load transfer efficiency level	Low LTE (<=50%)	%

Overlay Design Options and Desired Performance		Input	Unit
	Will repairs or retrofit of dowel bars be performed prior to overlay?	No	-
	Analysis period	10	years
	Threshold for reflective cracking amount (% of underlying joints reflected)	95	%
	Perform crack sealing when reflective cracking threshold is reached?	No	-
	Overlay life-extension by performing crack sealing	0	months

Figure E.2-2 Screenshot of input module showing user inputs for given demonstration of decision tree tool.

Also included within the input module is a section for the user to provide overlay layer specifications in terms of material selection, lift thickness, and unit costs. Figure E.2-3 shows a screenshot of the decision tree tool where the user has the ability to build an overlay cross section, and in this particular example Cell 990 is modeled. User defined mixtures can be entered in this location by selecting “User Defined ACOL” as the asphalt material type, and entering the

corresponding inputs (binder content, design air void, mix density and fracture energy from DCT testing).

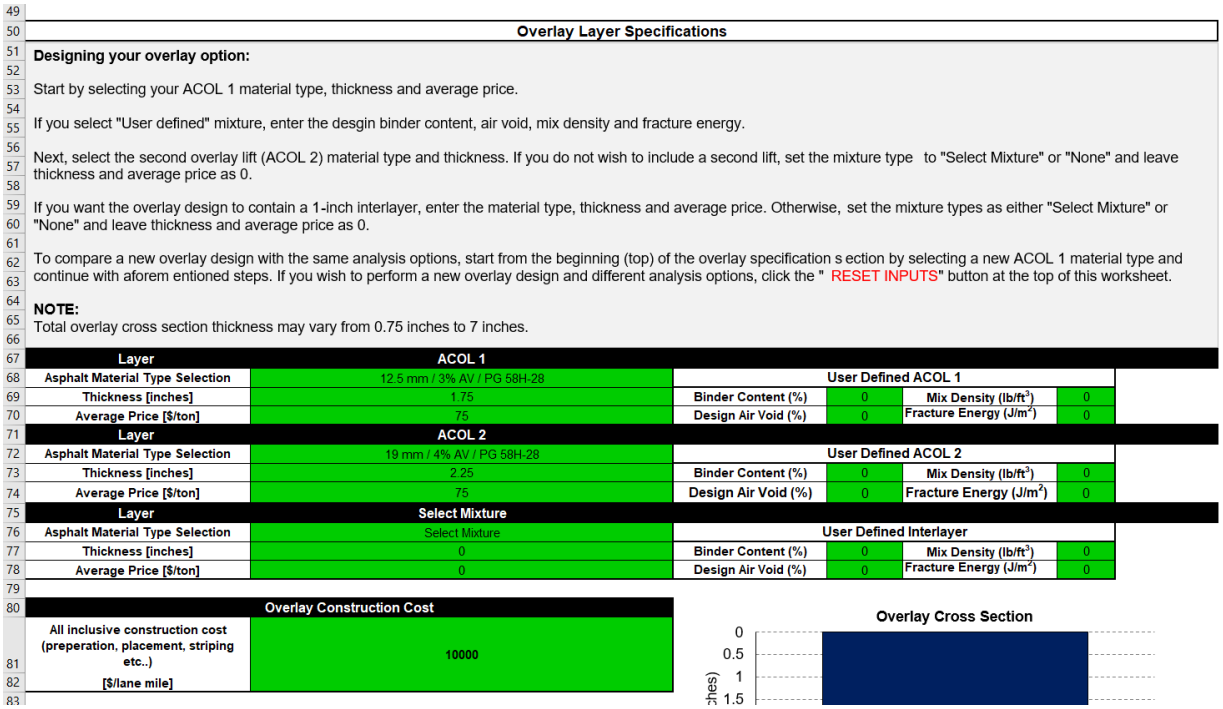

Overlay Layer Specifications

Designing your overlay option:

Start by selecting your ACOL 1 material type, thickness and average price.

If you select "User defined" mixture, enter the desgin binder content, air void, mix density and fracture energy.

Next, select the second overlay lift (ACOL 2) material type and thickness. If you do not wish to include a second lift, set the mixture type to "Select Mixture" or "None" and leave thickness and average price as 0.

If you want the overlay design to contain a 1-inch interlayer, enter the material type, thickness and average price. Otherwise, set the mixture types as either "Select Mixture" or "None" and leave thickness and average price as 0.

To compare a new overlay design with the same analysis options, start from the beginning (top) of the overlay specification s ection by selecting a new ACOL 1 material type and continue with aforem entioned steps. If you wish to perform a new overlay design and different analysis options, click the " RESET INPUTS" button at the top of this worksheet.

NOTE:
Total overlay cross section thickness may vary from 0.75 inches to 7 inches.

Layer	ACOL 1	User Defined ACOL 1			
Asphalt Material Type Selection	12.5 mm / 3% AV / PG 58H-28				
Thickness [inches]	1.75	Binder Content (%)	0	Mix Density (lb/ft^3)	0
Average Price [$/ton]	75	Design Air Void (%)	0	Fracture Energy (J/m^2)	0
Layer	**ACOL 2**				
Asphalt Material Type Selection	19 mm / 4% AV / PG 58H-28	User Defined ACOL 2			
Thickness [inches]	2.25	Binder Content (%)	0	Mix Density (lb/ft^3)	0
Average Price [$/ton]	75	Design Air Void (%)	0	Fracture Energy (J/m^2)	0
Layer	**Select Mixture**				
Asphalt Material Type Selection	Select Mixture	User Defined Interlayer			
Thickness [inches]	0	Binder Content (%)	0	Mix Density (lb/ft^3)	0
Average Price [$/ton]	0	Design Air Void (%)	0	Fracture Energy (J/m^2)	0

Overlay Construction Cost	
All inclusive construction cost (preperation, placement, striping etc..) [$/lane mile]	10000

Figure E.2-3 Screenshot of user input module for overlay layer specification to model Cell 990.

Once all user inputs have been entered, the output module will automatically generate an overlay design summary, truck traffic summary, LCCA results and predicted performance curves with respect to time in service and cumulative number of trucks. Figure E.2-4 shows an example of the output module for the given demonstration. Again, the dashed red and blue lines on the predicted performance curve plots represent the 95% upper and lower confidence intervals. For the model overlay scenario using Cell 990's pavement structure, truck traffic and existing LTE, one overlay constructions after the initial overlay will be required to reach the desired service life of 10 years. The estimated agency LCC of asphalt material in NPV is approximately $30,216 and

the estimated EAC is approximately $3,542 for the entire project scope (length=0.1 miles and number of lanes =2).

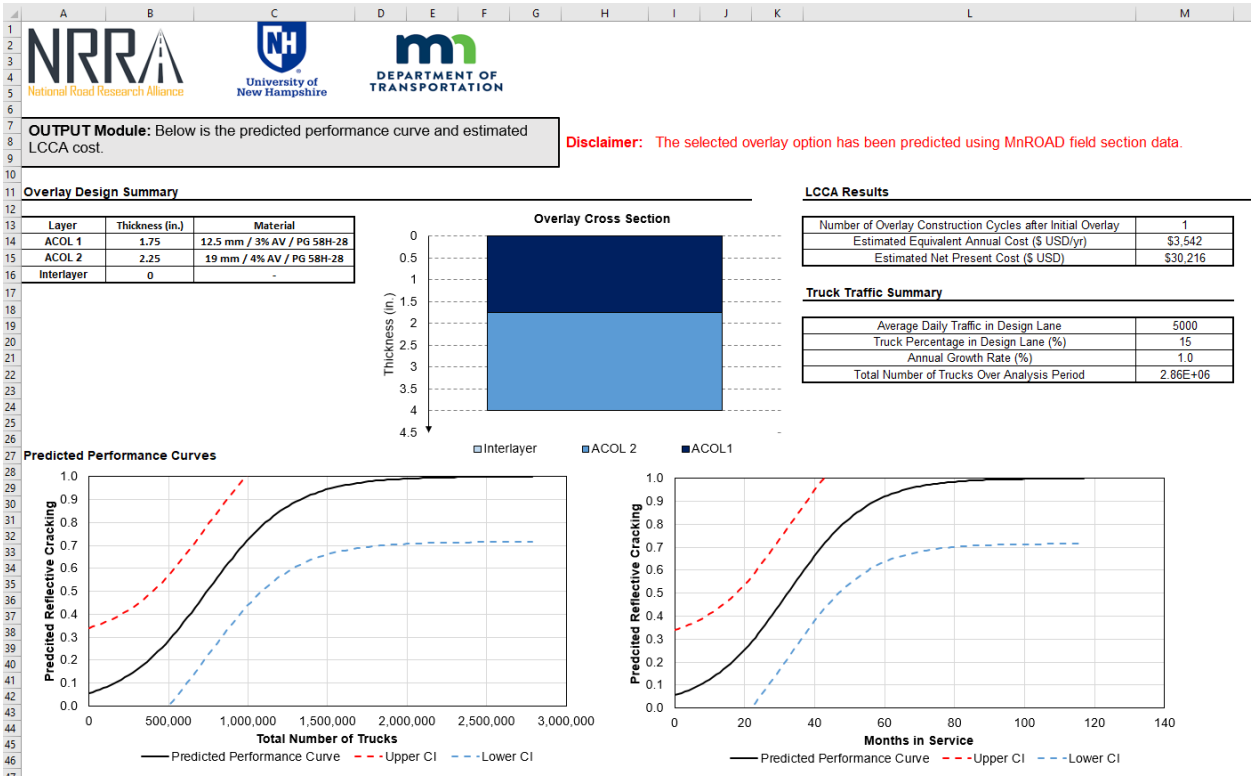

Figure E.2-4 Screenshot of output module for given demonstration of decision tree tool.

Figure E.2-5 and Figure E.2-6 provide a closer look at the predicted performance curves for Cell 990 in terms of total number of trucks and months in service respectively. These uniquely generated performance curves provide users with the ability to easily compared predicted reflective cracking amount with time or cumulative number of truck traffic at different cracking threshold levels.

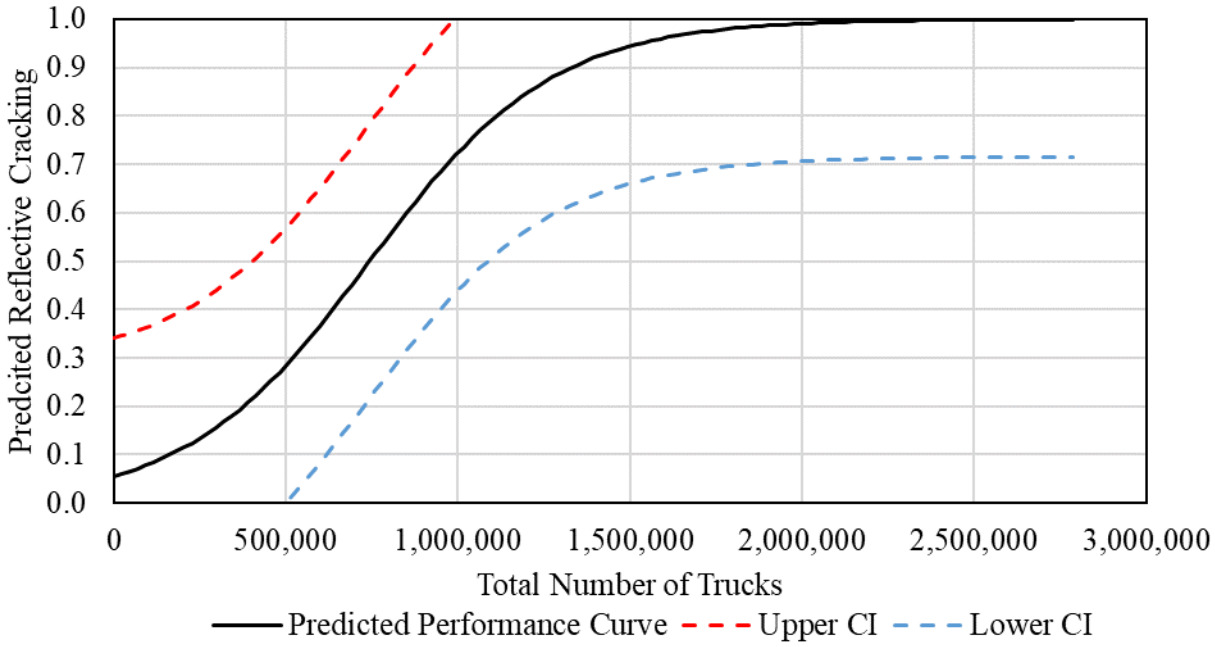

Figure E.2-5 Output example of predicted reflective cracking versus total number of trucks.

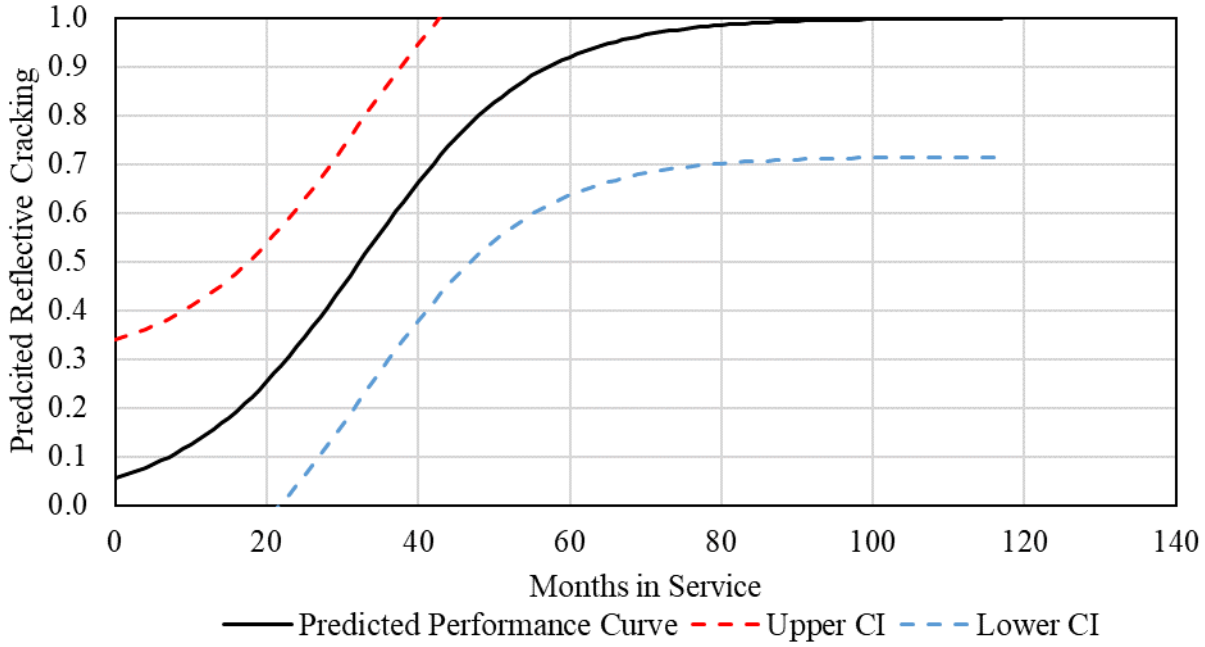

Figure E.2-6 Output example of predicted reflective cracking versus months in service.